University of Oxford

St. Cross College

D.Phil. Earth Sciences

Mathematical studies of Morphology in Early Life Palaeobiology

---

Author:

Renee Hoekzema

Supervisor:

Prof. Martin Brasier

November 13, 2015

Contents

Mathematical studies of Morphology in Early Life Palaeobiology

Abstract

The overarching topic of this thesis is the mathematical study of morphology, applied to palaeobiology, more specifically the palaeobiology of early life. The first part of this thesis concerns the study of growth in the enigmatic late Ediacaran macrobiota (579-541 Ma). A new framework is presented for quantitative comparison of the ontogeny of dickinsoniomorphs and rangeomorphs, and this setup is applied to the iconic Ediacaran taxa *Dickinsonia costata* and *Charnia masoni*. The methodology, based on measurements of branch/segment lengths at different stages of ontogeny, reveals an intricate, complex system of growth in both taxa. The segments of *Dickinsonia* grow in two stages of growth, a first phase of rapid growth and a second phase of slower inflation. After around 50 segments are present on each side of the axis, the rate of insertion starts to decrease while the growth of the organism

continues. I speculate that this switch might reflect a change from somatic to reproductive growth. Interestingly, a very similar mode of growth is found in the first order branches of *Charnia masoni*, which also grow in two distinct phases, and potentially can be seen to halt their insertion after around 18-20 branches are present on each side of the organism, while the organism continues to grow. In contrast, the second order branches do not follow this pattern but continue to be added. These modes of growth are reconstructed in a computer model. This model can be extended to other Ediacaran life forms, effectively generating a "morphospace" of rangeomorphs and dickinsoniomorphs.

The second part of this thesis focuses on the biological or abiological origin of the iconic trace fossil *Paleodictyon*, shaped like a hexagonal mesh. This ichnogenus occasionally displays incredible regularity, as well as a very high connectivity, a very broad environmental tolerance and a temporal range from the Cambrian until the present day. Despite extensive research on modern patterns, no organism has yet been identified as creator. These facts cast doubt on the biogenic interpretation of *Paleodictyon*. I propose the hypothesis that some of these patterns are created abiotically by regular hexagonal standing Faraday waves resulting from events such as earthquakes. This hypothesis is put to the test by means of experiments and computer modelling of the wave. In particular, a hexagonal pattern very similar to the most regular specimens of *Paleodictyon* could be formed in experiments and preserved on the surface of a calcium carbonate paste.

Extended Abstract

The overarching topic of this thesis is the mathematical study of morphology, applied to palaeobiology, more specifically the palaeobiology of early life. The thesis is divided into three parts. The first part concerns the study of growth in macro-organisms of the Ediacara biota. Measurements and analysis of the growth of the taxa *Dickinsonia* and *Charnia* are discussed, together with conclusions for biology. A growth model describing the growth of these taxa and other Ediacaran organisms with a branching morphology is introduced, and the Part concludes with a discussion of the phylogenetic position of Ediacaran "vendobionts". The second part concerns the Phanerozoic trace fossil Paleodictyon, proposing and testing an abiotic formation hypothesis that could be responsible for creating some or all structures previously assigned to this ichnotaxon. The third, concluding part summarizes the finds discussed in the thesis.

Part I concerns the study of growth within Precambrian macroscopic organisms of the late Ediacaran biota (579-541 Ma).

Chapter 1 gives an introduction to the Ediacara biota and the study of the origin of segmentation in bilaterians.

In Chapter 2 the measurements of segment lengths and counts of twenty well-

preserved specimens of the iconic taxon *Dickinsonia* are presented. Furthermore, building upon the interpretations of Ivantsov (2011), who suggested that *Dickinsonia* was responsible for feeding traces termed Epibaion, I propose quasi-passive locomotion to explain the feeding traces found for *Dickinsonia* and similar forms. This suggests that the organism may have changed its shape or chemistry to facilitate being passively moved by currents. In particular, I discuss the possibility that *Dickinsonia* was able to curl up its margins, explaining "touch-evasive" marks, as recently discussed in Evans et al. (2015), the folds observed in some specimens, and suction marks in feeding traces that suggest the organism was stripped off a mucilaginous mat from the margin upwards.

Chapter 3 presents the measurements of first and second order branches of four well-preserved specimens of *Charnia masoni* in different stages of ontogeny. I have measured the lengths of the first order branches, counted the number of first order branches and estimated the maximal number of second order branches visible on any first order branch. The chapter also gives an introduction to the concept of fractal or Hausdorff dimension and shows why it is mathematically obvious that *Charnia* has a fractal dimension of 2.

Chapter 4 introduces the concept of a morphospace, after which one is constructed in the form of a growth model. Then the measurements of *Dickinsonia* and *Charnia* are interpreted.

Within a three-dimensional visualisation of the measurements of *Dickinsonia*, these split into two groups, separating *D. costata* and *D. rex* specimens. The *D. costata* lie between two growth surfaces, interpretated as a contracted versus uncontracted specimens. The measurements confirm that *D. costata* grew

through both addition and inflation of segments. The measurements furthermore reveal that *D. costata* experienced a decrease in the rate of segment insertion while continuing to inflate in size, as the number of segments approached 50. This change in growth might be explained by a switch in life strategy from a somatic to a reproductive phase.

Dickinsonia is currently assumed to insert its segments on the apical end of the central axis, where the segments are smallest. However, measurements reveal that a basal mode of insertion is also consistent and cannot be dismissed.

Uncontracted specimens are found to have their longest segment at around 35-40% of the total number of segments, counted from the basal segment upwards. Contracted specimens, however, are consistently found to have an altered outline where the position of the longest segment has shifted down to around 25% of the total count. This new observation suggests that the wider segments towards the basal end contract less than the thinner segments towards the apex of the organism. This is consistent with the idea that *Dickinsonia* had an elastic body supported by internal pressure, which deflated post-mortem.

A growth model for *D. costata*, assuming apical insertion, is built based on segments that grow in two phases, as is revealed to be the case in the measurements. The model can be assembled into an animation, of which snapshots are shown in Appendix A.

Analysing the measurements of *Charnia* reveals similarities with *Dickinsonia*. The taxon also grows both through insertion and inflation of branches. The basal 38% of the branches appear to be of the same length, while the apical branches decrease linearly in length towards the apex. This has usually been interpreted as a sign of apical insertion, but analysis of the measurements show

that a basal branching model is also consistent, and there are features in the fossils that favour the latter interpretation.

The largest specimen is unusually large for the number of branches it possesses, which could indicate an insertion stop as was observed in *Dickinsonia*. Alternatively, differential growth of this specimen might have been the result of a disturbance in the environment.

Measurements of the second order branches reveal that the growth program of *Charnia* is potentially not as self-similar as proposed in Hoyal Cuthill and Conway Morris (2014). The outline of first order branch lengths shows that branches grow in two stages, the first one with a faster rate of growth and the second one with slower inflation of the branch lengths. An apically branching growth model is based on this assumption, together with measurements of the second order branches. Snapshots of the resulting animation are shown in Appendix B.

Towards the end of the chapter, I compare the growth programs of *Dickinsonia costata* and *Charnia masoni*, and describe how the growth model can arguably be extended to other Ediacaran macro-organisms. I then continue to review the morphology of these organisms, and I make a case for a common origin of the "vendobiont" growth plans.

Part II of this thesis concerns the origin of the hexagonal patterns ascribed to the ichnotaxon *Paleodictyon*. These occasionally exceptionally regular hexagonal meshes are found in marine and non-marine sandstones from the early Cambrian on. Modern patterns were found near the Atlantic mid-oceanic ridge (Ekdale (1980)), but a thorough study did not reveal an organism responsible for their creation (Rona et al. (2009)). Very similar patterns can be made

by means of the physical phenomenon of Faraday waves (standing waves on a surface), which can potentially be induced in the surface of the sediment by events such as earthquakes. Standing waves are governed by geometry and can form hexagonal patterns with a precise regularity. Chapter 5 explores the possibility that this phenomenon is responsible for some of the occurrences of *Paleodictyon* in the fossil record and on the modern sea floor.

To test this hypothesis, I have studied computer models of the three-dimensional waveform and velocity field, which help to understand how a waveform can create a lasting pattern in the sediment. Experiments showed that a hexagonal Faraday waves were easily induced on the surface of different mixtures of fine-grained sediment and water as the result of a simple vertical oscillation. In particular, a calcium carbonate paste captured the induced wave as a lasting relief in the shape of a hexagonal mesh on its surface, which was preserved for several days after the excitation. It is not yet clear whether Faraday waves would result in the creation of a tunnel network with vertical tunnels as found in the modern *Paleodictyon*, although a case can be made to suggest this.

Analysis of experiments inducing the Faraday waves on the surface of a silica dust suspension shows the presence of a square root relationship between the widths of the edges of the hexagons and their diameters. A study of measurements of hundreds of *Paleodictyon* ichnofossils documented in the literature show that this relationship is also present in the fossil record. Changes in the prefactor over time possibly relate to the rise of angiosperms during the Cretaceous and other changes in the global environment.

I discuss the biogenicity criteria put forward by Ekdale et al. (1984) for trace fossils, in particular those emphasized by Pickerill (1990) to assess the bio-

genicity of *Paleodictyon*, and whether these objections are resolved by the given abiogenic interpretation. Pickerill notes a lack of current orientation; generally uniform dimensions and the regularity of the pattern; presence of a thin lining and the presence of other trace fossils on the same bed as evidence for the biogenicity of *Paleodictyon*. Faraday waves are not current-related, therefore the first argument does not speak against this hypothesis. The uniformity and regularity are even more strongly a feature of standing waves than they are of biology. A thin lining could potentially be created by compaction of the sediment along the nodes of the wave, which were calculated in a computer model to lie along the boundaries of the hexagon edges. Experiments show that an increase in density occurs at the nodes of the waveform, in accordance with previous work inducing Faraday waves on calcium carbonate pastes in Nakayama et al. (2013). *Paleodictyon* belongs to the group of trace fossils known as graphoglyptids, which are commonly found together. Graphoglyptids are regular geometric patterns that share a tendency to subdivide an area into units of equal lengths (Rona et al. (2009)). This is reminiscent of standing waves, which are governed by their wavelength. Faraday waves occur in many different modes with different geometries. Therefore presence of other patterns on the same beds as *Paleodictyon* might tentatively be taken to suggest the abiogenicity of some of the patterns associated with graphoglyptids. A new list of considerations for the biogenicity of trace fossils is suggested especially to differentiate between biogenic graphoglyptids and abiogenic patterns resulting from standing waves.

Part I

A mathematical study of Ediacaran mophology: modelling, measurements and conclusions for biology

Chapter 1

Introduction to the Ediacara Biota

1.1 The discovery of a macroscopic Precambrian biota

The late Ediacaran macrobiota inhabited the seas of planet Earth during the last 40 million years of the Neoproterozoic era, just before the Cambrian explosion of complex life where it seemingly met its demise (Laflamme et al. (2013)). In 1946 a number of fossils from this period, including the segmented impessions of *Dickinsonia*, were discovered in shallow marine strata the Ediacara Hills of South Australia, which have since lent their name to the Ediacaran system (Knoll et al. (2006)). Initially the fossils were cautiously described as "Early Cambrian jellyfish" by their discoverer Reg Sprigg, a former geology student from the University of Adelaide (Sprigg (1947); Turner and Vickers-Rich (2007)). Their significance was only recognised when Martin Glaessner

wrote a number of papers on the finds together with his student Mary Wade from 1959 onwards (Glaessner (1959, 1961); Glaessner and Wade (1966)).
Around the same time the first macrofossils recognised to be Precambrian in age were discovered on the other side of the world in Charnwood Forest in Leicestershire, England. This set of beautifully preserved fossils included the iconic taxon *Charnia*. The Charnwood assemblage described by Trevor Ford was suggested to represent new forms of Precambrian algae (Ford (1958)). Ford also made the link to *Rangea*, a similar impression that had been identified in 1929 by Gürich from the Nama formation of what is now Namibia, but whose Precambrian age was not yet confirmed (Gürich (1929, 1933); Jenkins (1995)). Nowadays Ediacaran fossils are known from all over the world and paint the picture of a complex biota distinctly different from modern sea faunas (Narbonne et al. (2012)). Figure 1.1 gives an artist's impression of a typical community in the deep sea environment of what is now Charnwood forest.
A few key taxa of the late Ediacaran macrobiota are shown with their temporal range in Fig. 1.2. Most notable in terms of complexity are the "fractally" branched rangeomorphs, such as for example *Charnia*, *Rangea* and *Fractofusus*. Rangeomorphs are often described as frond-like. They generally have a central axis from which two or more vanes of branches grow, and these branches subdivide into smaller "higher order" branches, in a more or less self-similar way (Brasier et al. (2012)). The taxon *Charniodiscus*, while initially speculated to be associated to *Charnia* by Ford (1958), does not show a further subdivision of its branches. It does clearly posses a basal circular organ interpreted as a holdfast, as do a number of rangeomorph taxa, and it is occasionally grouped with the rangeomorphs, for example in Brasier et al.

Figure 1.1: An artist's impression of an Avalonian benthic community about 560 million years ago. Apart from the numerous frondose organisms, several other organisms are shown undergoing decay while the microbial mat is enveloping them. These have been suggested to explain features on the fossilized beds known as ivesheadiomorphs (cf. Liu et al. (2011a)). Figure appears in Liu et al. (2014), Fig.7. Artist: Charlotte Kenchington, used with permission.

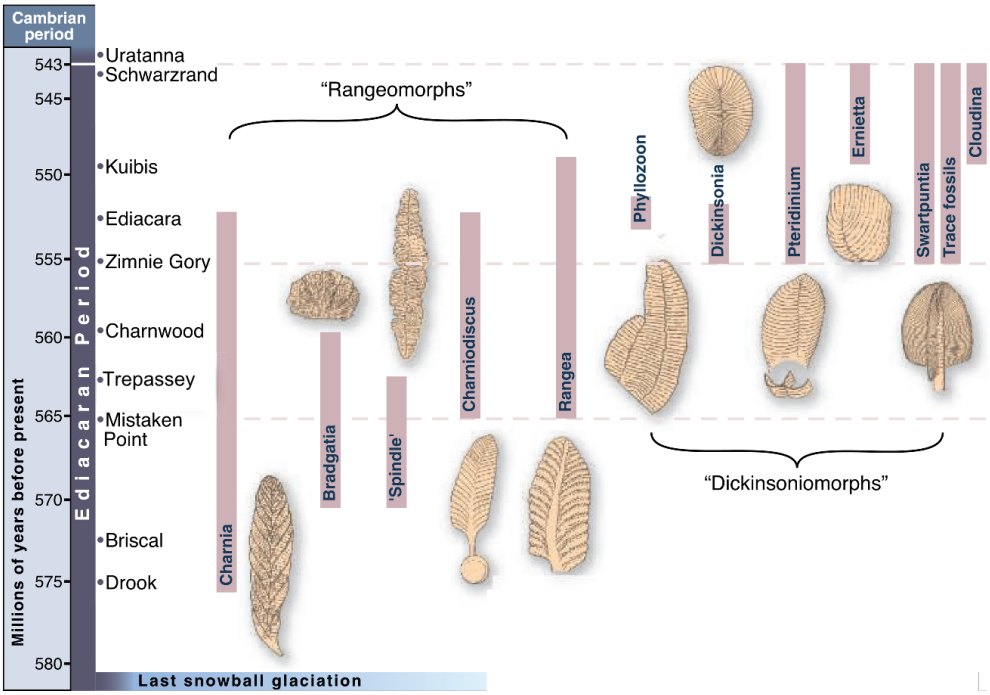

Figure 1.2: An overview of the temporal range of a few key taxa from the late Ediacaran macrobiota, with the localities marked on the left. The taxa grouped in this figure and this thesis as dickinsoniomorphs generally have a later range than the rangeomorphs. They also generally stem from a shallower marine environment. Figure adapted from Brasier and Antcliffe (2004).

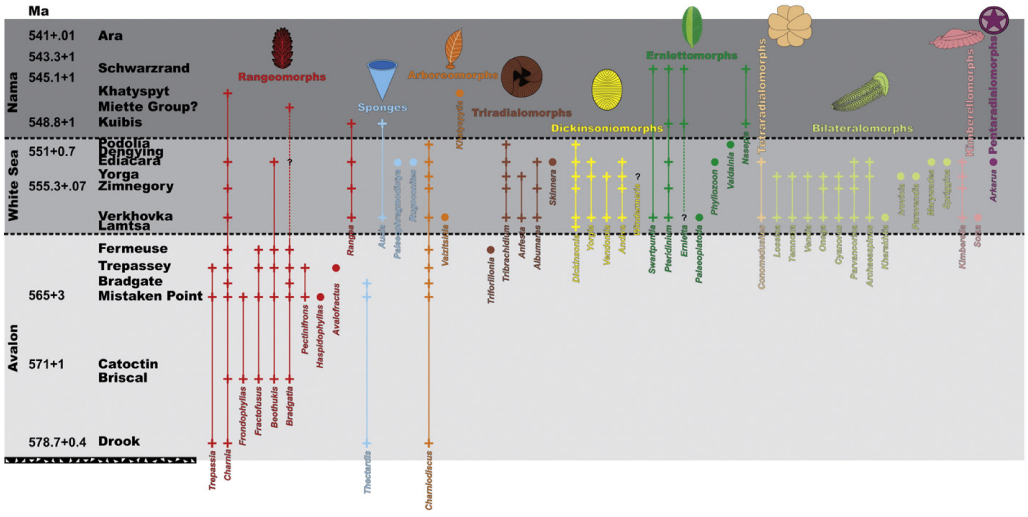

Figure 1.3: A finer subdivision of Ediacaran clades with their temporal distribution from Laflamme et al. (2013).

(2012).

Another group of complex macrotaxa are the dickinsoniomorphs. This group contains *Dickinsonia* and *Yorgia* living flat on the sediment. Dickinsoniomorphs generally have a simpler body structure than rangeomorphs, with a central axis from which segments originate that are not subdivided further. They are only found in younger Ediacaran deposits.

There are many more taxa with a single order of branching. Recently authors have suggested a finer subdivision of these taxa than is shown in Fig. 1.2. For example, Laflamme et al. (2013) suggests a subdivision of Ediacaran branching forms into rangeomorphs (e.g. *Charnia*, *Fractofusus*, *Rangea*,..), arboreomorphs (*Charniodiscus*), dickinsoniomorphs (e.g. *Dickinsonia*, *Yorgia*), erniettomorphs (e.g. *Swartpuntia*, *Pteridinium*, *Ernietta*) and bilateralomorphs (e.g. *Spriggina*). The overview of the grouping of these clades with their temporal range is shown in Fig. 1.3. A similar subdivision was suggested earlier in Xiao and Laflamme (2009) and Erwin et al. (2011b).

The branching Ediacaran macro-organisms mentioned above are the central object of study in Part I of this thesis. However, these are not the only lifeforms that inhabited the late Ediacaran seas. Discoid forms include both separately preserved holdfasts of rangeomorphs and separate organisms that are shaped like a disc or circular blob. Recent work suggests that the taxon *Aspidella* is actually the foothold of a charniodiscid (Tarhan et al. (2010)). On the other hand the taxon *Tribrachidium* is clearly a separate organism, posessing an intricate pattern on its dorsal side with a triradial symmetry. The discoid forms are split into three groups in Laflamme et al. (2013), namely the triradialomorphs, the tetraradialomorphs and the pentaradiolomorphs, based

on their three-, four- and fivefold patterns of radial symmetry (see Fig. 1.3). Other Ediacaran lifeforms include the protozoan *Paleopascichnus* (Seilacher et al. (2003), Antcliffe et al. (2011)), the macroscopic *Kimberella* that is regarded as a basal mollusc (Fedonkin and Waggoner (1997); Fedonkin et al. (2007b)), and some controversial sponge remains (McCaffrey et al. (1994); Höld et al. (1999); Love et al. (2009), disputed in Antcliffe (2013)). Towards the end of the Ediacaran the first biomineralizing lifeforms appear such as *Cloudina* and *Namacalathus* (e.g. Grotzinger et al. (2000)), which have been suggested to represent reef-building metazoans (Penny et al. (2014); Zhuravlev et al. (2015)). Recently an increasing number of tubular body fossils are found (e.g. Gehling and Droser (2009); Chen et al. (2014)), as well as potential animals (Liu and Matthews (2014)).

1.2 Localities and preservation of Ediacaran localities

Ediacaran fossils have been discovered in many places around the world. The best known localities are the Flinders Ranges in South Australia, the Nama Group in Namibia, Mistaken Point in Newfoundland, Canada, the White Sea region in Russia, and Charnwood Forest in Leicestershire, United Kingdom. The assemblages in each of these localities are distinct, although there can be many common taxa.

The Australian deposits reveal mainly shallow communities in with an epibenthic biota, including *Dickinsonia* (Gehling and Droser (2013)). The Nama Group is characterized by endobenthic forms such as *Pteridinium* and the

enigmatic frond-like form *Rangea* (Grazhdankin and Seilacher (2005)), after which rangeomorphs are named. *Rangea* was recently given a new reconstruction from Namibian specimens in Vickers-Rich and Ivantsov (2013). The Nama deposits stem from a shallow environment, but in contrast to the Australian sites also include carbonate units (Grotzinger et al. (2000)).

Newfoundland in Canada and Charnwood Forest in Leicestershire were both just offshore of the microcontinent of Avalonia during the late Ediacaran and share a similar presence of taxa. Both represent deep-marine slope deposits in the vicinity of a volcanic island arc (Wood et al. (2003)). However, the spindle-shaped rangeomorph *Fractofusus* appears in Newfoundland but not in England.

The White Sea region has a mixture of different communities, from a variety of depths, with many examples of dickinsoniomorphs but also a number of rangeomorphs and other taxa (Grazhdankin (2004)). The differences between communities were recently shown to correlate with environmental differences such as depth (Grazhdankin (2004); Gehling and Droser (2013)).

Whereas the shallower Australian assemblages were within the photic zone at the time of deposition, some of the Avalonian assemblages stem from a deeper marine environment. This means that for organisms such as *Charnia*, *Fractofusus* and *Bradgatia*, photosynthesis is one of the few potential modes of life that can be excluded.

Ediacaran fossils have an unusual type of preservation. The organisms are often preserved in situ surrounded by a intricate texture described as elephant skin. This texture is a fossilised microbial mat, which covered the sea floor at the time of burial (Callow and Brasier (2009); Gehling and Droser (2009)).

This mat structure likely caused the remarkable preservation of the Ediacaran imprints through bacterial precipitation of iron sulfides as described in Gehling (1999). The presence of the microbial mat, together with a lack of bioturbation and the lower oxygen concentration, resulted in a chemistry very different from the modern sea floors. The sediment had a strong redox gradient with an oxygenated surface and a reactive anoxic environment at a depth of only a few centimeters or even millimeters (Callow and Brasier (2009)).

An even more remarkable state of preservation was found at the Trepassey formation near Spaniard's Bay in Newfoundland (Narbonne (2004)). The bedding plane revealed an assemblage of Avalonian rangeomorphs with three-dimensional preservation, which showed that the rangeomorphs are composed of similar structural branching elements.

Some fossils on the bedding planes are less well preserved and show an irregular "pizza disc" structure. Liu et al. (2011b) interpreted these as decaying frondose organisms in various stages of decomposition, forming less regular taphomorphs. These are now known as ivesheadiomorphs (see for illustration Fig. 1.1).

1.3 Interpretations of biological affinities of Ediacaran macrofossil taxa

The first discoverers of Ediacaran taxa placed them within different groups of extant taxonomy. Sprigg (1947) initially interpreted the first Australian fossils as jellyfish. Ford (1958) suggested a potential affiliation with algae for *Charnia* and *Charniodiscus*. Glaessner reinterpreted *Dickinsonia* as an annelid worm

close to the extant *Spinther*, and *Charnia* and other rangeomorphs as sea pens, a modern group of cnidarians (Glaessner (1961); Glaessner and Wade (1966)). Other interpretations include a placozoan and a polypoid organism (Sperling and Vinther (2010) and Valentine (1992) respectively) for *Dickinsonia*, and a fungus for *Charnia* (Peterson et al. (2003)).

A new view was introduced in the eighties when Fedonkin, instead of making a comparison with modern taxa, compared the Ediacaran macro-organisms with each other. Based in particular on the pattern of branching he called metameric growth, Fedonkin posed that the Ediacaran forms were closely related and together formed a stem group of metazoans, within the new phylum Proarticulata (Fedonkin and Cope (1985b); Fedonkin (1998)).

Seilacher went one step further and proposed that all rangeomorphs, dickinsoniomorphs and discoid forms should be united in a clade of Vendobionta that was not basal to Metazoa at all (Seilacher (1989, 1992, 2007a)). Instead, he imagined vendobionts being fundamentally different to any form of extant life, perhaps representing some giant protists (Seilacher et al. (2003)). Seilacher interpreted the quilted, "mattress-like" appearance of the Ediacaran imprints as a sign of a common body structure of fluid-filled sacks held up by an internal pressure. This similar body construction was taken to hint at a common ancestry. Figure 1.4 shows a figure from Seilacher (1989), in which he explains the discussed similarities in Ediacaran body constructions.

In the last decade, detailed studies of the palaeoenvironment (e.g. Grazhdankin (2004); Gehling and Droser (2013)), palaeoecology (e.g. Liu et al. (2014); Droser et al. (2006)) and metabolism (e.g. Laflamme et al. (2009)) have revealed a more complex picture, demonstrating that the Ediacaran

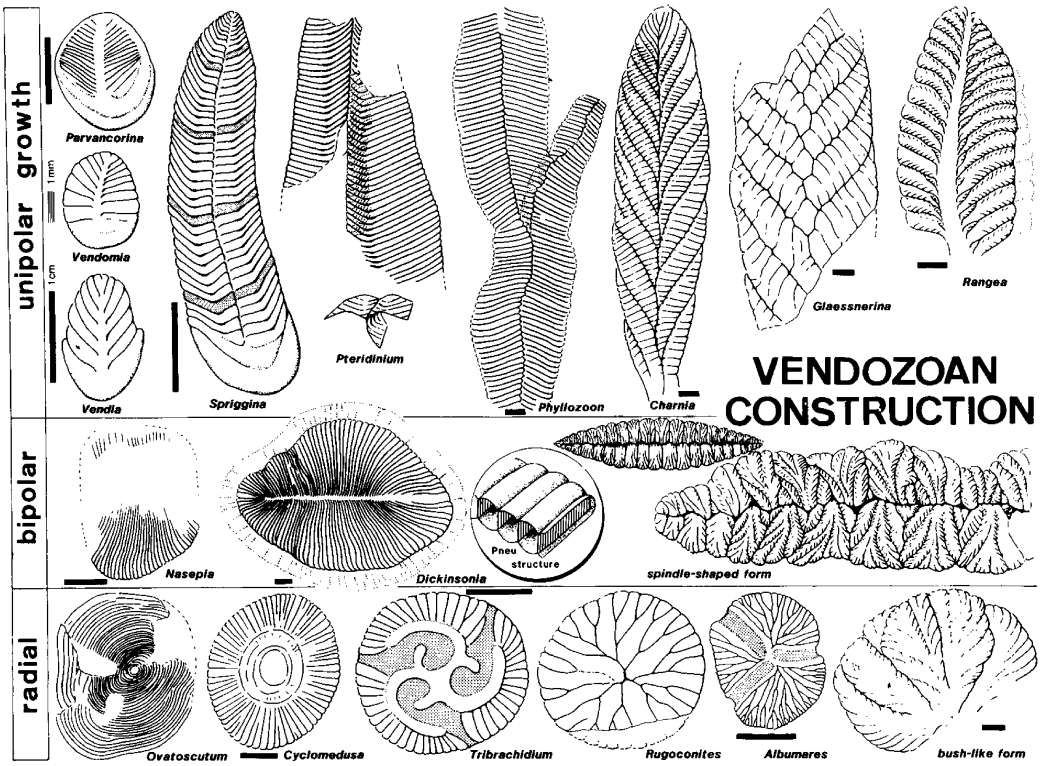

Figure 1.4: Original diagram showing the similar "quilted pneu" body structure of Ediacaran vendobionts from Seilacher (1989). The suggested similar construction of Ediacaran bodies subdivided into chambers was taken by Seilacher to hint at a common ancestry for the late Ediacaran macrobiota.

assemblages likely contained a diversity of communities in which different lifestyles were exercised. Hence the phylogenetic position of the Ediacaran macro-organisms with respect to each and the rest of life other is still a matter of debate.

1.4 The ontogeny of Ediacaran macro-organisms

After seventy years of studying Ediacaran fossils, many questions remain. A decade ago Brasier and Antcliffe (2004) argued for new, quantitative approaches to be applied, making use of analysis of morphology and a study of

growth programs. They emphasized the need for observation of the stages of ontogeny for determining phylogenetic links.

Since then a number of new methods have been applied. Antcliffe and Brasier (2007b) made a first attempt at building a morphospace for the Ediacara biota, based on the angles consecutive branches make with respect to each other. The morphospace was built on measurements of the angles of branches/segments. The angles were not modelled but expressed as a string of measurements, from which very little information could be derived directly. Unfortunately the article also contained some mathematical inaccuracies.

A better basis for the study of rangeomorph morphology was laid out in Brasier et al. (2012). This work suggests that all rangeomorphs have a similar architecture with a self-similar mode of branching. Hoyal Cuthill and Conway Morris (2014) built upon this work by using an L-system model to make the self-similarity exact. An L-system or Lindenmayer system (Lindenmayer (1968a,b)) is a simplified growth model used primarily for plants, in which a division rule is specified and then recursively implemented, leading to a self-similar shape. Thus rangeomorph branching, which appears self-similar, can be modeled in this way.

The resulting work is beautiful, but unfortunately does not yet answer many questions. Instead of testing whether the growth of rangeomorphs is self-similar, it assumes this is the case. The model has many free parameters, but does not seem to allow for varying some of the variables that distinguish between the ontogeny of different taxa, such as the position of the longest branch. In the model, the lengths of the branches vary linearly along the central axis, assuming that the basal branch is always the longest and the lengths

decrease at a regular pace towards the apex. In practice this is not the case for many taxa, for example for *Charnia masoni*. The basal roughly 35% of the branches are of a similar length, independent of how many branches there are. From there on the other 65% of the branches have regularly decreasing lengths towards the apex. This ratio of 65% "phase 1" branches versus 35% "phase 2" branches differentiates *Charnia masoni* from for example *Charniodiscus*, where the switch occurs close to the base. Because of this, the outline of the *Charnia* model from Hoyal Cuthill and Conway Morris (2014) looks different than the outline of fossils of *Charnia*.

The L-system model assumes apical insertion as the mode of generating the branches used by *Charnia*. This assumption is based on work by Antcliffe and Brasier (2007a) on the ontogeny of the taxon. This article disputed the proposed affiliation of *Charnia* with the sea pens put forward by Glaessner on the basis of apparent dissimilarities in mode of growth. It was argued that *Charnia* has a generative zone at the apex of the frond, where the branches are smallest, while pennatulaceans add their branches at the basal end of their frond-like morphology.

Ontogeny does not always reflect phylogeny and, vice versa, similarities in ontogeny do not give conclusive evidence that two clades are related. Some homologous structures diverge in development strategy over the course of evolution. For example, grasses have moved their generative zone to the base of the leaf to cope with the selective pressure of grazing animals. Salamanders are capable of regenerating lost limbs, in contrast to most other vertebrates (e.g. Yun et al. (2014)). The telencephalon, the embryonic structure from which the cerebrum develops, grows differently in teleost fish than in all other

vertebrates (e.g. Folgueira et al. (2012)), yet the brain is a homologous organ across these clades.

On the other hand, sometimes a body structure develops in a similar way in different clades even though it is not basal feature. For example, vertebrates developed wings three separate times, and McGowan and Dyke (2007) was able to study the wings of bats, birds and pterosaurs within a single framework as they are functionally similar. Bivalves and brachiopods both possess shells which grow in a similar way, described in a model by Raup (1966), but it is not ancestral to the two clades.

Despite these reservations, studying the ontogeny of organisms is a very helpful tool and can give clues for establishing phylogenetic relationships between organisms. In particular for a group of organisms as mysterious as the Ediacara biota, it is important to exploit any source of information available. Dickinsoniomorphs and rangeomorphs are found in many different stages of growth, therefore studying their growth is a possibility, which has thusfar has been explored very little.

1.5 The development of a segmented body plan

Recently, Gold et al. (2015) argued that *Dickinsonia* belonged to bilaterian animals based on its ontogeny. The authors used a database of protein alignments in living taxa to reconstruct a large phylogeny of animals and then applied ancestral state reconstruction to show that it is likely that basal bilaterians possessed a mode of growth known as terminal addition. This refers to segments, or iterated units, being inserted on one side of a central axis of the organism while the axis elongates. The ancestral state reconstruction

suggested that it was unlikely for this mode of growth to have been present in basal Eumetazoa and Metazoa, thus the authors conclude that terminal addition is a synapomorphy of Bilateria. The authors argue that *Dickinsonia* also grew via terminal addition and is therefore bilaterian.

Whether or not segmentation is basal to bilaterians is a fundamental question in the study of the evolution of complexity. Three modern animal phyla manifestly make use of a segmental organisation of their bodies: arthropods, annelids and chordates. Similarities in the embryonic development of the segmented body plan between these three phyla have led to the suggestion that the common ancestor of bilaterians was segmented as well. These similarities include the discoveries of the same molecular mechanisms appearing in multiple clades, such at the Notch signaling pathway for expression of genes involved in axial elongation and segmentation. Notch is central to somitogenesis of vertebrates (e.g. Dequéant and Pourquié (2008)), but has also been found to be involved in segmentation spiders (Stollewerk et al. (2003)), centipedes (Chipman and Akam (2008)) and cockroaches Pueyo et al. (2008). There is also evidence that Notch plays a role in the segmentation of annelids (Rivera and Weisblat (2009)). The Hedgehog singaling pathway is prominent in arthropod embryonic segmentation patterning and has also been shown to be active in establishing the segmentation pattern in the annelid *Platynereis dumerilii* (Dray et al. (2010)). Moreover, vertebrates, annelids and arthropods also, in most cases, superficially produce their segments in a similar manner, namely through terminal addition of the units.

It seems an obvious conclusion to suggest that segmentation is basal to bilaterians. However, this would imply that the character was lost or degenerated

in all but these three bilaterian clades, a process which must then, according to the current phylogenies, have happened around thirty times (Chipman (2010)). Also, there are differences between the modes of segmentation in the three main groups. Even though some of the same players are involved, there are many complex differences between the organisation of the genetic pathways that control segmentation. There are also differences in the role the segments play with respect to each other. For example, annelids and arthropods have clear boundaries separating the segments, which are of a different nature in both, while chordates do not have clear segment boundaries. During embryogenesis, all bilaterians form three germ layers during the process of gastriculation: the endoderm, the mesoderm and the ectoderm. In vertebrates segmentation occurs within the mesoderm, whereas in annelids and arthropods, segmentation starts within the ectoderm.

Chipman (2010) suggested the alternative hypothesis that the regulatory gene networks for axial elongation were present in basal bilaterians, but not yet employed in the structuring of a segmented body. They suggest these genes were then reinvented as signalling pathways for the regulation of segmentation multiple times. Marshall and Valentine (2010) similarly argued that the regulatory genes that are currently involved in the production of a complex body plan in bilaterians originally had a different function. Many of these genes were added to the metazoan genome in the stem groups of metazoans and eumetazoans, while the clades that branched off early in the evolution of metazoans (e.g. choanoflagellates; sponges; placozoans; ctenphores; cnidarians) all have a much simpler body plan. Thus, instead of segmentation as a synapomorphy of bilaterians, it might be that the gene networks useful for

the evolution of complex morphology were in place at the base of bilaterian radiation, but the adaption of these regulatory networks for the production of segmentation was invented multiple times.

As we map out the molecular mechanisms that determine the mode of growth of more and more modern bilaterian organisms, the chances are high that we will be able to differentiate to between hypothesis of co-option of regulatory genes and the hypothesis of a segmented Urbilaterian. Our understanding of the ancestral state of individual phyla is currently still diffuse, thus the reconstruction of the ancestral state of all bilaterians as given by Gold et al. (2015) might at this point be premature. Gold et al. label the mode of segmentation of many different clades as "terminal addition", but this label for the mechanism of growth may be too simplistic when compared to the variety and complexity of modes of segmentation found in modern bilaterians. For example, widening our investigation of arthropod segmentation from the study of the model organism *Drosophila melanogaster* to include other arthropods, has led to the conclusion that the ontogeny of the fruit fly is not at all representative of the ontogeny of all arthropods (Peel et al. (2005)). It turns out that different representative arthropods (e.g. crustaceans, spiders, myriapods and other insects) develop their segmented bodies in different ways, although many do add basal segments after a first embryonic stage. Peel et al. urge for the collection of more data on a wider range of arthropods before we can answer the question what the precise mechanism of segmentation of basal arthropods must have been. The same holds for other segmented bilaterian clades, especially for the annelids, of which little is currently known about different segmentation mechanisms. Recent palaeontological data has

suggested that the annelid head was originally a limb-bearing segment (Parry et al. (2015)). It would be interesting to compare this to the segmentation of the arthropod head, which is still not yet well understood (Peel et al. (2005)). A closer look at the database used by Gold et al. (2015) furthermore leads to some doubts about the representation of the bilaterian phylogeny. In the presented one of the two metazoan phylogenies (see Fig. 3 and 4A in the paper), 15 out of 22 of the included bilaterian clades are marked as having terminal addition, and the trade only needs to be lost four times, not thirty as suggested by Chipman (2010), to explain the included unsegmented forms from a segmented ancestor. In fact, the ancestral state reconstruction, the complicated time-calibration, the Monte Carlo simulation, etc. used by the team seem rather excessive given the fact that the database used will obviously yield the desired conclusion. 15 out of 22 studied bilaterians are labeled as possessing terminal addition, and no other organisms outside of the Bilateria are labeled as such, hence the ancestral state reconstruction concludes that terminal is a likely synapomorphy of bilaterians and less likely to have been shared with Eumetazoa or Metazoa. The second dataset, with a more complete representation of bilaterians, also appears to give a less conclusive outcome.
Relaying our focus back to the Ediacara biota, the question whether *Dickinsonia* represents a bilaterian animal is a different question. Does it indeed display the same mode of growth that Gold et al. argue was present in the ancestral bilaterians? Do we understand the ontogeny of *Dickinsonia* well enough to say this? And how well should the ontogeny resemble that of bilaterians to come to such a conclusion, given that we do not currently know what the ancestral mode of segmentation of bilaterians was like and given the

fact that similarities in ontogeny might not imply a phylogenetic affinity? Yet another question is how the rest of the Ediacaran macro-organisms, some of which show a remarkable amount of similarity to *Dickinsonia*, fit into this picture.

1.6 Studying Ediacaran ontogeny quantitatively

Runnegar (1982) first performed measurements of the ontogeny of *Dickinsonia costata*, and showed that the taxon maintained its aspect ratio during growth, in contrast to the annelid worm *Spinther arcticus* and the polychaete worm *Nereis diversicolor*. The segmentation pattern was also considered, and it was suggested that the segments form confocal parabolas, alhough this was not supported by measurements.

Seilacher (2007a) suggested that in *Dickinsonia*, *Phyllozoon* and *Pteridinium* each segment (quilt) initially expanded its volume but stopped after certain dimensions were reached. However, this statement was not backed up by a quantitative analysis and it turns out, as will be clear from the analysis in this thesis, that this claim is false for *D. costata*. Seilacher supported the view that *Dickinsonia* added segments on eiter side of its axis, while many authors since have assumed that the generative zone lay on the side of the axis where the segments seem smallest (e.g.Brasier and Antcliffe (2008); Gold et al. (2015); Sperling and Vinther (2010)).

For organisms with an iterated body structure, one can pose the question how much the unit grows compared to the rate of insertion of the units. Perhaps each unit is inserted and does not grow anymore after. I call this an insertional mode of growth. On the other end of the spectrum, it might be that all units

are already fully formed in an embryonic phase, before the organism starts growing, and then the units inflate over the lifetime of the organism. I call this an inflational mode of growth.

The latter occurs in the best studied arthropod of all, the fruitfly *Drosophila melanogaster*, in which all segments are patterned simultaneously in a very early stage of embryogenesis, when the embryo is still syncitial. This is similar to vertebrates which also form their somata in an embryonic phase. However, most other arthropods form only a small number of segments at an early embryonic stage and subsequently add segments from a posterior growth zone, thus combining the insertional and inflational strategies. Trilobites for example added segments at the posterior end of the thorax but before the last few segments called the pygidium, during their lifetime, until a set total number of segments was reached (the holaspis stage). They then continued growing for a while until maturity was reached (e.g. Benton and Harper (2009); Hughes (2003)). Many organisms with an ordered, iterated mode of growth apply a combination of the two mechanisms. For example, many plants insert leaves or branches along their stem and allow these to grow. However, this is not the case for the leaves of ferns, which fully form the frondlets of the leaf before inflating it to its mature size (Steeves (1963)). Rangeomorphs and dickinsoniomorphs had a body made up from iterated segments or branches, so the question of insertion versus inflation is one that can be asked for these organisms.

Sperling and Vinther (2010) argue that *Dickinsonia* is set apart from other Ediacaran lifeforms by its mode of growth, through both addition and expansion of segments. The authors state that different modes of growth are present in the Ediacaran macrobiota, suggesting different phylogenetic affini-

ties should be sought for the different groups. As an example, it is argued that *Pteridinium* grows solely through addition of segments, while *Charniodiscus* and *Fractofusus* grow by inflation of existing branches. However, reviewing the data on which these claims are based reveals that although one mode of growth is dominant, in fact both *Pteridinium* and *Fractofusus* appear to display a mix of the two modes of growth, just like *Dickinsonia*.

The measurements of *Pteridinium* specimens in Grazhdankin and Seilacher (2002), Fig. 7, reveals a correlation between segment (quilt) width and body length, as well as a correlation between segment number body length, suggesting that segments were inserted during growth, but also continued expanding after addition. Laflamme et al. (2009) suggest, after analysis of specimen length versus number of branches in *Fractofusus*, that although the taxon grows mostly through inflation, there is a period of branch addition during early growth. As Sperling and Vinther (2010) note and the data in chapter 2 and 4 shows, *Dickinsonia* slows the rate of insertion of segments in later stages of ontogeny, thus potentially displaying a similar switch from a insertional to an inflative mode as Laflamme et al. (2009) suggest occurs in the ontogeny of *Fractofusus*. The morphometric data of *Charniodiscus* in Laflamme et al. (2004) does not reveal a correlation between frond length and branch number for the taxon *Charniodiscus spinosus*, but seems to suggest a positive correlation for *C. procerus* (Laflamme et al. (2004) Fig. 5.4). Also the taxon *Charnia* is known to grow through both the addition of new branches and the expansion of existing branches (Antcliffe and Brasier (2008)). Thus it appears that the mode of growth of *Dickinsonia* might in fact be very similar to that found in other Ediacaran macro-organisms.

The ontogeny of different macrotaxa from the Ediacara biota has at this point not been studied to sufficient detail to provide the background to a statement such as made by Sperling and Vinther (2010). What different modes of growth are present within the Ediacaran taxa? How do they differ, and in what manner are they similar? The study of these questions requires, firstly, a framework to study and compare Ediacaran morphology and ontogeny.

To quantitatively study the growth of the Ediacaran macro-organisms as suggested by Brasier and Antcliffe (2004), we need to have a system for comparing different growth stages with each other. A feature shared by rangeomorphs and dickinsoniomorphs is a subdivision into branches/segments that connect to a central stem. Many taxa show a direct correlation between the sizes of specimens and the number of branches/segments. Thus, it seems these taxa grow through the insertion of these iterated features, as well as possibly through expansion of the existing ones. The addition of segments/branches can be used as an indexing of ontogenetic stages, within which it is easier to compare the progression of growth.

Part I of this thesis builds a framework to study growth and applies it to the taxa *Dickinsonia costata* and *Charnia masoni*. Growth is quantified by the measuring the lengths of segments/branches. In Chapters 2 and 3, I describe measurements of the segment/branch lengths of *Dickinsonia costata* and *Charnia masoni* respectively. In Chapter 4 these measurements are analysed, and I build a growth model that models the ontogenies found in the measurements. This reveals new insights into the complexity of the ontogenies of these taxa, as well as revealing similarities between the two modes of growth. The model can be extended to a geometric morphospace for vendobionts. Based on this

model and an analysis of other morphological features that are shared between different Ediacaran macrotaxa, I reconsider the question whether the iterated growth of vendobionts is derived from a common ancestor.

Chapter 2

The growth of *Dickinsonia costata*

2.1 Introduction

Dickinsonia (Sprigg (1947)) is an iconic member of shallower water communities of the Ediacara biota. It was discovered in the Ediacara Hills of South Australia as one of the first examples of macroscopic Precambrian fossils. The fossils are usually preserved in negative epirelief on the base of sandstone slabs, surrounded by the characteristic "elephant skin" structure of a fossilized microbial mat (Callow and Brasier (2009)). Apart from the Australian Ediacaran deposits, *Dickinsonia* is also found in the White Sea region in Russia (Martin et al. (2000)). *Dickinsonia* is known from the younger temporal range of the late Ediacaran macrobiota of around 560-550 Ma (Laflamme et al. (2013); Xiao and Laflamme (2009)).

Although the taxonomic classification of *Dickinsonia* has changed over the

years, it is currently widely regarded to be subdivided into five species: *D. costata* (Sprigg (1947)), *D. lissa* (Wade (1972)) and the larger forms *D. tenuis* (Glaessner and Wade (1966)), *D. brachina* (Wade (1972)) (similar in morphology to *D. tenuis*) and *D. rex* (Jenkins (1992); Fedonkin et al. (2007a)). The different species of *Dickinsonia* share a similar body plan that resembles the morphology found in a group of taxa of the Ediacara biota known as dickinsoniomorphs. The organisms were flat sediment recliners, round to oval in outline. From a central axis outward the body was divided into iterated features. These are here referred to as segments, following the terminology of Wade (1972), without meaning to imply a homology with bilaterian segmentation. In *D. costata*, a wide central segment can be identified on the basal end, which is referred to as the basal segment here.

Over the years many different interpretations of the biological affinities of *Dickinsonia* have been proposed. Initially *Dickinsonia* was placed within the phylum Cnidaria (Sprigg (1947); Moore and Harrington (1956)), as features around the margin of the holotype, shown in Fig. 2.2 D15, were interpreted as tentacles. These features, present only in some specimens, were later reinterpreted as contraction marks, and the taxon was reinterpreted as a polychaete worm (Glaessner and Wade (1966)).

A different approach was suggested by Fedonkin, who emphasized the morphological similarities of Ediacaran body plans (Fedonkin and Cope (1985a); Fedonkin (1998)). The author argued that a number of macroscopic Ediacaran taxa, among them *Dickinsonia*, should be grouped as basal Metazoa within a separate phylum Proarticulata. Seilacher took this hypothesis one step further and argued that the organisms belonged to a separate extinct kingdom

Vendozoa (later Vendobionta) (Seilacher (1989, 1992)).

In contrast to these views, recent research into palaeoenvironment (e.g. Grazhdankin (2004); Gehling and Droser (2013)), palaeoecology (e.g. Liu et al. (2014); Droser et al. (2006)) and metabolism (e.g. Laflamme et al. (2009)) demonstrates that Ediacaran assemblages likely contained a great diversity of communities with different lifestyles. Thus in recent publications the Ediacaran macro-organisms have been treated as discrete groups (e.g. Xiao and Laflamme (2009); Laflamme et al. (2013); Grazhdankin (2014)), potentially with little mutual phylogenetic affiliation despite similarities in morphology. In particular, this view places *Dickinsonia* within a clade of dickinsoniomorphs, a group of flat sediment recliners with a segmented body, together with *Yorgia* and *Andiva* among others.

There is increasing evidence that *Dickinsonia*, as well as other dickinsoniomorphs, was capable of active movement. The ichnotaxon *Epibaion*, consisting of similar-sized epirelief imprints associated with fossils of *Dickinsonia*, has been interpreted as feeding traces (Ivantsov (2001); Ivantsov and Fedonkin (2001); Ivantsov (2011)), suggesting that the organism fed on microbial mats. This has led to the proposition of a placozoan affinity for *Dickinsonia* (Rozhnov (2010); Sperling and Vinther (2010)), as placozoans are both mobile and feed through their bottom surface.

It has often been suggested that some specimens of *Dickinsonia* show signs of contraction (Brasier and Antcliffe (2008); Seilacher (1989); Runnegar (1982); Wade (1972)). The outline of some specimens appears blurred with occasionally radial grooves that are aligned with the segment boundaries. Runnegar (1982) noted that some specimens have the same number of segments but a

different overall size, in particular two specimens which are also examined in detail here (labeled specimen D17 and D18 in this chapter). This contracted state has been explained by some as a feature of biology and evidence for the presence of muscles in the organisms (Glaessner and Wade (1966); Runnegar (1982)). Others have interpreted it as a sign of taphonomic decay, suggesting that the physiology required a high internal pressure which might have "deflated" after death (Seilacher (1989); Brasier and Antcliffe (2008)). Contraction is visible as a shift in segment length direction (the height) of the surface of measurements in the three-dimensional parameter space of *Dickinsonia* that is constructed in the chapter.

This chapter presents measurements capturing the growth of the genus *Dickinsonia* quantitatively, with an emphasis on the most common species *D. costata*. The same methodology can be applied to other taxa within and potentially outside of the Ediacara biota. An understanding of ontogeny, and a framework within which to compare the ontogeny of different taxa, provides a new analytical tool for studying the Ediacara biota. This is useful for the understanding of biological affinities, since affiliations are often, though not always, reflected in ontogeny. A quantitative study of morphology and ontogeny is particularly important for the study of an enigmatic fossil group such as the Ediacaran macrobiota, as also argued in Antcliffe and Brasier (2008), since other methods to study this biota are not present or not known to be reliable, such as the comparison with modern analogues or nearest living relatives.

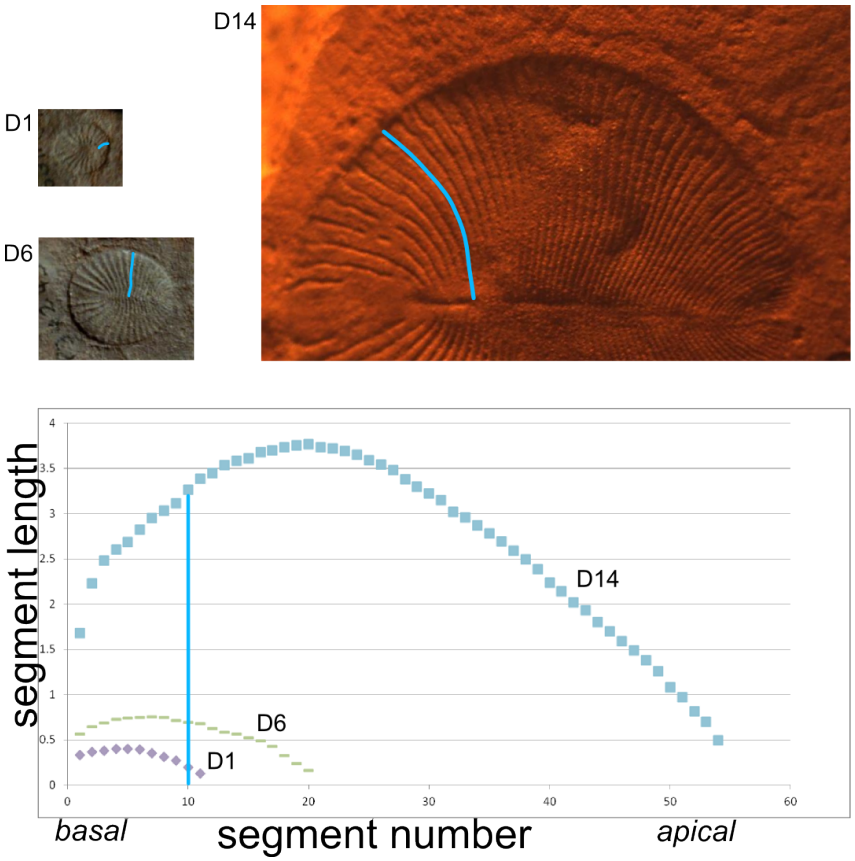

Figure 2.1: Measurements of the segment lengths of three specimens of *Dickinsonia costata* illustrate the methodology applied in this chapter. The length of each segment is measured from the central axis to the margin, following its curvature. These measurements are summarized in a diagram of segment length versus segment width. The tenth segments from the basal end are highlighted in three specimens of different sizes and total number of segments. Measurements are depicted in a diagram of segment lengths versus segment number along the axis. In later diagrams a third dimension is added, reflecting the total number of segments (segment count) of the specimens.
If one would assume that segments are inserted on the apical end of the organism, on the right side for all three specimens above, then segments at the same segment number are homologous. In specimen D1, the tenth segment would just have been inserted. In specimen D6 the tenth segment is one of the longest segments and lies halfway the axis. In specimen D14, which has 54 segments in total, the tenth segment is one of the wider segments on the basal end of the organism, and is not as long as the younger segments halfway down the axis, although it is longer than it was in the younger specimens. The diagram plots all measured lengths in one diagram. The lengths of the tenth segment is shown in blue in the diagram beneath.

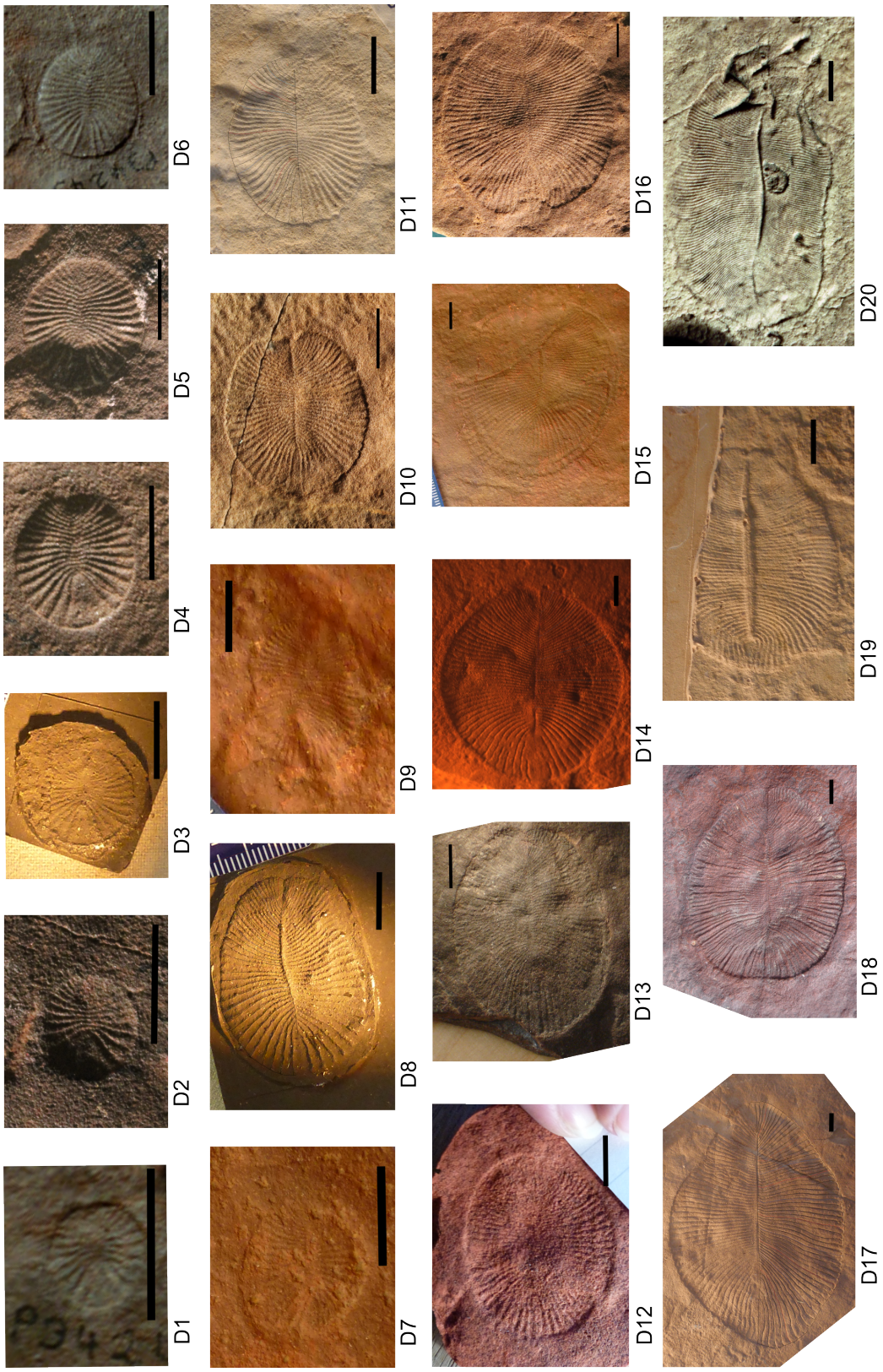

Figure 2.2: Pictures of the twenty specimens under study in this chapter. For details see Table 2.1. Each specimen is shown with the basal end on the left and the apical end on the right. Scale bars in each picture are 1cm.

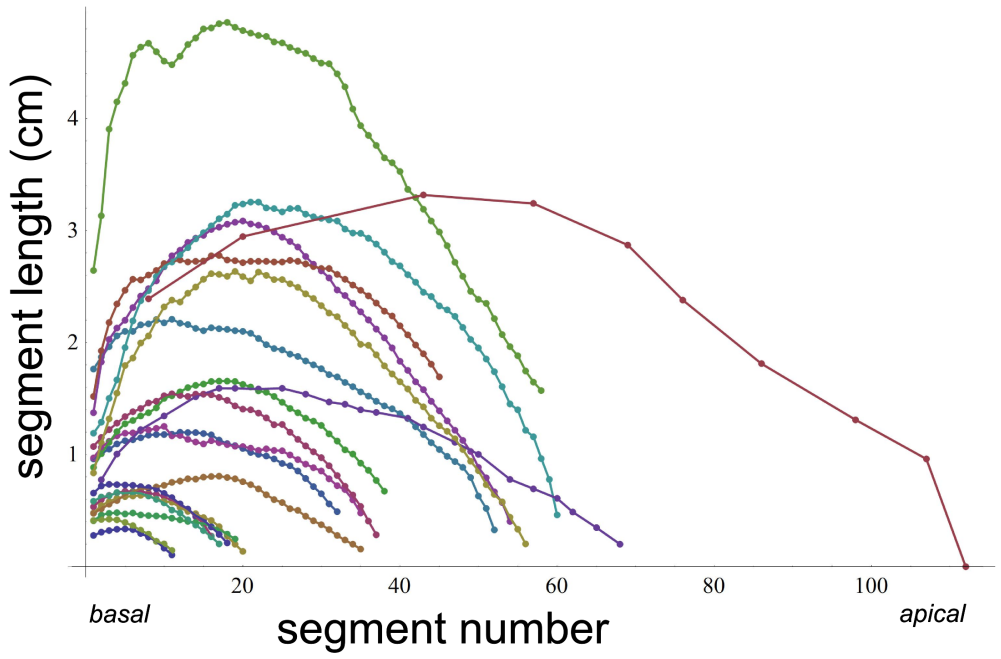

Figure 2.3: Measurements of segment lengths of 20 specimens of *Dickinsonia* described in Table 2.1. The horizontal axis shows segment number from the basal segment and the vertical axis shows length in cm.

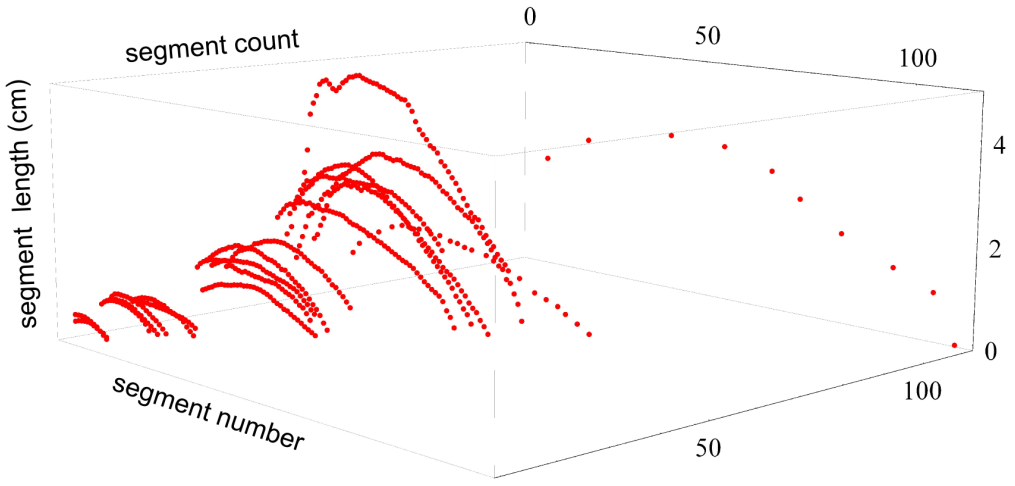

Figure 2.4: Measurements of the segment lengths of 20 specimens of *Dickinsonia* in a three-dimensional view of segment number and the segment count of each specimen, with the length of the segments on the vertical axis.

2.2 Materials and Methods

The growth of *Dickinsonia* is studied in this chapter by measuring the lengths of all individual segments of specimens. The lengths of the segments are measured from the axis to the margin of the specimen, following the natural curvature of each segment. This methodology is illustrated in Fig. 2.1. The measurements were performed by drawing lines following the segment margins on top of photographs of the specimens in the vector based graphics programs Inkscape and Adobe Illustrator. The length of the curved lines was then calculated in the program and compared with the length of a scale in the photograph to translate the measurements into centimeters. In each specimen the segments measurements were taken on one side of the central axis, the side on which the individual segments were most clearly visible. Test sampling on either side of the specimens indicates differences in segment lengths between both halves are negligable compared to the size differences between the specimens. The specimens were furthermore indexed by counting the total number of segments present on one side of the axis.

Because of the segmentated mode of growth of *Dickinsonia*, two scales of growth, namely size and segment number, can be measured independently and compared. The transverse widths of the segments vary gradually from widest on one end, here called the basal end, to thinnest on the other, is referred to as the apical end. The information of an individual segment is captured in three numbers: its length; its distance to the basal segment or "segment number"; and the total number of segments of the specimen, or "segment count". Segment length, segment number and segment count together form a

three-dimensional parameter space. The measurements of a single segment is a point in this space. A specimen forms a line within this space, with a point for each segment, all at the same segment count. A number of specimens in different stages of growth form an sequence that can potentially be interpreted as an ontogenetic sequence, which would form a surface within this three-dimensional parameter space, assuming that all specimens have followed the same ontogenetic path.

A methodology as described above requires specimens whose features are well-preserved. In order to capture information about the growth of the taxon, it is required that the measured specimens represent a wide range of ontogenetic stages. For this purpose twenty well-preserved specimens of the genus *Dickinsonia* were selected, mainly belonging to the species *D. costata*, which is most common. These specimens were selected in the first place because they appear to be the best preserved specimens from five different collections of Ediacaran fossils, each showing good tip-to-tip preservation and little taphonomic deformation. An overview of the specimens can be found in Table 2.1.

The specimens appear to represent a large range of ontogenetic stages of *D. costata*, with the smallest specimen less than one centimeter across and bearing 11 segments, while the larger specimens of *D. costata* span around 15 cm with up to 60 segments. All the specimens originate from Australia. Among them is the original holotype of *D. costata* from Sprigg (1947).

2.3 Measurements

2.3.1 Measurements of segment lengths

The result of the measurements of segment lengths is shown in Fig. 2.3. The collection of segment lengths form a curve for each specimen, with the longest segment nearer to the basal end of the organism. In Fig. 2.4 the segment length measurements are combined with the segment count on a third axis.

2.3.2 Uncertainty in measurements

The measurements of segment lengths carry uncertainty from both preservational deformation of the specimens and measurement errors. Within the measurement methodology itself the main uncertainty is generated by the choice of an outline that is taken as the boundary of the specimen. The relative uncertainty in choice of a margin is greater for the smaller specimens D1, D3, D6 and D7, and for specimens D7, D9 and D20 that show more taphonomic deformation. The position of the chosen margin was based on an assumed continuity of the margin and on the position of the widest circular imprints. This generates an error in the segment length measurements of around ±5%, which is small compared to the differences found between the specimens and therefore negligable for the purpose of this study. The longest segment of the widest specimen (D17) is about 750% the length of the largest segment of the smallest specimen (D1).

The taphonomic and biological deformation can be classified in radial contraction and non-radial deformations. Signs of radial contraction are present

for example in specimen D15, in the form of a circular groove parallel to the outline, with radial striations aligned with the segment boundary. The boundaries between the segments of specimen D18 are not as straight as those in other specimens, but instead appear more irregular as if deflated, which is also interpreted as a sign of contraction.

Deformation not due to radial contraction can be estimated visually by comparing the specimen with well-preserved specimens.The outline of a specimen can be deformed such that the margin no longer appears to curve smoothly as it does for most specimens. Specimen D20 shows significant taphonomic deformation, which results in a difference between the segment lengths on both sides of the specimen of about 25%. D20 is an outgroup specimen of the species *D. rex* and illustrates the difference with the species *D. costata* well. Replotting the data compensated for the 25% error either way does not change the interpretation of the data. Other specimens show deformation to a lesser extent, for example specimen D17 has a dented outline. This is likely due to biological variations in growth or another biological process, as the rest of the specimen seems undeformed. The dented outline can be seen in the resulting plots of the data but does not influence the interpretation. For each specimen the measurements are performed on one side of the central axis. In each case the side is chosen that appears least deformed by taphonomic processes.

The tectonic deformation associated with the specimens is minimal and can be neglected here. This can be estimated from the fact that the outlines of specimens of *Dickinsonia* appear round and not sheared, even though they are found with different orientations (e.g. Evans et al. (2015)).

The segment count also carries some uncertainty as not all segment bound-

aries are clearly visible. The observation that the segments are spaced at fairly regular widths was used to fill in some of the missing information. Repeated count of the number of segments, as well as comparison with a reported segment count found in the literature for some specimens, allows for an estimate of the uncertainty in segment count of 1 segment for the smaller specimens and up to 5 segments for the larger specimens. Shifting the measurements by this amount along the segment count axis has little effect on the interpretation, as can be seen by considering Fig. 4.11.

2.3.3 Position of the longest segment

Each set of measurements in Fig. 2.3 takes the shape of a smooth curve of segment lengths that is smaller to either end of the organism and has a maximum in the middle. An interesting question to ask is where this maximum is realized, in other words, where the longest segment lies with respect to the number of segments. An overview of this data is given in Table 2.1. All specimens have their longest segment closer to the basal segment in terms of segment number, below 50% of the segment count, counted from the basal end . Among all 20 specimens it varies between 17% to 45% of the segment count with a mean at $(33 \pm 8)\%$.

2.4 Feeding traces

An important factor in considering the possible biological affinities of *Dickinsonia* and related forms is the discovery of (feeding) traces *Epibaion waggoneris* associated with dickinsoniomorphs in the White Sea region (Ivantsov (2001,

2011)). The fact that these feeding trails are all of the same size tells us that the production of the trails occurred on a much shorter timescale than the growth of the organism. This is also confirmed by the lack of regeneration of the microbial mat.

The existence of the feeding trails is indicative of the biology of the organisms. In particular, it suggests that the organisms in some way fed on or by means of the microbial mat, destroying it in the process, and that the entire lower surface was involved in this process. A possible scenario is therefore that the organisms were feeding through their entire lower surface by means of osmotrophy.

Unfortunately the feeding traces do not immediately tell us about the mode of mobility. There are no visible dragging or trace marks that would indicate passive movement by turbulent flow, as some have suggested (Dzik and Ivantsov (1999)). There is also no trace of a creeping or sliding motion of the organism. The trails are simply a collection of positive imprints, often found together with a single negative imprint representing the body fossil, like a collection of foot prints, of which the last contains a boot. As there are no marks of creeping of the organism from imprint to imprint, one might suggest that the organism lifted itself of the mat entirely to move into ints next position. This could have occured through a semi-passive mode of transport. For example, the organism might have been able to control the strength of the adhesive forces, adhering to a piece of microbial mat when landing, then after digesting "letting go", and as a result be transported some distance passively by currents. This would agree with the observation that the traversed distance differs along the track, with frequent overlap. Presumably the organism

was benefitting from renewing the covered microbial mat, so why would it not move off its own shadow entirely if it had the ability to move freely?

Following this line of thought, there are several ways in which the organism might have stimulated a passive transport by currents, for example: a) The adhesive strength of the microbial mat could have reduced significantly by its digestion, so this process might have had a purpose apart from feeding; b) The organism might have been able to curl up its margins slightly to allow the current to scoop it up. This is an alternative explanation for some of the "touch-evading" imprints that have been seen, where *Dickinsonia* seems to have deformed its outline to avoid touching another organism, such as Ivantsov (2011) Pl. 1 fig. 1. and it might account for the formation of folds. More generally, *Dickinsonia* regularly found with a "missing piece" along its periphery, which was explaned in Evans et al. (2015) as marks left by sediment flowing underneath the organism as it was slightly lifted off the microbial mat. Evans et al. showed that these "missing pieces" are aligned with the current even if the organism was not. This process could also be linked to the blurred or unclear outline that is occasionally observed in dickinsoniomorphs. Ivantsov (2011) notes that some tracks are reduced platforms, meaning that only the central and apical region of the body made an imprint while the margins and basal side did not. It is possible that the latter parts of the body would have been curled upward slightly.

Another argument in favour of the curling margins hypothesis is given by the V-shaped features occasionally found within the imprints of the segments of the feeding traces of the dickinsoniomorph *Epibaion waggoneris*, shown in Fig. 2.5. These were explained by Ivantsov (2011) as possible imprints of

cilia on the bottom surface of the organism transporting nutrient particles to the boundaries of the segments. However, these imprints also resemble the pattern of marks that is created by the adhesive effects of lifting something off a sticky surface. If the body of the organism were to be lifted up off the sticky microbial mat in a motion from the margin inwards, one would expect similar V-shaped adhesion marks to be formed where the rounded segments used to be. This explanation of the marks in Fig. 2.5 suggests that the organisms were lifted from the mat curling up from the margin, as opposed to crawling away from the traces.

Figure 2.5: V-shaped features within the imprints of the segments in the feeding traces *Epibaion waggeronis*, an ichnotaxon whose imprints are morphologically similar to and associated with *Dickinsonia costata*, suggest that the segments curled up from the margin inwards leaving adhesion marks in the feeding traces. See Ivantsov (2011) Pl.2 fig.4.

Other mechanisms can be thought of that could assist passive transport, such

as bubbles of gas being freed by the microbial mat, fluids being expelled by the body or a change in the density of the organism. The viability of such mechanisms could be validated with experiments simulating these conditions.

Table 2.1: List of specimens with specifications. SAM: South Australian Museum; UCMP: University of California Museum of Paleontology; BGS: British Geological Survey; OUMNH: Oxford University Museum of Natural History.

Name	Number of segments	Longest segment number	Longest segment relative position	Previous classification	New classification	From	specimen/ cast location	specimen number
D1	11	5	0.45	*D. costata*	*D. costata (slightly contracted)*	Australia	SAM	A032
D2	11	3	0.27	-	*D. costata (uncontracted)*	Australia	SAM	P30310
D3	16	7	0.44	*D. costata/ Dickinsonia sp.*	*D. costata (uncontracted)*	Australia	UCMP/Cambridge	UCMP149039/-
D4	17	6	0.35	-	*D. costata (slightly contracted)*	Australia	SAM	P34228
D5	18	3	0.17	-	*D. costata (uncontracted)*	Australia	SAM	P34273
D6	22	7	0.32	*D. costata*	*D. costata (contracted)*	Australia	SAM	A032
D7	23	4	0.18	*Dickinsonia sp.*	*D. rex*	Australia	OUMNH	AW.90
D8	35	12	0.34	*D. costata/ Dickinsonia sp.*	*D. costata (slightly contracted)*	Australia	UCMP/Cambridge	UCMP149039/-
D9	36	10	0.28	-	*D. rex*	Australia	OUMNH	AW.94
D10	37	11	0.30	-	*D. costata (uncontracted)*	Australia	SAM	-
D11	38	17	0.45	*Dickinsonia sp.*	*D. costata (contracted)*	unknown	Cambridge	-
D12	41	17	0.41	*D. costata*	*D. costata (slightly contracted)*	Australia, Ediacara Hills	BGS/SAM	-
D13	52	11	0.21	*Dickinsonia sp.*	*D. costata (slightly contracted)*	Australia, Ediacara Hills	OUMNH	AW.89
D14	54	20	0.37	*D. costata*	*D. costata (uncontracted)*	Australia	SAM	J683
D15	55	17	0.31	*D. costata*	*D. costata (slightly contracted)*	Australia	OUMNH	AW.00120
D16	56	19	0.34	-	*D. costata (contracted)*	Australia	SAM	-
D17	58	18	0.31	*D. costata*	*D. costata (uncontracted)*	Australia	Cambridge	-
D18	60	21	0.35	*D. costata*	*D. costata (contracted)*	Australia	? (Runnegar)	-
D19	68	25	0.37	*D. costata/ Dickinsonia sp./ D. rex (juv.)*	*D. rex*	Australia	UCMP/Cambridge/SAM	UCMP149009/-/ P18888
D20	111	43	0.39	-	*D. rex*	Australia	SAM	A027

Chapter 3

The Growth of *Charnia masoni*

3.1 Introduction

Charnia (Ford (1958)) was the first macrofossil to be accepted as being of Precambrian origin and can therefore be considered as a turning point in Precambrian palaeontological research (Antcliffe and Brasier (2008)). It is still central in the study of the late Ediacaran macrobiota as it appears in many different deposits around the world. Apart from Charnwood Forest, where it was discovered, it is also known from Mistaken Point, Newfoundland (e.g. Clapham et al. (2003)), from the White Sea region (e.g. Grazhdankin (2004)), from the Olenek Uplift in Siberia (e.g. Knoll et al. (1995)), from Northwestern Canada (e.g. Narbonne et al. (2014a)) and from the Rawnsley Quartzite and other localities in South Australia (e.g. Gehling and Droser (2013); Glaessner (1962)). It has the longest known temporal range of any Ediacaran genus, spanning 20 million years (Antcliffe and Brasier (2008)).
The enigmatic body structure of *Charnia masoni* is shown in Fig. 3.1. This reconstruction was based on laser scans and reveals the self-similar branching

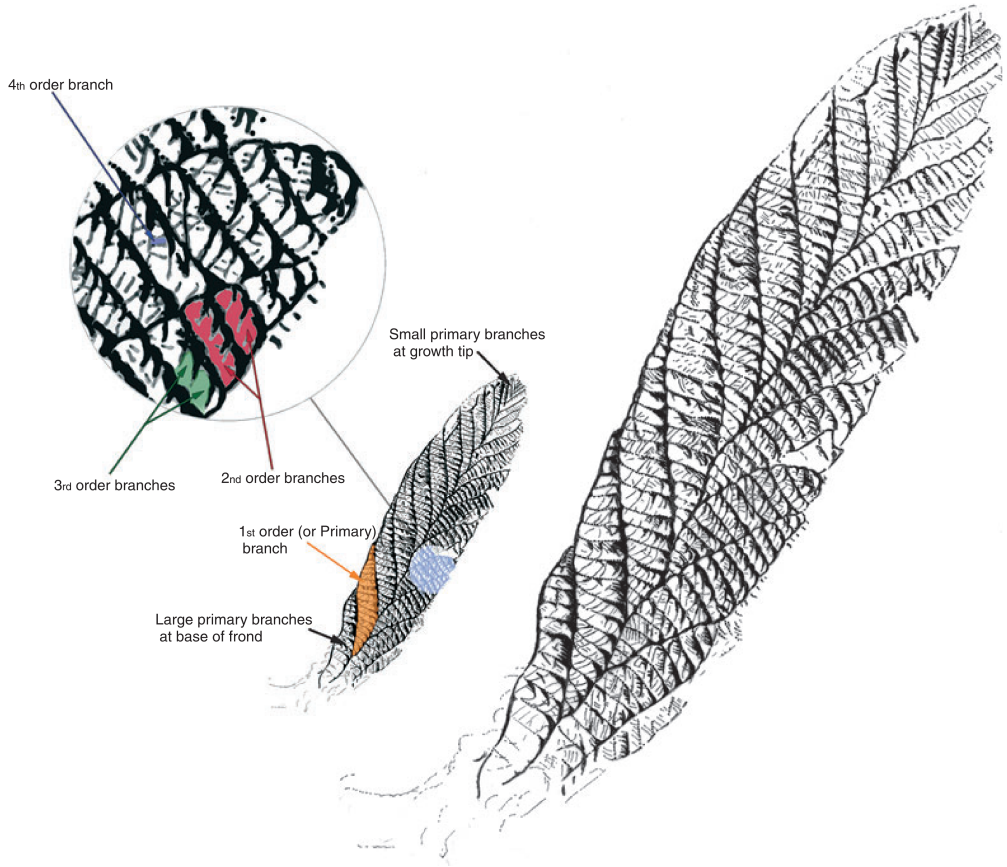

Figure 3.1: Reconstruction of *Charnia masoni* from laser scans of the holotype (Ford (1958). The alternating first order branches are further subdivided in second order branches, which themselves show subdivision into third and possibly even fourth order branches. Specimen is 20.8 cm long.). Drawing by Martin Brasier. From Antcliffe and Brasier (2008) fig. 2.

pattern of the taxon (Antcliffe and Brasier (2008)). The first order branches, which grow in an alternating pattern, are subdivided into higher order second, third and possibly fourth order subbranches.

Glaessner assigned *Charnia* to the phylum Cnidaria because of its body structure, with branches to either side of a central stem, resembling that of the modern pennatulaceans (sea pens) (Glaessner (1961, 1962)). However, this superficial similarity was argued to be convergent by a comparison of the ontogeny of both forms (Antcliffe and Brasier (2007a)). The authors argue that *Charnia* inserted new branches at its apical pole (see Fig. 3.1), while pennatulaceans insert them on the basal side of their stem. Pennatulaceans moreover do not show the off-set symmetry, generated by an alternating branching pattern, that is so clear in *Charnia* (Antcliffe and Brasier (2007a, 2008)).

Charnia is usually considered as a member of the rangeomorphs, which have similar branching patterns and are generally believed to be monophyletic and unique to the Ediacara biota (e.g. Xiao and Laflamme (2009); Narbonne (2004); Laflamme et al. (2013)). The rangeomorphs are sometimes considered as a part of a larger clade that groups much of the Ediacaran macro-organisms together, for example into a metazoan phylum Proarticulata (Fedonkin and Cope (1985b); Fedonkin (1990, 1998)), or a clade of Vendobionta that is not related to Metazoa at all (Seilacher (1989, 2007a)).

In this chapter measurements of the ontogeny of *Charnia masoni* are presented. The lengths of the branches are measured as a function of the number of branches in four well-preserved specimens of *Charnia* in different stages of ontogeny. I furthermore discuss the results of Hoyal Cuthill and Conway Morris (2014) for the fractal dimension of *Charnia* and other rangeomorphs. I will

show how the fractal dimension or Hausdorff dimension can be estimated directly by considering the branching pattern of the taxa *Charnia*, *Avalofractus* and *Bradgatia*.

Table 3.1: Table with details of the four specimens of *Charnia masoni* used in this study. BGS stands for the British Geological Survey and Oxford for the collection of Martin Brasier at the University of Oxford. CF stands for Charnwood Forest, Leicestershire, UK.

Name	**Number of 1^{st} order branches**	**Maximal number of 2^{nd} order branches**	**Origin**	**Cast location**	**Specimen number**
A	15 ± 1	11 ± 1	CF	BGS	GSM 105988
B	22 ± 1	13 ± 1	CF	BGS	GSM 105979
C	28 ± 1	15 ± 1	CF	Oxford	(cast of holotype)
D	36 ± 2	21 ± 2	CF	BGS	GSM 105873

3.2 Materials and methods

The material used in this study consists of casts of four well-preserved specimens of *Charnia masoni* in different stages of growth (Fig. 3.2). Details are presented in Table 3.1. Three of the specimens, A, B and D, were photographed at the British Geological Survey. The fourth specimen, C, is the *Charnia masoni* holotype from Charnwood Forest. It was photographed from a cast at Oxford. All casts were taken in Charnwood forest, Leicestershire and are all from the same North Quarry bedding plane, including the holotype. Only four specimens were available for study, but as these four cover a wide range of ontogenetic stages and show good preservation, it is possible to derive a substantail amount of information about the ontogeny of the organisms. Similar to the way in which single well-preserved fossils can be used to derive information about the morphology of an organism, it is also possible to study a

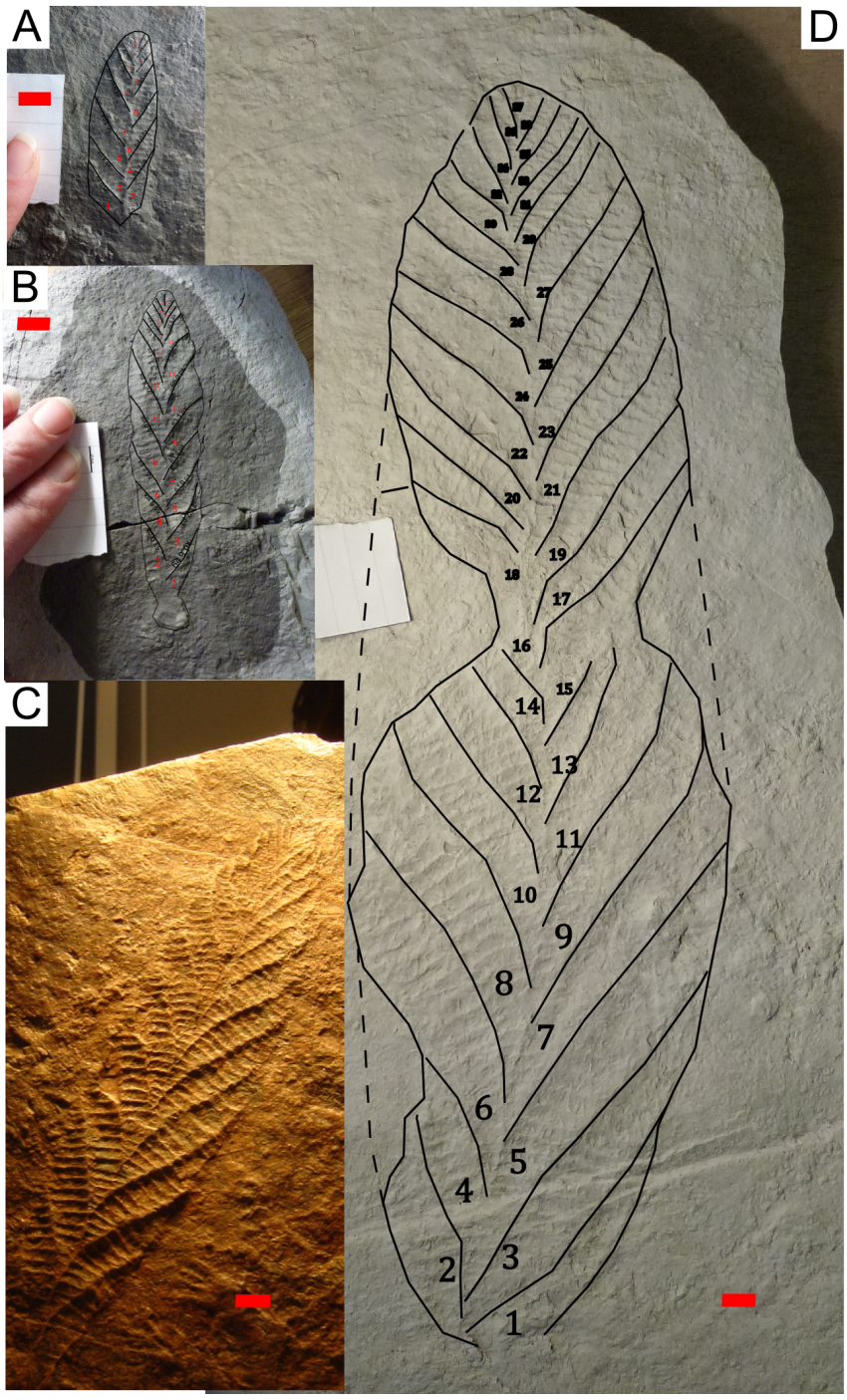

Figure 3.2: Four well-preserved specimens of *Charnia masoni* in different stages of ontogeny, all from Charnwood Forest. The red scales are 1 cm. The numbers label the branches from the basal to the apical pole of the axis and correspond to the branch numbers used in the measurements.

small number of well-preserved specimens to derive detailed information about ontogeny.

A, B and especially the holotype C are well-preserved specimen with a minimal amount of taphomic deformation, with all first order branches visible and many discernible second order branches. D has suffered some pre-burial deformation, possibly some twisting or partial twisting around its axis halfway along its length. Nonetheless the very basal branches and the branches towards the apical side are well-preserved and are not deformed. See Wilby et al. (2011) for a discussion of the geological setting of Charnwood Forest. As tectonic deformation affected all four specimens similarly and the specimens do not seem to have been affected by shear forces, the tectonic deformation of the specimens is neglected.

The growth of the first order branches was reconstructed on the basis of their lengths and the number of branches per specimen. The number of first order branches or branch count was counted on both sides of the central axis, with even numbers on one side and odd ones on the other side. Less visible apicl branches were reconstructed based on their regular distribution and the extrapolated decrease in width of the branches. The estimated uncertainty in branch count is 1 to 2 branches, which comes down to 4 - 7%.

Branch lengths were measured by measuring the lengths of the curved ridges between the branches. The length of this ridge was then taken as the length of the branch above (on the apical side of) this ridge. The method of taking these measurements relied on tracing the ridges in the vector-based drawing programs InkScape and Adobe Illustrator and letting the program calculate their length. I traced the outline of the form to make sure the interpreted outer

edge was consistent throughout the measurements. The uncertainty in the branch length measurements resulting from measurement error was established by repeated measurement to be not significant. There is uncertainty resulting from taphonomic deformation, especially on the basal side of specimen D. Also either biological variation or taphonomic deformation results in a consistent offset between the lengths of the left and right branches in some places, in particular the apical branches of D. Combined, this gives an uncertainty of up to 20% on the individual branch lengths of specimen D, and less for the other specimens. The interpretation of the measurements does not rely only on the individual lengths, but the outline of branch lengths along the whole specimen, which carries much less uncertainty because of repeated sampling. This error is therefore small compared to the differences between the specimens. The basal branches of the largest specimen are about 650% the length of the basal branches of the smallest specimen.

The second order branches are harder to measure as they are not always clearly visible. One variable that could be established reliably in every specimen was the the maximal number of second branches present on any first order branch. This number was measured by giving an estimate of the number of second order branches visible on each of the first order branches. The second order branch number was based on the maximal values of this, taking into account which first order branches were best preserved. The uncertainty on this number is estimated to be 1 second order branch for specimens A, B and C, and 2 for specimen D.

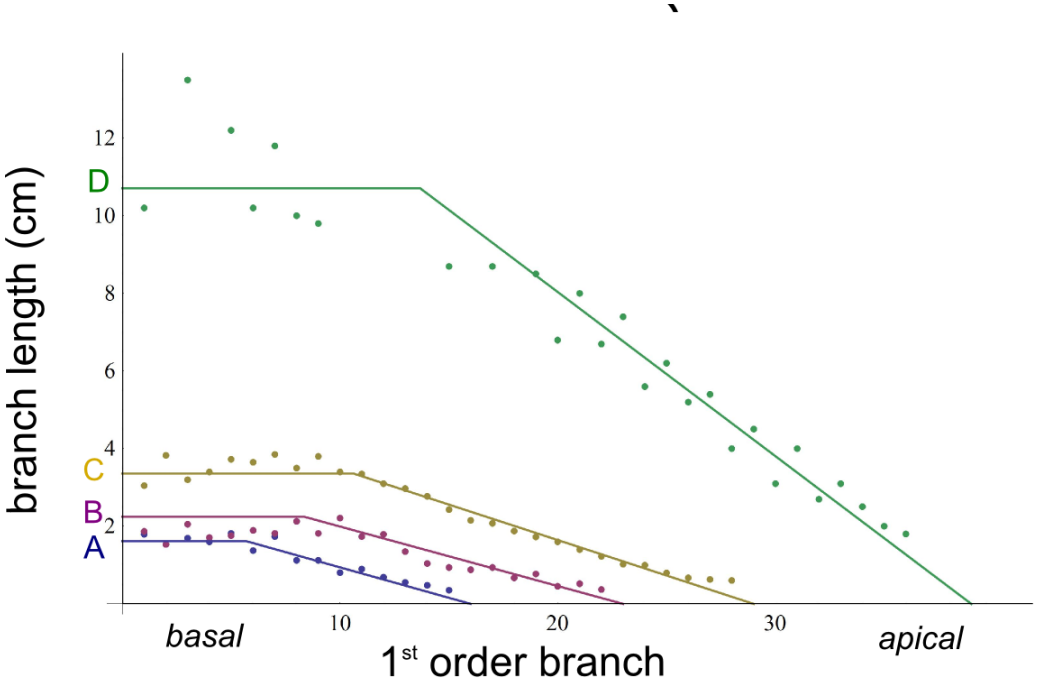

Figure 3.3: Measurements of four well-preserved specimens of *Charnia masoni* and model outlines. The model curves are constant up to 38% of the branch count of each specimen, after which they linearly decrease to zero.

3.3 Measurements

3.3.1 First order branching

The measurements of the lengths of the first order branches of all four specimens are shown in Fig. 3.3. The sets of measurements of specimen A, B and C follow a similar pattern. The 35-40% of the branches at the basal end of each organism are of more or less the same size. The other 55-60% of first-order branches decrease linearly in size with respect to branch number in the direction of the apical pole. A similar linear decrease in branch size towards the apical end of the organism can be observed in specimen D. What is going on at the basal end of the orgamism is not entirely clear because of the deformation

of this specimen. However, the drawn outline represents the same model as is drawn for the other specimens, with the first 38% of the branches being of similar size and decreasing linearly towards the apex, and this model seems to fit the measurements appropriately.

The holotype of *Charnia masoni*, specimen C, is the clearly best preserved specimen studied in this chapter, and it also shows the modeled behaviour most clearly. Therefore slight deviations from the pattern of the measurements of especially specimens A and B are likely to be due to deformations.

The value 38% has some significance as ratio of 0.38 versus 0.62 is known as the golden ratio, which appears often in the ontogeny of different lifeforms, especially plants (e.g. Livio (2002)). There the golden ratio can be present for example in the angle distribution of consecutive leaves around a stem, which arguably allows the leaves to make optimal use of the sun light. The appearance here implies in particular that the ratio of the number of basal branches (B) of similar size and the number of apical branches (A), with linearly increasing lengths, equals the number of apical branches divided by the total number of branches:

$$\frac{B}{A} = \frac{A}{(A+B)}. \tag{3.1}$$

It is not yet clear why this relationship should hold for the organisms, but if its presence is confirmed it may be relevant for our understanding of the biology behind the growth program, as the golden ratio usually occurs as the result of an optimalization.

In Fig. 4.18, the branch number and branch length measurements are combined with the branch count of each specimen in a three-dimensional plot. A

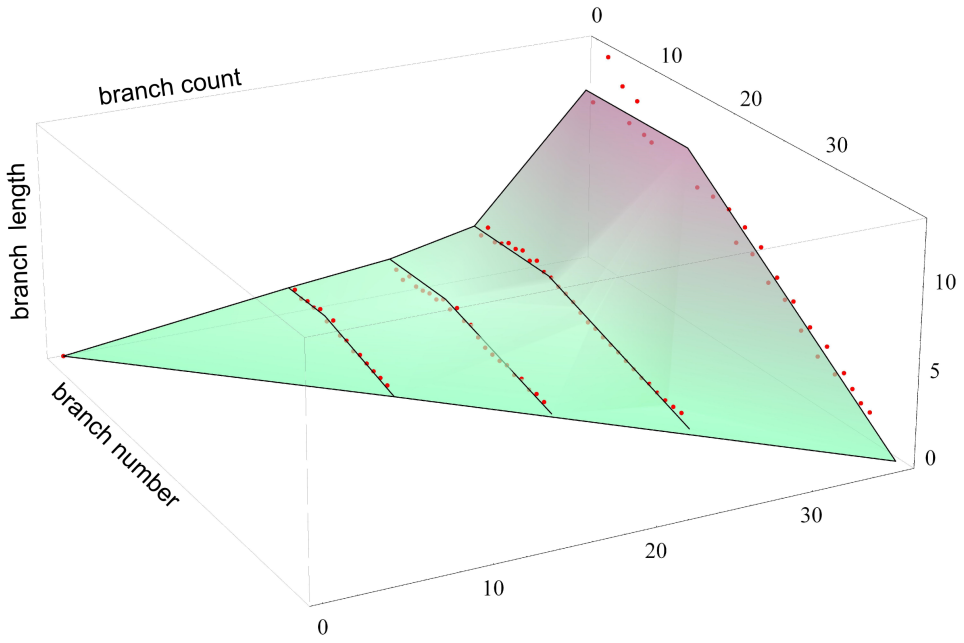

Figure 3.4: The measurements of four specimens of *Charnia masoni* shown in a three-dimensional plot with the branch count on the third axis. A growth surface is drawn through the four model outlines and the point (0,0,0), which stands for a start of ontogeny (i.e. zero branches and zero lengths).

surface connecting the modelled outlines is added to guide the eye. The surface increases in height very regularly with the first three sets of measurements, and rises more steeply towards the fourth, specimen D. These measurements will be further discussed in Chapter 4.

3.3.2 Second order branching

Fig. 3.5 shows the measurements of the maximal number of second order branches found on a single first order branch of the *Charnia* specimens, compared to the number of first order branches on each specimen. The specimens A, B and C appear to line up with each other, but not with the value (0,0) or with specimen D. An interpretation of these measurements will be discussed in Chapter 4.

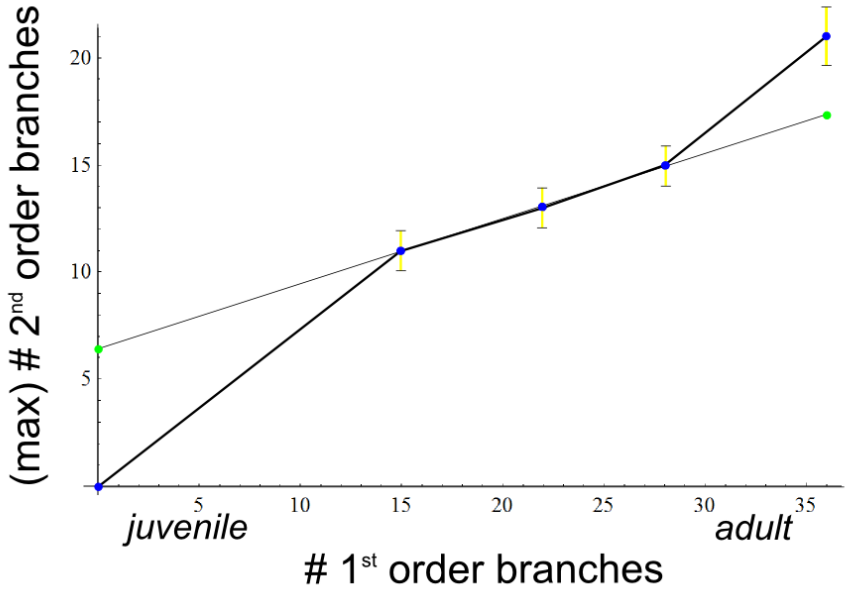

Figure 3.5: Measurements of the maximal number of second order branches versus the number of first order branches in the four measured specimens. The specimens A, B and C line up with each other, but not with (0,0) or with specimen D. The thick line is drawn from (0,0) through the measurements while the thin line follows the behaviour of A,B and C. The error bars, as discussed in the previous section, are shown in yellow.

3.4 Fractal dimension

Hoyal Cuthill and Conway Morris (2014) present estimates for the fractal dimension of a number of rangeomorphs based on box-counting of the branching skeleton of their models. By branching skeleton I mean the set of one-dimensional curves that form the axes of all the branches. The estimates range from 1.6 for the taxon *Avalofractus* with separated branches to 2.4 for the taxon *Bradgatia* that shows a more spacefilling method of growth. In fact, a study of the growth program of *Bradgatia* shows that it is creating a negatively curved surface, which explains why it is never neatly preserved on the bedding surface, as a negatively curved surface cannot be stretched out to a flat surface.

These fractal dimensions can also easily be calculated directly by using the definition of Hausdorff dimension. The Hausdorff dimension can be calculated as follows. For a given fractal F and a given radius r, take the least number N_r of discs of radius r that are needed to cover the shape such that each point of the fractal is enclosed in at least one such disc. Now let r tend to zero. Consider the following expression:

$$H_s(F) = \lim_{r \to 0} N_r \cdot r^n. \tag{3.2}$$

For a given value of s, some positive number, $H_s(F)$ is either zero, a finite number or infinite. It turns out that for any fractal F, there is a unique value of s such that $H_s(F)$ is finite. This value the Hausdorff dimension n of F. If F is any normal shape, such as a cirlce, then n will be its normal dimension, i.e. 1. If F is a fractal then n can be any positive real number smaller or equal

to the dimension of the space F is embedded in.

To get some understanding of the idea behind this definition, compare the expression for H_n with the expression of the circumference of a circle ($2\pi r$), the area of a circle (πr^2), the area of a sphere ($4\pi r^2$) and the volume of a sphere ($4/3\pi r^3$). Note that we always need to raise the radius r to the power of the dimension of the shape we are considering. Analogously, the finite value of H_n for n the Hausdorff dimension is in some sense the "n-dimensional" volume. Consider for example the Sierpiński carpet shown in Fig. 3.6. As one covers the shape with smaller and smaller discs, we don't need to cover the hole in the middle, and the more and more holes that fall on smaller scales. Hence one needs less discs than expected for the surface. Therefore it can be expected that the Hausdorff dimension is smaller than 2. Indeed, a short calculation that I will leave out here suffices to show that the Hausdorff dimension of the Sierpiński carpet is $\frac{\ln 8}{\ln 3} = 1.8928$.

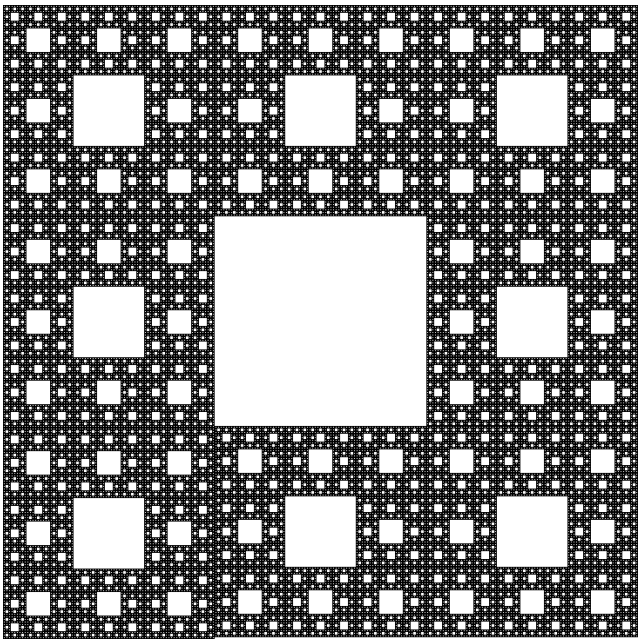

Figure 3.6: Illustration of the Sierpiński carpet.

Now consider the Hilbert curve shown in Fig. 3.7. The Hilbert curve is constructed from an iterative procedure, which at each step replaces a piece of the graph with a more complicated piece according to some set rules. Fig. 3.7 is the state of this curve after five iterations. As the number of iterations tends to infinity, the curve becomes entirely plane filling. If we want to cover this plane-filling curve with discs, then as the curve does not leave any holes, we will need the same number of discs as we would need to cover the plane itself. Therefore the Hausdorff dimension of this curve is just 2.

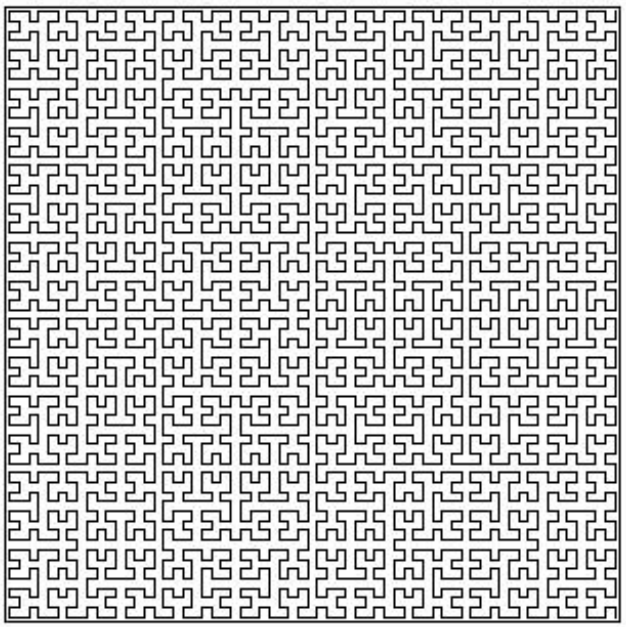

Figure 3.7: Illustration of the Hilbert curve.

Assume that the fractal branching patterns of *Charnia* continues at smaller and smaller orders indefinitely. At every stage, every branch is divided up into smaller branches. Therefore the branching skeleton of *Charnia* also does not leave any holes, hence it is a plane-filling curve. Thus it follows immediately that the fractal dimension of *Charnia* is 2. Fractal dimensions of objects in nature should be considered a heuristic measurement, since in the real world

subdivision is never indefinite and true fractals do not exist.

In the taxon *Avalofractus*, as opposed to *Charnia*, subsequent branches are separated from each other. Thus, there are holes in the branching skeleton. If we try to cover this graph with discs, we will again need less discs than for a plane, thus the Hausdorff dimension is less than 2.

Whereas *Charnia* only branches within a two-dimensional plane, some other rangeomorphs, such as particularly *Bradgatia*, do not only fill up a plane but branch into three dimensions. In particular, *Bradgatia* constructs a hyperbolic surface as it branches. A hyperbolic surface is a surface that is too big to be flattened out to a plane, such as a saddle. Hyperbolic surfaces are used in nature to optimise surface area, such as for red blood cells. The fact that *Bradgatia* branches in a hyperbolic manner can be derived from the fact that every branch flares out with a wide angle as it grows, which would necessarily take up more space than fits on a plane. This appears to happen at different orders, thus the hyperbolicity of the plane increases with the increasing orders of branching. At the same time the branching pattern is plane-filling on this surface. Hence the Hausdorff dimension of *Bradgatia* is higher than 2.

Chapter 4

Building a Growth Model for Ediacaran vendobionts

4.1 Introduction

Our understanding of the biology of extinct lifeforms rests on the interpretation of the morphology of fossils, the associated palaeoenvironmental and palaeoecological information and inferred affinities to extant lifeforms whose biology we already understand. For the Ediacara macro-biota, it is not clear whether there is a direct affiliation to modern, or even Cambrian lifeforms, so understanding the body structure of the organisms relies primarily on our interpretation of their morphology.

Recent decades have seen a rise in the use of advanced techniques for the quantitative study of morphology in palaeobiology (e.g. Gould (1991); McGhee (1999); Niklas (1994)). One method of studying and comparing morphology is given by a morphospace. A morphospace is a space meant to describe and

compare phenotypes of organisms. Morphospaces are central in morphometrics, the statistical description of the morphology of biological organisms. On the other hand it is used in the study of evolutionary biology, where it underlies the idea of an adaptive landscape. The first approach is usually referred to as an empirical morphospace, and the second as a theoretical morphospace. Mathematically the spaces are based on the same concept, but the mode of collecting data and interpreting results differs (Mitteroecker and Huttegger (2009)). Morphospaces can be used to study evolution in manifold ways.

An example of the use of a morphospace in the morphometric sense is given by Shen et al. (2008). The presence or absence of 50 morphological characters was noted for 272 occurrences of Ediacaran species. From this a morphospace was constructed to show that the different assemblages of the Ediacara biota (Avalon, White Sea and Nama) share a similar morphospace. Therefore the authors argued that the Ediacara biota can be described as an "Avalon explosion" in analogy to the Cambrian explosion.

Another example of is given by McGowan and Dyke (2007), where it was explored whether flying vertebrates suffer competitive exclusion from each other by measuring six parameters of the limbs of 795 species of nonavian dinosaurs, birds, pterosaurs and bats. Principle component analysis was used to project the high dimensional data onto a low-dimensional subspace. Then the separation of the different data clouds was studied within the projected plot. In this paper, the authors showed that the different flying vertebrates occupy distinct sections of morphospace, hence it was concluded that the clades do not suffer competition from each other. This example also shows that distinct phylogenetic affiliation can result in separation within a morphospace.

From a third point of view, Foote (1989) and Foote (1990) revealed an increasing morphological disparity of trilobites during the Cambrian and Ordovician through the use of Fourier analysis on the shape of their cranidium. Thus the direction of evolution can occasionally be studied with morphospaces.

A different approach to the study of morphology is presented by the creation of a theoretic or geometric morphospace, a space of geometric shapes that is spanned by a few parameters (e.g. Raup (1966); Niklas (1994); Fortey and Bell (1987); Tyszka and Topa (2005)). Varying the parameters generates a substantial proportion of the morphologies that are observed in nature for the studied group of organisms. Such a model can then be used in the study of the biology of the organisms. For example, if certain values of the parameters are not attained in a natural morphology, it could be that there are either physical or selectional reasons to explain the associated shape is not viable. By studying which values of the parameters in the morphospace are attained over time, one can study the evolution of the group of organisms.

The study of geometric morphospaces inspired a way of thinking about morphology on a macroscopic scale (see McGhee (1999)). An adaptive landscape is an abstract morphospace, thus not actually constructed, that is used for example to consider how species move between fitness optima while under selective pressures (e.g. Gavrilets and Gravner (1997)). It is not clear whether such a space would still have a sense of geometry and whether our Euclidean way of considering these morphospaces actually makes sense, as argued in Mitteroecker and Huttegger (2009).

A classic example of a geometric morphospace is the model for shell coiling in molluscs and brachiopods of Raup and Michelson (1965); Raup (1966).

Assuming that the aperture of the shell is circular, the Raup model uses three parameters to define a two-dimensional shape. This shape is generated by tracing the surface that is swept out by an expanding circle as it is transported perpendicularly along a spiral (see Fig. 4.1). The parameter D parametrizes the rate at which the spiral expands from the axis about which it rotates. The expansion rate W parametrizes the rate at which the circle expands, assuming it has zero diameter at the origin of the spiral. The parameter T measures the vertical translation of the spiral in the direction of the coiling axis. An extra parameter S that measures the eccentricity of the circle can be added to generalize the model (Raup (1966)). Fig. 4.2 shows how the parameter space of the model, spanned by the parameters W, D and T, is occupied with shells occurring in nature within the regular ammonoids, the bivalves (pelecypods), the gastropods and the brachiopods.

Note that two taxa do not need to be closely related to each other to be described by the same morphospace model. Bivalves and brachiopods for example do not belong to the same phylum, but they both fit well in Raup's shell coiling model. This illustrates the fact that similarities in morphology and even ontogeny do not necessarily imply homology of the growth mechanism.

Nonetheless, phylogeny can be explored with a geometric morphospace. For example in the parameter space of Raup's morphospace (Fig. 4.2), different clades form different regions. This appears to reflect the fact that shells from for example bivalves and bracchiopods have a non-homologous developmental program. If one can smoothly go from one morphology to another passing through other forms that have also been realised then it is more plausible, although not proven, that the two are related. If alternatively the parameter

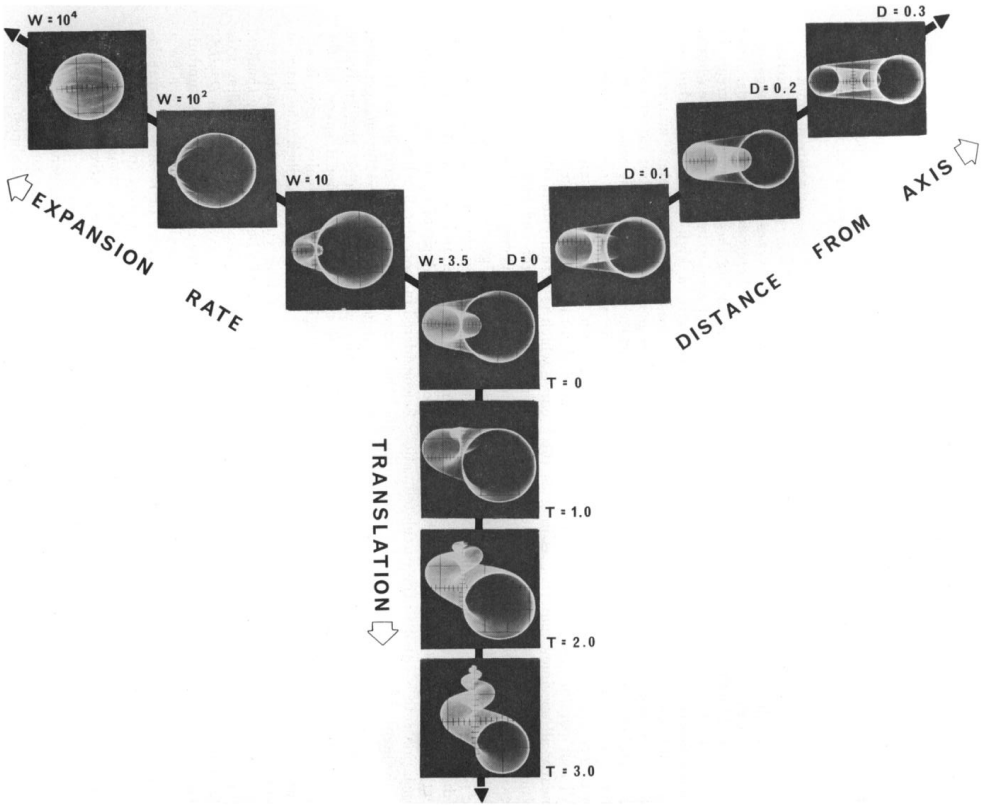

Figure 4.1: A visual explanation of the shell coiling morphospace of Raup. By varying the three parameters W, D and T, most regular mollusc morphologies can be described by the model. Raup (1966) fig. 2.

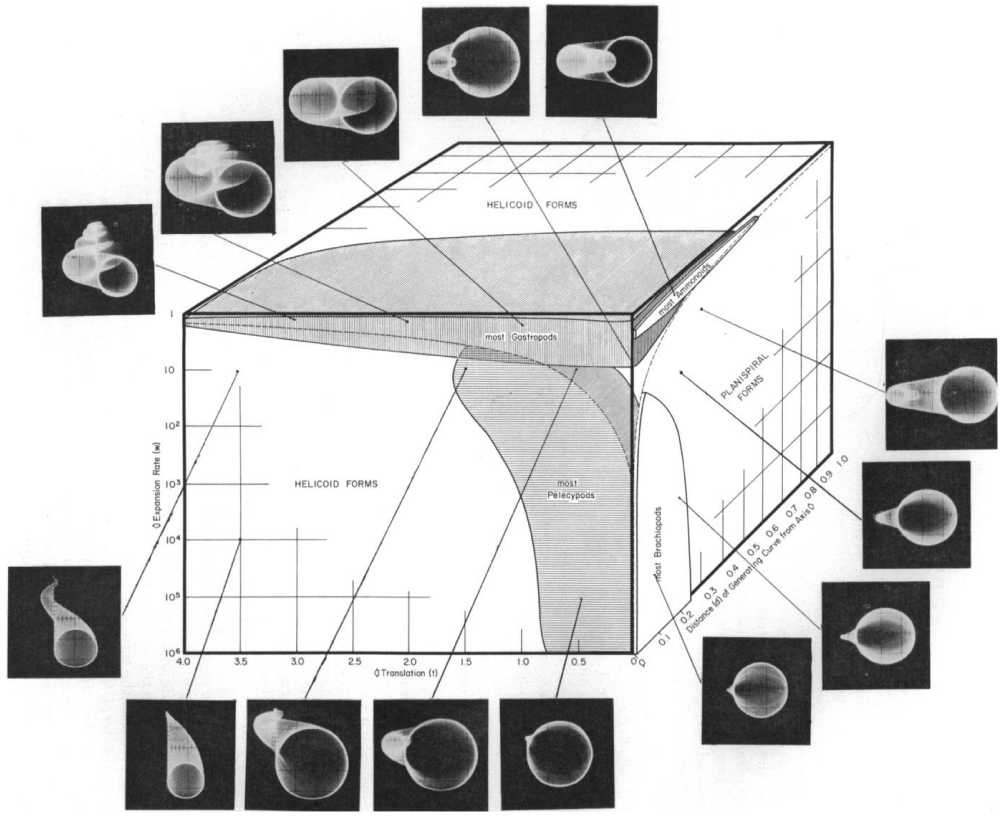

Figure 4.2: Occupation of the parameter space or morphospcae of the Raup shell coiling model, spanned by the parameters W, D and T, with shells occurring in nature within the regular ammonoids, the bivalves (pelecypods), the gastropods and the brachiopods. Raup (1966) fig. 4.

space splits up into different groups which separate in the parameter space, then it is plausible that the organisms within each group are more closely related to each other than to the organisms in the other group.

In this chapter I build a growth model for rangeomorphs and dickinsoniomorphs of the Ediacaran macrobiota. This growth model is governed by a few parameters, three for the model of *Dickinsonia costata* and *Charnia masoni*, which can be extended to four to describe a larger class of vendobionts. By varying these parameters many of the morphologies of rangeomorphs and dickinsoniomorphs can be simulated. It is an example of a geometric morphospace. Like the Raup shell coiling model, phylogenetic affilation of the represented taxa is not assumed, but can be studied by looking at the parameter space of the model. However, unlike the Raup model, every point in the parameter space in this model stands not for a single mature morphology, but for an entire growth sequence of an organism.

First I explain the assumptions and the setup of the growth model, which is based on the growth of branch/segment lengths over time. Then the measurements of *Dickinsonia costata* and *Charnia masoni* are analysed and the growth model is adapted to either. Finally the sets of measurements and growth models are compared and I explain how to extend the model to other taxa. Comparing the ontogeny and morphology of different taxa in the Ediacara macrobiota I make a case for the ancestral origin of the mode of growth of these organisms.

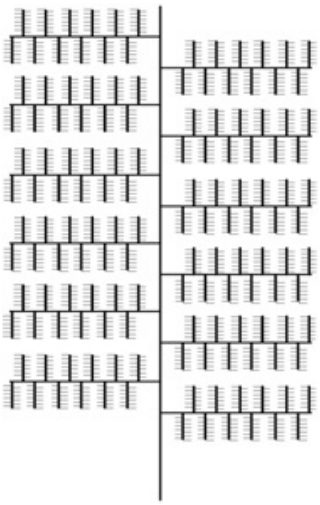

Figure 4.3: A schematic drawing of the branching structure of rangeomorphs. The shown braching pattern has three orders of self-similarity.

4.2 Growth model

4.2.1 How to build a growth model

A geometric model is built from a basic setup of a geometric shape and a choice for how to vary this setup with parameters. For example, the Raup morphospace has as a basic setup of the geometry the traced-out movement of an expanding circle along a spiral. Within this setup three parameters can then be varied to alter the shape. The setup of the vendobiont growth model built here is a schematic form with a stem and branches to either side, such as displayed in Fig. 4.3. Initially I will only consider first order branches. The branch lengths are varied not by setting their lengths one by one, but by making use of the relationship between consecutive branch lengths.

Two obstacles need to be overcome in the construction. Firstly, different specimens that clearly do belong to the same taxon have different numbers

of branches and I want to represent each taxon with a single point in the morphospace. Secondly, if we choose every branch length as an independent parameter, then one ends up with as many continuous parameters as branches in our model, which would make the dimension unnecessarily high. This would also include a lot of superfluous forms which are not realised in nature, such as the example in Figure 4.4a, determined by 100 parameters. This is because the morphologies occurring in nature have a constraining relationship between the lengths of consecutive branches, i.e. the lengths are close together because the growth program is similar and at a similar stage for consecutive branches. This greatly constrains the amount of variation, as illustrated in Figure 4.4b, which is determined by a single parameter.

The solutions to these two obstacles are as follows. Firstly, I can build the morphospace in the form of a growth model, such that every point in the morphospace encodes an entire growth sequence. Then specimens from the same taxon with different branch numbers can be viewed as snapshots in an ontogenetic sequence, and the entire ontogeny of the taxon can be described by a point in the morphospace. Secondly, in the growth model we should make use of the relationship between consecutive branch lengths instead of treating them as independent parameters. One way to build a model describing branch lengths in a branching/segmented organism is therefore to give a description of branch insertion and lengthening over time.

4.2.2 Assumptions of the model and their justification

The model I build relies on a number of assumptions about the growth of the organisms that are described by the model. I here state the different assump-

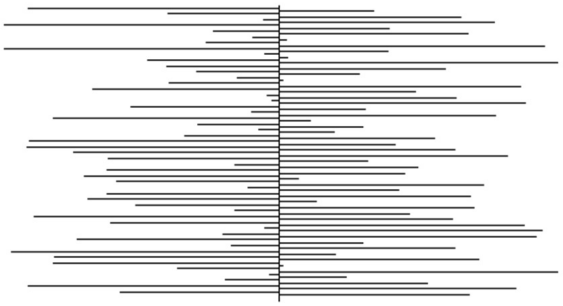

(a) A schematic drawing of a first order branching pattern with a random assignment of branch lengths. The set of these shapes is spanned by a 100-dimensional space with one independent variable for each branch.

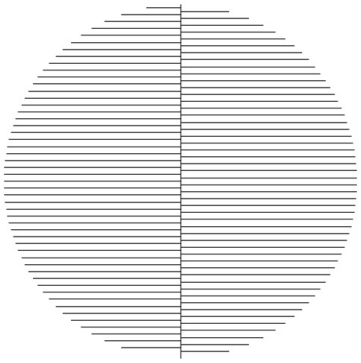

(b) A first order branching structure with 100 branches given by a single parameter, namely the radius of a circle.

tions and consider whether they are justified in the case of the description of rangeomorph and dickinsoniomorph growth. I also consider whether they hold in other organisms with comparable modes of growth such as segmented bilaterians.

Branches are added during ontogeny

In the model it is assumed that branches are added over time, i.e. that the branch number grows or is stable, but does not decrease during growth. It is known that many Ediacaran macro-organisms show a correlation between the number of branches and the size of the organism, hence it is a safe assumption that growth occurred through the addition of branches in some way or another. Modern segmented animals do not decrease the number of segments, although many modern arthropods, e.g. insects, fuse some of their segments together into tagma. This process is known as tagmosis. There is currently no evidence of such a process occurring in rangeomorph and dickinsoniomorph.

Branches grow during ontogeny

Secondly, it is assumed that branches grow over time, i.e. that the lengths of the branches does not decrease. It could be that the branches stop lengthening, but in principle it is assumed in the model that the lengths do not decrease. This refers to an uncontracted state of the organism. If the organism is capable of contraction then the measured value of the lengths can be smaller than expected, as will become clear with the discussions of the measurements of *Dickinsonia*. For segmented bilaterians, it is generally the case that the segments increase in size or stay the same size during ontogeny. Measurements of *Dickinsonia* and *Charnia* show that the branch lengths increase with the number of branches.

Alternating branches

In the basic setup of the model I assume that the branches are added one by one alternatingly on the left or right side of the central axis. This alternating pattern of branch insertion is seen in rangeomorphs and referred to as a glide plane of symmetry (e.g. Antcliffe and Brasier (2007a); Brasier et al. (2012)). Whether this special off-set symmetry is also present in *Dickinsonia* is a matter of much debate. Fedonkin argues that it is present (e.g. Fedonkin (1998)) in dickinsoniomorphs and it is argued to be present in *Dickinsonia* in Brasier and Antcliffe (2008). Gehling et al. (2005) and Gold et al. (2015) argue that the segmentation pattern in *Dickinsonia* is symmetric. In case of the latter, the organisms would show bilateral symmetry, which might suggest a possible phylogenetic link to Bilataria. Alternatively, if the segments appear on either side of the axis in an alternating fashion this might suggest a link to

rangeomorphs. The dickinsoniomorph *Yorgia* clearly has an off-set branching pattern. The transverse widths of the segments of *Dickinsonia* are small compared to the lengths scales of deformation on the specimens, such that it is hard to quantitatively study whether the segmentation pattern is off- set or symmetric. Therefore this is left out of the picture in the current quantitative study of ontogeny. Either interpretation is consistent with the presented study. The growth model can be adapted to show symmetric branching.

Apical insertion

The growth model is based on the assumptions that the organisms grow through insertion of the branches on one end of the central axis of the organism, analogous to the terminal addition mode of growth found in many bilaterians. It is currently widely assumed in the literature that *Dickinsonia* and *Charnia* grow in this way. In both taxa the generative zone is speculated to lie at the end of the organism where the branches/segments are smallest. In sections 4.3 and 4.4 I will consider whether this assumption is justified by the measurements presented in this thesis.
Basal and apical insertion can both be described by the model as it is symmetric, so the resulting diagrams can be reflected or rotated to display the other mode of insertion. For a different mode of insertion of branches, e.g. bipolar insertion, the model can be adapted.

Organisms follow similar ontogeny

I will build a single growth surface that should in principle reflect the modelled ontogeny of a species. Hence there is the subtle implicit assumption that

the members of the species follow a very similar growth plan, with similar lengths of the branches at a similar stage. The measurements of *Dickinsonia costata* indicate that the organisms studied follow a similar growth program. The four specimens of *Charnia* studied in this thesis also show a consistent growth program. However, these specimens are from the same bedding plane in Charnwood Forest. It is possible that the specimens of *Charnia* on a different bedding plane would have followed a different growth surface because of environmental influences on growth.

All the programming for the model was done in Wolfram MATHEMATICA, version 9.0, which is a particularly suitable for rendering complex graphics such as the growth surfaces.

4.2.3 Simple model of branch insertion and growth

To illustrate how the model works I will first explain a simple example of a growth sequence that can be generated. Assume that branches are inserted at a constant rate, and grow at a constant and uniform rate α. The branches are furthermore separated by a constant branch width. A diagram of the lengths of all branches over time is shown in Fig. 4.5a. This diagram represents every branch with a line. We can also put the branch number on a third axis and represent the same information in as a surface, as shown in Fig. 4.5c. I call such a three-dimensional diagram with branch number, branch length and time on the three axes, a growth surface. Fig. 4.5b shows a snapshot of the resulting morphology, after the insertion of 15 upper branches, or 30 branches in total. The first branch is the longest as it has has the most time to grow at a constant rate.

This model is entirely determined by one parameter, the growth rate α. Although the other two parameters, the branch insertion and the branch width, can be given a different value, the resulting morphology can be rescaled and the time parameter can be reparameterized, such that the resulting ontogeny is considered the same. A change in α effectively changes the aspect ratio of the morphology, the relationship between the widths and the lengths of the branches.

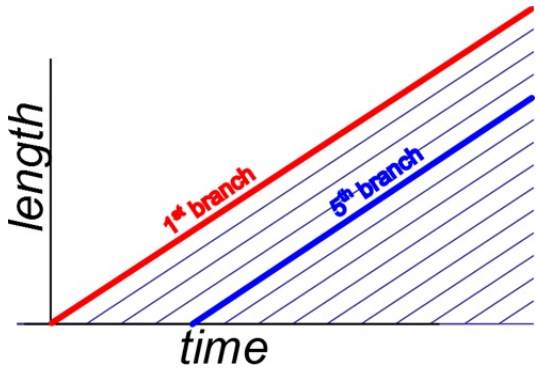

(a) A simple growth model has branch insertion at regular intervals and these branches grow linearly as a function of time with rate α.

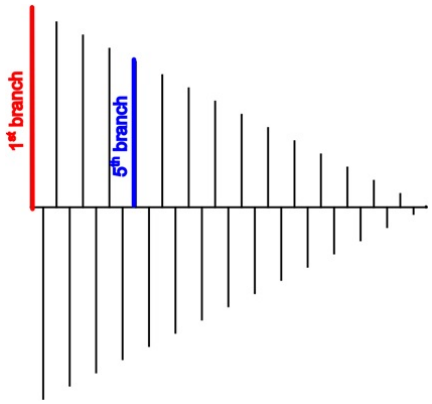

(b) An intermediate form of the simple model described by 4.5a after the insertion of 15 branches.

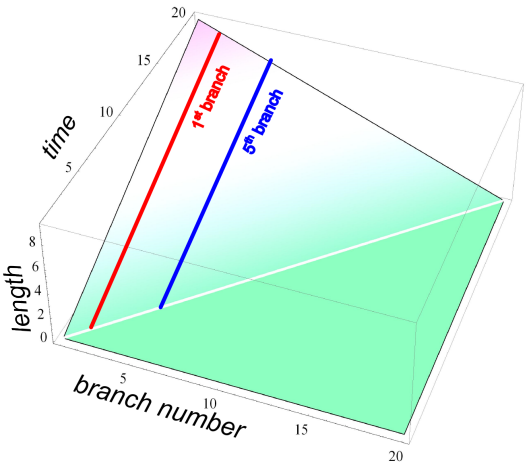

(c) The growth surface of the simple growth model.

Figure 4.5: Simplest growth model.

4.2.4 Introducing growth stages

In the simple model the oldest branches always remain the longest as they have had the most time to grow. This is still the case if the insertion rate is not constant. This behaviour can be changed by introducing growth phases. For example, suppose that there is a set mature maximal length L at which the branches stop growing. This model is illustrated in Fig. 4.6a, which is illustrated in three dimensions as before in Fig. 4.6c. A snapshot of the morphology after the insertion of 15 upper branches is given in Fig. 4.6b.
The time of the onset of the mature growth phase T is constant and can be expressed as L/α, so we can also consider α and T as the two variables that determine this model. Fig. 4.7 presents an initial "morphospace" that is given by varying the two variables α and T, where we only show the snapshots of the morphologies after the insertion of 15 upper branches.

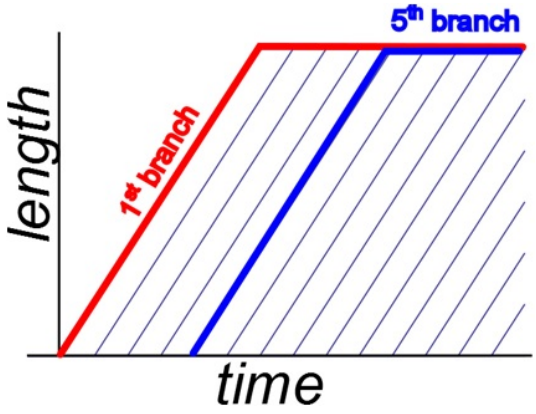

(a) A model with growth phases. Initially branches grow with growth rate α, but they switch to a mature growth phase after a fixed time T.

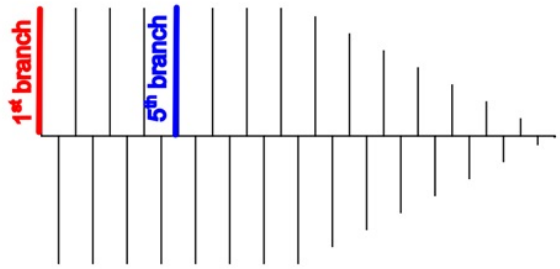

(b) An intermediate form of the growth sequence described by 4.6a after the insertion of 15 (upper) branches.

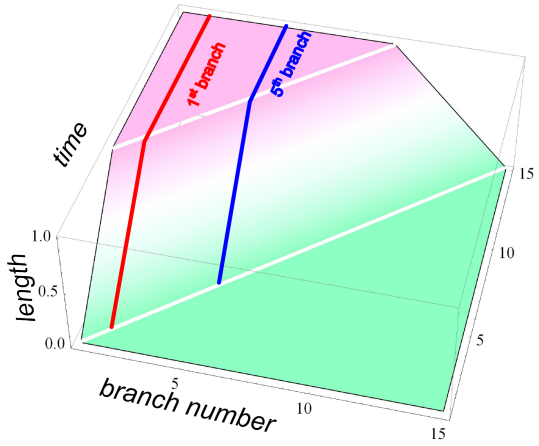

(c) The growth surface corresponding to a simple model with two growth phases.

Figure 4.6: Model with growth stages.

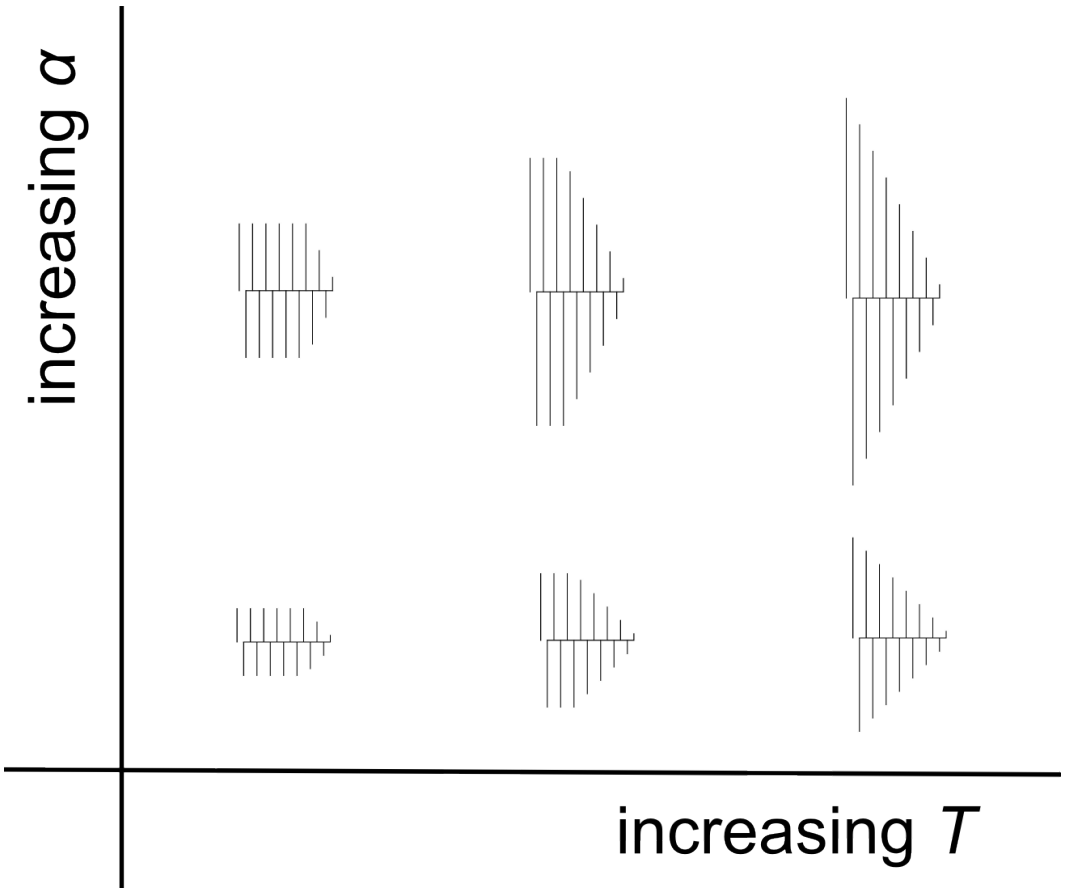

Figure 4.7: Diagram explaining the idea of a "morphospace" for the model with two growth stages. Shown is the parameter space of the model, spanned by the growth rate α and T, the duration of the juvenile growth phase. Six snapshots of the resulting ontogenies are shown, each one at the point where 15 upper branches have been inserted.

4.2.5 Symmetric growth

A generalisation of the above model is to allow the delay time T for a branch to switch from the juvenile to the adult phase, to vary between the branches. With this adaptation it is possible for the branches in the middle of the organism to grow longer than the oldest branches. This allows for a rounded shape as we see for example in the taxon *Dickinsonia costata*, where the most basal and most apical branches are smaller than the ones halfway along the axis.
One way to achieve this is to let T, the duration between the insertion of a branch and the onset of its mature phase, grow as a function of the branch number k. A simple assumption is that T is a linear function of k. In particular, it is possible to choose $T(k)$ so that the form will be symmetric throughout its entire growth. This happens precisely when the $T(k)$ equals the time it took before the branch k was inserted. As branches are inserted at a constant rate in the current model, one can set one unit of time to equal the insertion of one branch. Then the time is parameterized by the number of branches of the organism. We can then write the condition for the model to become entirely symmetric in the equation $T(k) = k$.
Such a system of "symmetric growth" could be a functionally beneficial property for an organism, because it allows a branching organism to maintain the same geometry over its entire life while it grows. Because this model fixes T in a unique way, this model again is determined only by the parameter α. The model is illustrated in Fig. 4.8.

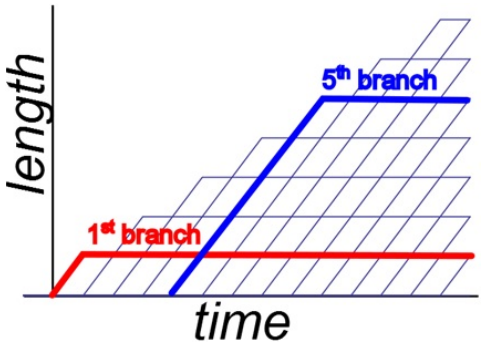

(a) Symmetric growth model in which every branch first grows with growth rate α before switching to the adult (full-grown) phase after a time $T(k) = k$ in such a way that the resulting shape is always symmetric, even though growth only occurs at one end of the central axis.

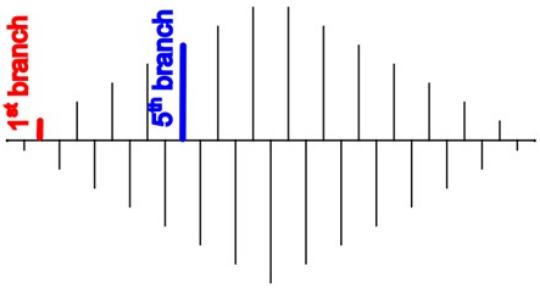

(b) An intermediate form of the growth sequence described by 4.8a after the insertion of 15 (upper) branches.

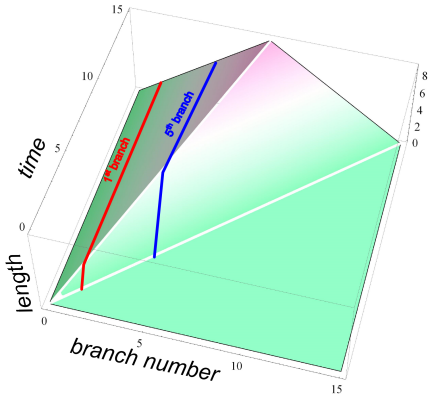

(c) The growth surface of the symmetric growth model.

Figure 4.8: Symmetric growth.

4.2.6 Inflationary growth

Charnia, in terms of branch lengths, looks more or less like a morphology such as Fig. 4.6b generated by the growth model with two stages. However, the measurements from Chapter 3 tell us that the basal branches, although they have a similar size, do still grow over time, only slower than the apical branches. This can be modelled by generalizing the growth model with two stages by allowing the second stage to have a nonzero growth rate. I call this mode of growth inflationary. The model is illustrated in Fig. 4.9.

Note that every snapshot of the inflationary growth model looks like a snapshot from an ontogeny of the earlier two stage growth model with a set mature length. This reflects the fact that also within the fossil record, it would not be possible to separate these two growth programs by looking at a single specimen. By comparing multiple specimens, as I did in Chapter 3, it is possible to differentiate between these two modes of growth.

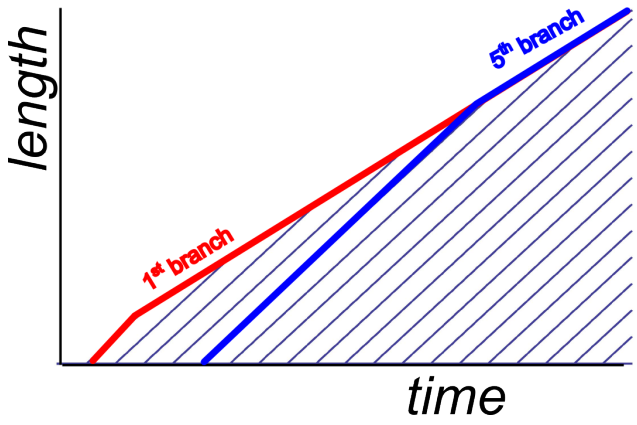

(a) Inflationary growth model, in which every branch grows until it has caught up with the basal branches and then continues to grow at a slower, inflative growth rate.

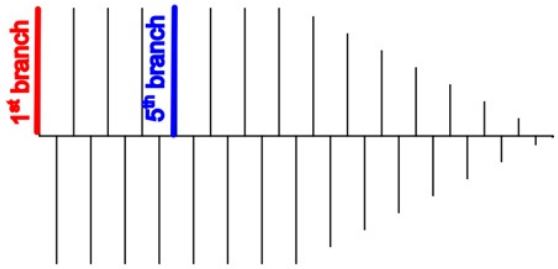

(b) A snapshot of an ontogeny generated by the inflationary growth model shown in Fig. 4.9a after the insertion of 15 (upper) branches.

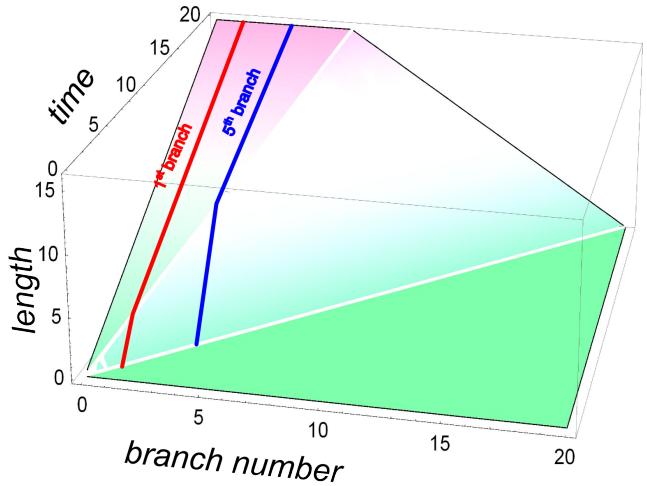

(c) Growth surface of the inflationary model.

Figure 4.9: Inflationary growth

4.3 *Dickinsonia costata*: interpreting measurements and building a growth model

In this section I will discuss and interpret the measurements of twenty specimens of *Dickinsonia* presented in Chapter 2. Then I will build a growth model for *Dickinsonia costata* based on these measurements.

4.3.1 Interpretation of measurements

A first question to ask in the description of the ontogeny of *Dickinsonia* is how well segment insertion is correlated with the growth of the segments. It has been implicitly assumed in the literature that segment insertion can be considered a measurement of age and correlates with size, for example in Runnegar (1982). If one concludes that some organisms are found in a contracted state from the fact that two organisms with a similar segment count have different sizes, then one is implicitly assuming that the normal state of affairs for uncontracted organisms is that segments have the same length if the segment count is the same. This might not be the case for example if the ratio of the two modes of growth, inflational and insertional, depends on the environment. Biological variation between organisms might also contribute to substantial differences in methods of growth within the population.

It is convenient for the interpretation of the data to plot three guiding surfaces as shown in Fig. 4.10 and 4.11, connecting sequences of measurements to each other. Each surface increases gradually in height (segment lengths) with increasing segment count. The specimens of the species *D. rex* are more elongated and have a larger number of segments compared to their size than *D.*

costata specimens. This is captured by the fact that they lie on the lowest blue surface, which is flatter and lower than the rest of the specimens. The blue surface consists of specimens D7, D9, D19 and D20. The latter two can clearly be identified as *D. rex* on the basis of their elongated shape and high number of segments. The smaller two specimens have not previously been identified as *D. rex* but are differentiated from the *D. costata* by their elongated shape. The *D. costata* specimens lie on, and between, the higher red and green surfaces[1]. The fact that the 16 *D. costata* specimens are constrained between these two surfaces indicates that the studied specimens have followed a similar growth plan in which segment insertion correlates with inflation.

There are different processes that contribute to distributing of the specimens between the red and green surface, instead of consituting to a single growth surface. On the one hand, factors such as biological variation in the growth program have contributed to variation in the growth surface within the living population. On the other hand, taphonomic processes have led to deformation of the specimens, altering their outline and overall size. Another contributing factor is contraction, which might be due to either taphonomy or biology. Features in the fossils can also indicate contraction, such as those found in D15 and D18. Specimen D15 (the original holotype of *D. costata*), shows radial grooves aligned with the segment margins along its rim. These features were once interpreted as tentacles (Sprigg (1947)) but are nowadays interpreted as signs of contraction of the specimen. D18 has a "loose skin" appearance with folded segment margins, and was interpreted by Runnegar (1982) as a highly contracted *D. costata* specimen. Indeed D15 lies between the red surface and

[1]In fact specimen D13 lies partly below the green surface, but its basal segments are larger thus I have not included it in the green surface.

the green surface and D18 lies on the green surface, well below the red surface. Hence contraction is indeed a factor that contributes to the distribution of the specimens between the two surfaces, by shrinking the specimens towards the green surface.

The surfaces drawn from the data represent growth surfaces: the outline of segment lengths as a function of segment count. As growth correlates with segment count, the segment count in some sense parameterizes the age of the organisms. However, it is not possible to derive an absolute time sense of time from this data, as it is not known what the absolute rate of insertion of the segments was. The rate of insertion of segments might also not have been constant, thus a relative sense of time is difficult to obtain as well.

Both the red and the green *D. costata* surfaces curve increasingly upward at around 40-60 segments (Fig. 4.11). This can either be explained as an increase in the rate of growth of the segments, or as a decrease in the rate of insertion of segments. The second interpretation is consistent with the fact that *D. costata* is generally found with up to 50-60 segments (e.g. Fedonkin et al. (2007a)). Thus it appears that segment insertion slows down and possibly eventually stops entirely, while the growth of the segments continues. This is consistent with a claim in Sperling and Vinther (2010).

4.3.2 Apical insertion versus basal insertion

The transverse widths of the segments varies gradually from widest on one end, here called the basal end, to thinnest on the other, referred to as the apical end. Also the lengths of the segments decreases to zero towards the the apical end. This end is therefore usually interpreted as the generative

zone where new segments are inserted (Runnegar (1982); Sperling and Vinther (2010); Brasier and Antcliffe (2008)). This interpretation is implicitly based on the idea that the apical segments are small because they are younger. Another interpretation would be that the apical segments were inserted at a time when the organism was still much smaller and are therefore older. This is the hypothesis of basal insertion.

If the apical segments are youngest and are continually inserted from a generative zone given only by the very apical end of the axis, then the most apical segment at a later time is not necessarily expected to be larger than a previous apical segment. They are after all, assuming apical insertion, not homologous structures, and their initial size is determined by the size of the generative zone which is assumed to be given only by the very apical endpoint of the axis. The idea of apical insertion is based on the idea that the apical segments are inserted starting from a similar very small size and grow over time (e.g. see Fig. 2.1). In fact, it has probably been assumed that the hypothesis of basal insertion of segments fails because the apical segments at a later stage might occasionally be smaller than those at an earlier stage. Then basal insertion would imply that the segments decrease their length, which would contradict the reasonable assumption that the segments do not significantly decrease their length (except for through contraction, which can also be seen in the rest of the specimen as well).

In Fig. 4.12 I have plotted the lengths of the segments as a function of the number of segments of four specimens with a well-preserved outline: D2, D4, D10 and D14. Specimens D2, D10 and D14 are uncontracted specimens inside the red surface in Fig. 4.10. D4 lies very slightly below this surface, but has

the least deformed outline compared to the specimens close to it hence it is preferably used in a study of individual segment growth.

In Fig. 4.12a, the segment measurements are connected based on the assumption of apical insertion. In Fig. 4.12b the segments measurements are connected based on the assumption of basal insertion. It turns out that neither of these models requires the segments to decrease their length over time, hence neither hypothesis can be refuted on the basis of the assumption that segments increase their length. In Fig. 4.12a, the apical insertion assumption leads to the conclusion that segments grow at a faster rate compared to segment insertion initially, but slow their relative growth rate after they have been the longest segment, and continue to grow at a steady lower rate.

In Fig. 4.12b, the basal insertion assumption leads to the conclusion that segments are inserted at a non-zero length that is given by the side of the basal segment as they split off from the basal segment. After insertion, they continue to grow at a steady low rate, as can be seen in the almost horizontal lines connecting the most apical (i.e. oldest for basal insertion) segments. Note that the fan-shape given by the outlines of segments that appear for the first time at a given specimen, is in this case an artefact of the sampling, since we expect them to be inserted with a non-zero length (i.e. vertically) at an earlier stage.

Thus, either one of the models can explain the measurements without contradicting the assumption that the segments do not decrease their length over time. Can either hypothesis explain why the other hypothesis works too? The fact that the apical segments line up very well in Fig. 4.12b could reflect a steady increase in the size of the apical generative zone. On the other hand,

basal insertion can explain why the basal segments increase their size steadily: the basal segment grows and as a result the segments splitting off from this segment are larger.

Figure 4.13 shows the measurements from Chapter 2 presented from the point of view of basal insertion. Whereas in the earlier presentation of the data in Fig. 2.3 and Fig. 4.10, the segment number of each segment was counted from basal segment up, they are now counted from the apical segment up. Thus, assuming basal insertion, homologous segments appear on the same vertical line in Fig. 4.13a. Comparing Fig. 4.13a to Fig. 2.3, we see the apical regions in Fig. 4.13a (left side of the diagram) resemble each other in terms of size and slope. This would be natural within the basal insertion hypothesis as these segments are homologous, only grow steadily. However, in terms of the apical insertion hypothesis, one might argue that the generative zones are similar, while the shape and growth of the older segments diverges. Hence, the fact that the apical regions of the specimens are similar does not necessarily refute the apical insertion hypothesis.

Is there direct evidence for basal or apical insertion? In specimen D14, shown in Fig 4.14, the segments on the very basal end of the specimen are only halfway separated from the basal segment. One might interpret these segments as being in the process of splitting off from the basal segment. Other basal segments also do not seem to continue all the way to the central axis, even though this is the case for the apical segments. This might indicate that these segments have also not fully split off. However, note that a few of the segments in the basal region seem to have a boundary that is interrupted in some places. This looks like a taphonomic feature, hence it could be that the discontinuation of

the boundary in other places is due to taphonomy as well. Thus far I have not found similar features in other specimens. I am not aware of any direct evidence in favour of the apical insertion hypothesis.

All in all, basal insertion cannot be refuted based on the measurements of twenty well-preserved *Dickinsonia* specimens. In fact, there is some tentative evidence in favour of basal insertion as opposed to apical insertion. Thus, the basal insertion hypothesis should be taken seriously in the future. This is relevant as Gold et al. (2015) uses the assumed apical insertion of *Dickinsonia* to interpret the taxon as a basal bilaterian.

Apical and basal insertion are not the only two possible modes of insertion of segments. Others include insertion on either end as proposed by Seilacher, or insertion halfway the organism. The latter occurs in many arthropods, whose generative zone is not entirely at one end of the organism but preceded or followed by a fixed number of segments. In trilobites, for example, the thoric segments were inserted on the anterior side of the pygidium, the fused posterior tagma consisting of 1-30 segments (Benton and Harper (2009)). Both these alternative modes of segment insertion cannot be excluded for *Dickinsonia*, although there are arguments against either. Insertion on either end is doubtful given the clear asymmetry of the two ends compared to the strong similarity of the segments to each other. Apical insertion implies a generative zone from which segments grow from a relatively small size, whereas the basal end has a large central basal segment from which segments would split off. It is not unthinkable, but quite unlikely, that the organism would possess two growth zones of a different nature. One might in such a case also expect that there would be a distinction between the segments originating from either end, but

instead the features and measurements of the segments varies smoothly from one end to another.

Arguments against insertion halfway the organism are given the absence of a distinguished segment along the axis of the organism, as well as the fact that the widths of the segments vary continuously along the axis. If one segment functioned as a generative zone, then we might expect this fundamental distinction in biology to be reflected in the morphology of the segment in some way. *Dickinsonia* is found with a large variation in the number of segments, thus if the segments were inserted halfway the axis, then we would expect to find examples of the organism in the process of splitting off a segment halfway, if this were its mode of growth. In contrast, the segment widths vary gradually along the axis. If the segments split somewhere along the axis then it would be expected that at a certain point the segment would be either significantly wider or smaller than its neighbours, and this is not something I have observed in the 20 specimens studied in this chapter. Note that for example trilobites are not, generally, found in the process of adding a segment. However, this is because trilobites grew through molting, thus at every point the exoskeleton only possessed a discrete number of segments. There of molting of *Dickinsonia*, nor is it likely that the organism would need to molt, given that it was soft-bodied, as supported by the way its body adapted to the curvature of the bed (e.g. see Fig. 4.14).

4.3.3 Other conclusions from the measurements

Measurements confirm that *Dickinsonia* grew through both addition and expansion of segments, as suggested in Sperling and Vinther (2010). The au-

thors furthermore suggested that the rate of segment insertion in *D. costata* decreased all throughout ontogeny. The measurements confirm that a decrease in segment insertion rate is likely, although the upward bend in the growth surface presented in Fig. 4.10, seen from the side in Fig. 4.11, arguably suggests that the decrease in rate occured later in ontogeny as a switch in the growth program. This switch in growth program might indicate the switch to the reproductive phase of *D. costata*, which is a reason for organisms to change their mode of growth (Stearns (1992)).

When comparing the larger specimens from the red and green surfaces in Fig. 4.10, one notices that the shape of the outline of the measurements differs between the two. This is illustrated in Fig. 4.15. The outline of segment lengths of a number of the uncontracted specimens (red) is markedly more rounded than the outline of the contracted specimens (green). In particular, the position of the longest segment seems to have shifted towards the basal end of the specimen. This find suggests that the segments towards the apical end of the organism contract more than the wider segments on the basal end. A possible explanation is that the contraction of the segments was related to the "elastic" body structure of *Dickinsonia*, held up by some internal pressure, and contracted by the release of this pressure. An elastic shape that is held rigid by an internal pressure will tend its shape as close as possible to a round sphere. This lowers surface area compared to volume and therefore reduces the tension in the elastic hull. A thin rod-like shape will thus try to shrink along its long axis and expand in the direction of its short axes. Like a rod-like balloon, when deflated the thin segments will mostly first reduce their length and secondarily reduce their widths. This effect is less strong for the wider

segments. Therefore the contracted or deflated segments might appear more equal in length, resulting in a flattened curve of measured segment lengths. Alternatively, the observed relatively larger contraction in the apical segments compared to the basal segments, could be related to a reduced elasticity of the basal segments due to the greater size, or their difference in age. In either case, the difference in outline between the uncontracted and contracted specimens are consistent with a taphonomic interpretation of contraction, but it does not contradict a biological interpretation.

4.3.4 A growth model of *Dickinsonia costata*

The model constructed in the previous section can now be tailored to the measurements of *Dickinsonia costata* from Chapter 2 to form a growth sequence that represents the ontogeny of *Dickinsonia costata*. This growth model assumes apical insertion of the segments, although I have shown it cannot be concluded from the measurements whether the taxon grew through apical or basal insertion. A growth model for *D. costata* based on basal insertion can be built in a very similar way. The model furthermore displays *Dickinsonia costata* as having an off-set symmetry, while some authors argue that the taxon is instead symmetric. The model can be adapted to show a symmetric branching pattern without changing the parameters that define the growth surface of the model.

Dickinsonia costata has a rounded shape, i.e. the oldest segments are shorter than the younger segments in the middle. Therefore I start from the symmetric growth program. However, as is discussed in Chapter 2, the longest segment of the outline is not in the middle but at $(33 \pm 8)\%$ the segment count of the

specimen. I have set the position of the maximal segment at 38%, which is the position it has in specimen D14 which has the best preserved outline of the specimens (see Fig. 4.14). This position of the longest segment can be adapted from the symmetric growth program by setting the duration of the first growth phase as follows:

$$\frac{T(k)}{k} = \left(\frac{1}{0.38} - 1\right) \approx 1.62. \tag{4.1}$$

This happens to be close to ϕ, the number that is referred to as the golden ratio.

As can be seen in Fig. 4.10, and more clearly in Fig. 4.12a, segments grow in a first stage with faster growth rate and, as they become the longest segment, they switch to a second phase with a decreased growth rate. Thus the second growth phase is not stagnant as suggested by the symmetric growth model, but inflative as in the inflationary model.

Finally, the measurements tell us that at around 50-60 segments on either side of the axis, the insertion slows down while growth continues. This will be modeled with an insertion stop at 50 branches. If the growth program for individual segments were to continue as before, then the youngest segments would eventually become the longest. Instead a similar outline is preserved. Thus after the insertion stop all segments grow at the same rate. It might be that this growth rate is much lower, or higher, than the earliergrowth rates. This is impossible to determine from the measurements as the absolute timescales cannot be determined. Here I have set the inflative growth rate after the insertion stop to be the same as the second growth rate, such that at the insertion stop, all the segments in the first phase switch to the second

phase while the segments already in the second phase continue their growth normally.

The reconstructed growth program is illustrated in Fig. 4.16a, where I have set the insertion stop to be lower such that it is easily captured in the diagram. In the three-dimensional growth surface, Fig. 4.16c, the insertion stop is set to 50 branches. A snapshot of the resulting ontogeny is shown in Fig. 4.16b. Here the angles are set to vary linearly from the basal to the apical side, leaving a wider angle at the basal end where the basal segment is located. I have added an outline to provide better resemblence between the model and the fossil material.

The widths of the segments is constant, although this is not the case for the segments of *Dickinsonia costata*, which vary supralinearly in width from the apical end to the basal end. There are two reasons why this is not assumed in the model. Firstly, the lack of curvature of the segments prevents the model from looking more like the fossil material if the widths are set to vary. Secondly, the model is not initially meant to capture the variation of segment widths, which is too detailed for the initial model to describe. Fundamentally the model reconstructs the growth surface of *D. costata*, which is also what is reconstructed from the measurements in Chapter 2. The shape of the growth surface is the object that can be varied between taxa, and that contains the information that I wish to study with the model. One can add extra features for the purpose of making the model appear similar to a single taxon, which can help to study the ontogeny of a single taxon. However, this would only clutter the morphospace that is used for comparison with other taxa.

Like the fourth parameter in the Raup shell coiling model, which describes the

eccentricity of the aperture of the shell, can be added later on to refine the model, a second growth surface can be added to this model to describe the widths of the segments/branches. Effectively, this would describe the lengths of the second order branches of rangeomorphs over time in a similar way as the currently model describes the lengths of the first order branches.

The assumption of constant width of the branches works well for the purpose of recreating a similar morphology. The widths of the segments are set to increase slowly over time after the insertion stop, such that the aspect ratio of the segments does not vary too much. The entire ontogeny from timestep 1 to 200 is shown in Appendix A. Here each timestep up to 100, when insertion stops, corresponds to the insertion of a new segment on either the upper or the lower side of the axis.

The model of *Dickinsonia costata* can be adapted to resemble the morphology of the other species within the genus *Dickinsonia*. For example, introducing a flattening of the growth surface while setting the insertion stop very high leads to a morphology similar to *Dickinsonia rex*. *D. lissa* can be recreated by with an even flatter growth surface and a high insertion stop. *D. tenuis* resembles *D. costata* but with the widths of the segments smaller compared to the lengths, and also a higher insertion stop. *D. brachina* is similar in morphology to *D. tenuis*.

Runnegar (1982) concluded from measurements of the length and width of many specimens of *Dickinsonia costata* that the taxon grows isometrically, i.e. the aspect ratio is preserved throughout ontogeny. This is also reflected the model of *D. costata* constructed here in the sense that the cross-sections of the growth surface at different times are isometrically related.

Figure 4.10: Measurements of twenty well-preserved specimens of *Dickinsonia* shown in a three-dimensional diagram of segment number from the basal end up and segment length versus segment count (total number of segments of a specimen). Labels refer to the numbering of specimens used in Table 2.1. The measurements can be naturally divided into three separate smooth growth surfaces such that the lengths of segments do not decrease significantly over time. The lowest, blue surface consists of specimens of the species *D. rex*, which clearly separate from the *D. costata* specimens that make up the red and green surfaces. The latter represent the boundaries of the variation found in the *D. costata* measurements. The red surface is interpreted to represent the uncontracted appearances of *D. costata* and the green surface contracted specimens, in accordance with features found in the fossils. Specimens in between the surfaces are coloured dark green.

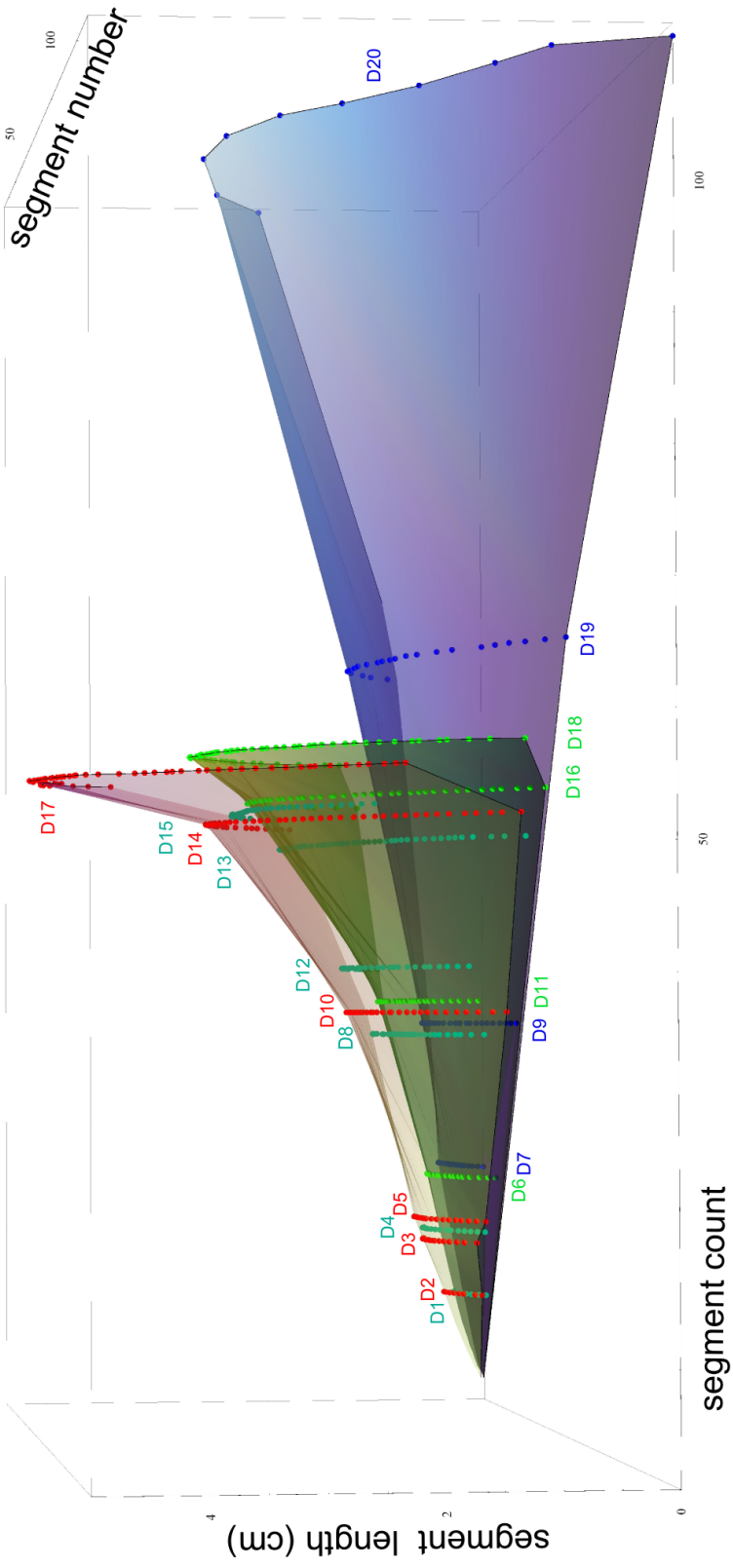

Figure 4.11: A side view of the measurements and growth surfaces presented in Fig. 4.10. The red and green surfaces, interpreted as uncontracted and contracted specimens of *D. costata* respectively, show a steepening of the slope as a function of segment count. This might indicate a decrease in segment insertion while the segments continue to inflate in size.

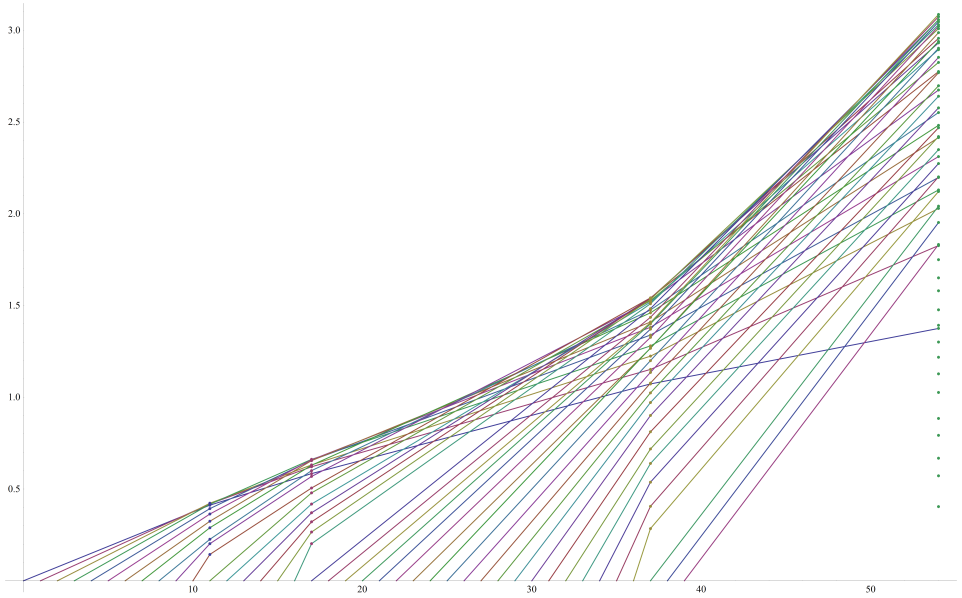

(a) Apical insertion

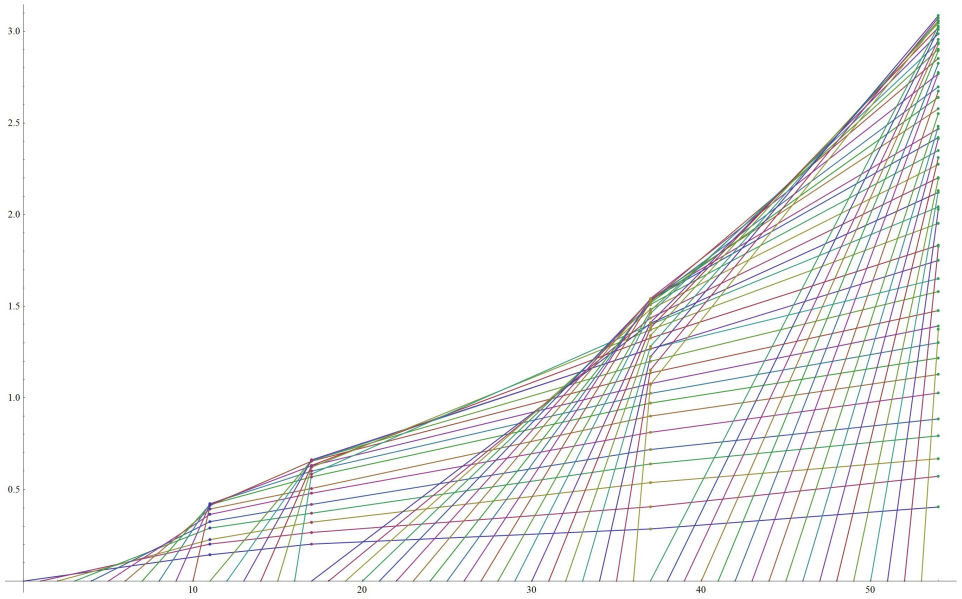

(b) Basal insertion

Figure 4.12: The measurements of the segment lengths of D2, D4, D10 and D14 seen from the side, with segment number of the specimens on the horizontal axis and segment length vertically. In (a) the segment measurements are connected based on the assumption of apical insertion. Within this hypothesis, the segments grow faster initially and later decrease their rate compared to segment insertion, so that younger segments become longer and the overal outline of the shape is rounded. In (b) the segments measurements are connected according to basal insertion. Within this hypothesis, the basal segments have the same length as the side of the basal segment when inserted, and then grow steadily at a low rate compared to the insertion rate. The upward fanning appearance of the new segments is an artefact of the low sampling. It is very striking that the apical segments, which in (b) are the first to be inserted and thus the lowest lines, line up perfectly, which is consistent with basal insertion but is not directly predicted by apical insertion.

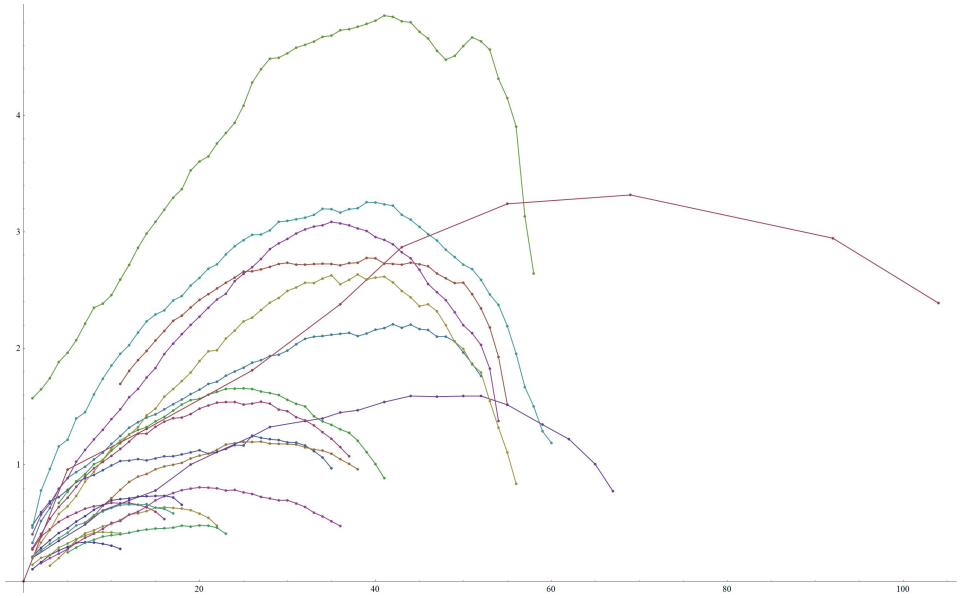

(a)

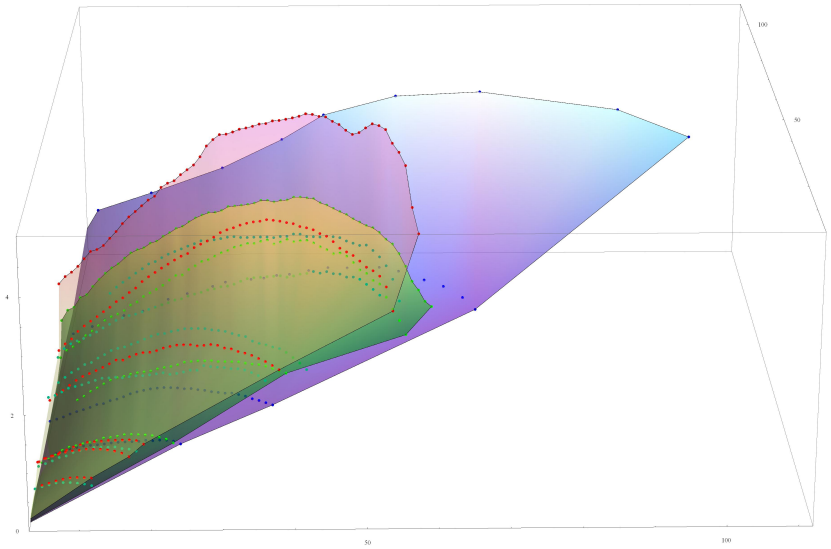

(b)

Figure 4.13: Measurements of the twenty *Dickinsonia* specimens presented with the segment number counted from the apical end, i.e. from the point of view of basal insertion. Note that the apical regions, on the left side in (a), are very similar to each other in slope and size. In (b), the measurements are again shown in a three-dimensional plot with segment number and segment count versus segment length on the vertical axis.

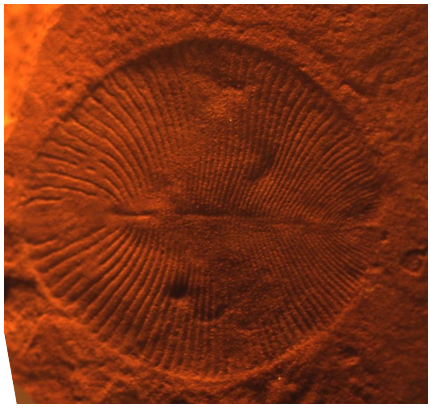

Figure 4.14: Specimen D14 arguably showing segments splitting off from the central basal segment.

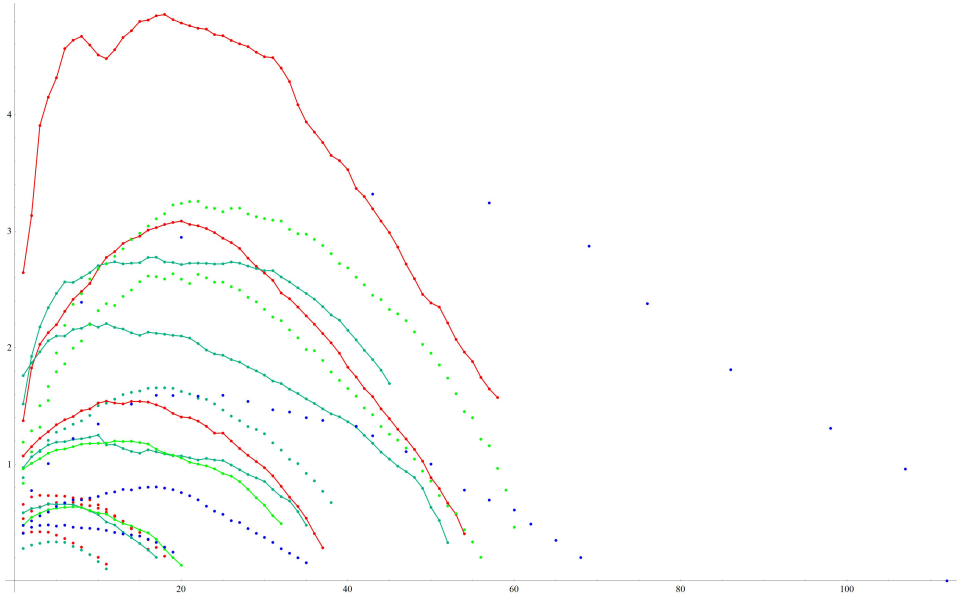

Figure 4.15: Measurements colour-coded for their position on the growth surfaces in Fig. 4.10. The connected measurements show differences in the outlines of the uncontracted specimens (red) and the outlines of the contracted specimens (green). In particular, the position of the longest segment has in many cases shifted towards the basal end of the specimen.

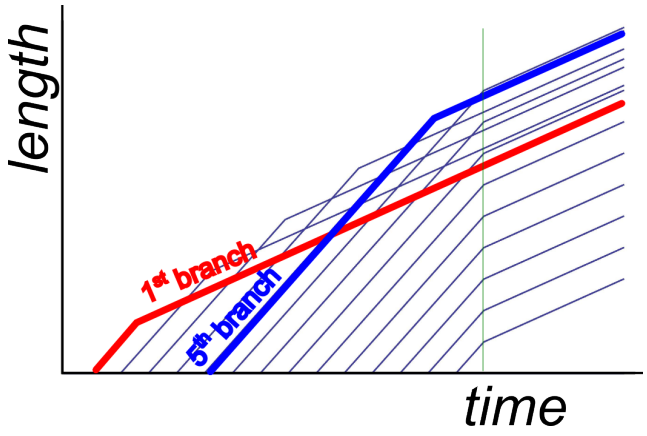

(a) Branch lengths over time of the model representing the growth of *D. costata*.

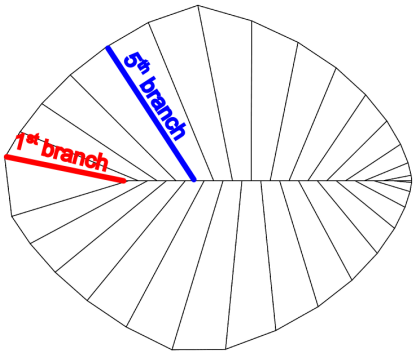

(b) A snapshot of an ontogeny generated by the *D. costata* growth model shown in Fig. 4.16a after the insertion of 15 (upper) branches.

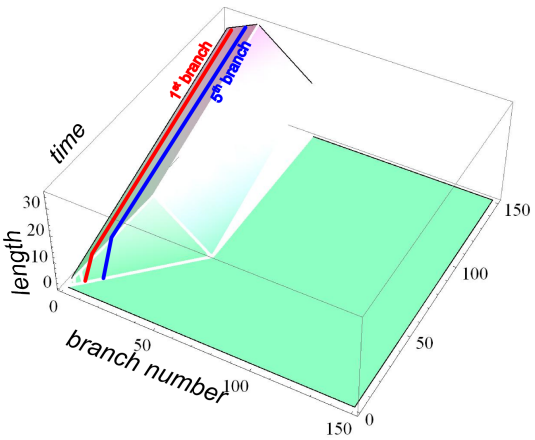

(c) Modeled growth surface of *D. costata*.

Figure 4.16: Reconstruction of the growth of *Dickinsonia costata*.

4.4 *Charnia masoni*: interpreting measurements and building a growth model

In this section I will discuss the interpretation of the measurements of four well-preserved specimens of *Charnia masoni*. Then I present a growth model based on these measurements.

4.4.1 First order growth

Fig. 4.18 shows the measurements collected in Chapter 3 of the first order branch lengths of four well-preserved specimens of *Charnia masoni* from Charnwood Forest. The measurements are red dots in a three-dimensional diagram of the branch number, counted from the most basal branch upwards on either side, the branch count of the entire specimen, and the branch lengths in cm vertically. For each specimen a model outline is drawn, given by a constant line for the basal 38% of the branches and a linear slope towards zero for the apical branches. These outlines are connected in Fig. 4.18 to form a surface. In Antcliffe and Brasier (2008), the authors pose the question whether *Charnia* grows through inflation or insertion of branches, or a combination of the two. It is concluded that both modes of growth are present, based on qualitative comparison of two specimens: the larger one of the two has more and larger branches. This conclusion is supported by the measurements shown in Fig. 4.18. The larger organisms have a larger number of branches, so branch insertion correlates with growth and the organisms made use of an insertional mode of growth. On the other hand, all branches appear to increase their length as the organism grows, suggesting that the organism grew not only

through insertion of new branches but also through inflation of the existing ones.

The three youngest specimens, A, B and C, (first three from the left in the diagram) line up with each other and with (0,0,0). The point (0,0,0) stands for zero branches and zero length. If one assumes that these three organisms adequately reflect an ontogenetic path, then one can try to predict what the organism looked like at an earlier stage of ontogeny. The fact that these three specimens line up with each other and with zero indicates that the organism started out with no first order branches and that the growth rate was linked to the insertion rate one-to-one. One option is that branch insertion rate was constant over time and branch growth was linear, but an absolute timescale cannot be derived from these measurements.

The fourth specimen, D, shown on the right in Fig. 4.18, is larger than expected for its branch count. This appears to indicate a switch in the growth program of *Charnia*, slowing down or stopping the insertion of branches while the growth of the organism continued. This switch might have occurred at a branch count of 30-35 branches (counted on both sides of the specimen). There are also alternative explanations for the observed difference. Wilby et al. (2015) reported a less detailed morphometric study of the specimens of *Charnia* found on Bed B in Charnwood Forest, including the four specimens A, B, C and D studied in this chapter. Two specimens in the assemblage, specimen D and another even larger, but less well preserved specimen, reveal a much greater size compared to their branch count. Wilby et al. argue in favour of an explanation in terms of non-overlapping cohorts. They argue that the two large specimens might have been the only survivors of a disruption

event, after which they had the bed for themselves and changed their mode of growth in response to the changed environment. The bed was then recolonised by a new cohort of younger *Charnia*, making up the smaller specimens.

If the growth of specimen D is indicative of a switch in the growth program of *Charnia*, then this switch might signify the onset of the reproductive phase. Trilobites, for example, first completed the insertion of their segments, then continued their growth inflatively for a while before starting their reproduction. Wilby et al. argue that the switch of growth mode is unlikely to respresent maturity of the specimens as there are only two specimens on the bed showing this mode, and also elsewhere large specimens of *Charnia* are rare. However, how many individuals within a given population are in a reproductive stage is a non-trivial question. Many organisms are capable of producing a large amount of offspring. For invertebrates, reproductive output is usually a linear function of the body mass, hence reproductive success depends on size and it is thus advantageous to invest in growth (Sebens (1987)). On the other hand, investing energy in growth reduces the energy available for reproduction. Also, growth takes time and hence there is a risk of mortality. If the gain in reproductive success by gaining size outweighs the risk of not surviving the time needed to grow to that size, then it will be advantageous to grow to a very large size.

The Ediacara biota lacked predation entirely, thus the life history of organisms might have looked very different than it does today. The mortality risk was given by disruptions of the environment or competition with the neighbours, which were for large part of the same species as the ecology of the Ediacara biota was not very diverse and tiered (e.g. Narbonne et al. (2014a); Liu et al.

(2013); Xiao and Laflamme (2009)). It could be that waiting with maturation until a large size was reached was advantageous for the organisms, even though only a few members survived to that stage. Especially if the neighbours on the same bed were closely related to each other, for example if they spawned at the same time from the same parent(s). In the case of asexual reproduction, neighbours might have been clones, thus the survival of one organism would ensure the survival of the genome of all the organisms. There is evidence for colonization of a bed asexually outwards by a single or a few organisms in the case of the rangeomorph *Fractofusus* (Mitchell et al. (2015)). Arguably this type of spawning is also indicated by the community succession found in Liu et al. (2013). Thus, it seems quite plausible that the two large specimens on Bed B are in fact the parents of all the other smaller *Charnia*'s on the bed.

A new observation here is the apparent division of the branches into two differentiated groups. In specimens A, B and C, the basal branches have a similar size while the apical branches decrease linearly in length towards the apex. This distinction between the two groups of branches is clear in the three measurements but it not immediately visible in the specimens. Specimen D has suffered deformation in the relevant area of the specimen so it cannot be resolved whether it follows the same model outline. In Fig. 4.17, I have drawn an outline around the specimen showing a reconstruction of the original margin. Assuming this reconstruction is accurate, the outline is similar as that of the holotype C and a similar division of the branches is expected. As will become clear when building the growth model for *Charnia*, this distinction might indicate a difference in growth phase of the individual branches.

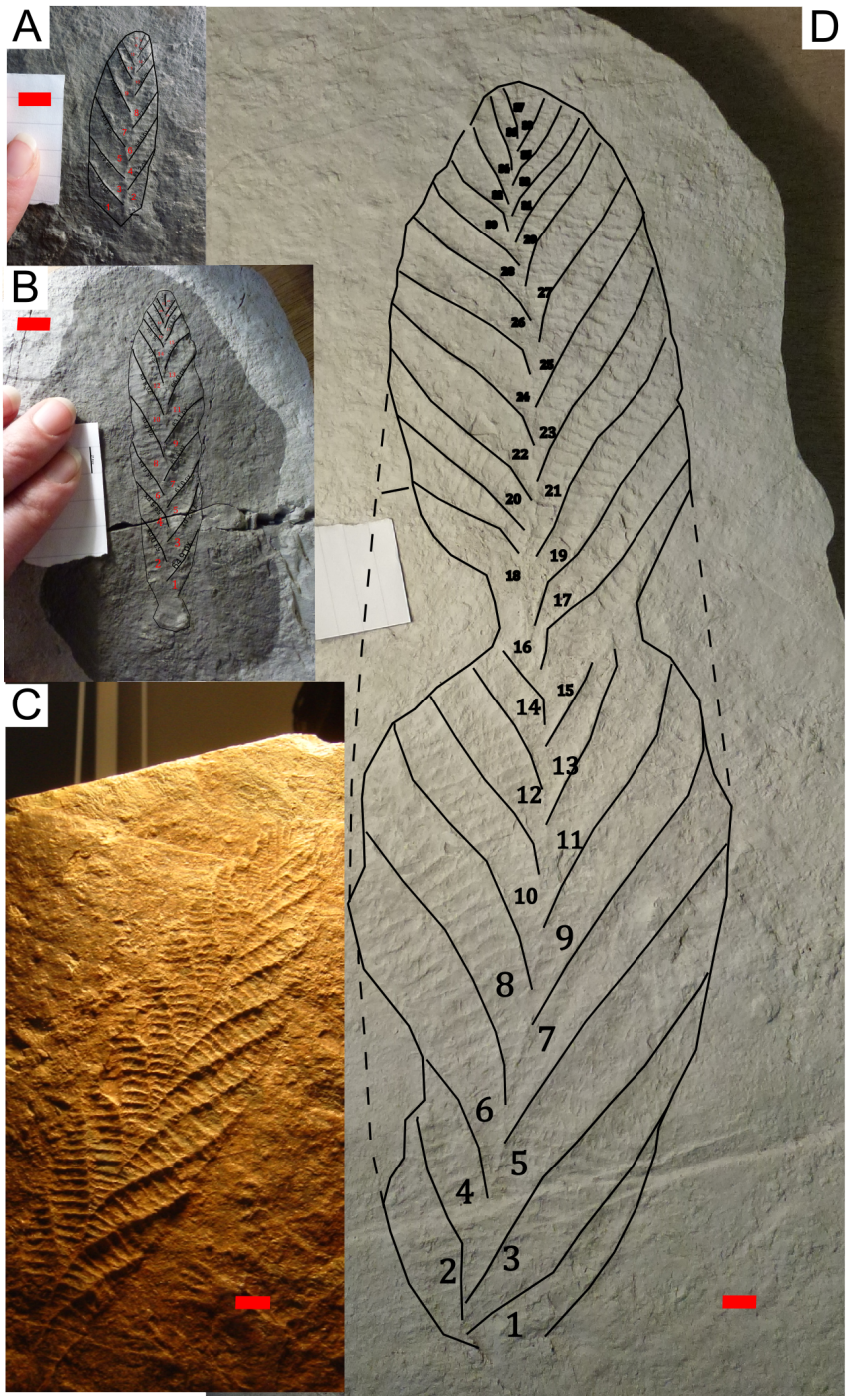

Figure 4.17: Four well-preserved specimens of *Charnia masoni* in different stages of ontogeny, all from Charnwood Forest. The red scales are 1 cm. The numbers label the branches from the basal to the apical pole of the axis and correspond to the branch numbers used in the measurements.

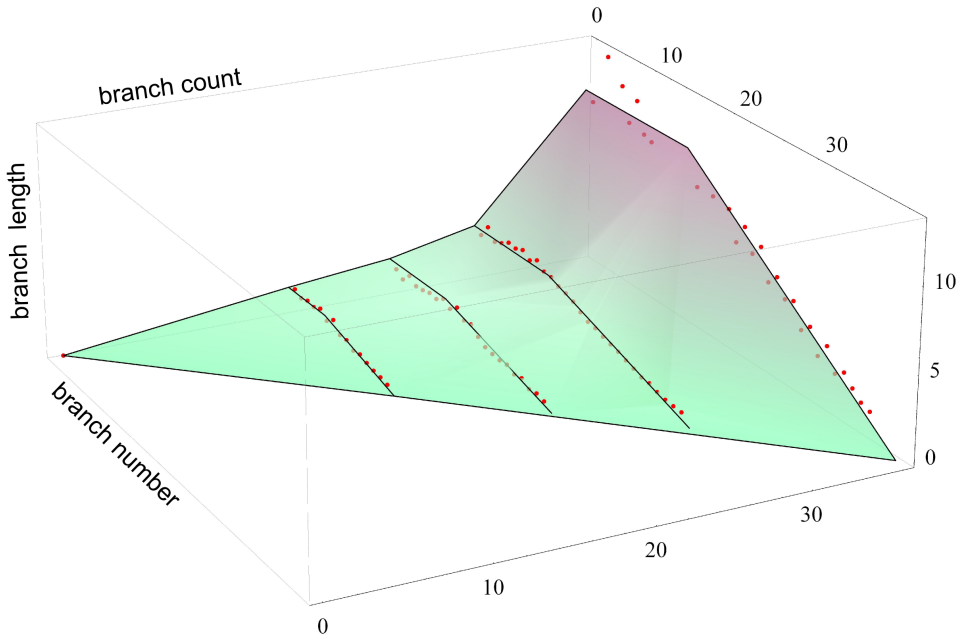

Figure 4.18: The measurements of four specimens of *Charnia masoni* shown in a three-dimensional plot with the branch number and branch count of the specimen versus branch length vertically. A growth surface is drawn through four model outlines and the point (0,0,0), which stands for a start of ontogeny.

4.4.2 Apical versus basal insertion

In Antcliffe and Brasier (2007a) it was argued that *Charnia* grows by inserting branches at its apex, based on the fact that the branches are smallest on the apical end. However, no arguments were given for why the smallest branches should necessarily be the youngest. In principle the apical branches might be smaller because they were inserted at a time when the organism was smaller, i.e. the small size might indicate they are oldest. In Fig. 4.19 the same measurements as before are plotted assuming a basal insertion program. In the side view of this plot, Fig. 4.19a, it is clear that the apical branches measured in each subsequent specimen are larger than those measured in the smaller specimens. Hence, a basal insertion program does not contradict the assumption of non-decreasing lengths for these four measurements.

If we consider the most basal branch in specimens B, C and D in Fig. 4.17, then we see that this branch is in all three cases less wide than the other basal branches, and also does not seem to have the same curving shape. One could argue that these branches are in the process of being inserted, and are thus evidence for a basal branching mode of *Charnia*. Note also that such a branch is not present in specimen A, where the most basal branch has a similar width as the one above. This can be argued to be curious from the point of view of apical insertion, as one then assumes that such an abnormal basal branch must either have been present at the start of ontogeny, or alternatively grown differently than its neighbouring branches. In order to explore the hypothesis of a basal branching pattern for *Charnia*, the presence of such an abnormal branch could be studied, as well as the lengths of the most apical branches in different stages of ontogeny. This possibility cannot be dismissed as it has

been thus far in the literature.

Another method to study basal versus apical insertion is presented by the presence of second order branches. If one can show that basal branching would imply a decrease in the number of second order branches present on a given first order branch over time, then this would be evidence against basal branching. However, this would require a reliable measurement of the number of second order branches present on a single first order branch, which is difficult as most *Charnia* specimens are not preserved in enough detail.

Note that apical and basal branching are not the only two possible modes of branch insertion. Similar arguments as I presented for *Dickinsonia*, concerning the regularity of the branches of *Charnia* and the asymmetry of its apical and basal ends, can be given to oppose alternative modes of brancing such as bipolar insertion or insertion halfway along the axis.

4.4.3 Second order branching

Comparing the growth of the first and second order branches gives us information about the self-similarity of the growth program of *Charnia*. Recently the growth of rangeomorphs such as *Charnia* was modelled in Hoyal Cuthill and Conway Morris (2014) with a self-similar Lindenmayer system (L-system) growth program, such as the ones often used to model the growth of plants (Lindenmayer (1968b,a)). Measurements of the self-similarity of rangeomorph growth can be used to test this assumed growth program.

Even though the morphology of *Charnia* appears almost[2] self-similar, this does not imply that the growth program is self-similar as well, as assumed in Hoyal

[2]Note for example that the second order branches are more alike than the first order branches as they all seem to have the same width (e.g. see Fig 4.17).

Cuthill and Conway Morris (2014). A self-similar growth program would grow in a similar way at different orders. One example of a self-similar mode of growth would be one in which division at different orders is coupled, and this is also what appears to be implied by the use of an L-system to describe growth. In such a growth model, perhaps second order branch insertion would be faster or slower than first order insertion, but there would be a simple relationship between the two. If the first and second order insertion would differ by a constant rate, then measurements of the number of first order branches versus the number of second order branches of specimens of *Charnia* would lie on a straight line such as suggested in Fig. 4.20.

Measurements of the maximal number of second order branches as a function of the number of first order branches are presented together with the surface of first order growth in Fig. 4.21. For specimens A, B and C the rate between first order insertion and second order insertion is constant. However, two interesting features appear. Firstly, the number of second order branches seem to have risen more steeply than expected in the early stages of ontogeny of *Charnia*. Secondly, the number of second order branches of specimen D is greater than expected, indicating that second order insertion has continued along with the inflation of the first order branches, while the insertion of first order branches has slowed down or ceased.

The steep rise of the number of second order branches at the early stages of growth of *Charnia* might indicate that every first order branch is already formed with a number of second order branches. This number of second order branches at the formation of a first order branch is predicted by these measurements to lie between 6 and 7. Analysis of very small specimens of

Charnia might resolve whether this is the case, such as the ones found in Newfoundland described in Liu et al. (2013). This indicates that very young specimens of *Charnia* might not look quite like the more mature organisms. The growth model constructed below features an extrapolation of the growth program from the measurements of these specimens, including their second order branch insertion. This gives some indication what the young *Charnia*'s might have looked like, although it is quite likely that the growth program changed over the course of ontogeny, so extrapolations back to a very early stage might not be reliable.

4.4.4 Smallest branches

It has been suggested that *Charnia* has more finer first order branches towards its tip than are visible in the fossils, subdividing to a degree beyond what we can observe (e.g. Hoyal Cuthill and Conway Morris (2014)). One can ask how I know that I have counted all the first order branches of a *Charnia* specimen, that there are no more finer branches that cannot be seen at the apex. The answer is simple. The first order branches decrease linearly in length towards the apical pole. If this pattern would be continued for more branches than we can see, then in specimens A, B and C, the next branch would in fact already hit the zero line and have zero length. From the point of view of an apical growth program, it might be the case that there are "budding branches" at the pole, but then these have to be in a different growth phase than the apical branches, a"phase 0". These budding branches all have to have a similar small length and the curve of branch lengths would have to make a sharp

kink to become asymptotic or parallel to the x-axis. This kink would have to take place at the branch number that I have counted as the total number of branches. Therefore it would not have any implications for the growth model to introduce these "phase 0" budding branches. Biologically, this analysis means that although we cannot rule out the further subdivision at the apex of *Charnia*, we can say that if there is further subdivision, then these budding branches have to be in a different, dormant phase before starting their proper growth.

A similar analysis can be applied to the growth of the second order branches. These all have a similar width along a single first order branch, so budding second order branches have to follow a particular growth program, where they first grow quickly to match the width of the other branches and then inflate slowly along with the other ones. Whether or not there are many dormant budding second order branches at one end of the first order branch is not relevant for the growth program nor a parameter that we can ever measure in the fossil record.

The research in this chapter shows that *Charnia masoni* had an intricate growth program. In contrast to the straightfoward model of growth that is suggested in Hoyal Cuthill and Conway Morris (2014), the branches appear to have grown in at least two distinct phases, the organism might have altered its mode of growth during its ontogeny and applied different rules at different orders.

4.4.5 A growth model of *Charnia masoni*

The growth model can now be adapted to describe the ontogeny of *Charnia masoni* based on the measurements from Chapter 3. I will assume apical insertion, but a different model can be written on the same principles that models *Charnia* with basal branching.

The model of inflative growth already describes the ontogeny quite well. I set the percentage of branches that is in the second phase compared to the first phase to 38% in accordance with the model outlines shown in Fig. 4.18. Therefore the onset of the second inflative growth phase is set to:

$$\frac{T(k)}{k} = 1/0.38 - 1 \approx 1.62 \approx \phi. \tag{4.2}$$

The first and second growth rates α and β can then be tuned accordingly, such that the basal branches still catch up with each other to a have a similar size. This happens precisely if the following equation holds:

$$\alpha \cdot \phi = \beta \left(1 + \phi\right), \tag{4.3}$$

so

$$\frac{\alpha}{\beta} = \frac{\phi}{1+\phi} = 0.62 = 1 - 0.38. \tag{4.4}$$

Interestingly this growth model for *Charnia* is uniquely defined as a special point within the morphospace (up to scale) by the condition that the basal branches are of the same size and the switch in program occurs at the golden ratio.

If one assumes specimen D to be indicative of the ontogeny of *Charnia*, then

first order branch growth appears to show a decline or stop in the insertion of branches. This will be modeled with a branch insertion stop with an onset at 35 branches in total. Again I assume that at this point all the branches switch to the second growth phase, such that the overall geometry of the morphology is preserved. The reconstructed model for the growth of first order branches is shown in Fig. 4.22a, and the three-dimensional growth surface is shown in Fig. 4.22c.

Fig. 4.22b shows a reconstuction of the morphology after the insertion of 15 branches on the right of the axis. An entire overview of the ontogeny in 50 timesteps is presented in Appendix B. At each timestep a branch is inserted on either the left or the right side of the axis, up to 35 when the first order branch insertion stops and the organisms continues to grow with an inflative mode of growth.

In this reconstruction, the angles are set to be similar and close to 30 ° from the vertical for the basal branches, and edging towards the vertical for the apical branches. This is achieved by setting the angles to be

$$\theta(x) = \frac{\pi}{6}\left(1 - x^3\right), \tag{4.5}$$

where x is more or less the fraction of the branch number relative to the total number of branches at a certain time, or more specifically,

$$x = \frac{k+1}{n+1}, \tag{4.6}$$

where k is the branch number and n is the total number of branches at a given time.

The widths of the branches are not set to be constant, but to be proportional to the branch length, plus a small time-dependent component. These values are loosely based on measurements of branch widths of the specimens.

The reconstruction in Fig. 4.22b and Appendix B also feature the growth of second order branches. These are added according to the measured values shown in Fig. 4.21. Explicitly, the number of second order branches on the largest basal first order branches equals:

$$n_2(t) = 6 + \rho t. \tag{4.7}$$

Here the time t is parameterized by first order branch insertion up to the branch insertion stop. The "6" stands for the number of "budding" second order branches that was predicted by the measurements to be present from the moment the first order branch is inserted. The insertion rate ρ of second order branches compared to first order branches was calculated from the measurements shown in Fig. 4.21 to be 0.3 second order branches per first order branch. I assume that this insertion continues at a similar pace when the first order branch insertion stops. It is suggested by the fact that in Fig. 4.21 the growth surface depicting the lengths of the first order branches and the curve representing the number of second order branches both curve upward quite steeply after the first order branch insertion stop, at the last set of measurements. Analysing the figure more closely one can see that it is actually suggested that the second order insertion rate decreases a little, as the difference in slope is greater for the surface than for the line of second order measurements. This is not modelled here.

The number of second order branches along each of the first order branches is

furthemore set to decrease slightly towards the tip as follows, in a way that is similar to the observed decrease in number of second order branches towards the apex of the specimens:

$$m(x) = \left(1 - x^4\right) + 0.02, \tag{4.8}$$

where we then set

$$k_2(k,t) = \lfloor m\left(\frac{k}{t+1}\right) \rfloor, \tag{4.9}$$

where $k_2(k,t)$ is the number of second order branches as a function of the first order branch number k and time t and $\lfloor . \rfloor$ is the floor function that evaluates to the nearest integer lower than the argument.

The second order branches of *Charnia* are in this model added at the tip of the first order branches, which is what is generally assumed, in analogy to the assumed apical insertion of first order branches. However, this is a choice and it is not derived from the measurements. Whether the second order branches are added at the tip or the base of the first order branches is an interesting question for study. The model by Hoyal Cuthill and Conway Morris (2014) assumes that the insertion is apical. This is also what one assumes when stating that the growth of *Charnia* is self-similar. Even if the *morphology* appears self-similar, the *growth* is not self-similar unless the generative zone is on the same end of the branch at different orders. The second order branches have a very similar width along a first order branch. This can be taken to indicate that at least the insertion of the branches was either apical or basal, or both, along the first order branch, as a generation in the middle presumably would create width differences at certain stages, which are not observed.

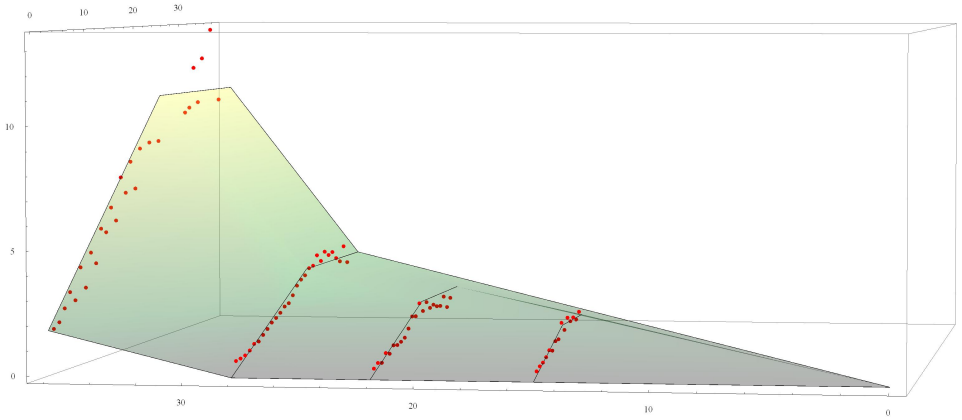

(a)

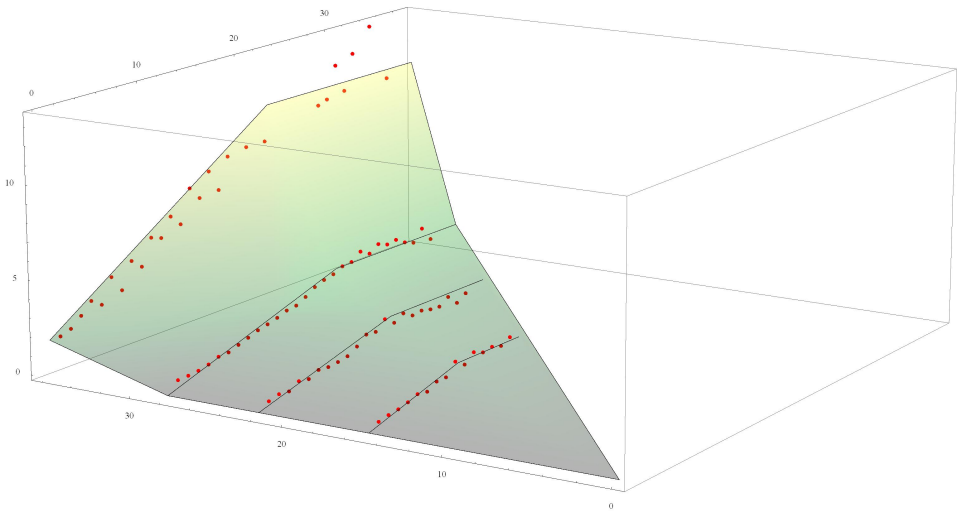

(b)

Figure 4.19: The measurements of four specimens of *Charnia* plotted with an inverted branch count axis, i.e. assuming basal insertion rather than apical insertion.

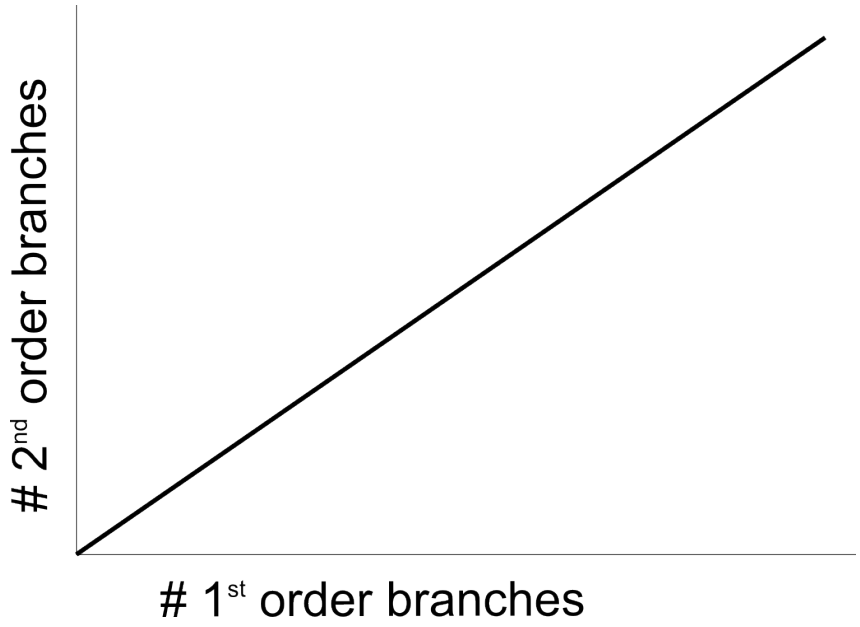

Figure 4.20: A hypothetical diagram of first versus second order branch count showing a one-to-one correspondence of the rate of insertion of the first and second order branches, as would be expected if the growth at different orders would be coupled through self-similarity.

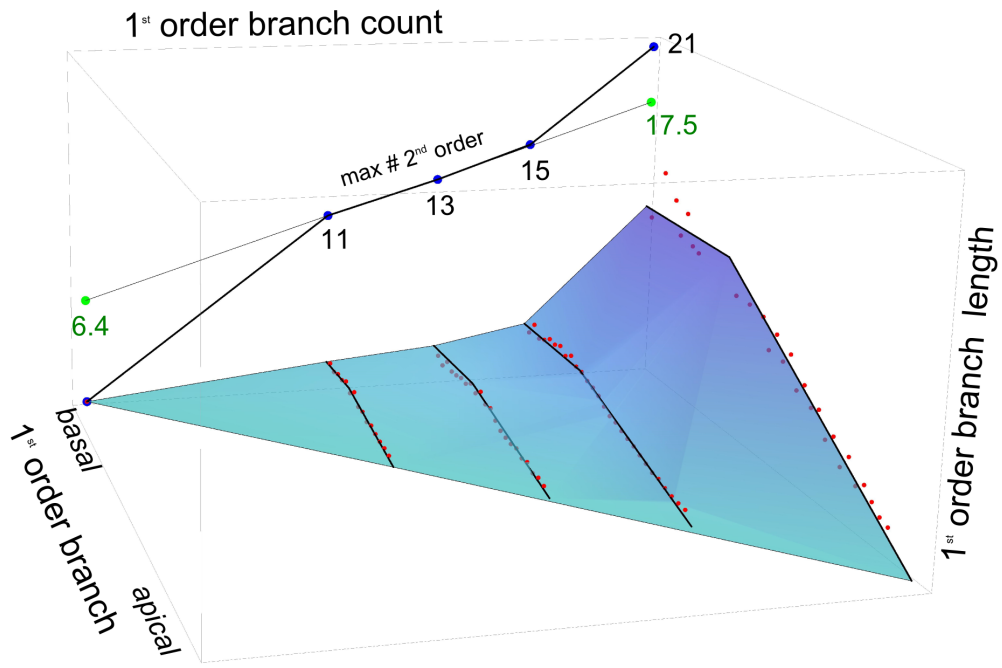

Figure 4.21: First and second order measurements shown together. The maximal number of second order branches of specimens A, B and C line up with each other, suggesting that over this period in ontogeny the addition of second order branches is coupled to the insertion of first order branches. However, A, B and C do not line up with 0, suggesting that the a number of second order branches is inserted faster in the early stages of ontogeny, or perhaps that the first order branches start out their growth with a number of second order branches in place. A, B and C also do not line up with D, suggesting that while first order insertion has slowed down in D compared to its growth, second order branch insertion has continued. The measurements are in different units thus not to the same scale.

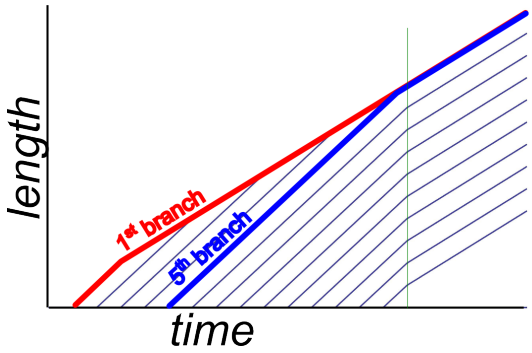

(a) Reconstructed growth program of the first order branch lengths of *Charnia masoni*. The green line represents the insertion stop, after which all branches switch to the second growth phase.

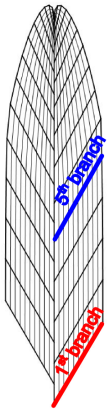

(b) A snapshot of an ontogeny generated by the inflationary growth model shown in Fig. 4.22a after the insertion of 15 (right) branches.

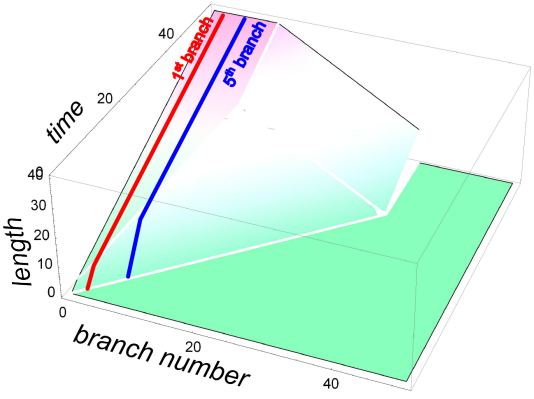

(c) Three-dimensional growth surface representing the same information as Fig. 4.22a.

Figure 4.22: Growth model reconstructing the growth of *Charnia masoni*.

4.5 Comparing the ontogeny and morphology of Ediacaran macro-organisms

4.5.1 Comparing the growth models of *Dickinsonia costata* and *Charnia masoni*

Although the morphology of *Dickinsonia costata* and *Charnia masoni* is at first sight quite different, measurements show that the growth of the taxa was quite similar. In particular, the organisms both grew through both insertion and inflation of units. As discussed in Chapter 1, this mode of growth is common for organisms with an iterated mode of growth. It therefore does not immediately imply that the mode of growth is ancestral to the two clades. However, Sperling and Vinther (2010) claims that *Dickinsonia* is set apart from other Ediacaran clades by its mode of growth because it grows through both insertion and inflation, but this does not appear to be the case.

In both clades, assuming either apical or basal insertion, each branch grows faster initially and later slows down its growth rate. The ratio of the branches in either phase remains the similar througout ontogeny, and it is similar in both taxa, around 30-40%, set to 38% in the model. *Charnia* also potentially shows a similar slowing down or stop of the branch insertion as is found in the measurements of *Dickinsonia*. Hence, the growth models for *Dickinsonia costata* and *Charnia masoni* are very similar, as is clear when comparing Fig. 4.16a and Fig. 4.22a.

Assuming apical insertion, in both taxa the duration of the first growth phase seems to be roughly the value of the golden ratio times the time it took for

the branch to be inserted initially. One might imagine that the branches are already present as "budding branches" before they start growing. In that case the ratio between the time the branches spend in the budding phase and in the first growth phase is also the golden ratio. It is not clear how this value is encoded in the biology. It is also at this point not clear whether it is coincidental or whether the appearance of this value has a biological function. Preliminary measurements of specimens of the genus *Charniodiscus* show that the relationship is not present in this taxon, at least not in the same straightfoward manner as the position of the longest branch along the axis.
The two growth models of *Dickinsonia costata* and *Charnia masoni*, by which I mean the growth surfaces in Fig. 4.16c and Fig. 4.22c that describe the branch lengths, are determined by two variables, namely the ratio of the two growth rates α and β and the insertion stop value I. I am not considering an absolute scale of the organisms. The *D. costata* model has a value $\beta/\alpha = 0.4$, which is modelled after the measurements, while for the *C. masoni* model the value is $\beta/\alpha = 0.62$, determined by the fact that the basal 38% of the branches are of similar length. Note that the higher value ratio in *Charnia* results in basal branches that grow relatively faster, and can thus be of the same length. As mentioned before, this is a special balanced point which is uniquely defined. The value of the insertion stop is set to 100 for the *D. costata* model and 35 for the *C. masoni* model.

4.5.2 Extending the model to other Ediacaran organisms

Sperling and Vinther (2010) has suggested that the vendobionts represent dif-

ferent clades because their ontogeny is different. Interpreting this in terms of a theoretical morphospace, the authors suggest that the taxa split up into distinctly different groups of organisms with different modes of growth: insertion, inflation and a combination of the two modes. The growth model presents a way to describe this theoretical morphospace. The method of measuring branch lengths as presented in Chapters 2 and 3 can be used to reconstruct the empirical growth surface, which can be used to construct the model surface. The growth model can differentiate between the inflational and insertional modes and describe a smooth spectrum in between. It also describes the geometry of the organisms in more detail. For example, it describes that the growth program for *Dickinsonia costata* and potentially also for *Charnia masoni* switches from an insertional and inflational to a purely inflational mode.

It seems to be the case for multiple other Ediacaran forms, for example *Charniodiscus* and *Dickinsonia rex*, that the relative position along the stem of the longest branch, potentially representing the growth phase switch of the branches, remains the same throughout ontogeny. This ensures that the overall geometry of the body is preserved. It should be noted that this constant ratio of longest branch number versus total branch number, represents a balance in the growth program between the insertion rate and the duration of the first growth phase. Assuming a constant rate of branch insertion over time, up to the insertion stop, this balance translates itself in the growth model as a linear form for the duration of the first growth phase, so $T(k) = \gamma k$ for some constant γ. For *D. costata* and *C. masoni* the value of γ is about 1.6. If for example *Charniodiscus* can be described by the growth model then γ has

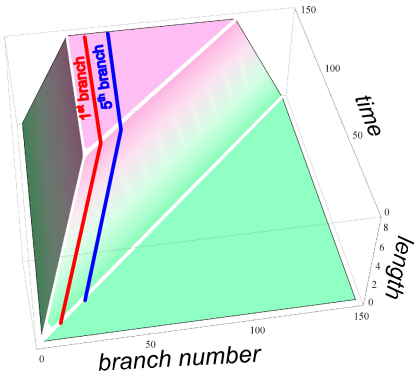

(a) A flattened growth surface.

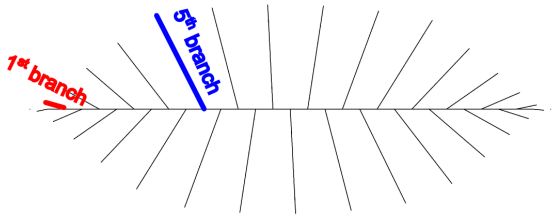

(b) The resulting morphology after the insertion of 15 upper branches.

Figure 4.23: A generalization of the growth model introducing a flattening of the growth surface allows for the description of a *Fractofusus*-like morphology.

to be between $2.3 - 4.6$. This represents the fact that the longest branch of *Charniodiscus* is closer to the basal end of the organism, at $18 - 30\%$ of the number of branches.

The model can be described by three parameters, namely the insertion stop I, the ratio between the two growth rates β/α, and the rate at which the duration of the first growth phase increases with branch number, γ. There are a number of taxa, such as *Dickinsonia lissa*, *Dickinsonia rex* and *Fractofusus*, that have smaller branches at both the basal and the apical end, but whose middle branches are all of similar size. To model this, a single new parameter can be introduced to the model, that regulates a flattening of the growth surface, in the way that is represented in Fig. 4.23a. The parameter is given by the time F at which the flattening initiates. This new parameter can be used to construct a growth model for *Fractofusus*, of which a snapshot is shown in Fig. 4.23b.

How well do the growth models built here for *Dickinsonia costata* and *Charnia masoni* describe the behaviour observed in the measurements? The growth

models fundamentally describe the shape of the three-dimensional growth surfaces, which in turn describe the branch lengths as a function of time and branch number. This information can be compared with the growth surfaces found through the measurements of *Dickinsonia costata* and *Charnia masoni*. However, the measurement surfaces are parameterized as a function of the branch count, whereas the growth model is given as a function of time. Up to the insertion stop the models assume that one branch is inserted per unit of time, so we know how to translate from one to the other. After the insertion stop we do not know what the relationship between time and growth is, but we can assume that the growth continues at a constant rate. Considering this, we can translate between the measurement and model growth surfaces and evaluate how well the two match. For *Charnia masoni*, the match is very good, as each of the sets of measurements is already described quite well by an outline taking the shape of a flat plateau on the basal side, and decreasing linearly towards the apical end. This is also what the cross sections of the growth model surface look like. Hence the growth model surface is similar to the measurement surface. The *Dickinsonia costata* measurements mainly show a more rounded surface, both in terms of the outlines at each point in time, indicating that the switch between the first and second growth phases of each segment is not as abrupt, and the fact that the insertion seems to slow down over a period instead of stopping abruptly.

A study of similarities and differences of the ontogeny of different Ediacaran clades can help us to study macroevolutionary trends within the late Ediacaran macrobiota, a major open problem (e.g. Xiao and Laflamme (2009)). With the use of the growth model, characters of growth can be defined, next to the mor-

phological characters that were given in Brasier et al. (2012) for rangeomorphs, and are extended to dickinsoniomorphs at the beginning of this chapter. These can be analysed to study the phylogeny and macroevolutionary trends of the Ediacaran macrobiota. For example, the mode of growth can be determined to be insertional, inflational, or a combination of the two modes. The value of the insertion stop I allows for a continuous spectrum of modes between the combined mode and the inflational mode. On the other hand, lowering the second growth rate to zero, hence the parameter β/α to zero, creates a continuous spectrum of growth modes between the combined mode and the insertional mode of growth. So determining this parameter for Ediacaran taxa allows us to determine whether a continuous spectrum of modes of growth is present in the Ediacara biota or a distinct modes as suggested by Sperling and Vinther (2010). Measurements of a number of well-preserved specimens in different stages of ontogeny, such as is presented in Chapters 2 and 3, is can be used to establish these ontogenetic characters. But as we have seen in these chapters, every such analysis can be very valuable for the study of the species itself, and reveal new insights into the biology of each taxon.

4.5.3 Other aspects of Ediacaran morphology

The late Ediacaran macro-organisms share many similarities in their morphology. In particular, the dickinsoniomorphs and rangeomorphs share a "quilted' morphology with a body that is divided into many segments or branches (Fedonkin (1998); Seilacher (1989); Brasier and Antcliffe (2004), see also Fig. 4.24). All the structures referred to by Seilacher as "quilted pneu" structures are referred to as branches from the point of view of the growth model. The

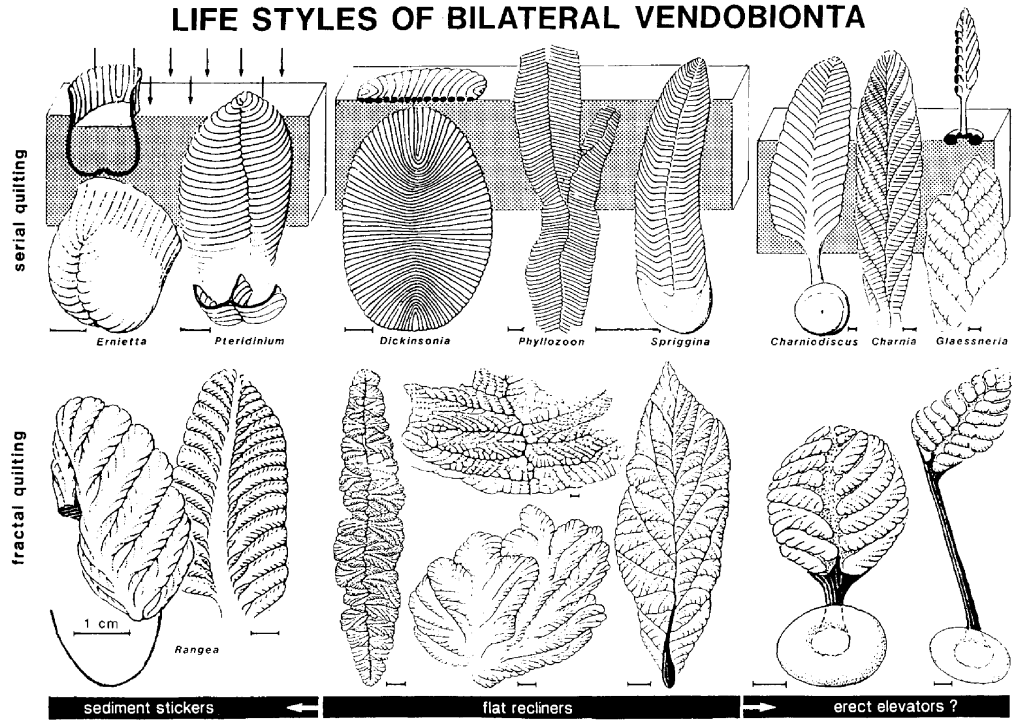

Figure 4.24: Mode of "quilting", i.e. first order or higher order branching, versus mode of life of various Ediacaran macro-organisms. Although the terminology from Seilacher is adopted here, no phylogenetic affiliations are assumed in the construction of the growth model. Seilacher (1992) fig. 1.

fact that the branching structures of different clades are morphologically similar does not automatically imply that they are homologous. The similarities could be due to convergence, for example because this body structure gave a selective advantage for the mode of life of the different taxa individually. In this section I will review the morphologies present within a subset of the Ediacara macro-biota given by the rangeomorphs and dickinsoniomorphs, as well as discussing the morphology of some members of the erniettomorphs, arboreomorphs and bilateralomorphs as defined in Erwin et al. (2011a) and Laflamme et al. (2013).

Within both the rangeomorphs and the dickinsoniomorphs, organisms possess a central axis from which the branches originate. For some taxa these branches lie within a plane, to either side of the axis, similar to a leaf, for example in *Charnia* and *Dickinsonia*. In other taxa the branches sprout from the axis within multiple planes oriented rotationally around the axis and referred to as "vanes" (rows in Brasier et al. (2012)). There are six of these for the taxon *Rangea* (Vickers-Rich and Ivantsov (2013)), three for *Pteridinium* (Seilacher (2007a)), and potentially three for *Fractofusus* (Narbonne et al. (2014b)). For other taxa, such as the rangeomorph *Bradgatia*, it remains unclear whether a central axis of growth is present, although it has been suggested based on the similarity to other rangeomorphs (Brasier et al. (2012)).

The primary morphological character on the basis of which rangeomorphs are distinguished from dickinsoniomorphs, erniettomorphs and arboreomorphs is the mode of branching. Whereas the branching or segmentation pattern of dickinsoniomorphs only features segments radiating from the central axis, the branches of rangeomorphs generally individually subdivide further into "higher

order" subbranches. The taxon *Charniodiscus*, the key taxon in the arboreomorphs, shows a single order of branching but is morphologically very similar to *Charnia* and other rangeomorphs. It possesses an upright morphology and a holdfast. It has therefore often been compared or grouped with rangeomorphs. It is grouped with rangeomorphs in Fig. 1.2.

It has been noted in recent years that there are many differences between the different groups of Ediacaran macro-organisms that have been separated as potentially monophyletic over the past years (i.e. Laflamme et al. (2013); Xiao and Laflamme (2009); Erwin et al. (2011b)). Dickinsoniomorphs generally represent later times and shallower deposits, see Fig.1.2. The rangeomorph *Rangea* is an exception to this rule as it is mostly associated with the later and shallower Namibian taxa such as *Ernietta* and *Pteridinium*. Also the position in the sediment of rangeomorphs and dickinsoniomorphs generally differs, see also Fig. 4.24. Whereas many rangeomorphs, apart from a number of taxa such as *Fractofusus*, are thought to have held an upright position, reaching upwards from the sea floor (e.g. Clapham and Narbonne (2002)), *Dickinsonia* is thought to have laid flat on the sediment, and *Pteridinium* and *Ernietta* had an endobenthic lifestyle (Grazhdankin and Seilacher (2002)). The rangeomorph *Rangea* is also thought to have lived endobenthically (Seilacher (2007a); Vickers-Rich and Ivantsov (2013)). Dickinsoniomorph *Swartpuntia* might have held a position more similar to rangeomorphs, as suggested by the reconstruction by Narbonne et al. (1997). A different reconstruction by Brasier shown in Fig. 4.25 visualizes *Swartpuntia* as a three-vaned version of *Dickinsonia* with one vane standing upright (Brasier, pers. comm.). The overall geometry of this new reconstruction, with two vanes to either side and

a third vane standing upright into the water column, is similar to the new reconstruction for a three-vaned *Fractofusus* by Narbonne et al. (2014b).

Dickinsonia and *Yorgia* have been associated with feeding traces, as discussed in Chapter 2, which has implications for their inferred ecology. It has been taken as potential presence of musculature (Gehling et al. (2005)), although the discussion in section 2.4 suggests that the traces could also be generated semi-passively. No such traces have been associated with rangeomorphs, erniettomorphs or bilaterianomorphs. *Dickinsonia* is also the only Ediacaran genus showing signs of contraction (e.g. Runnegar (1982); Wade (1972)), which has been taken either to indicate the presence of musculature (Gehling et al. (2005)), or the passive post-mortem deflation of a fluid-filled body (Brasier and Antcliffe (2008); Seilacher (1989)). The results from section 4.3 can be taken as evidence for the latter, as measurements show that the degree of contraction correlates inversely with the width of the segment, which is consistent with a hydrodynamic model of the deflation of fluid-filled elastic units. However, this find is not necessarily inconsistent with contraction as the result of musculature.

4.5.4 Characterizing rangeomorph and dickinsoniomorph morphology

Brasier et al. (2012) introduced a system for describing rangeomorph morphology through a set of morphological characters. I discuss a subset of these below and extend them to the dickinsoniomorphs where possible.

Brasier et al. suggest the concept of rotated and furled branches that is illustrated in Fig. 4.26. The first order branches of *Charnia* do not seem to have

(a) (b)

Figure 4.25: Reconstruction of *Swartpuntia* as a dickinsoniomorph with three vanes, from drawings of a specimen of unknown origin. Drawing and reconstruction by Martin Brasier (unpublished).

second order branches on either side, but we see only one row of second order branches. Brasier et al. proposed that this reflects that the first order branches are rotated such that we see only one side of the second order branches that attach to it, as shown in Fig. 4.26 **E**. Such a mode of growth would create extra external surface area, but this area would be rotated inward. This character is not meaningful for dickinsoniomorphs as higher order subdivision has not been observed so we cannot see the orientation of the first order branches. In Fig. 4.26 they correspond to **H** and **I**, just like *Charniodiscus*.

Furling refers to the way the branches of rangeomorphs such as *Charnia* are "tucked away" into the creases between the branches, as opposed to the apparently freely moving branches of for example *Bradgatia* (see Fig. 4.26). Dickinsoniomorph segments also seem to be rounded and attached (e.g. Seilacher (1989)), so one could say that dickinsoniomorphs have furled branches.

Another important concept emphasized in Brasier et al. (2012) is the concealment of the stem or growth axis that occurs in some rangeomorphs such as *Charnia* and *Fractofusus*, but not in others such as *Charniodiscus* and

Avalofractus. The concealment creates a zig-zag suture along the central axis behind which a "stem" is potentially concealed. As noted by Seilacher (1989), *Phyllozoon* also has a zig-zag suture where one expects a stem to be, whereas it does only have one order of branching. So one might say it also has a concealed stem. This is not the case for some other dickinsoniomorphs such as *Dickinsonia*. *Phyllozoon* is grouped with either dickinsoniomorphs (Brasier and Antcliffe (2004)), or alternatively with the erniettomorphs (Laflamme et al. (2013)), and is found in similar settings as *Dickinsonia* in Russia and Australia (Brasier and Antcliffe (2004)).

The presence of a holdfast is another discrete character in the analysis of Brasier et al. (2012). Taxa such as *Charniodiscus* and *Primocandelabrum* clearly posses a holdfast. For other taxa such as *Charnia* the holdfast is less clear but presumably present (Brasier et al. (2012)). Seilacher (1989) homologized the "head" of *Spriggina* with the holfasts of rangeomorphs. One might push this idea further and suggest a homology between the axis/holdfast of *Charnia* and *Charniodiscus* and the axial bulb of *Rangea* (as described in detail in Vickers-Rich and Ivantsov (2013)) and possibly also the axis and basal segment of *Dickinsonia*. This would fit in the growth model as these features are all central with a larger structure at the basal end, opposite the proposed generative zone if one assumes apical insertion. However, this does not imply a biological homology and further research is needed to make this claim.

The angles at which the first order branches depart from the stem in rangeomorphs is considered another character in Brasier et al. (2012). In many rangeomorphs such as *Charnia*, *Rangea* and *Avalofractus*, the branches are more or less parallel at the basal end of the organism and make a more acute

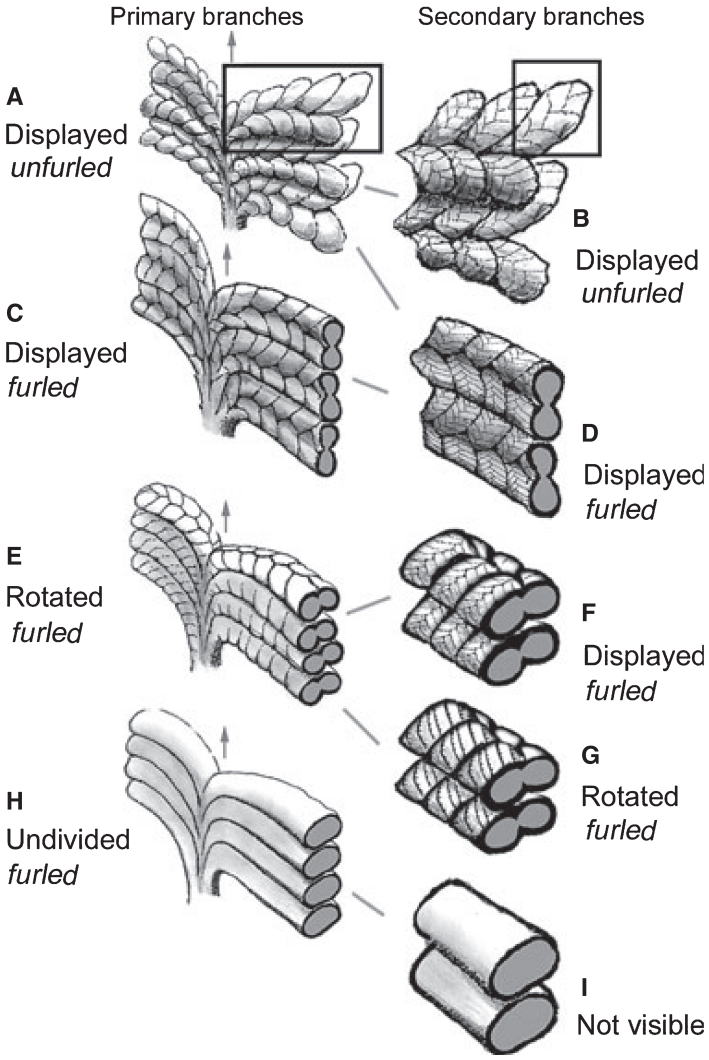

Figure 4.26: An illustration of the characters *displayed* versus *rotated* and *furled* versus *unfurled*. Each of the shown combinations is observed in the fossil record. **A-B** is present in mature specimens of *Bradgatia*; **C-D** is present in juvenile specimens of *Bradgatia*, suggesting that the branches "unpack" as they reach maturation; **E-F** is present in *Beothukis*; **E-G** is present in *Charnia*; and **H-I** is present in *Charniodiscus* and I suggest here that it is also present in dickinsoniomorphs. From Brasier et al. (2012).

angle towards the apical end, such that there is no open space left over at the apical end of the organism, which there would be if all branches were parallel. In other rangeomorphs such as *Bradgatia* the angles vary more along the stem or branch. This is referred to as radiate in the model by Brasier et al. (2012). In many dickinsoniomorphs, such as the different species of the genus *Dickinsonia*, a similar set of angles can be seen at the apical end, but in these taxa the basal branches do not curve upward but instead also close the gap to the basal segment by curving downward. As the angles vary continuously along the axis, they are mostly perpendicular to the axis more or less halfway along.

As the organisms were soft-bodied, the angles of the branches tend to vary with preservation. In fact, the precise angles and curvature seem to have been determined by hydrostatics of the elastic body structure. This is supported by the manner in which the segments or branches tend to change their form and angle but not their size or surface when folded or overlapping some relief, see for example the specimens in Brasier and Antcliffe (2008), fig. 1, 2 and 8. In principle this hypothesis could be tested with computer modelling. One could program boundary conditions for fluid-filled rods that are attached laterally, the "quilted pneus" of Seilacher, and one could numerically solve hydrostatic equations to see whether they would indeed display the curvature and angles observed in the morphology of dickinsoniomorphs and rangeomorphs. In the model I have regarded the angles and curvature as non-essential for the morphology. The branches are approximated as straight features, as programming curved branches would have a great cost on the time needed to render the figures. Continuously radiating angles of branches are added for the models of

Dickinsonia and *Charnia* in a way that is similar to their fossil appearance. Brasier et al. (2012) furthermore discuss the shape of the outline of the organism, which is referred to as "inflation". This character can be taken to mean the position of the longest branch along the stem. Proximal refers to a position of the longest branches at the basal end, distal refers to a position towards the apical end, medial refers to a position roughly halfway along the axis and moderate inflation means that the branches are more or less of the same length along the axis. Measurements in Chapters 2 and 3 show that in fact there is a lot more information about morphology and ontogeny hidden in the branch lengths and the position of the longest branches along the stem. The lengths and widths of the branches together determine much of the outline and appearance of the fossil.

4.6 Discussion

Serial growth by means of the repetition of iterated features is a common phenomenon among multicellular organisms, and even single-celled foraminiferans form tests with repeated chambers. The giant ciliate *Zoothamnium* gives an example of a colonial iterated mode of growth. Molecular data suggests that this mode of growth in plants and other bikonts evolved independently from that in animals (e.g. Gold et al. (2015)), thus it evolved at least twice, but potentially a number of times independently.

Many of the Ediacaran macro-organisms have a share a similar body plan with a central branching axis around which rounded branches ("quilts") are displayed, which make up the entire body of the organism, except for a central basal feature such as a basal segment or a holdfast in some clades (see

Fig. 4.24). Is this mode of division into repeated units in Ediacaran macroorganisms an ancestral feature of these clades? Table 4.1 gives a list of morphological, environmental, biological and ontogenetic characters that were discussed in the previous sections. It gives examples of taxa within the dickinsoniomorphs, erniettomorphs, arboreomorphs and rangeomorphs possessing these characters.

Most of the given characters are not limited to a single group. In particular, the number of vanes, rows of branching distributed radially around the growth axis, varies both in the fractally branching rangeomorphs and in the serially branching erniettomorphs. These vanes were shown to have an exchangeable biological function in the taxon *Pteridinium*. Grazhdankin and Seilacher (2002) described cases where the three vanes, which form a boat-like shape in the taxon with all three pointing vanes upwards, had interchanged places, rotating around the axis by a third. Also the vanes in the rangeomorph *Rangea* appear very similar, according to the symmetric reconstruction in Vickers-Rich and Ivantsov (2013). The presence of multiple vanes with a similar biological function has no analog in modern taxa, and is particularly not present within Bilateria.

It is striking that the number vanes appear to vary within groups of taxa that are currently thought of as monophyletic, such as the rangeomorphs, which are grouped together because of their intricate fractal mode of branching. This flexibility in developmental program is in stark contrast with the bilaterian symmetric body plan, which has been preserved consistently for over 500 million years. This does not necessarily imply that either of the Ediacaran groups cannot be ancestral to the biletarian body plan, since the appearance of extra

vanes could be a lost pathway in bilaterian evolution. However, its presence within both fractal and serially branching Ediacaran forms, while similar features are not readily found within in other organisms with ordered growth, suggests an ancestral origin of the "vendobiont" branching morphology.

Sperling and Vinther (2010) suggest that the similarities in Ediacaran morphology are not reflected in ontogeny. The authors argue that distinct modes of growth are present: inflational (*Fractofusus*, *Charniodiscus*), insertional (*Pteridinium*) and a combination of the two (*Dickinsonia*). Measurements in this thesis show that the ontogeny of *Charnia* shows similarities with that of *Dickinsonia*, contradicting the argument that *Dickinsonia* is set apart by its mode of growth. The growth model and the resulting morphospace in this chapter furthermore shows that it is possible to move between these three modes can be connected in a continuous way and in fact should be thought of a continuous spectrum of modes. It remains to show whether this morphospace of modes of growth is indeed filled in a continuous manner by clades in the Ediacara biota. A similar variation of modes of segmentation is found in arthropods. Fruit flies form their segments at an embryonic stage and grow inflationally, while many other arthropods insert segments over their lifetime while growing, displaying a mode of an insertional an inflational mode of growth. Thus dissimilarities in ontogeny do not always imply a non-homologous developmental program.

One could argue that the similarities in morphology and ontogeny between Ediacaran organisms could be convergent. The environment of the Ediacaran seas was very different from modern environments, thus perhaps a fine branching morphology was a selective advantage in these environments, and was thus

acquired multiple times. However, in recent years the Ediacaran clades have been shown to be set apart in palaeoenvironment (e.g. Grazhdankin (2004); Gehling and Droser (2013)), palaeoecology (e.g. Liu et al. (2014); Droser et al. (2006)) and metabolism (e.g. Laflamme et al. (2009)). The life positions varied between the clades, from an endobenthic to an upright position (see Table 4.1), and hence the mode of life must have differed between Ediacaran clades. It is unlikely that a similar morphology would be preferred in each of these modes of life. Hence it is more likely that the branching pattern was ancestral to the clades, and derived and adapted in different settings to suit different modes of life.

Table 4.1: The table below gives a list of morphological, environmental, biological and ontogenetic characters and marks whether there is a taxon within the dickinsoniomorphs, erniettomorphs, arboreomorphs and rangeomorphs possessing the character.

Characters	Forms with 1 order of branching			Forms with fractal branching
	Dickinsoniomorphs	Erniettomorphs	Arboreomorphs	Rangeomorphs
morphological characters				
2 vanes	*Dickinsonia*	*Phyllozoon*	*Charniodiscus*	*Charnia, Avalofractus, Beothukis...*
>2 vanes		*Swartpuntia, Pteridinium*		*Rangea, Fractofusus?*
axis displayed	*Yorgia*		*Charniodiscus*	*Avalofractus*
axis concealed		*Phyllozoon*		*Charnia, Fractofusus,*
symmetry across axis	*Dickinsonia?*			-
off-set symmetry	*Yorgia*	*Phyllozoon*	*Charniodiscus*	*Charnia,...*
life position				
upright		*Swartpuntia?*	*Charniodiscus*	*Charnia*
sediment reclining	*Dickinsonia, Yorgia*	*Phyllozoon?*		*Fractofusus*
endobenthic		*Ernietta, Pteridinium*		*Rangea*
environment				
shallow	*Dickinsonia,...*	*Ernietta,...*		*Rangea*
deep			*Charniodiscus*	*Charnia,...*
movement				
feeding traces	*Dickinsonia, Yorgia*			
contraction	*Dickinsonia*			
ontogeny				
only insertion		*Pteridinium?*		
only inflation			*Charniodiscus?*	*Fractofusus?*
inflation and insertion	*Dickinsonia*			*Charnia*
insertion stop	*Dickinsonia*			*Charnia?*

Part II

Mathematical methods to distinguish biological and abiological fossilised morphology

Chapter 5

Testing an abiotic formation hypothesis for the trace fossil *Paleodictyon*

Abstract

Paleodictyon is an iconic trace fossil found in deep-marine, shallow-marine and lacustrine sediments from a Cambrian age to the present day. It consists of a hexagonal relief network that occasionally shows perfect regularity. Despite extensive study, no organism has yet been identified as creator of the *Paleodictyon* trace. In light of this, and its unusual shape and broad environmental tolerance, *Paleodictyon* has been speculatively interpreted to (also) arise from a physical mechanism instead of a biological cause. The phenomenon of a Faraday wave, a standing wave on a plane, is both capable of forming hexagonal lattice patterns, and can plausibly occur in the environments in which

Paleodictyon is observed. An experiment inducing a hexagonal waveform in a calcium carbonate paste showed that a hexagonal relief pattern was indeed preserved on the sediment surface after a short excitation. It is not yet clear whether the Faraday waves can form a network of tunnels, although this can be made plausible using computer simulations of the waveform and its nodes and velocities. Measurements from experiments inducing a Faraday wave in non-submerged fine-grained siliceous pastes show a square root relationship between the diameter of the hexagons of the excitation and the width of the regions that form the ridges between hexagons in the excitation. A review of measurements from the literature reveal a similar square root relationship is present in fossil specimens of *Paleodictyon*. Some occurrences of *Paleodictyon* and potentially also other very regular graphoglyptids may have been formed by subaquaous Faraday waves. A list of criteria is proposed to distinguish between biogenic and abiogenic trace fossils with regular geometry.

Figure 5.1: Example of *Paleodictyon nodosum* from the Eocene. Note the incredible regularity of the hexagonal pattern. In some areas only the mid-edge points of the hexagons are elevated. Picture from Rona et al. (2009).

5.1 Introduction

Paleodictyon (Murchison et al. (1850)) is a trace fossil famous for its mystery. It has been studied extensively and appears as a key taxon in many standard works in ichnology such as Seilacher (2007b); Ekdale et al. (1984); Bromley (1990). The ichnogenus *Paleodictyon* consists of a regular or distorted hexagonal pattern and is captured in fossilised sea beds from the Cambrian to the modern day. An example is shown in Fig. 5.1. *Paleodictyon* is most commonly found in flysch deposits from abyssal depths, but has also been described in shallower deposits (Paczesna (1985); Jensen et al. (2013); Stanley and Pickerill (1993); Metz (2012); Fursich et al. (2007); Hantzpergue and Branger (1992)) and lacustrine palaeoenvironments (Archer and Maples (1984); Pickerill (1990); Lan and Chen (2010)). It is commonly interpreted to have consisted of a tunnel network, preserved through distal turbidite flows,

on the lateral margins of a turbidite deposits where only a thin layer of fine sediment is deposited, and the predepositional sediment remains fairly undisturbed (Ekdale et al. (1984); Ekdale (1985)). The hexagonal tunnel system of *Paleodictyon* is then cast by an influx of the turbiditic sediment which preserves the pattern as a positive epirelief impression.

Paleodictyon is a commonly observed member of the *Nereites* ichnofacies, an assemblage of trace fossils associated mainly with deep sea flysch deposits (Seilacher (1967)). It belongs to the graphoglyptids, group of complex geometrical trace fossils. This group includes the ichnotaxa *Cosmoraphe*, which forms a regular meandering pattern (Fig. 5.3A), and *Spiroraphe*, which forms an Archimedean spiral (Fig. 5.3F, Fig. 5.4). These complex geometrical patterns are often collectively described as agrichnia (from the Greek agricola for farmer) because of a modern interpretation of these patterns as traces of burrowing animals "farming" bacteria in the tunnels of their burrows, which they then revisit frequently to collect organic matter for sustenance (Ekdale et al. (1984); Seilacher (2007b)). This hypothetical behaviour would explain how these organisms thrive in very oligotrophic deep sea conditions (Olivero and Lopez (2010)).

In the seventies, a modern version of *Paleodictyon* was discovered in pelagic deep-sea sediments during a series of deep-sea dives in the Atlantic and the Pacific (Rona and Merrill (1978); Ekdale (1980)). A thorough study of multiple specimens from the Atlantic mid-oceanic ridge led by Peter Rona (Rona et al. (2009)) showed that the modern examples consist of a hexagonal network of tunnels, with vertical tubes halfway along the edges of each of the hexagons connecting the tunnel network to the surface of the sediment. These features

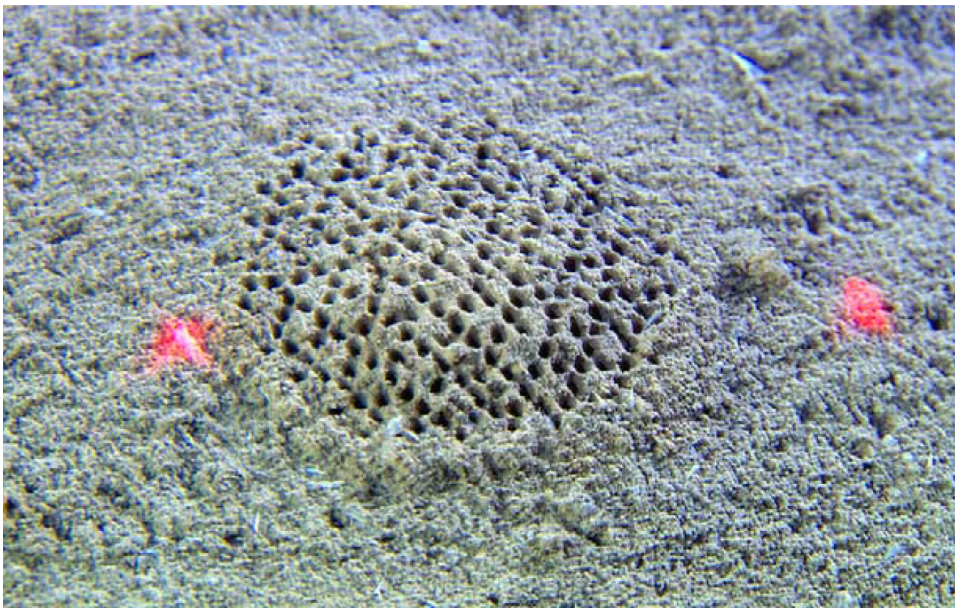

Figure 5.2: A photograph of a modern pattern similar to *Paleodictyon* found near the Atlantic mid-oceanic ridge by the submersible *Alvin*. The holes are vertical tunnels that appear halfway the edges of the hexagonal pattern that is hidden a few millimeters below the surface of the sediment. The sediment is flocculate and compressible. Therefore the tunnel walls could potentially be formed through compression of the material without an agglutinating agent. The red laser lights indicate a separation of 10cm. Picture from Rona et al. (2009).

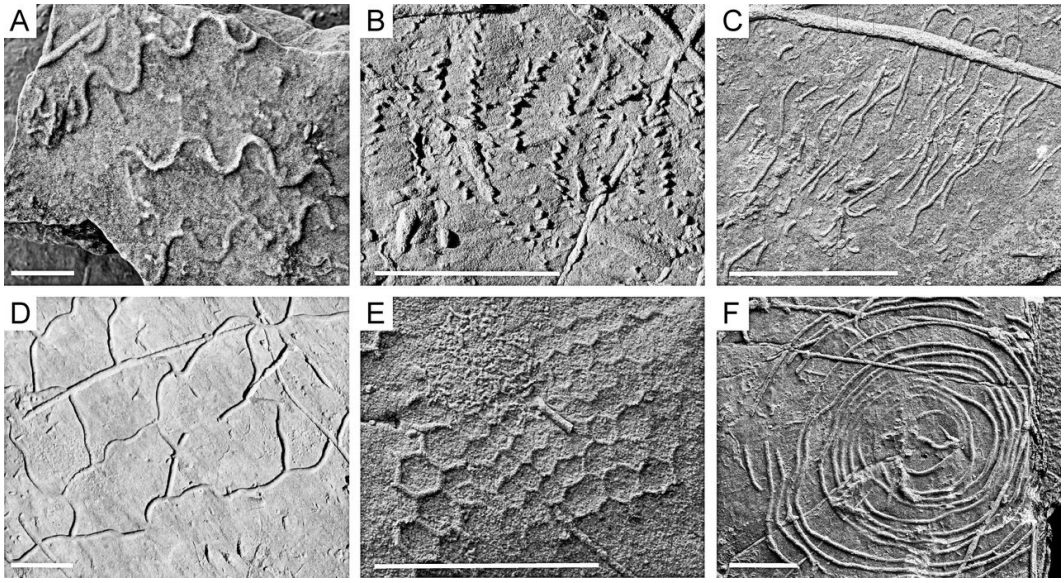

Figure 5.3: Graphoglyptid traces from the Eocene Guipúzcoan Flysch of Zumaia, Spain. A) *Cosmorhaphe*, B) *Helicolithus*, C) *Helminthorhaphe*, D) *Megagrapton*, E) *Paleodictyon*, a specimen less regular than the one in Fig. 5.1, F) *Spirorhaphe*, a slightly distorted specimen. In general Spiroraphe has the shape of an Archimedean spiral. Figure from Lehane and Ekdale (2013) Fig. 1, photographed in Eocene deposits in Spain. As noted by Rona et al. (2009), a feature that graphoglyptids have in common is the subdivision into parts of equal scale across occasionally large patterns.

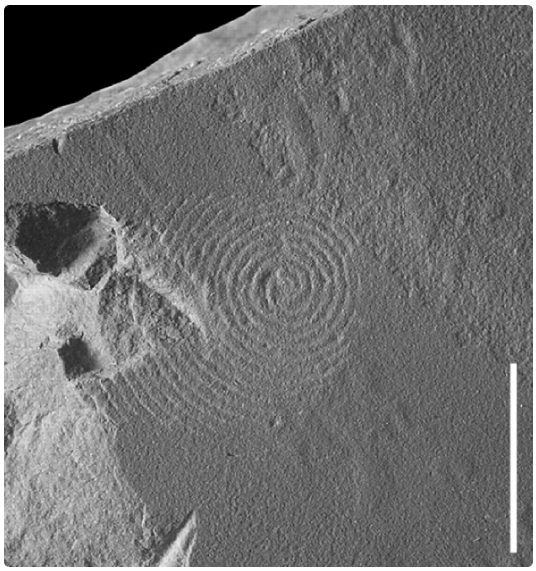

Figure 5.4: A very regular specimen of *Spirorhaphe azteca* from an Early Permian intertidal flat. After Minter et al. (2006).

halfway along the edges are consistent with similar features in the fossil ichnospecies *Paleodictyon nodosum* as shown in Fig. 5.1 (Seilacher (2007b)). A photograph of one of the modern patterns from above the sediment, showing the holes where the vertical tunnels meet the surface of the sediment, is shown in Fig. 5.2.

Despite the extensive research of multiple modern specimens by Rona et al. (2009) no traces were found of an organism responsible for creating *Paleodictyon* and the origin of the patterns remains uncertain. Most authors assume that *Paleodictyon* and other graphoglyptids are burrows produced by small endobenthic organisms (Miller (2014)). Garlick and Miller (1993) made a computer simulation of the process of burrowing *Paleodictyon*, which led them to conclude that the precision involved in producing the pattern is unlikely for a vermiform organism or protist. They suggested a small crustacean could be responsible. However, Honeycutt and Plotnick (2005) concluded from calculations of the total length of the tunnels that it would be unlikely for any small metazoan to burrow and maintain such a vast underground network.

Alternatively *Paleodictyon* has been described as a body fossil. Swinbanks (1982) suggested xenophyophores as possible makers, after finding modern tests of these deep sea protozoans shapes as (irregular) polygonal tubes. This option was carefully considered and refuted by Rona et al. (2009), based on differences in morphology and the absence of barium crystals that are characteristic of modern xenophyophores. Instead the authors give their support to two different hypotheses. On the one hand they maintain the explanation as the traces of "farming" endobenthic organisms. On the other hand they support an alternative hypothesis put forward by Rona and Merrill (1978),

suggesting that the pattern is the compressed body of a hexactinellid sponge. Both these hypotheses however raise the question of why careful analysis of the patterns did not show any differences in chemistry between the patterns and the surrounding sediment, nor any consistently associated eukaryotic genetic signature. The mysterious nature of *Paleodictyon* and other graphoglyptids was recently reviewed in Miller (2014), wherein the author wonders whether the "stubborn problem" of the biological interpretation of graphoglyptids will ever be solved. Miller writes:

> Since my last attempt to sum up what we know/infer about these distinctive structures from a biological point of view (Miller (1991)), there have been ingenious attempts to interpret constructional morphology, behavioural ecology and taxonomic affinity of the trace producers; but I am not sure we have made much progress.

Paleodictyon's precise geometric regularity, the difficulty of finding an associated organism and its occurrence over a time span of 500 million years, compels one to examine the option that these hexagonal patterns are not produced by biology but are instead the result of some physical process. This possibility has been examined several times in the past. Kummel and Teichert (1970) interpreted similar polygonal structures as ripple marks. Boyd (1975) noted that similar hexagonal patterns could be produced by synaeris, subaqueous shrinkage cracks resulting from a changing chemistry. However, neither these mechanisms can explain the regularity of the hexagonal mesh that is present in many examples of *Paleodictyon*. Pickerill (1990) discusses biogenic versus abiogenic interpretations, concluding that the described specimens of *Paleodictyon* are of biogenic origin, based on the following grounds: a lack of current

orientation; generally uniform dimensions and the regularity of the pattern; presence of a thin lining and the presence of other trace fossils on the same bed.

In this chapter I propose a new physical mechanism as a candidate for the origin of some or all *Paleodictyon* impressions, that a hexagonal two-dimensional standing wave is induced in the surface of the submerged sediment, driven for example by an earthquake, can be fixated in the sediment to form a tunnel system by a sorting and compaction effect on the grains. Two-dimensional standing waves are known as Faraday waves and were first described by Faraday in 1831 (Faraday (1831)). A common mode of Faraday wave is a perfectly regular hexagonal waveform, while other frequently occurring modes are spirals, stripes, square patterns and more irregular quasi-crystals.

With experiments I show that these hexagonal waves form readily on the surface of a suspension or paste and that a regular hexagonal mesh pattern can indeed be preserved in a paste long after the excitation occurs. Computer models of the velocity field within the waveform, based on the numerical solution of the Navier-Stokes equation from Périnet et al. (2009), help to understand how the waveform can induce the fixation of the pattern. A process for the formation of tunnels is proposed in the chapter, but an experimental verification is beyond the scope of this work as it requires a more elaborate experimental setup. Measurements of the experiments show that for moving standing waves on the surface of a suspension, there is a square root relationship between the diameters of the hexagons and the widths of the strings that form the edges of the hexagons of the wave. A large dataset of measurements of *Paleodictyon* patterns collected from the literature show that this square root relationship

is also present in the fossils.

In this chapter I will first explain Faraday waves and how the hypothesis that *Paleodictyon* patterns are created by this phenomenon works. This leads us to two main questions that need to be answered in order to establish the hypothesis. Firstly, is it likely that Faraday waves occur on the surface of submerged sediment? Secondly, how would the oscillating and short-lived Faraday waves lead to the observed fixed pattern in the substrate? Sections 5.3 and 5.4 discuss these questions and the experiments and modelling that was performed to address them. In section 5.5 size measurements of *Paleodictyon* occurrences in the fossil record are analysed and shown to reveal a clear square root relationship. The chapter is concluded with a list of criteria to distinguish trace fossils of biological origin from those created by Faraday waves.

5.2 The Faraday wave hypothesis for the formation of *Paleodictyon*

Faraday waves are standing waves on a vertically vibrated two-dimensional medium. They were first described by Michael Faraday in 1831 (Faraday (1831)) and have since become a well-studied phenomenon within the physics literature (e.g. Kumar (1996); Douady and Fauve (1988); Kudrolli et al. (2001); Edwards and Fauve (1994); Cabeza and Rosen (2007); Périnet et al. (2009)). Any two-dimensional fluid interface or surface, when vibrated in the vertical direction, can display this particular type of standing wave, which forms geometrical patterns on the surface. The waveform can have many appearances, but most commonly forms a striped, ringed or spiralling pattern,

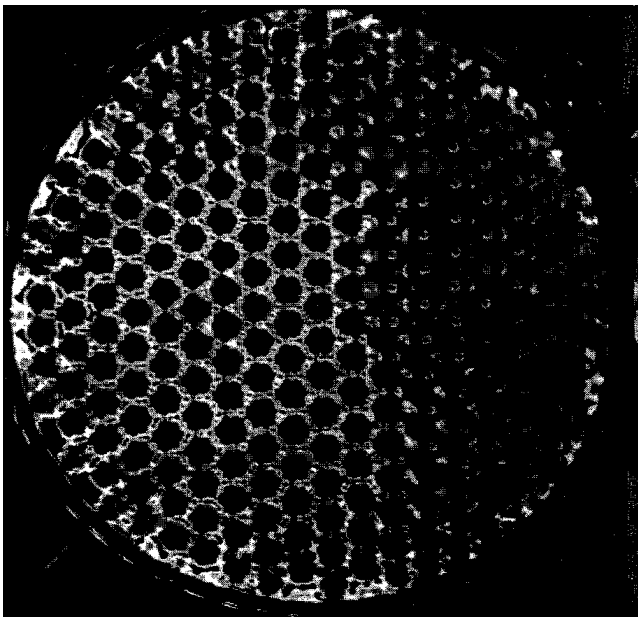

Figure 5.5: Photograph of a hexagonal Faraday wave pattern on a Newtonian fluid (Kudrolli and Gollub (1996)).

a regular square or hexagonal lattice or a quasicrystalline pattern (see Fig. 5.5). The selection of the mode depends on the frequency and amplitude of the vibration and properties of the medium such as viscosity.

To the general public the phenomenon of Faraday instability is best known in the form of the rings that appear on the surface of water when one taps a glass (for example in the famous scene in Jurassic Park where the rings in a glass of water betray the proximity of the *Tyrannosaurus rex*). With the right combination of frequency and amplitude it is also possible to initiate a hexagonal vibration in a glass of water, although this mode is often not very clearly visible because of the high wave celerity and translucency of water.

Instead of the surface of the water, I here consider the possible occurrence of Faraday waves within submerged sediment. Suspensions of sediments can themselves act as fluids. If a sediment is submerged and its upper layer is in

suspension in the water, then the interface of the suspension with the clear water can behave as an interface between fluids. Consider, for example, the fluid motion of a soft layer of clay on the bottom of a pond when disturbed. This type of fluid or interface has a very low celerity. Therefore a source with a low frequency, such as an earthquake, will produce a pattern with a small wavelength, as we can see from the wave equation:

$$\lambda = v/f, \tag{5.1}$$

where λ is the wavelength, v is the wave velocity and f is the frequency of the wave.

Footage from the submarine *Alvin* from the IMAX film *Volcanoes of the Deep Sea* shows the sediment near the modern *Paleodictyon* specimens flowing as a fluid when the submarine touches the sediment (see Fig. 5.6). In fact, from this footage it is possible to estimate the flow velocity of the sediment, a fluid property that is related to the wave velocity, to be around 1 cm/s. One can therefore estimatethat the wave velocity is roughly around 1 cm/s or lower. In the wave equation, if v is of the order of magnitude of 1 cm/s, then a frequency of 1 Hz has a wavelength of 1 cm. Models of the hexagonal Faraday wave, which I will discuss later in the chapter, give us a relationship between the wavelength and the sizes of the hexagonal mesh as represented in Fig. 5.7. If the wavelength is 1 cm, then edges of hexagons have a size of 0.7cm, which is the same order of magnitude of the edge lengths of *Paleodictyon* patterns.

Within this hypothetical framework, the next question to ask would be: what is the source of the vibrations with frequencies around 1 Hz? *Paleodictyon* patterns are indicative of flysch deposits and can therefore occur in areas with

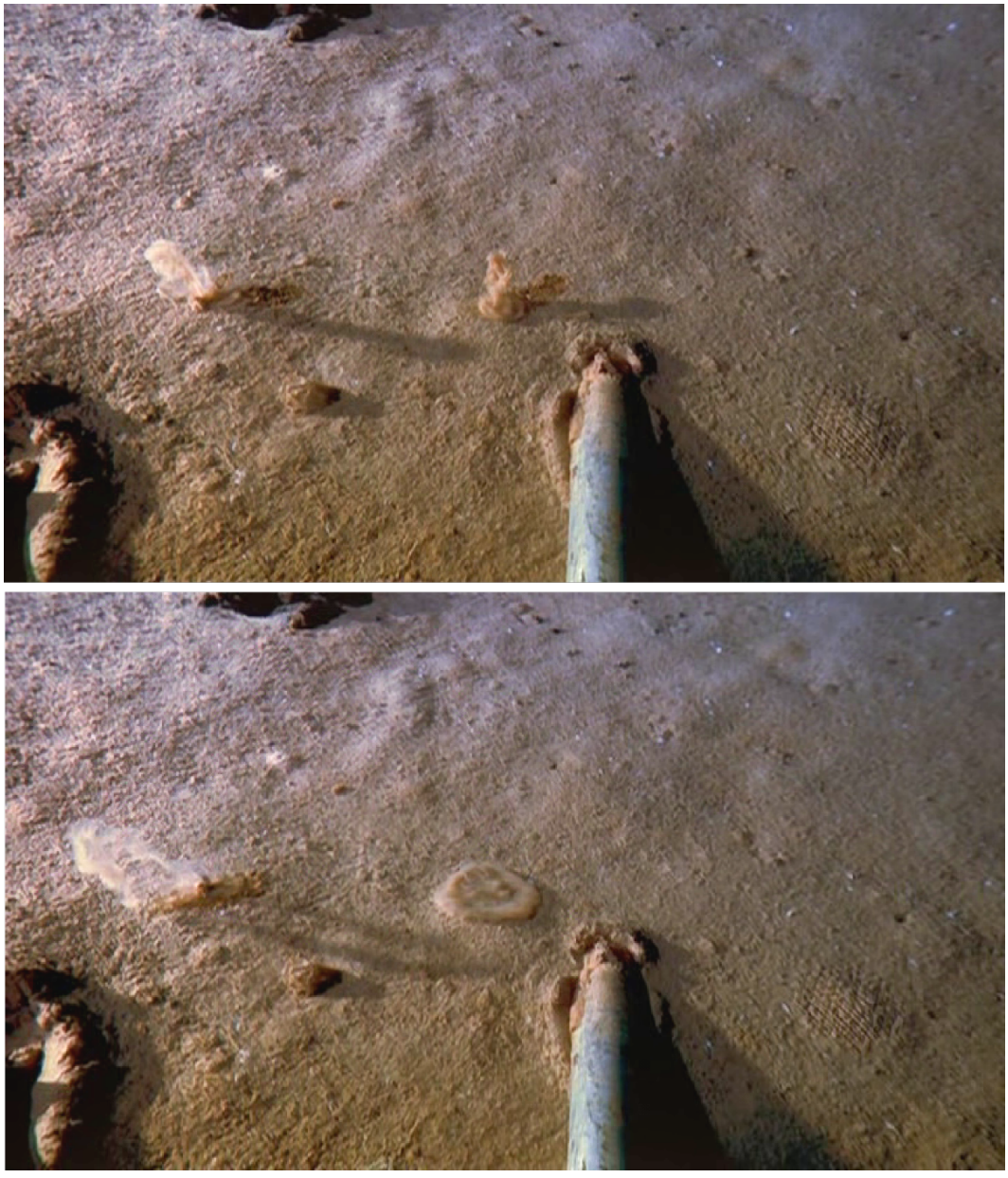

Figure 5.6: Snapshots of sediment flow in the immediate vicinity of modern *Paleodictyon*-like tunnel system permit the calculation of a rough estimate of the sediment flow velocity (1-2 cm/s). Snapshots taken 3 seconds apart. A specimen *Paleodictyon* can be seen to the right of the flowing sediment. Footage from the IMAX film *Volcanoes of the Deep Sea*.

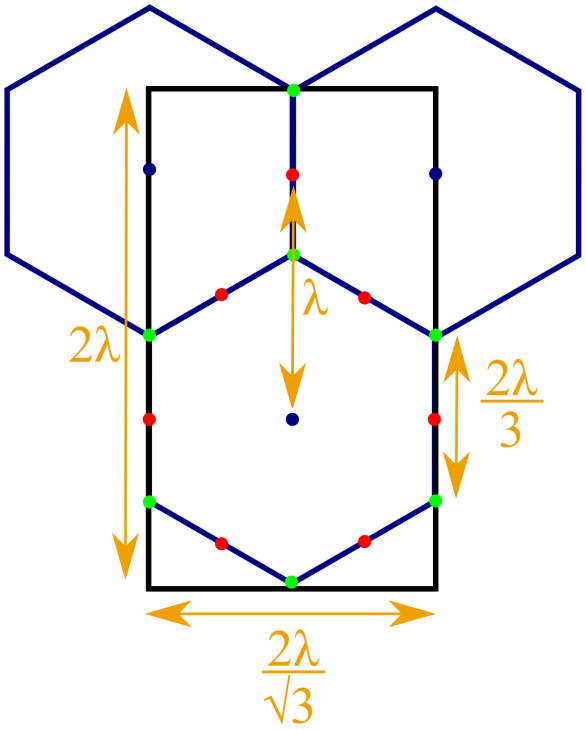

Figure 5.7: This diagram shows the relationship of the wavelength of the main driving frequency of a hexagonal Faraday wave compared to the resulting hexagonal mesh. We see that a single edge measures $2\lambda/3$. The long diagonal of the hexagons is twice the length of an edge, so it is $4\lambda/3$. After Périnet et al. (2009).

much seismic activity, which could potentially provide a source of vertical vibrations that might excite a standing wave. We know that modern specimens are found near deep sea volcanic vents which are zones of frequent seismic activity. Earthquakes often have spectra that range from very low frequencies up to around 1 Hz. So earthquakes form a potential source of vertical excitations that would lead to the formation of Faraday waves on two-dimensional interfaces.

What is acting as an interface for the Faraday wave? Suspended sediments can act as fluids and admit waves, even within a liquid. The modern hexagonal patterns studied in Rona et al. (2009) is present at a depth of 2-3 mm below the surface of the sediment, so it seems the actual interface of the wave might lie beneath the observed sediment surface, and the wave induces the formation of small tunnels within the sediment. If the sediment is loosely packed, then the density at which the sediment fluidizes as a result of vibrations can lie slightly below the surface of the sediment, and this could act as an interface for the Farday wave. Alternatively there might be a lens of water present underneath a layer of sediment, or the sediment can be composed of two layers of different composition, which form an interface slightly below the surface. As shown in Rona et al. (2009), the sediment where the modern specimens of *Paleodictyon* are found is indeed composed of two layers, a red metalliferous sediment covered by a grey calcareous lutite veneer of up to 1 cm thick.

Fluidized sediment is likely to form a non-Newtonian and often visco-elastic fluid. Faraday waves on visco-elastic fluids have been shown to have several special properties, in particular the ability to form isolated patches of the hexagonal mode as seen in Fig.5.8 (Wagner et al. (1999)), which might explain

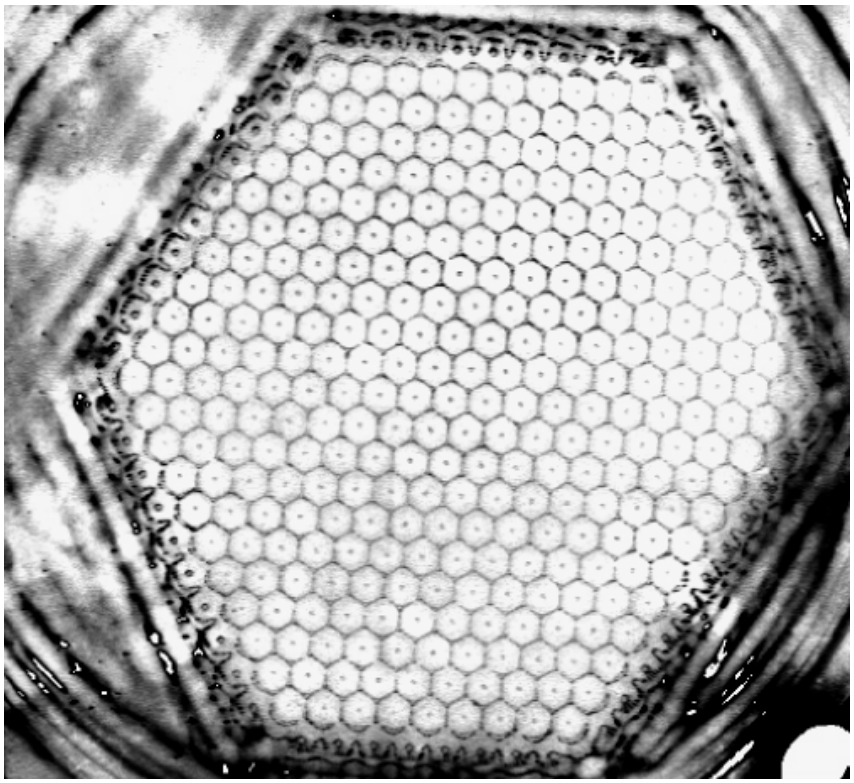

Figure 5.8: Experiment on a viscoelastic fluid shows a mode of an isolated patch of hexagons. From Wagner et al. (1999).

why *Paleodictyon* typically appears as isolated patches.

If such a Faraday wave occurs at a small depth within the sediment, how would this cause a pattern of tunnels to form? In order to answer this question one needs to examine two things. First one needs to know how the wave might sort the grains to create empty spaces. Modelling the fluid velocity field can help to understand possible sorting or memory effects that might play a role in this. Secondly one needs to understand the sediment in which *Paleodictyon* occurs, to understand whether and how the sediment might compact to support a tunnel network. In modern times, the deep sea substrate is predominantly comprised of degraded biomatter or "marine snow" that has taken a long time to sink through the water column. This material is often flocculated and

compressible. This is also the case for calcareous lutite layer in which the modern *Paleodictyon* is found, as can be seen in the photograph of one such pattern in situ, in Fig. 5.2.

The Precambrian ocean and ocean sediments were very different from the modern ones for various reasons, such as the lower concentration of oxygen and the resulting dissolution of calcium carbonate, the different composition of settling biomatter, the lack of bioturbation rounding the sediment grains and the fact that part of the sea floor was covered with a microbial mat tying the sediment together. These differences would have made the occurrence and preservation of Faraday waves less likely, as discussed in more detail in section 5.4.

After establishing a general understanding of the Faraday wave hypothesis above, there are two steps in establishing it as a viable hypothesis for the origin of *Paleodictyon*. First one needs to study the potential occurrence of a hexagonal Faraday wave on the sediment interface. Secondly one should consider how this wave could form the lasting pattern in the sediment, which can later be cast in a turbiditic flow and thereby preserved as "trace fossils".

5.3 Likelihood of occurrence of a hexagonal Faraday wave

In this section we will discuss whether hexagonal Faraday waves could occur on the surface of a submerged deep sea sediment. Faraday waves have been known to occur in a multitude of systems. Their behaviour on the surface of a fluid or an interface between fluids as the result of vertical oscillations is

a well-studied topic (e.g. Kudrolli et al. (2001); Edwards and Fauve (1994); Périnet et al. (2009); Wagner et al. (1999)). However, Faraday waves have also been observed in many other systems, such as a magnetically driven ferrofluid surface (Pi et al. (2000)), a Bose-Einstein condensate (Engels et al. (2007)), as solutions to certain reaction-diffusion equations (Ke et al. (2006); Dolnik and Rovinsky (1999)) and in gas-fluidized powders (Li and Liu (2008)).

The formation of *Paleodictyon* patterns always occurs subaquously. Therefore the surface of the water cannot be the two-dimensional medium of the hypothesized Faraday wave. Below the surface, the water itself cannot transport the transverse waves that are required for the waveform. The waves must therefore occur on the surface of the sediment or on an interface within the stratified sediment-water mixture itself. This can occur if the sediment is fluidized and thus behaves as a liquid, for example under the influence of vibration (liquefaction) or because the mixture has the right grain/water ratio (fluidization). In a mixture of sand and water, the latter occurs if the water content is one third. With this ratio the mixture is on the verge of two states: either the grains just touch each other, in which case the mixture behaves as a solid, or they do not touch and are in suspension in the water, such that the mixture behaves as a liquid.

For very loosely packed sediment, the water content of the mixture might cross this critical level at some depth beneath the actual surface of the sediment. This could explain why in modern *Paleodictyon* specimens, the hexagonal pattern itself is not present at the surface of the substrate but occurs a depth of a few millimetres. This might also be explained by a stratifaction of the sediment into two layers with different properties. The sediment in which the modern

Paleodictyon patterns was found to be composed of a metalliferous substrate with a calcareous lutite layer on top. As the two grain/water mixtures fluidize, they behave as two fluids with different properties and the interface between the layers might therefore act as an interface of fluids.

Such mixtures of sediment and water usually behave as a non-Newtonian fluid. This means that they obey different mechanics than normal (Newtonian) fluids. An example of a non-Newtonian fluid that is well-known to the public is a mixture of corn flour and water, which behaves like a fluid but on which one can also stand if one moves quickly. Many suspensions of colloidal or flocculate particles behave this way. It is also possible for a paste to fluidize under the influence of vibration and return to a solid when the vibration ceases.

Wagner et al. (1999) experimented with the formation of Faraday waves on viscoelastic fluids, which are a type of non-Newtonian fluid. They showed that this type of fluid admits a range of alternative standing wave modes, among them a mode that that looks like an isolated patch of regular hexagonal lattice, as shown in Fig.5.8. It is unclear whether such behaviour extends to other types of non-Newtonian fluids. If it does, then as we expect submerged sediment to behave in a non-Newtonian manner, this could explain why the *Paleodictyon* specimens usually do not cover an entire surface but often appear in rounded isolated patches.

Some reported specimens of *Paleodictyon* do cover a large surface. The giant specimen described in Wetzel (2000) covers 0.5 m by 1 m, with hexagon diameters between 8 and 13 cm. A specimen shown in Lehane and Ekdale (2013) fig.4 A covers an area of roughly 25 cm by 25 cm with hexagon diameters of 8-9 mm.

It is not entirely clear whether a single frequency of the seismic spectrum would need to be amplified in order to create a hexagonal Faraday wave, or whether a mixed signal might also suffice. There have been some experiments that combine two frequencies to see what the resulting pattern is. Kudrolli et al. (1998) finds that a combination of two frequencies with different non-integer ratios give rise to a number of new "superlattice" patterns, but hexagonal patterns also arise. It can also happen that a single frequency is singled out by a resonance in the substrate. Resonance often occurs on larger scales for earthquakes. For example, resonance, in other words a standing wave, in the Kathmandu basin during the 2015 Gorkha earthquake resulted in the collapse of many buildings (Galetzka et al. (2015)).

The occurrence of Faraday instability on a fluid interface is the result of a vertical vibration at an amplitude exceeding a certain critical amplitude, which depends on different physical properties of the situation such as the wave velocity of the interface and the viscosity of either fluid. The selection of the pattern can then be represented in a phase diagram of frequency versus amplitude, see for example Wagner et al. (1999) Fig. 2 or Cabeza and Rosen (2007) Fig. 6. This phase diagram is different for every experiment, depending on the properties of the medium. However, a comparison of phase diagrams from different experiments also shows many similarities. In particular, the hexagonal mode typically occurs at low frequencies, at the lowest amplitudes exceeding the critical threshold. This is also noted in Kudrolli and Gollub (1996), where the authors conclude that the hexagonal pattern is observed at low frequency over the entire viscosity range studied in their experiments on Newtonian fluids. The experiments on viscoelastic fluids by Wagner et al.

(1999) show that the isolated hexagonal patterns are found in a region of phase space with low frequencies at the lowest amplitudes that exceed the critical threshold.

The fact that Faraday waves typically take on a hexagonal mode at low frequencies and at the amplitudes that just exceed the critical amplitudes is consistent with the idea that hexagonal Faraday waves could be induced on a seafloor by an earthquake. Although one cannot say for certain what the wave celerity of the proposed medium is, it is known that the frequency spectrum of earthquakes extends downwards to very low frequencies, but not upwards to high frequencies. One also does not know directly what the critical amplitude of such a medium is, but the pattern that is formed at the lowest amplitudes crossing critical threshold is expected to be the most abundant.

5.3.1 Materials and methods

In order to test whether hexagonal Faraday waves form easily on a suspension or paste, a number of experiments were performed. The experiments imposed a vertical excitation on the surface of a sediment/water mixture with different compositions. It was not technically feasible to perform the experiments under water, so the medium of the vibrations was the interface between the suspended/fluidised sediment and the air instead of the sediment and the water. The main difference between a subaqueous setting and the setting that the experiments were performed in is the difference in wave velocity. As water has a high surface tension, the wave velocity of the sediment suspension exposed to air is higher than the wave velocity at the surface of a sediment mixture that is submerged.

The setup used to perform these experiments consists of a strong magnet, above which a plastic circular dish with an inner diameter of 106 mm is suspended with a coil worked into the plastic. Applying an alternating sinusoidal current to the coil makes it move up and down at the same frequency as the current applied to it. The output signal is sinusoidal. Frequency and amplitude can be varied independently by varying the current. The frequency range of the setup lies between 1 and 50 Hz. The maximal displacement of the dish is about 5 mm.

A range of materials and mixtures were subjected to vertical oscillation by means of the device. It seems that fine-grained materials were easier to excite, presumably because suspensions of finer grained material have a lower critical amplitude. Fig. 5.9 shows a snapshot of the hexagonal wave mode created in one of the experiments. The material consisted of around two parts silica dust and one part water, totalling to a volume of 300 ml which created a past with a depth of around 0.5 cm.The silica dust has a lognormal grainsize composition with D_{10}, D_{50} and D_{90} at 3.7, 32 and 97 μm. The experiment shown in Fig. 5.9 also contains a small component of bentonite (around 50 ml). The bentonite was left out of the other experiments and is thought to have had little effect on the behaviour of the mixture.

The experiment in Fig. 5.9 was performed at a frequency of around 25 Hz. Because of the high surface tension of water, the wave velocity on the surface of a sediment/water mixture exposed to air is higher than one would expect for a sediment surface that is submerged. Therefore the frequency range used in the experiments creating hexagonal patterns of a reasonable size is higher than is expected to be the relevant range in the case of a *Paleodictyon*-creating

Figure 5.9: Snapshot of an experiment creating a hexagonal Faraday wave mode on the surface of a mixture of two-thirds silica dust and one-third water, with a component of bentonite. Scale bar is 1cm.

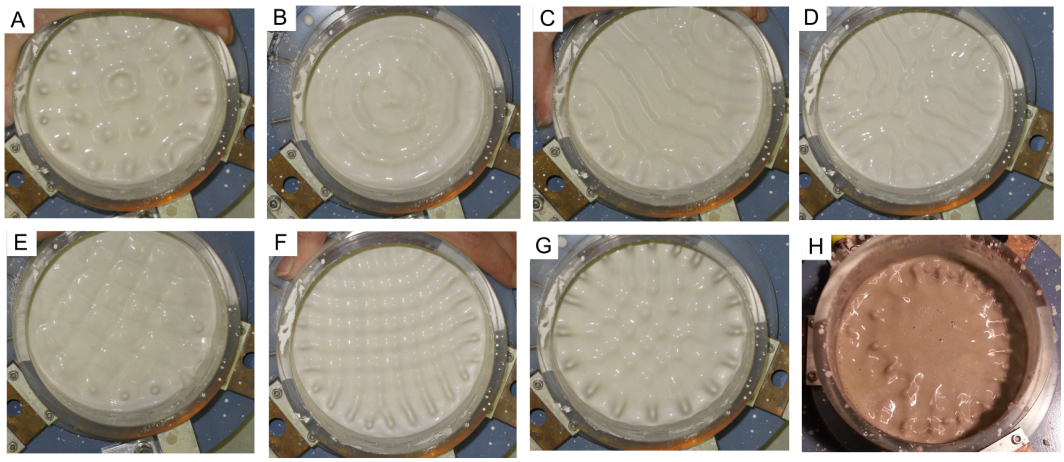

Figure 5.10: Other patterns formed in the experiments: A) quasi-crystalline; B) rings; C) stripes; D) coexisting stripes and hexagons; E) square; D) smaller squares; G) hexagonal with radial boundary effects; H) ribbon of transverse excitations. Experiments A-G consist of a silica dust/ water mixture, while experiment H was perfomed on the same mixture as Fig. 5.9 containing a component of bentonite.

wave.

A series of experiments was performed with the silica water mixture as described above. Different modes of the Faraday pattern could be created on the surface, hexagons and squares on the whole surface or a part, combined with stripes, rings and spirals or sometimes singular excitations or ribbons of transverse excitations, see an overview in Fig. 5.10. The equipment was not reliable enough to map out a detailed phase diagram of this behaviour. Sorting and settling of the suspensions as a result of the vibrating forces altered the physical properties of the mixture and changed its behaviour over time, causing the patterns to switch between different modes. Alternatively, density variations that resulted from the induced patterns also seemed occasionally to stabilize this pattern, such that the same mode in the same position would be reinitiated after the vibration was halted for a short time.

5.3.2 Experimental Results

The experiments showed that Faraday waves in the hexagonal mode occur readily in this setting, for different types of grain and water content. Comparing the large diameter hexagonal patterns induced at low frequency with small hexagonal modes created with higher frequencies, it became clear that the widths of the upwards excitation between the hexagons was relatively smaller for the larger hexagons. This scale-dependence of the Faraday wave has to come from scale-dependence in the medium. Within the hypothesis that these waves can create a system of tunnels, one would expect that these "edge" excitations are responsible for the formation of the tunnels in *Paleodictyon*. Therefore the widths of these excitations should be related to the widths of the tunnels. The widths of the tunnels, which are cast to form the "riblets" between hexagons in fossilised specimens of *Paleodictyon*, are well documented in the literature and are therefore an interesting quantity to study.

Fig. 5.11 shows measurements that were taken from snapshots of nine experiments, including the experiment in Fig. 5.9. The snapshots are taken at the instance in the period of the wave when the hexagons are clearly visible and divided by upward edge excitations. On the horizontal axis measurements of the widths of the hexagons are presented and on the vertical axis measurements of the widths of the upward excitations are shown. The best fit for the exponent is 0.55 ± 0.08. Thus the measurements are adequately described with a square root relationship of the form:

$$y = \alpha\sqrt{x}, \tag{5.2}$$

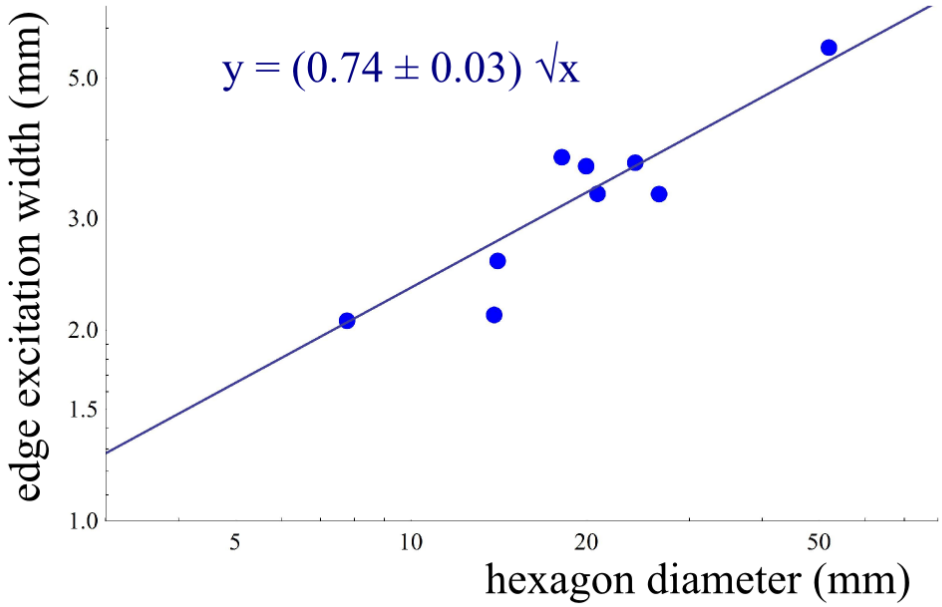

Figure 5.11: Loglog plot of measurements from nine experiments in which the hexagonal Faraday mode was induced on the surface of a mixture of silica dust and water. Shown horizontally are the diameter of the hexagons and vertically the width of the upright ridge between the hexagons in a snapshot of the wave, such as can be seen in Fig. 5.9. The measurements form a square root relationship.

with x the long hexagon diameters in mm, y the widths of the edges in mm and α a dimensionful quantity that is dependent on the medium properties and in this case is fitted to $0.74 \pm 0.03\sqrt{mm}$. This fit to the measurements has an R^2 value of 0.87.

5.3.3 Experiments on deep sea sediment

To create a closer analogue to the situation in which *Paleodictyon* is formed, experiments were performed with fresh Antarctic sea sediment from a recently extracted core. The sediment comes from the neighbourhood of the Totten Glacier in East Antarctica from a depth of around 700m. Samples were taken at 6-10 cm beneath the sediment surface. The sediment core is composed mostly of degrading biological matter from phytoplankton blooms.

Initially the critical amplitude of the core sample could not be exceeded with the experimental setup. However, the mixture seemed homogeneous and in possession of a small surface tension, possibly through the binding effects of the degraded biomatter, see also Fig. 5.12 A. The the sediment was diluted with water, and after this procedure Faraday waves could be induced its surface. Stripes, rings and spiral modes were easily formed at frequency ranges of 25-35 Hz, see Fig 5.12 C-G. Isolated excitations not covering the entire surface (Fig. 5.12 B) indicated that the sediment likely behaves in a non-Newtonian manner. After the vibration ceased the mixture showed signs of wave-induced sorting effects, as shown in Fig. 5.12 H. The hexagonal Faraday mode could not be induced in this sediment, most likely because of limitations in the range of the experimental setup.

The experiments performed in this section suggest hexagonal Faraday wave is

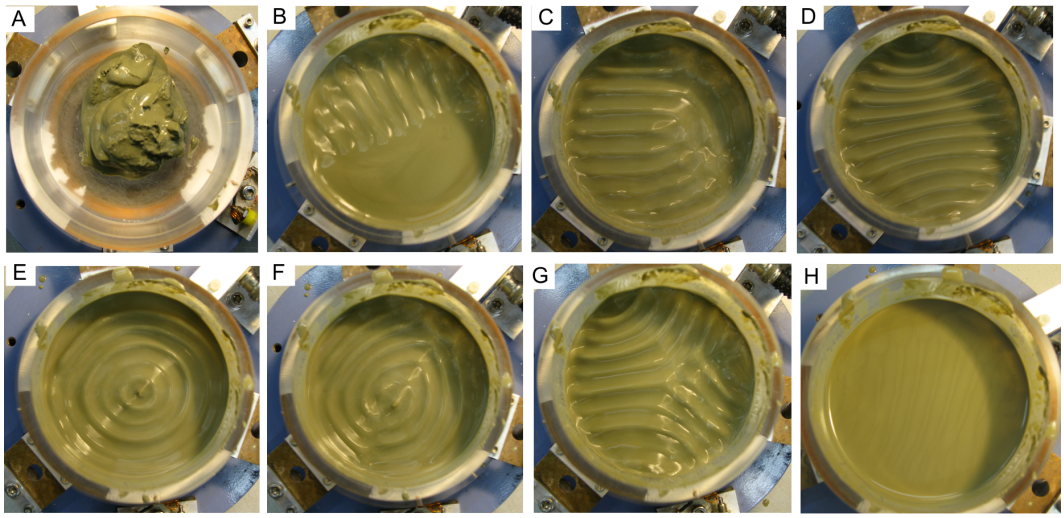

Figure 5.12: Experiments on Antarctic sediment show a number of Faraday wave modes. A) The sediment before dilution; B) Striped mode covering only a part of the surface; C) Transition between circular and striped pattern; D) Stripes; E) Rings; F) Spiral; G) Distorted stripe pattern; H) Stripes are visible on the surface of the sediment after the vibration has ceased. The difference in colours indicate a separation of grain types has occurred through a sorting effect induced by the wave.

likely to occur on a fluidised sediment or the surface of a suspension in the presence of a source of vertical excitation. Whether it is possible to create these patterns subaquously at a small depth in the sediment cannot be tested with the experimental setup that was available. However, the physics of subaquous fluidized sediments is similar to that of fluidized sediments exposed to air, thus in principle it should also be possible

5.4 Fixation of a pattern

It is well-known within the field of sedimentology that waves or movement of fluid/sediment mixtures induces sorting effects, resulting in relief, density or grain size gradients. For example cross-bedding, the lithified evidence of migration of ripples and dunes in the direction of fluid flow, is an example of how fluid movement is captured by sediment sorting and eventually by geology. A similar effect will create density variations in a suspension when submitted to a standing wave. The question in this section is how precisely the sorting effects induced by a hexagonal Faraday wave influence the sediment. More specifically, can such a wave induce the formation of a network of tunnels in a hexagonal lattice, with vertical tunnels halfway along the edges, as found in the modern specimens of *Paleodictyon*.

Recently Nakayama et al. (2013) studied the effect of Faraday waves on calcium carbonate pastes. It turns out that the position of the nodes and antinodes of a Faraday wave that is imposed on the paste for a short time, controls the position of desiccation cracks that form days later when the paste dries. A memory effect within the $CaCO_3$ paste is responsible for this, presumably

a process of either aligning molecules or locally changing the density of the paste, or both.

Nakayama et al. have researched the influence of Faraday waves on a calcium carbonate paste for the circular, striped and rectangular modes of the Faraday wave, but not yet for the hexagonal wave mode. In this section I report the results of imposing a hexagonal pattern on a calcium carbonate paste. Nakayama et al. find that desiccation cracks are formed at the nodes of the waves, where the velocity field is minimal integrated over the period of the wave. The experiments presented here suggest that in the nodal regions the paste becomes more dense and therefore dryer when exposed to air, which might explain why desiccation cracks appear at the nodes in the experiments in Nakayama et al. (2013).

5.4.1 Preserving a Faraday wave and the absence of Precambrian patterns

What physical properties does the sediment need to have to preserve a network of tunnels if these were formed by a wave? Two minimal requirements are as follows:

(a) The sediment should be influenced by the wave, i.e. the critical amplitude of the forcing required to bring the sediment in motion should be higher than amplitude of the wave. It could be hard to bring the sediment into motion for example if it is bound. (b) The sediment should allow for the preservation of a tunnel system without an agglutinating substance. This can be improved if the substance is flocculate or (inelastically) compressible, so that forcing the sediment more easily results in a permanent shape being preserved. Also,

Ekdale et al. (1984) noted that production and preservation of deep sea trace fossils is correlated with the calcium carbonate content, which increases the strength of the sediment. As shown in Nakayama et al. (2013) and with the experiment below, calcium carbonate also possesses a memory effect that make it more likely to capture a wave.

Furthermore, in the specific case at hand it might be relevant that the substrate is stratified into two layers, and that the wave occurs on the interface between the two fluidised sediments. The substrate in which the modern patterns are found is described to consist of two layers, carbonate lutite and underlying red metalliferous sediment.

Most Phanerozoic abyssal deposits were created by a continuous fine rain of biomatter settling through the water column (Ekdale et al. (1984)). The degraded organic matter is compacted into bacterially bound floccules or faecal packages to form a stratified nepheloid layer. This slowly settling, flocculate mixture is called marine snow. Pictures taken by the submarine Alvin show that the substrate is flocculate, see Fig. 5.2. It is characterized as calcereous ooze in Rona et al. (2009). Rona et al. describe the boundaries of the tunnel networks in the excavated specimens of *Paleodictyon* as agglutinated, yet they do not find a difference in chemical composition between the pattern and the surrounding sediment. It might be that the tunnel walls seem agglutinated because they are made up of compressed floccules. It is also clear from the footage of Alvin landing on the substrate that the sediments flow and move around easily, see also Fig. 5.6. So it seems that the conditions (a) and (b) are satisfied in the modern sediments.

Phanerozoic seas were very similar to modern seas, when compared to the

Precambrian seas which were very different in composition. Nonetheless the composition of marine sediments has changed over the course of the Phanerozoic. For example during the late Mesozoic, the rise of angiosperms resulted in an increase in plant detritus deposited in the seas. Around this time there is also a rise in the number of occurrences of *Paleodictyon*, and graphoglyptids in general, and Seilacher (1974, 1977) and Uchman (2003) propose that the two are related (see also Ekdale et al. (1984)). If *Paleodictyon* is formed by standing waves, then its formation is closely related to the physical properties of the sediment. Biological matter increases the flocculate behaviour of the sediment and could therefore increase the probability of preserving a Faraday wave. This might explain the increase in occurrences of *Paleodictyon* during the late Mesozoic. Section 5.5 discusses the data by Uchman showing variations of size measurements of *Paleodictyon* over time and discusses whether these variations may be related to changes in the physical properties of the sediment.

There are many ways in which Precambrian deep sea sediments differed in composition and physical properties from Phanerozoic sediments. Although there must have been a lot of bioproduction in the Precambrian seas, most forms of phytoplankton only became dominant in the Phanerozoic (e.g. Falkowski et al. (2004)) thus the content of settling biomatter was different. The different composition of both the biomatter and the ocean itself resulted in differences in composition of the settling sediments. The lack of oxygenation of the water column resulted in the dissolution of calcium carbonate, which also was not produced in the same quantities because of the apparent lack of biomineralising organisms. The sediment was therefore depleted of calcium carbonate

compared to modern ocean sediments. Once settled, the sediment would be unperturbed by bioturbation, which evolved during the Late Ediacaran/Early Cambrian. It would in many places be covered by a microbial mat, fixating the sediment in place, exhibiting a strong redox gradient in the upper few millimeters of sediment (e.g. Callow and Brasier (2009)). Recently Harazim et al. (2015) stressed how fundamentally bioturbation modified the redox gradient, mineralogy, posorsity, organic content and fabric of muds. McIlroy et al. (2003) already showed that bioturbation increases weathering of minerals, rounding grains, and influences porosity and permeability of the resulting facies. Callow and Brasier (2009) write:

> It is beyond doubt that the appearance of infaunal bioturbation and metazoan biomineralization across the EdiacaranCambrian transition irreversibly affected the nature of marine sediment architecture and biogeochemistry.

All in all, the minimal conditions (a) and (b) were unlikely to be met in the Precambrian ocean. Therefore it is unlikely that one finds a preserved Faraday wave in Precambrian sediments, and this could explain why no Precambrian occurrences of *Paleodictyon* have been recorded.

5.4.2 Model

I have modelled the waveform based on the three-dimensional hexagonal pattern solution to the Navier-Stokes equations on an interface between two liquids calculated numerically in Périnet et al. (2009). The aim is to establish whether it is likely for the Faraday waveform to induce the formation of tunnels in the geometry that is found in the modern specimens of *Paleodictyon*,

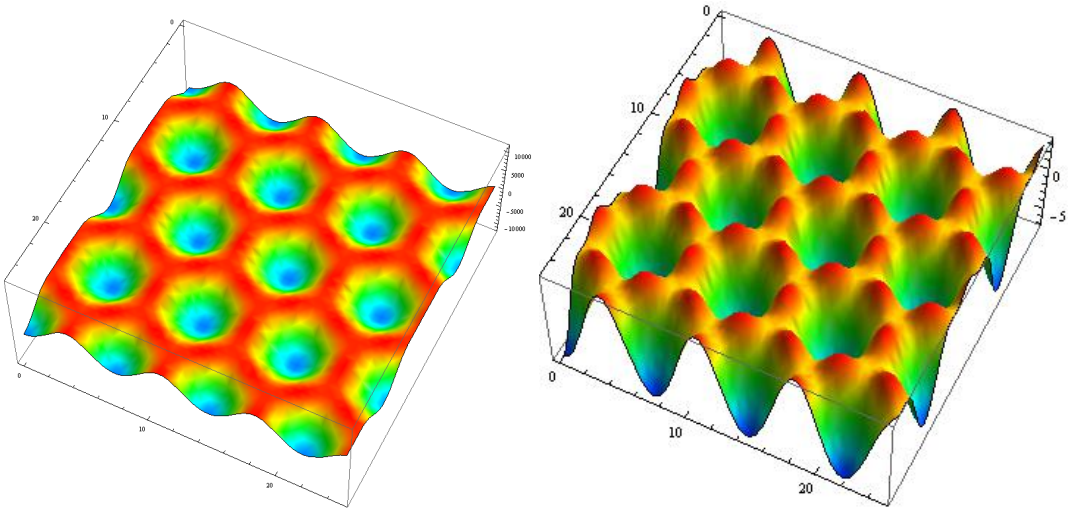

(a) (b)

Figure 5.13: Two snapshots of the simulation, modelled in Mathematica after the numerical solution to the Navier-Stokes equation from Périnet et al. (2009). Figure 5.13b shows that the mid-edge points of the hexagonal pattern are special points in the waveform. The mid-edges are special points in the *Paleodictyon* patterns, which have a vertical tube at these locations.

i.e. a horizontal hexagonal pattern with upward tunnels halway the edges, by considering the expected displacement of particles induced by the movement of the interface and the velocity field within the liquids.

The modelled movement of the interface between the two fluids is shown completely in Appendix C.1, together with the underlying equations. The interface continuously displays the symmetry of a hexagonal grid. During an instance of the period of the wave the edges of the hexagons are seen as upward excitations, as shown in Fig. 5.13a. For a large part of the period of the wave, the mid-edge points, which in the modern patterns feature the upward holes, form special points in the waveform with an upward displacement, as shown in Fig. 5.13b.

Fig. 5.14 shows the maximal vertical displacement of every point on the in-

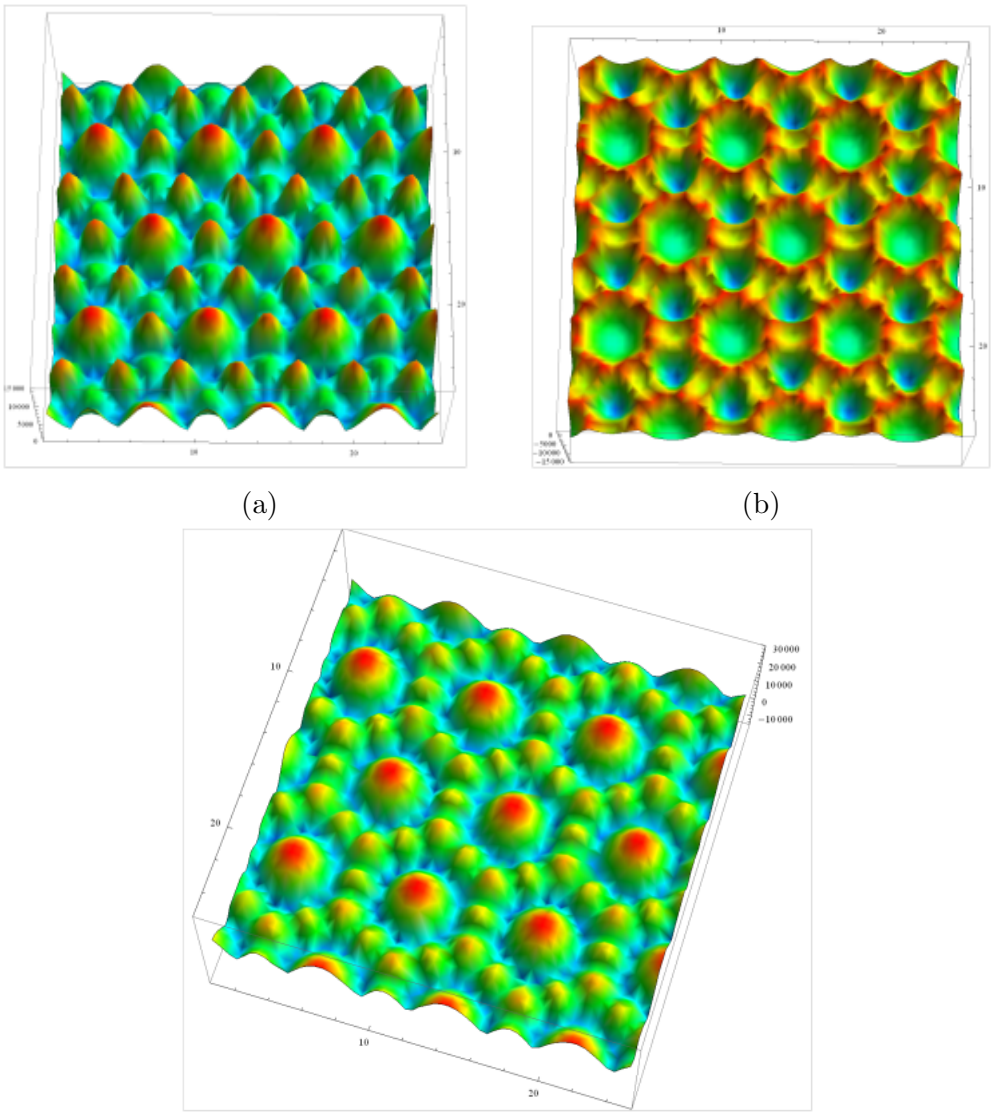

(a) (b)

(c)

Figure 5.14: Maximal upward (5.14a) and maximal downward (5.14b) displacement of points on the interface. Note that the mid-edge points extend further upward, whereas the vertices extend further downwards. Fig. 5.14c shows the absolute value of the vertical displacement of each point on the interface integrated over the period of the wave.

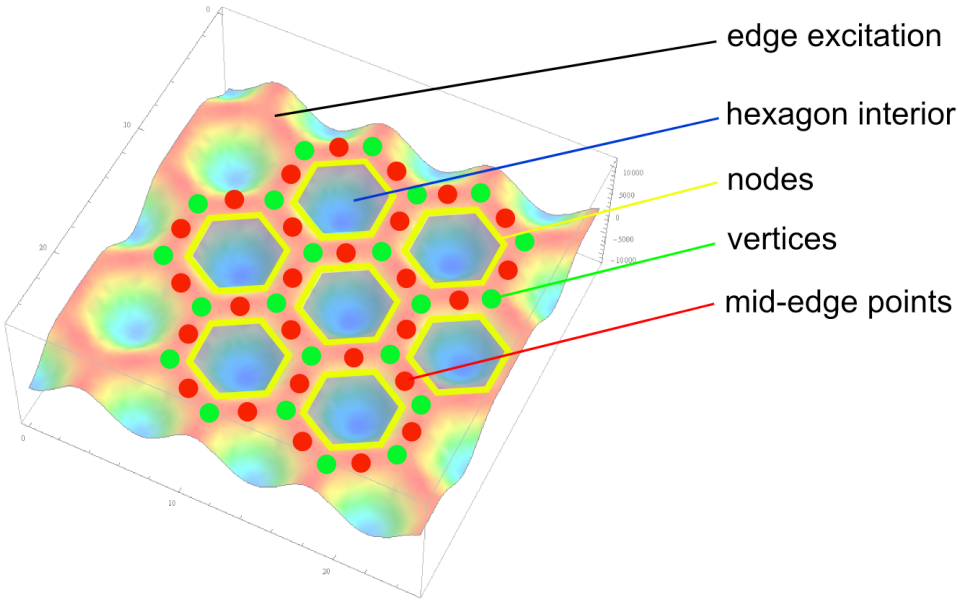

Figure 5.15: A diagram defining different areas of the waveform.

terface, upwards in (a), downwards in (b) and the difference of these two, the maximal absolute displacement of every point, is shown in (c). The regions within the hexagons move up and down equally, while the mid-edge points move upwards more, and the vertices of the hexagons are more displaced downwards. The nodes of the waveform are formed by the lines between the interior of the hexagon and the edge excitation of the hexagon. The pattern of nodes is illustrated in Fig. 5.15.

These simulations are based on an interface of which the physical properties are not influenced by the wave, unlike the sediment-water mixture, which can change its composition locally as a result of the exerted pressures. Experiments suggests that this has a stabilizing effect on the wave.

Appendices C.2.1 and C.2.2 show the three-dimensional velocity field within the two fluids in snapshots at 48 moments of the period with an equal time

interval. Suspended particles respond to the velocities of the fluid, thus one can estimate the expected first order sorting response of the sediment from the velocity field. Only a first order approximation can be made from this model because the interaction of the sediment with the system alters the physical boundary conditions of the dynamical equations. Hence the behaviour of the waveform is expected to differ slightly in the presence of a suspended sediment, and moreover to alter over time as the sediment sorts and restricts the motion of the fluid. A snapshot of the velocity field seen from above in Fig. 5.16 shows that there is an interval during the period of the wave when the velocity vectors along the edges are aligned with the edges. Thus it can be expected that the particles are transported longitudinally along the edges.
So from the models the following information can be derived:

- The lines between the edges and the hexagons form nodes in the plane of the interface. The experiment discussed below suggests that this would lead to an increase in density along these regions.
- There are moments in the velocity field when the velocity vectors lie along the edges.
- The mid-edge points of the interface mainly move upward.

This information suggests the occurrence of the following mechanism that would induce the formation of tunnels in the shape of a *Paleodictyon* pattern:

- In a compressible medium the increase in density along the nodes leads to a region of compacted sediment in the plane of the interface. This might form walls of the tunnels. The experiment and the pattern of nodes on

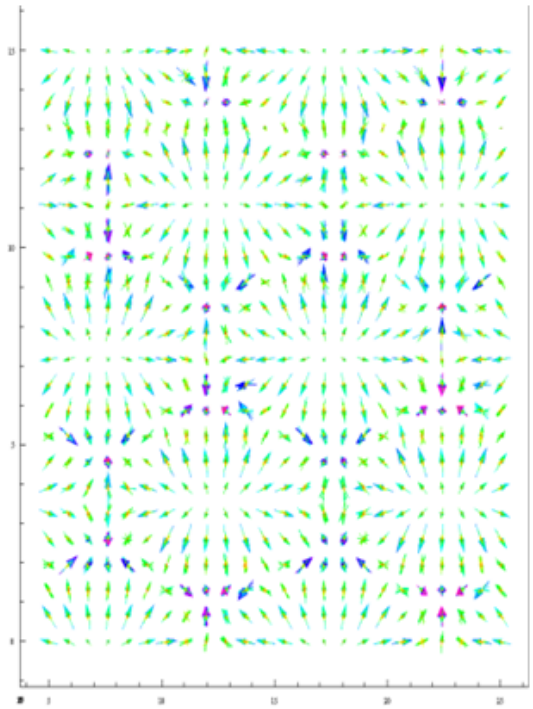

Figure 5.16: A snapshot of the three-dimensional velocity field seen from above shows that small currents are induced along the edges at some point during the period of the wave. These currents transport the particles along and from the edges, which are antinodes of the pattern.

the interface can only suggest this in two dimensions, so whether compaction also takes place above and below the formed tunnels is unclear.

- The velocity vectors along the edges induce longitudinal currents along the edges, where the density is lower, and sweeps up the particles, forming the hollow interior of the tunnels.

- The upward movement of interface at the mid-edge points hits the surface of the sediment and expels the suspended particles from the tunnels onto the surface of the sediment. This empties both the hexagonal tunnel systems and the paths leading up from the mid-edge points to the surface, and creates a slight elevation of the surface on top of the pattern, where the expelled material is deposited. This elevation is observed in the modern specimens of *Paleodictyon*.

Thus based on the modelling it is reasonable to suggest that a Faraday wave could induce movements of suspended particles that would lead to the formation of a system of tunnels similar to those found in the modern specimens of *Paleodictyon*.

5.4.3 Calcium carbonate experiment

Using the same apparatus as was used for the experiments described in paragraph 5.3.1, I performed the same experiment with a calcium carbonate paste. This paste was mixed from a fine $CaCO_3$ powder (48 ml) and water (35 ml) such that the mixture was at the verge of fluidization. A hexagonal Faraday wave was induced at a frequency of 20Hz for about 6 seconds. Directly after the vibration ceased, a relief pattern was visible in the surface of the paste. This

Figure 5.17: Experiment vibrating a calcium carbonate paste. On the left a snapshot of the experiment, which induced a hexagonal Faraday wave in a paste of $CaCO_3$ for 6 seconds. The wave was immediately preserved as a hexagonal pattern of relief in the surface. On the right is a photograph of the paste three days after the excitation. The raised surface forms a pattern of double hexagons, consistent with the pattern of nodes of the oscillation shown in Fig. 5.14. The hypothesis here proposed is that if this oscillation occurs slightly below the surface of the sediment, the nodal regions of the oscillation compact the sediment to form the boundaries of the tunnels, which form between these regions under influence of longitudinal currents, see Fig. 5.16. Scale bars 1cm.

pattern was still visible after three days of drying at room temperature, after which the experiment was ended. In Fig. 5.17 a snapshot of the excitation and a photograph of the pattern after three days are shown.

A careful examination of the relief that was left on the surface of the paste shows that the nodes are raised, whereas the anti-nodes are lower. The antinodes are formed by the hexagon interiors, the vertices and the mid-edge points. Nakayama et al. (2013) performed a number of experiments inducing a Faraday wave on the surface of a calcium carbonate paste and drying the experiment in a drying chamber. The desiccation cracks that appeared on the surface

after drying appeared to lie preferably on the nodes of the various modes of Faraday waves, among them the square lattice. This rectangular mode has a less complicated waveform than the hexagonal mode. The experiment described here was not dried to check whether the same law for the formation of desiccation cracks holds. In order to see whether this is the case, the depth of the paste should also be adjusted such that the characteristic spacing between the cracks is similar to the wavelength of the Faraday wave.

Although the desiccation crack experiment was not replicated here, the relief pattern found after the hexagonal excitation has not yet been documented before. The relief pattern explicitly follows the nodes of the hexagonal waveform, which were calculated here for the first time. The relief was visible on the surface of the paste immediately after the vibration ceased and is therefore not a result of dessication, but is directly produced by the memory/sorting effects of the paste. The relief was visible for three days until the experiment was destroyed.

The find that the nodes are elevated in the surface gives us a new insight into the causes for the formation of desiccation cracks along nodes. The rise in the surface suggests that particles were accumulated in these regions, suggesting that the density of particles in the paste has increased at the nodes. A higher accumulation of particles implies a lower presence of water, so a dry area in the paste. This might explain why the cracks are more readily formed here, since the water acts as an agglutinating agent between the grains preventing the formation of cracks.

The experiment explained here is relevant for the proposed hypothesis in two ways. Firstly it shows that hexagonal Faraday waves can induce some form

of sorting in suspensions or pastes, resulting in a lasting pattern. Secondly, it shows that the sorting of particles behaves in ways that can be predicted from a computer model of the wave, and it supports the physical mechanism proposed in the previous subsection that would result in the formation of a *Paleodictyon*-like tunnel system.

5.4.4 Can Faraday waves fixate a hexagonal pattern?

This section considered the physical properties of the sea floor sediment, computer models of the interface movement and 3D velocity field of a hexagonal Faraday wave and an experiment in which the hexagonal pattern was fixated on the surface of a paste. The aim was to resolve whether it is reasonable to suggest that a tunnel system like the excavated specimens of *Paleodictyon* found on the modern sea floor could be formed by the forcing of a hexagonal Faraday wave. The experiment above shows that a wave can result in the formation of a permanent hexagonal pattern in the sediment. It has not yet been established experimentally whether tunnels, and in particular vertical tunnels, can be formed through such a process. It is proposed here that flocculate marine sediment can be compressed through a physical process to form tunnels, and that there is a mechanism by which a Faraday wave can induce this process in a layer of loosely packed sediment, if it occurs on an interface slightly below the surface. Both these claims are quite complicated and cannot be proven until an experiment forms the actual pattern.

5.5 Comparison with *Paleodictyon* from the fossil record

The previous sections argued that hexagonal Faraday waves are likely to occur on the sea floor sediment and that they are capable of forming a lasting hexagonal lattice in a sediment, potentially also a system of tunnels similar to the modern *Paleodictyon nodosum*. Even if Faraday waves can create *Paleodictyon*-like patterns, this does not yet necessarily show that there are *Paleodictyon* patterns found in the fossil record that were created by Faraday waves. This section puts forward evidence that directly links measurements from experiments of hexagonal Faraday waves and measurements from occurrences of *Paleodictyon* in the fossil record.

In Fig. 5.18 A I present an overview of ranges of hexagon diameter of *Paleodictyon* specimens versus their age in millions of years. The data to compile this graph was taken from 22 papers which themselves compiled data from other papers as listed in Appendix C.3. Although incomplete, this data covers a wide range of times and sizes.

Specimens of *Paleodictyon* have been reported in sediments from an early Cambrian age through to the Cenozoic. As one would expect as a result of the sampling bias, a greater variation of sizes is found in recent times, but otherwise the hexagonal patterns are similar in size over time, as shown in Fig. 5.18 A. This data does not support the hypothesis that there is a directional shift in the sizes of *Paleodictyon* over time, as proposed in Seilacher (1977).

The measurements are plotted on a logarithmic axis, which is natural as they appear to be lognormally distributed. This last statement is supported by

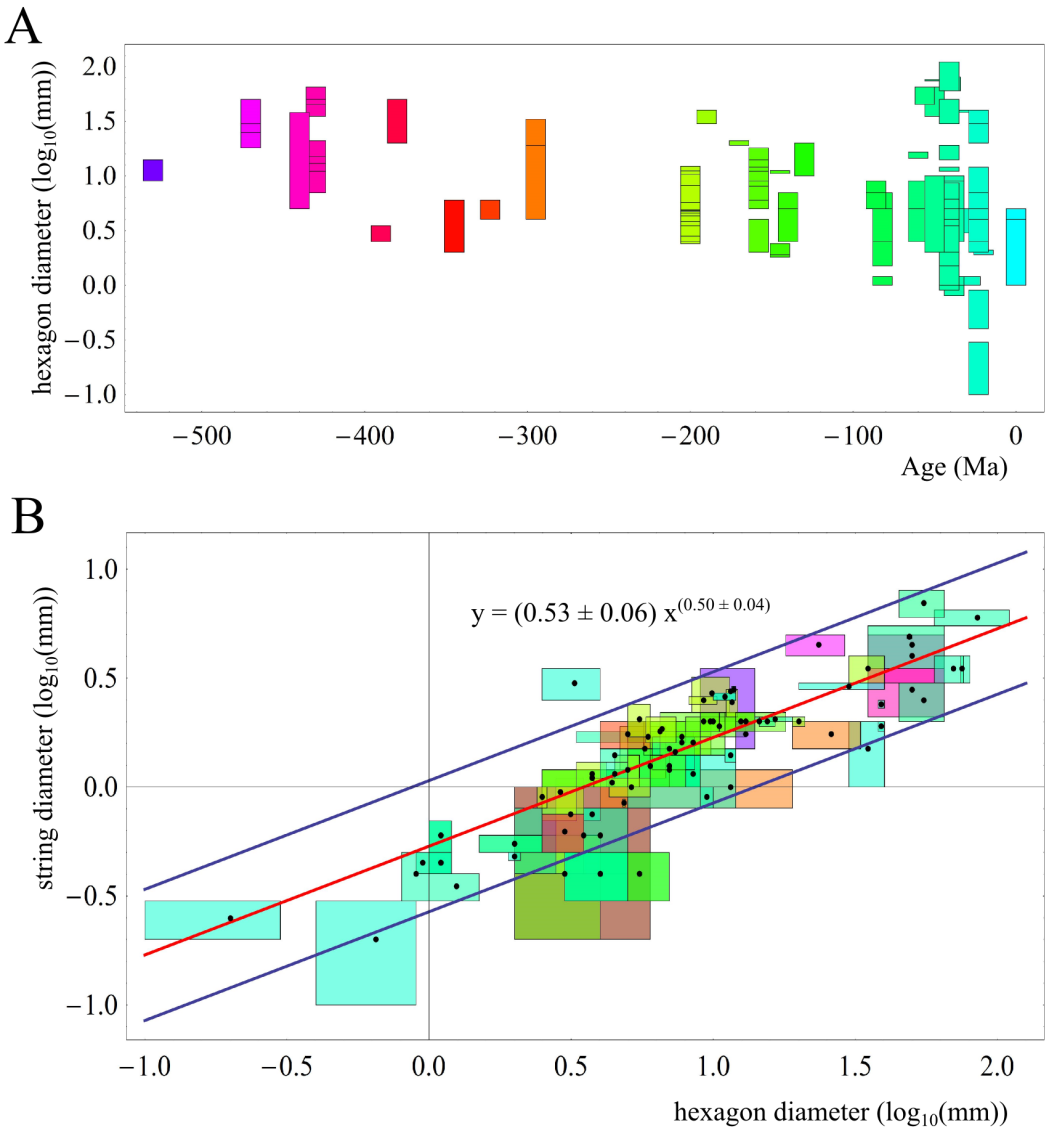

Figure 5.18: A) Measurements of *Paleodictyon* from the literature (see Appendix C.3) as a function of geological time. There is no clear shift in the mean size of the patterns, though as one might expect for both preservational and sampling arguments, the smallest and largest patterns are found in the Cenozoic.
B) A loglogplot of measurements of the mesh diameter versus the string diameter from the literature, colour coded for their age. The black dots show the centroid of each estimate. The mesh measurements cover three orders of magnitude and the string diameter two orders of magnitude. The data follows a square root relationship (red line and equation). There does not appear to be a clustering into species of the specimens of *Paleodictyon*.

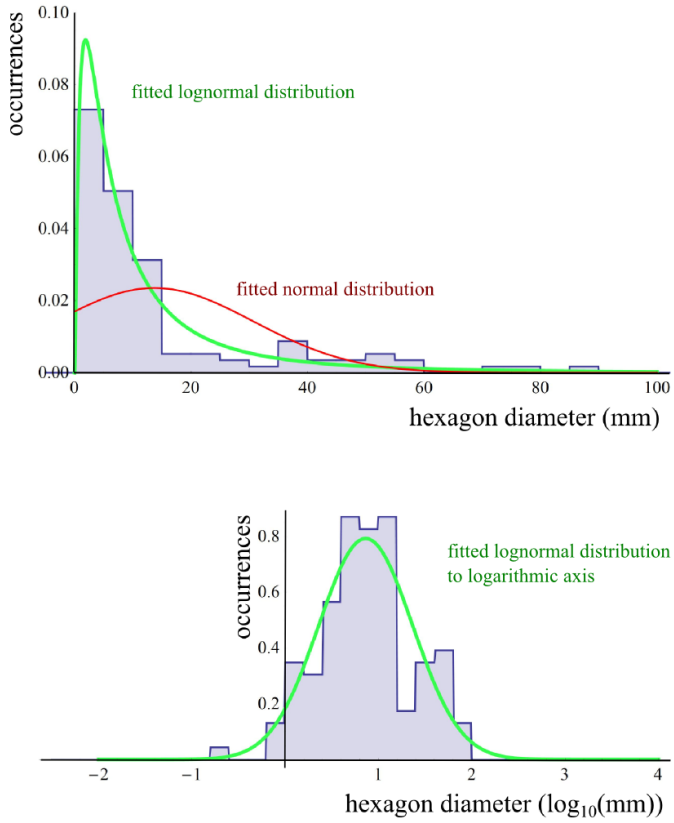

Figure 5.19: Histogram plots of mesh size measurements of *Paleodictyon* specimens shows these are lognormally distributed.

statistical analysis and is visualised in Fig. 5.19 which shows the binned distributions of the measurements themselves and of their logarithm.

5.5.1 Hexagon versus string size

The classification of *Paleodictyon* into ichnospecies is problematic, and has been renewed several times (e.g. Seilacher (1977); Ksikiewicz (1970); McCann and Pickerill (1988); Crimes and McCall (1995); Uchman (1995); Miller (2014); Seilacher (2007b)). There is currently no consensus concerning the ichnotaxonomic classification. In the classification by Uchman (1995) two measurements

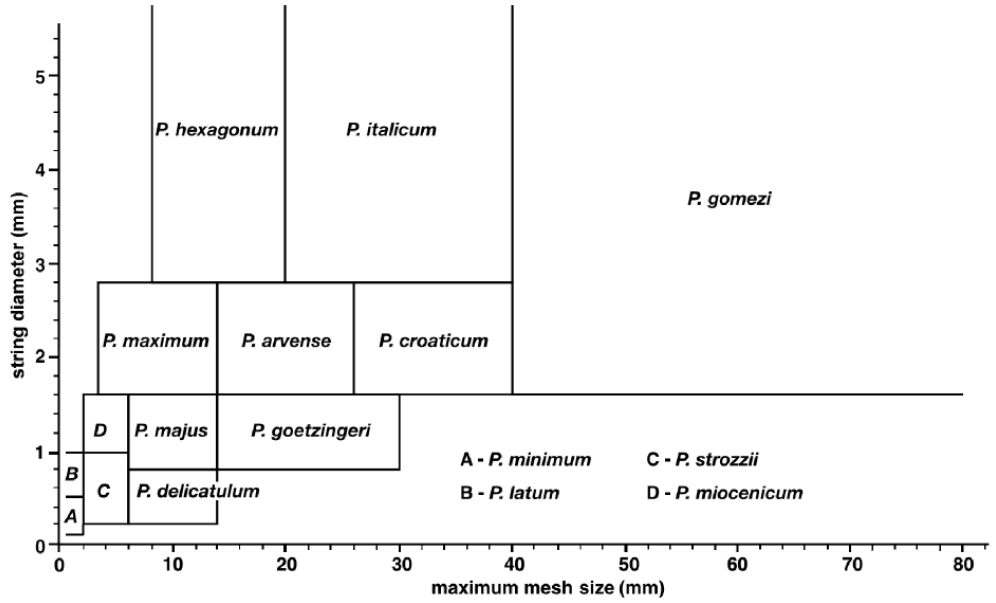

Figure 5.20: Classification into ichnospecies of *Paleodictyon*, Uchman (2003) Fig. 10.

of the ichnofossils are taken as a basis for ichnospecies assignment, namely the diameter of the hexagons and the width of the hexagon ridges or strings. This classification is shown in Fig. 5.20. These two measurements are plotted in Fig. 5.18 B, colour coded according to their age with the same colours as were used in Fig. 5.18 A.

As was noted by Uchman and is clear from Fig. 5.18 B, there is no clear grouping into ichnospecies of the size measurements of *Paleodictyon*. Instead the measurements seem to be spread around a square root dependence. The fitted function, red in the diagram, is given by:

$$y = (0.54 \pm 0.06)\, x^{(0.50 \pm 0.04)}, \tag{5.3}$$

where y is the string or ridge diameter and x is the hexagon diameter.

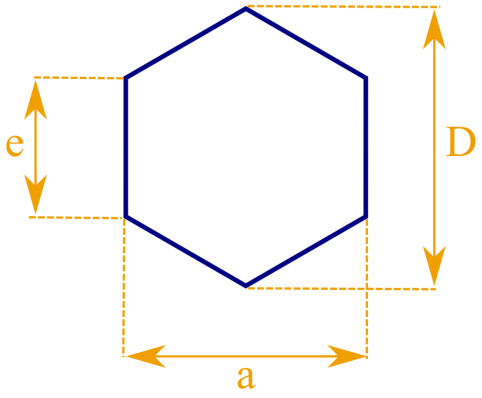

Figure 5.21: Diagram showing the different lengths in a hexagon, the long diameter D, the short diameter a and the edge length e, whose mutual relationship is shown in equation 5.4.

Although it is clear what is meant by the string width, it is not immediately clear what is meant by the diameter of a hexagon. As shown in figure 5.21, there are three different lengths in a regular hexagon that one might consider as the diameter. There is the length of an edge e, the length of the small diagonal a and the length of the big diagonal D. In a regular hexagon these three quantities obey the following relationships to each other:

$$D = \frac{2}{\sqrt{3}}a = 2e. \tag{5.4}$$

The two black lines in the diagram describe the uncertainty that originates from interpreting the given diameter x as either the longest diagonal D or the short edgelength e. It should be noted that some of the scatter of the measurements might therefore originate from differences in measurement technique. This is represented by the two black lines in diagram 5.18. We should also expect some scatter in the physical data, for example as a result of the flattening of the ridges, which often appear slightly ellipsoidal in cross section.

All in all measurements of the mesh diameter (x) versus string width (y) of *Paleodictyon* ichnofossils seem to be adequately described by the relationship $y = 0.5\sqrt{x}$ and do not seem to be grouped as one would expect as a result of ichnospecies differences.

5.5.2 Link to Faraday waves

A similar square root relationship was found in measurements from nine experiments inducing a hexagonal Faraday waves on a mixture of fine silica dust and water. With the diameter of the hexagons in the excitation on the x-axis and the widths of the excitations that form the edges of the hexagons on the y-axis, the following relationship holds:

$$y = \alpha\sqrt{x}, \tag{5.5}$$

where α was fitted to $0.74 \pm 0.03\sqrt{mm}$.

This relationship reflects a physical constraint for Faraday waves. The physics of this system is currently not yet understood well enough to explain why a square root might be present. One would expect the behaviour to be related to higher order effects that relate to the interactions of the different modes that contribute to the hexagonal Faraday wave (see Appendix C.1) and how this relates to intrinsic scales of the liquid or interface. The constant α encodes the magnitude of this interaction and thus relates to the intrinsic properties of the material. One expects the presence of the square root to be universal for the hexagonal mode while the value of α varies with the properties of the sediment.

Finding a square root relationship in the ichnofossil record supports the hypothesis that the Faraday wave is responsible for the formation of *Paleodictyon*. The value of α that we find when averaging over specimens of *Paleodictyon* from all eras is 0.54, which is in the same order of magnitude as the value 0.74 that is found in the experiments.

5.5.3 Changes in size over time

Plots very similar to Fig. 5.18 B have been compiled by Uchman (2003) for different time periods to study the variations in sizes of *Paleodictyon* over time and to link these to environmental changes. This data is shown in Fig. 5.22. The lines in the background refer to the species division in Fig. 5.20. Geological time since the Cambrian is split into four periods and for each period the distribution of mesh versus string sizes of specimens of *Paleodictyon* is shown.

I have fitted one or two square roots to the data presented in each plot in Fig. 5.22. Particularly for the Triassic-Jurassic (panel B) and the Paleogene (panel D), the variation in sizes of *Paleodictyon* is adequately described by a square root. The different values of the prefactor α of the are shown in Table 5.1. The weighted average of these values is 0.5, close the value of α found for the data plotted in Fig. 5.18 B, indicating that the two datasets show similar behaviour.

These variations in sizes of *Paleodictyon* over time were argued by Uchman (2003) to be indicative of variations in the marine environment induced by environmental changes. The paper gives an overview of the complex processes that influence ocean productivity over the course of the Phanerozoic.

The ocean biosphere greatly influences the composition of the sediment. Therefore it is to be expected that the sediment properties and therefore the value of α would vary over time. If the hexagonal Faraday wave hypothesis for the origin of *Paleodictyon* is confirmed, then it would be possible to study the physical properties of the palaeo-sediment in a new way by measuring the sizes of *Paleodictyon* specimens. For example, the datasets in Fig. 5.22 suggest that conditions were more stable during the Paleogene and the Triassic-Jurassic than during the Cambrian through to the Permian and in the Cretaceous, with respect to certain aspects of the behaviour of the sediment. Indeed, the ocean conditions are known to have been stable from the Devonian to the Middle Jurassic. However, there is a marked difference between the stable situations in the Triassic-Jurassic and in the Paleogene, with the value of α lowering from 0.7 to 0.4.

The lower α is, the smaller the ridges of the hexagons are compared to the hexagon diameters. Smaller ridges reflect stronger interaction and probably an increased influence of higher order effects on the waveform. A lower value of α therefore probably reflects that the sediment suspension has more self-interaction. This self-interaction can be the result of large molecules and particles binding to each other within the sediment and increasing its cohesion. The lowering of the value of α from 0.7 in the Triassic-Jurassic to 0.4 in the Paleogene might reflect the diversification of angiosperms during the Cretaceous, which resulted in an increase of terrigenous detritus being deposited in the seas. This altered the sediment composition, increasing the input of organic matter, mainly cellulose (Uchman (2003)). Cellulose is a polysaccharide usually bound in a linear chain of thousands of units and which also forms hy-

drogen bonds, so it is especially cohesive. The lowering of the value of α could therefore be explained by an increased cohesion due to the influx of cellulose in the deep sea sediment. Uchman (2003) already noted an influence of the rise of angiosperms on the trace fossils, but writes it is hard to explain.

The Paleozoic measurements show a mixture of higher and lower values of α. I have drawn lines corresponding to $\alpha = 0.9$ and $\alpha = 0.3$. This could indicate that during the Paleozoic there were different environments, with different physical properties, in which Faraday waves were preserved. Note that eukaryotic phytoplankton only became dominant during the Mesozoic, while currently being responsible for over 45% of the Earth's net primary production (Falkowski et al. (2004)). The radiation of phytoplankton increased nutrient recycling and could, arguably, have stabilised the ocean environment, preventing the build-up of organic matter. The absence of such a stabilising mechanism might explain why in some area's during the Paleozoic the value of α was very low, potentially reflecting a cohesive layer of built-up degrading biomatter.

Table 5.1: Values of α over time, based on the measurements collected in Uchman 2003. These variations might be attributed to changes in the physical properties of the sediment. Age Plot in Fig. 5.22.

Age	**Plot in Fig. 5.22**	**Value of α**
Cambrian, Ordovician	A	0.9 ± 0.1
Ordovician,Silurian, Permian, Carboniferous	A	0.3 ± 0.1
Triassic, Jurassic	B	0.7 ± 0.1
Cretaceous	C	0.9 ± 0.1
Cretaceous	C	0.4 ± 0.1
Paleogene	D	0.4 ± 0.1
Weighted average		$\mathbf{0.5 \pm 0.1}$

5.6 Discussion

How does the Faraday wave hypothesis relate to the arguments that were raised by Pickerill (1990) to establish that *Paleodictyon* was biogenic? Pickerill argued that *Paleodictyon* had to be biogenic based on four arguments: a lack of current orientation; generally uniform dimensions and the regularity of the pattern; presence of a thin lining and the presence of other trace fossils on the same bed. How does the abiogenic hypothesis proposed in this chapter compare with these points?

Faraday waves are not caused by a current, thus they are not expected to be aligned with the current. They might be deformed by a current after their production, but current alignment is not a necessary characteristic. Regularity often implies that a pattern is of biogenic origin. However, perfect regularity is very rarely attained by biology. At the same time the presence of a uniform wavelength throughout the pattern is a fundamental feature of a standing wave and indeed the Faraday modes form perfectly regular geometrical patterns. As for a lining of the specimen walls, computer modelling and the experiment with a calcium carbonate paste suggest that the density of the sediment increases at the tunnel boundaries. Therefore a thin lining of the tunnel walls might indicate that the flocculate sediment is compacted under the force of the vibration, according to the pattern of nodes in the waveform.

Lastly, the Faraday wave hypothesis should also be able explain the co-occurrence of *Paleodictyon* with other trace fossils, namely the graphoglyptids. As *Paleodictyon* is commonly found together with other graphoglyptids, it seems improbable that *Paleodictyon* is formed abiotically while the other grapho-

glyptids are proper trace fossils.

Graphoglyptids are regular geometrical patterns that have a tendency to subdivide a pattern in bits of equal lengths (Rona et al. (2009)). This is reminiscent of standing wave which has a fixed wavelength. There is also a striking similarity between some taxa of graphoglyptids and some other modes of Faraday waves. In particular *Spirorhaphe*, forming a regular Archimedean spiral, is very reminiscent of the spiralling Faraday modes such as the one shown in Fig. 5.12 F. The meandering *Cosmorhaphe* could potentially be formed by the mode that I encountered in experiments resembling a ribbon of transverse excitations, an example of which is shown in Fig. 5.10 H. Other forms with a strong meander such as *Helminthorhaphe* (Fig. 5.3 C) are sometimes similar to striped modes such as Fig. 5.12 B-D,G. The mode selection of Faraday waves is sensitive to variations in the amplitude and frequency of the driving excitation. Therefore one would expect other modes to occur in the same setting. So one can potentially argue that some of the other graphoglyptid patterns might be formed by different modes of Faraday waves.

Uchman (2003) finds a higher diversity of graphoglyptids since the Cretaceous, and also Seilacher (1974) believed that highly patterned graphoglyptids became more abundent at the end of the Mesozoic because of the radiation of angiosperms. Perhaps this can be explained by the increase in cohesion of the sea sediment, and a resulting increase in the amount and diversity of Faraday wave patterns that were preserved.

However, a number of modern burrowing organisms are known to create very regular patterns. For example, the modern paraonid polychaete *Paraonis fulgens* creates spiral-shaped burrows that are also quite similar to *Spirorhaphe*,

as shown by Minter et al. (2006). Clearly not all regular trace fossils can be the result of standing waves. Graphoglyptids essentially form a spectrum of geometrical shapes, which vary in morphology from perfect regularity to only superficially regular forms. Hence there is a need for a way to differentiate biogenic trace fossils which are geometrically regular from patterns formed by Faraday waves.

In order to consider the possibility that a trace fossil is created by a Faraday wave, the list of criteria for biogenicity of trace fossils, given by Ekdale et al. (1984) and interpreted by Pickerill (1990) to consider the biogenicity of *Paleodictyon*, should be updated for the special consideration of trace fossils displaying geometric regularity. I propose the following points to be considered for future reference, apart from trying to identify biological markers such as faecal pallets or altered chemistry.

Does the specimen show a clear repetition of a single scale or "wavelength" throughout the pattern?

As Faraday waves are standing waves, a connected pattern that results from such a wave must obey the physical rules of a standing wave. Particularly, the whole pattern displays the same wavelength at formation. The pattern may be disturbed after its formation, for example through currents or tectonic deformation. If the length scale of a trace were to vary across the pattern in a manner that can not be explained by such deformation, then this is evidence in favour of a biogenic interpretation of the specimen.

How regular is the geometry?

Faraday waves in principle have a regular geometry and therefore the resulting pattern is expected to be regular at the time of formation. There are some exceptions in the case of an inhomogeneous medium, in which case a mode can be isolated, variable or curved (i.e. see Fig. 5.10, especially H). Given a specimen one can try to estimate whether deviation from regularity can be explained through such a mechanism.

After a sediment pattern is formed by a Faraday wave, it might be distorted before, during or after burial. For example, the pattern might be fluted in the direction of the current. Monaco (2008) describes post-formational deformation of *Paleodictyon* and other graphoglyptid patterns. Experimental work on cohesion within the patterns could reveal how much a Faraday pattern can be deformed without breaking up entirely, and how irregular formed patterns can be.

If a specimen displays some overall geometry such as a lattice symmetry, then one can consider and measure how regular this pattern is. One can then consider whether the way in which the specimen deviates from regularity can be the explained by post-formational distortion under the influence of currents, degradation, the process of burial or tectonic deformation. If this is not the case, for example because a lattice-type trace is not at all regular, then this is evidence for a biogenic origin.

Does there exist a mode of Faraday waves capable of creating this pattern?

If a specimen is found to possess a recurring "wavelength" and is regular, then the next question to consider is whether it is possible for the dispayed pattern to have been formed by a Faraday wave. Faraday waves occur in many different modes. The classic modes are given by circles, stripes, squares and hexagons. In the 1990's it was found that many more modes with more complexity are possible, such as spirals (Edwards and Fauve (1994), see Fig. 5.23), quasi-crystalline patterns, superlattices and beaded stripes (Périnet et al. (2012)). For a given homogeneous medium, the selection of the mode depends on the amplitude and the frequency of the vertical excitation. As a general rule, fluids with more complex behaviour such as non-Newtonian fluids will have a more complex phase diagram with more possible modes (e.g. Wagner et al. (1999)). Fig. 5.24 illustrates a complex mode of Faraday wave, composed of a hexagonal superlattice encompassed by curved stripes, appearing on the surface of a viscoelastic fluid. Combining different forcing frequencies also results in a wider variety of patterns occurring (Edwards and Fauve (1994)). If a medium is not homogeneous, or if it differentiates as the result of the wave, then yet other modes can appear with a more local behaviour, for example a ribbon of transverse excitations (e.g. Fig. 5.10 H), or modes with irregularities and singularities (places where the symmetries of the pattern are broken).
A more subtle side of the question above is given by the following problem: given a certain mode of Faraday wave, what pattern will it leave in a sediment subjected to it? The pattern is expected to have the same overall symmetries as the waveform. However, it is not immediately clear how particles in the

suspension will respond to the forcing presented by the waveform, also because the velocities within the waveform are not known for every mode. One expects the nodes of the waveform to be important for the formation of a resulting pattern or sorting effect. If one can determine the position of the nodes through a model of a waveform, then a better prediction for the resulting sediment pattern can be made.

Identifying the nature of surrounding trace fossils

The biogenicity of a trace fossil should not just be considered on its own, but as a part of a given assemblage of trace fossils. Are the trace fossils found closeby, or similar ones found elsewhere, clearly of biogenic or abiogenic origin?
For a given ichnotaxon, can one find conclusive evidence one way or the other? For trace fossils with a modern analog, which is the case for a number of graphoglyptids (Ekdale (1980)), we can try to identify an organism responsible for the creation of the pattern by looking for it. On the other hand, we can try to recreate the a pattern in experiments that looks exactly like one of the ichnotaxa. If other graphoglyptids are produced by Faraday waves, then a relationship between widths of riblets and the recurring wavelength can again be expected. Potentially even a square root behaviour, because the same physics underlies the waveforms. This relationship is also something one can look for in specimens.

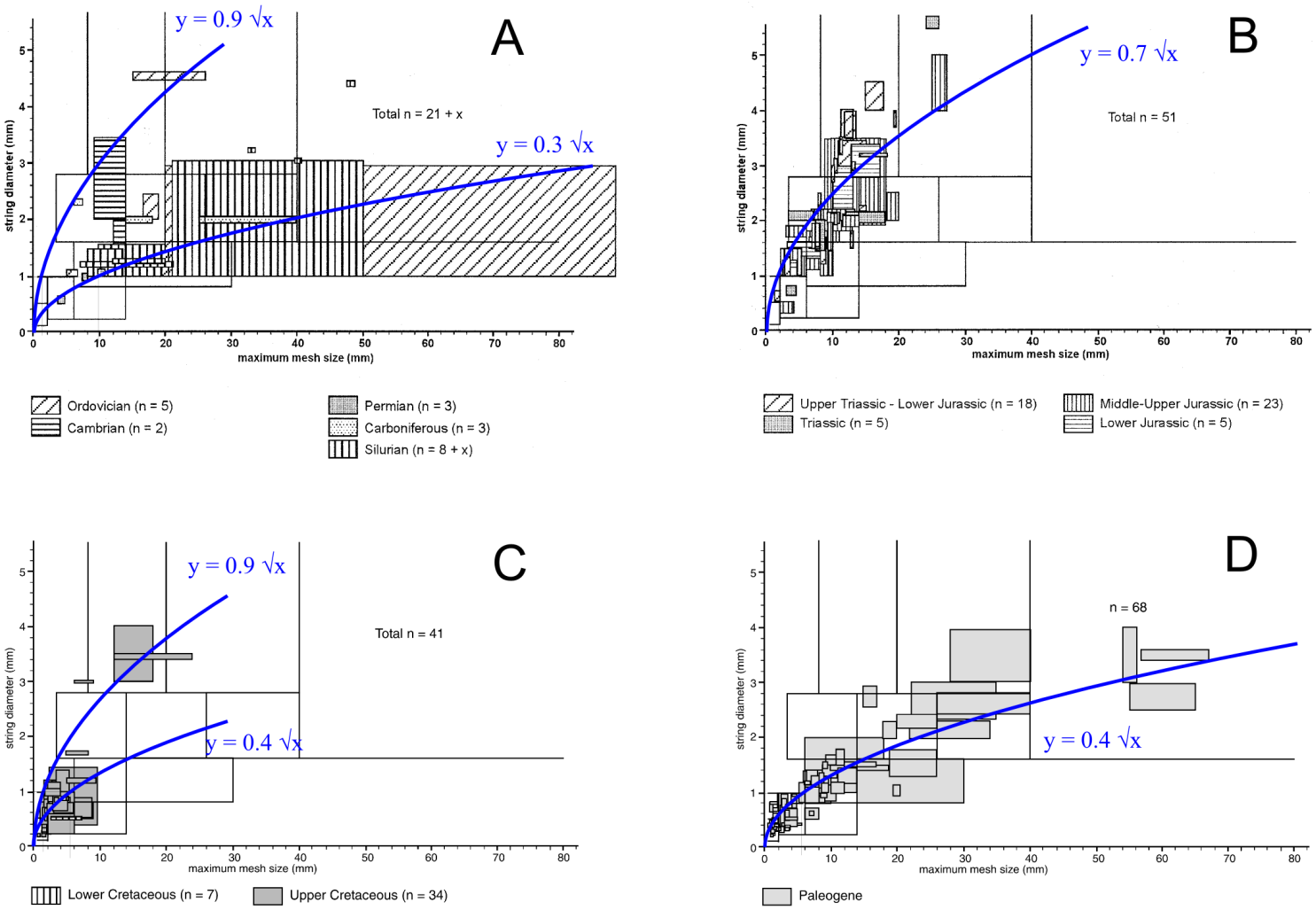

Figure 5.22: Measurements from *Paleodictyon* specimens across the fossil record, collected by Uchman (2003), indicate the potential presence of a square root relationship with different prefactors α at different times. Plots from Uchman (2003).

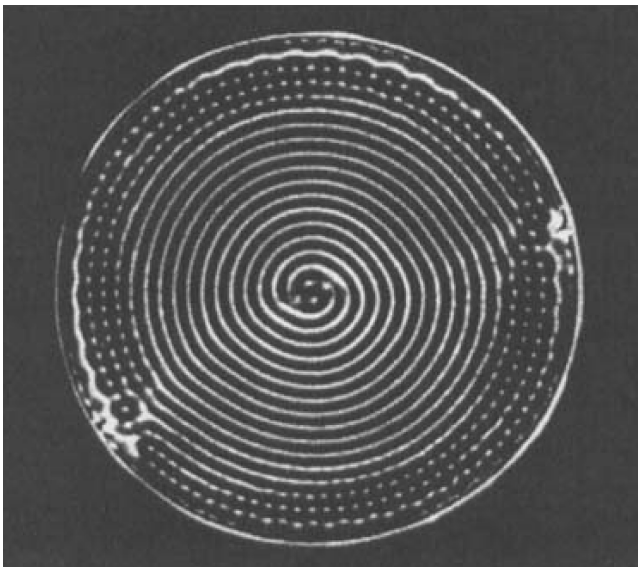

Figure 5.23: Example of a spiral Faraday wave. Edwards and Fauve (1994) Fig. 10.

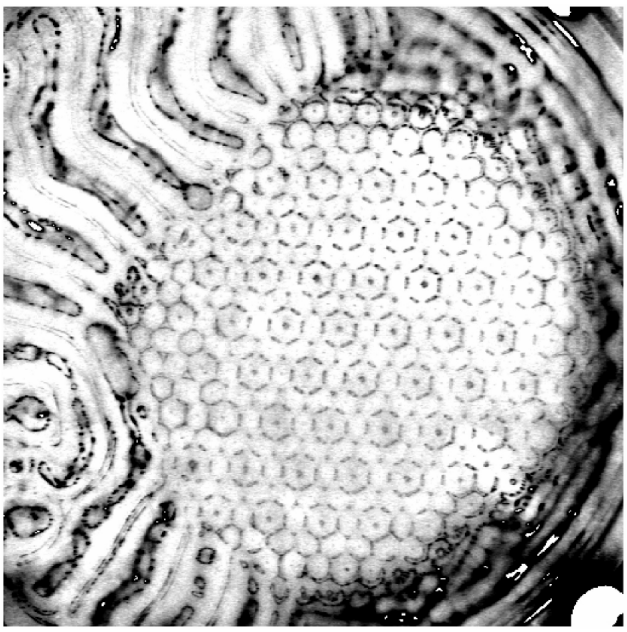

Figure 5.24: Example of a Faraday wave on a viscoelastic fluid illustrates how a non-linear medium can result in complex geometric modes. Wagner et al. (1999) Fig. 4.

Part III

Conclusion

Chapter 6

Conclusion

6.1 Concluding Part I

A major part of my doctoral research has focused on the development of new techniques for the study of growth in the late Ediacaran macrobiota. The techniques that were developed are applied in this thesis to the iconic Ediacaran taxa *Dickinsonia costata* and *Charnia masoni*. This application has revealed new insights into the development and biology of these two taxa, and revealed links between the growth programs of the two. The techniques developed in this work can be applied to a wide range of taxa from the Ediacaran period and other periods.

It would be interesting to study organisms with an iterated mode of growth outside of the Ediacara biota using the mode of presentation of measurements and potentially the growth model presented in this thesis. Examples of taxa and features that can be studied include: the size of the segments in segmented bilaterians, the size of leaves on a plant, e.g. fronds of a fern leaf, and the giant thiotrophic colonial ciliate *Zoothamnium*, which also shows it-

erated branching (Bright (2014); Kloiber et al. (2009); Laurent et al. (2009)). It would for example be interesting to quantitatively compare the mode of growth of *Dickinsonia* with that of the annelid worm *Spinther*, with which it has often been compared (Manton and Harding (1967); Runnegar (1982)).

Gold et al. (2015) argued that the "terminal addition" mode of growth of *Dickinsonia* places the taxon within the Bilateria. In Chapter 4, I argued that the morphology and mode of growth of many of the Ediacaran macro-organisms is derived from a common ancestor. Hence, the placement of *Dickinsonia* within Bilateria should be re-evaluated from the point of view of a united mode of growth for "vendobionts". This would imply a bilaterian placement of vendobionts, since Gold et al. (2015) argues that this mode of growth is a synapomorphy of Bilateria.

Within this larger group, there is some evidence against a link with the Bilateria. For example, specimens of *Pteridinium* have been found to cross-cut each other and continue growing (Grazhdankin and Seilacher (2002)). This shows a greater flexibilty of growth program than is present in any modern bilaterian. Furthermore, many vendobionts share a distinct off-set mode of branching, which contradicts the bilaterian mode of growth. This could be interpreted as a lost pathway in bilaterians, together with the apparently lost ability to produce multiple vanes surrounding the axis.

Alternatively, one might argue that vendobionts have a more basal placement within the phylogeny and separately evolved a complex mode of growth, which is distinct from those found in extant taxa. As argued by Chipman (2010) and Marshall and Valentine (2010), many of the genetic pathways that were useful for developing a complex body plan were present very early in the history

of life. If these pre-adapted genomes could easily be employed to generate complex body plans, as these authors argue, then perhaps these were independently adapted by the vendobionts to generate a unique mode of growth. As Marshall and Valentine (2010) argues, the pathways that generated these unique morphologies might have been mediated by developmental pathways that have now gone extinct.

6.2 Concluding Part II

In Chapter 5, I proposed the hypothesis that the phenomenon of Faraday waves occurring in the subaqueous sediment surface might be responsible for the formation of many specimens of the iconic hexagonal trace fossil *Paleodictyon*. This hypothesis may solve a number of mysteries that have surrounded *Paleodictyon* for a long time (see for example Miller (2014)).

For example, it would explain how a perfectly regular, highly interconnected and occasionally vast hexagonal network is formed, which has been argued to be difficult from the perspective of a burrowing organism (Garlick and Miller (1993); Honeycutt and Plotnick (2005)). Standing waves are non-local phenomena and are naturally regular across a large area, or appear in local patches in the case of a viscoelastic fluid. On a sediment with slight density variations less regular modes of Faraday waves occur, as is clear from experiments. Hence, very regular and less regular hexagonal patterns, across a larger area or in a small patch can potentially be formed by Faraday waves.

The hypothesis would explain why a thorough study of the modern specimens of *Paleodictyon* by Rona et al. (2009) did not reveal any trace of the presence of a creating organism. Also the common, but not exclusive (Fur-

sich et al. (2007)), occurrence of *Paleodictyon* in oligotrophic environments (Olivero and Lopez (2010); Uchman (2003); Miller (2014); Uchman (2004); Seilacher (1977)), as well as the appearance of *Paleodictyon* in a variety of aquatic environments, from the deep sea (e.g. Ekdale (1980)) to lake settings (e.g. Pickerill (1990)), would be explained if the pattern is of abiological origin. The occurence of regular specimens of *Paleodictyon* from the Cambrian until the present time can be explained by the rise of metazoan burrowers in the Cambrian, but would be consistent with the differences in sediment composition. Measurements of two sizes in the specimens of *Paleodictyon* reveals a square root relationship that is also present in the measurements from experiments. Changes in the prefactor of this relationship over time can be explained by the rise of angiosperms and a resulting increase in sediment cohesion.

The Faraday wave hypothesis is testable. Future experiments can show whether or not a *Paleodictyon*-like pattern can indeed be formed by a standing wave. These experiments will require an experimental setup that is potent enough to vibrate a reasonable body of water along with a layer of sediment at a considerable amplitude, such that the critical amplitude of the submerged sediment surface is exceeded while interference of surface waves of the liquid can be minimized. This is somewhat challenging as the low wave velocity of submerged sediment implies that lower frequencies should be applied, and lower frequencies require higher amplitudes to reach a similar critical acceleration. As was shown in the experiments, sorting effects can occur that capture the pattern of a Faraday wave in the sediment. However, for the sediment to form tunnels while submerged, the sediment has to be able to support tunnels. Therefore the sediments used in an experiment need to be more similar to the modelled

situation than silica dust is. Flocculate sediments are hard to create in a lab, so it is probably best if samples of natural marine sediment can be used, such as the Antarctic core samples that were used in Chapter 5.

If the hypothesis turns out to be true, then this has a number of consequences for the field of ichnology. The biogenicity of some ichnotaxa should be carefully reconsidered, especially of graphoglyptids. The chapter concluded with a list of considerations that may help determine the biogenic or abiogenic nature of trace fossils. The hypothesis might also bear consequences for studying palaeoenvironments. The size relationships of *Paleodictyon* vary over time, and this may be the result of changes in the physical properties of the sea floor sediment. Measurements may help us to understand the variables that influence these physical properties, such as evolution of phytoplankton and the radiation of angiosperms. Moreover, the absolute mesh size of *Paleodictyon* would be determined by the frequency of an earth quake, and the mode selection (what sort of pattern is formed), would be influenced by the amplitude. Thus, studying *Paleodictyon* might potentially reveal insights into the physical properties of the sediment and palaeoseismometry.

Acknowledgements

For financial support that made this research possible I would like to thank the Prins Bernhard Cultuurfonds, the Hendrik Mullerfonds, the Langerhuizen Stipendium, the VSBfonds, the Vreedefonds and the Genootschap Noorthey.

To my supervisor Martin Brasier, who sadly passed away one month before the submission of this thesis, I am deeply grateful. I will never forget his kindness and support, and his eternal enthusiasm. I regret that he will never see this thesis finished.

Alex Liu I want to thank for stepping in at the last moment and being a great help with proofreading the chapters and providing excellent feedback. I want to thank Roger Benson for a number of helpful discussions and proofreading my growth model chapter. I thank David Pyle, Chris Ballentine and Richard Walker for useful help planning the submission of the thesis.

For the second part of this thesis, I want to thank my collaborator Maarten Kleinhans at the University of Utrecht Department of Physical Geography for the use of lab space and very useful and fun collaboration. Rudi Borkus from the Utrecht Physics Department for a great help with the experimental setup. The technicians of the Utrecht Physical Geography I want to thank for help with the experiments, in particular Henk Markies for helping me

out in his spare time. The technicians of the Utrecht Physics Department I thank for material loan. Francesca Sangiorgi from the Earth Science Dept of Utrecht University I would like to thank for providing the core sediments from Antarctica. I want to thank Nicholas Périnet for a useful email exchange and providing the data for the model of the hexagonal Faraday waves.

I would like to thank my friends for their support during the last years, especially William Nash, Michael Stock, Fern Dowdall, Ashley Norris, Hanne Wouters, Robert Kropholler, Henry Bradford and Anna Grebenchtchikova. I would like to thank my parents for their incredible love and support. My family, my sisters Elseline and Tessa and little nephews Timo, Florian and Sava and little niece Jasmijn. I thank my partner's parents Ike van den Berg and Jos Wasserman. Last but not least, I thank Thomas Wasserman, my partner in love and science.

Appendices

Appendix A

Growth model for *Dickinsonia costata*

The next few pages show the growth model for the taxon *Dickinsonia costata* reconstructed in Chapter 4. The morphology is shown in 200 timesteps, where each timestep represents the insertion of one branch for as long as the branches are inserted. The insertion stops after 100 branches. The snapshot at the moment of the insertion stop is framed to indicate when this transition occurs.

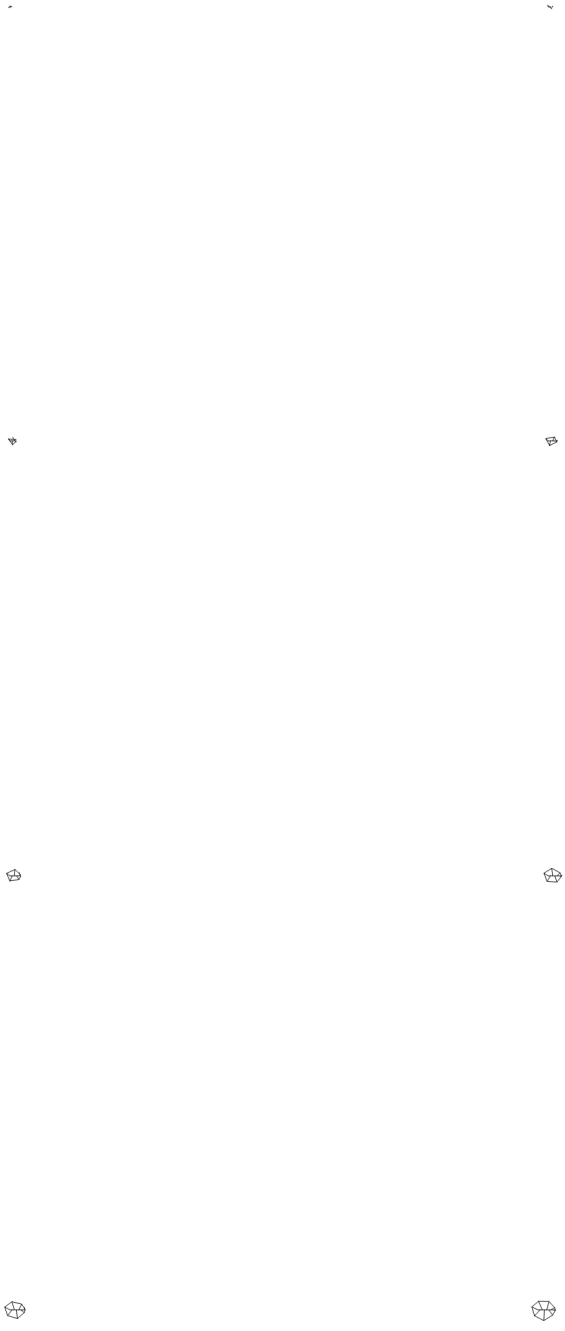





















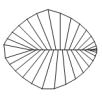
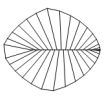

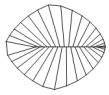
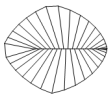
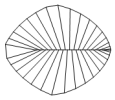
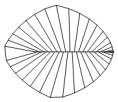
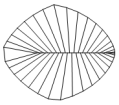
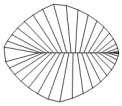
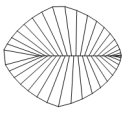
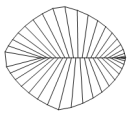

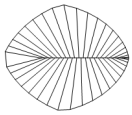
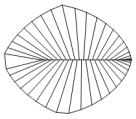
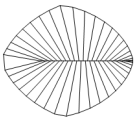
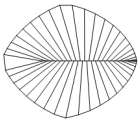
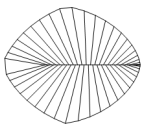
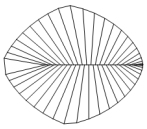
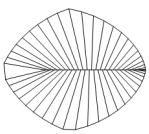
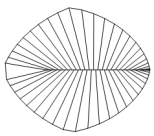

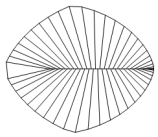
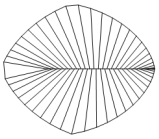
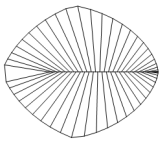
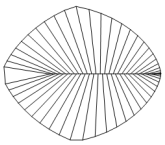
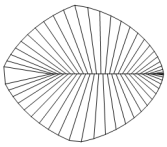
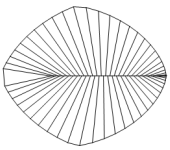
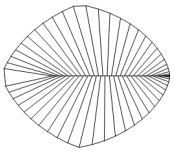
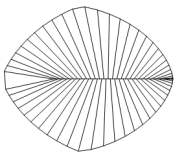

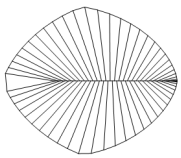
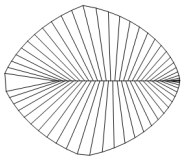
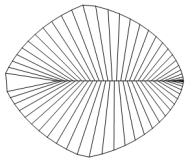
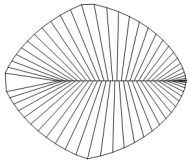
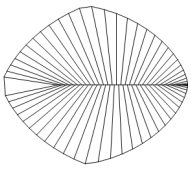
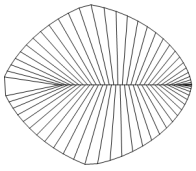
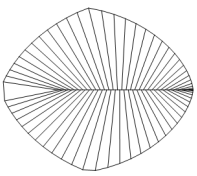
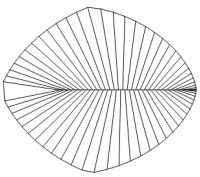

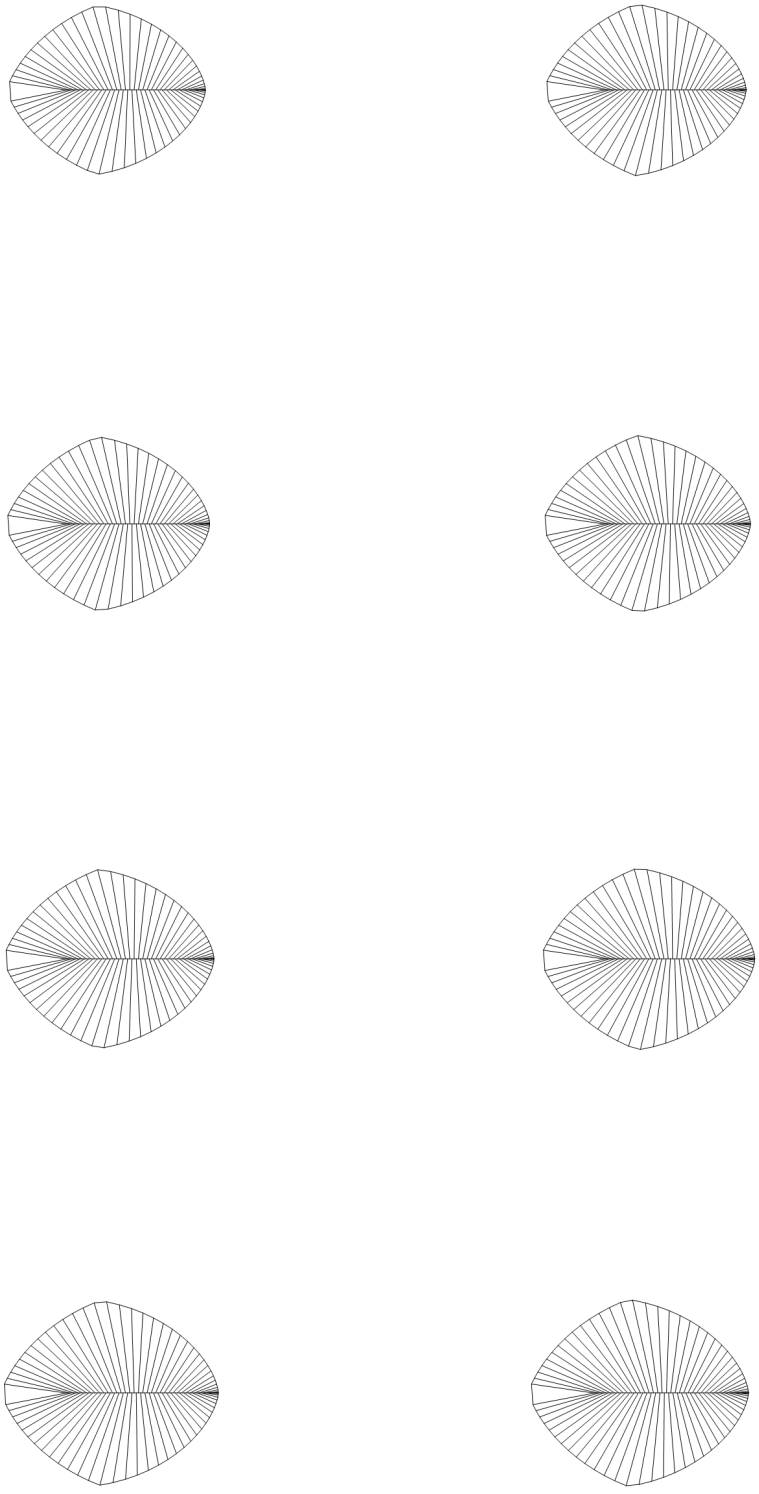

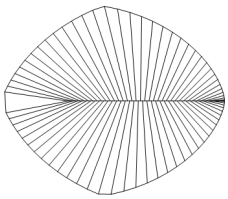
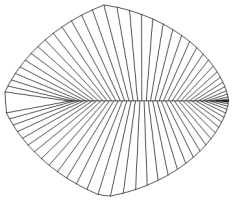
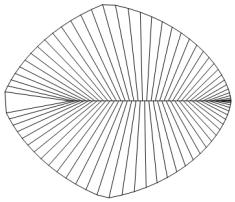
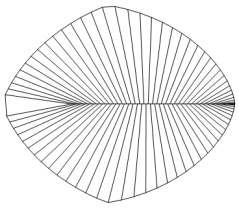
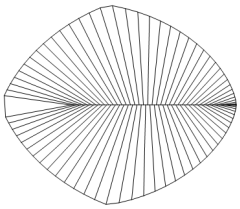
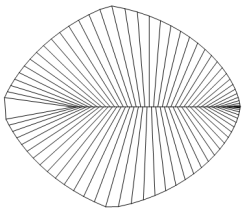
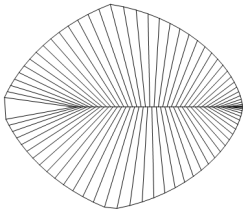
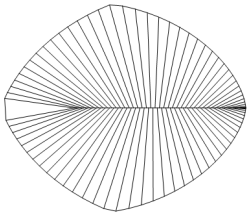

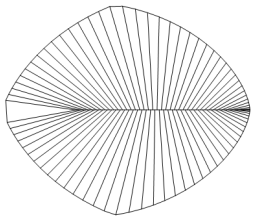
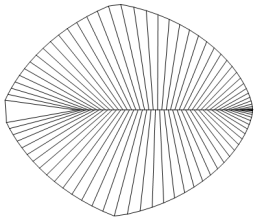
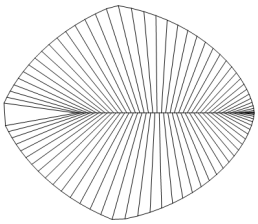
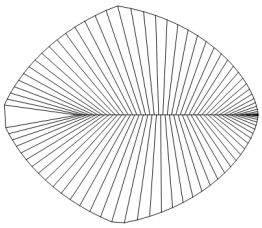
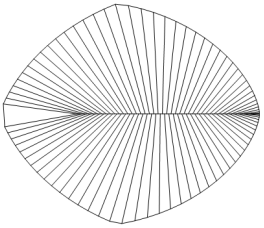
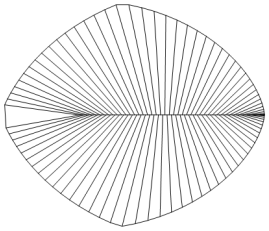
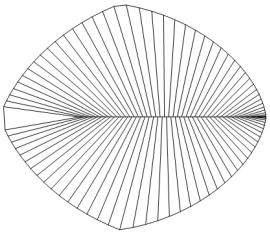
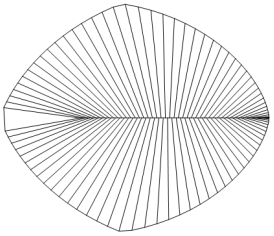

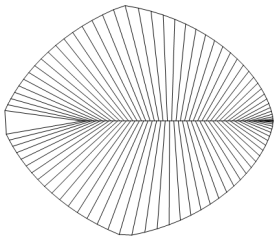
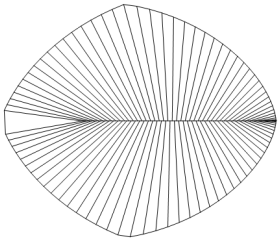
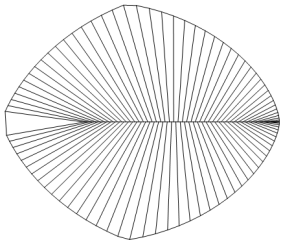
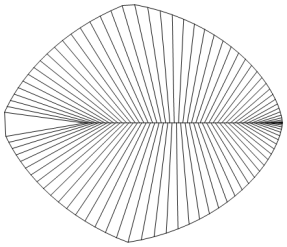
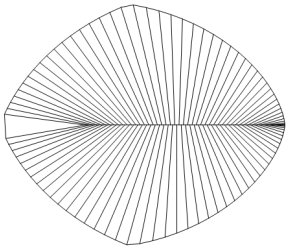
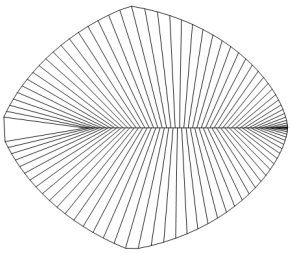
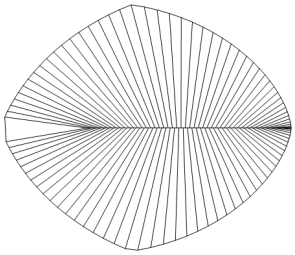
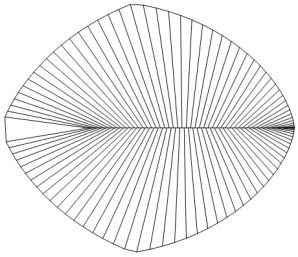

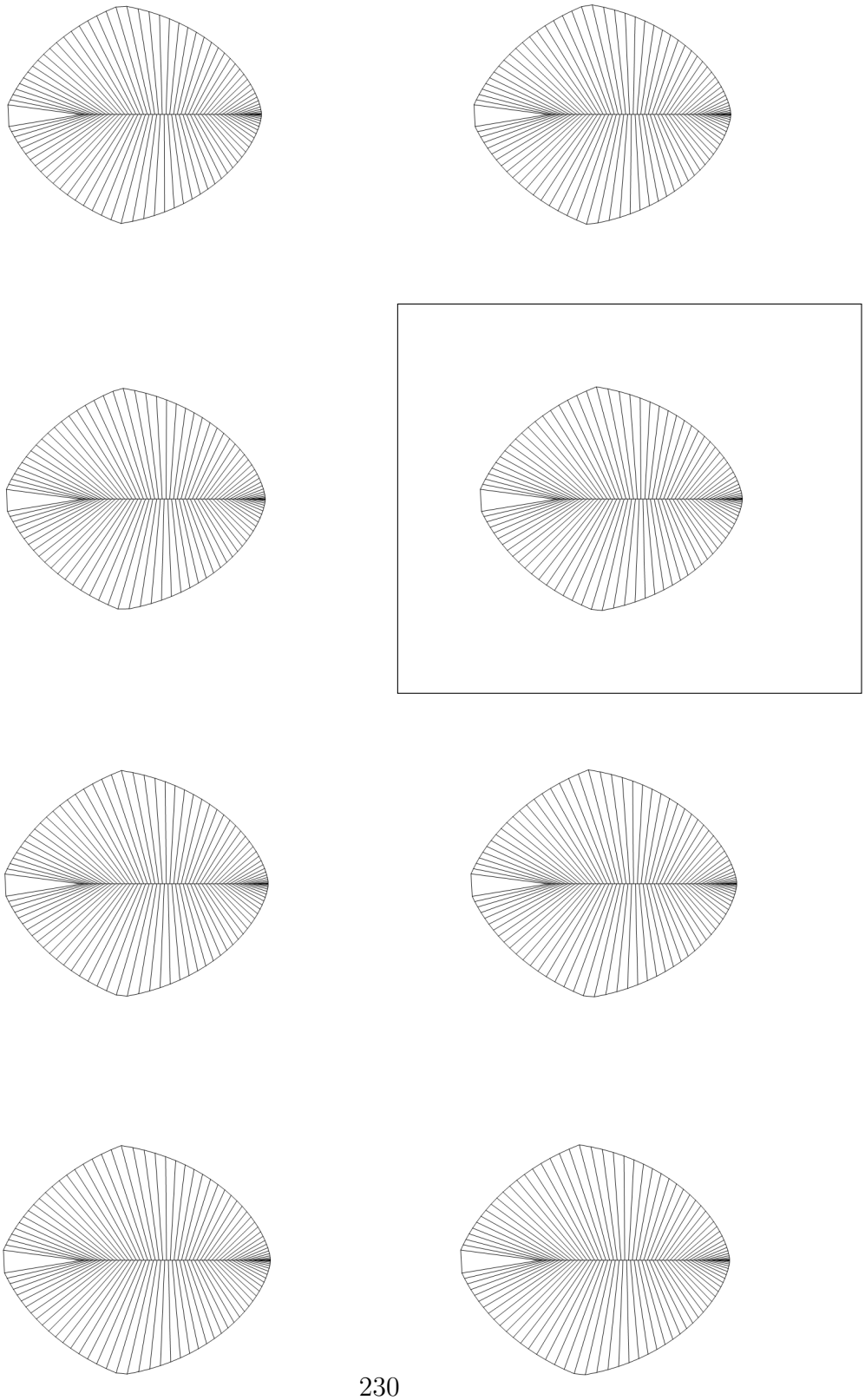

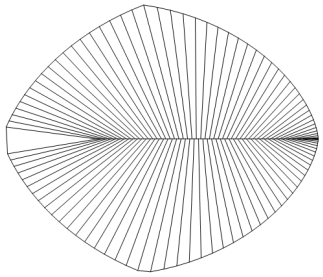
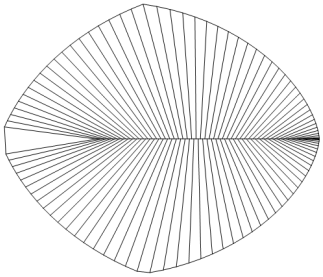
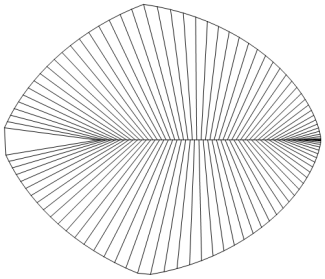
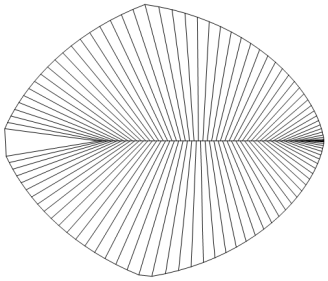
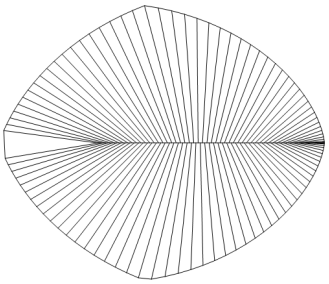
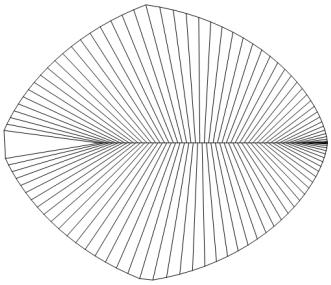
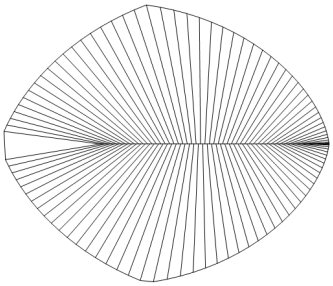
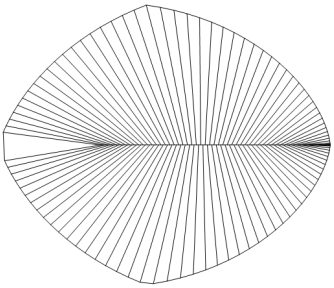

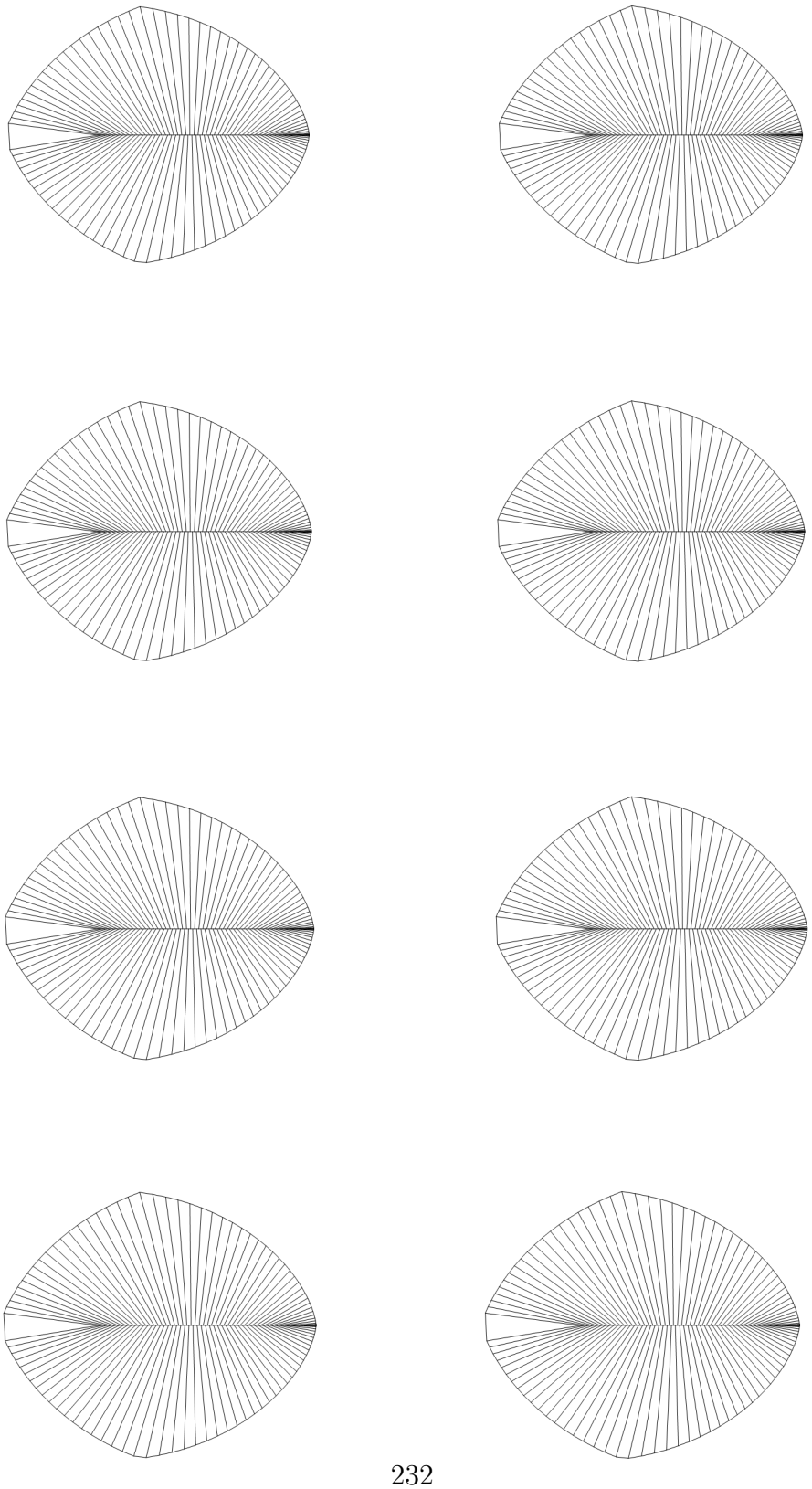

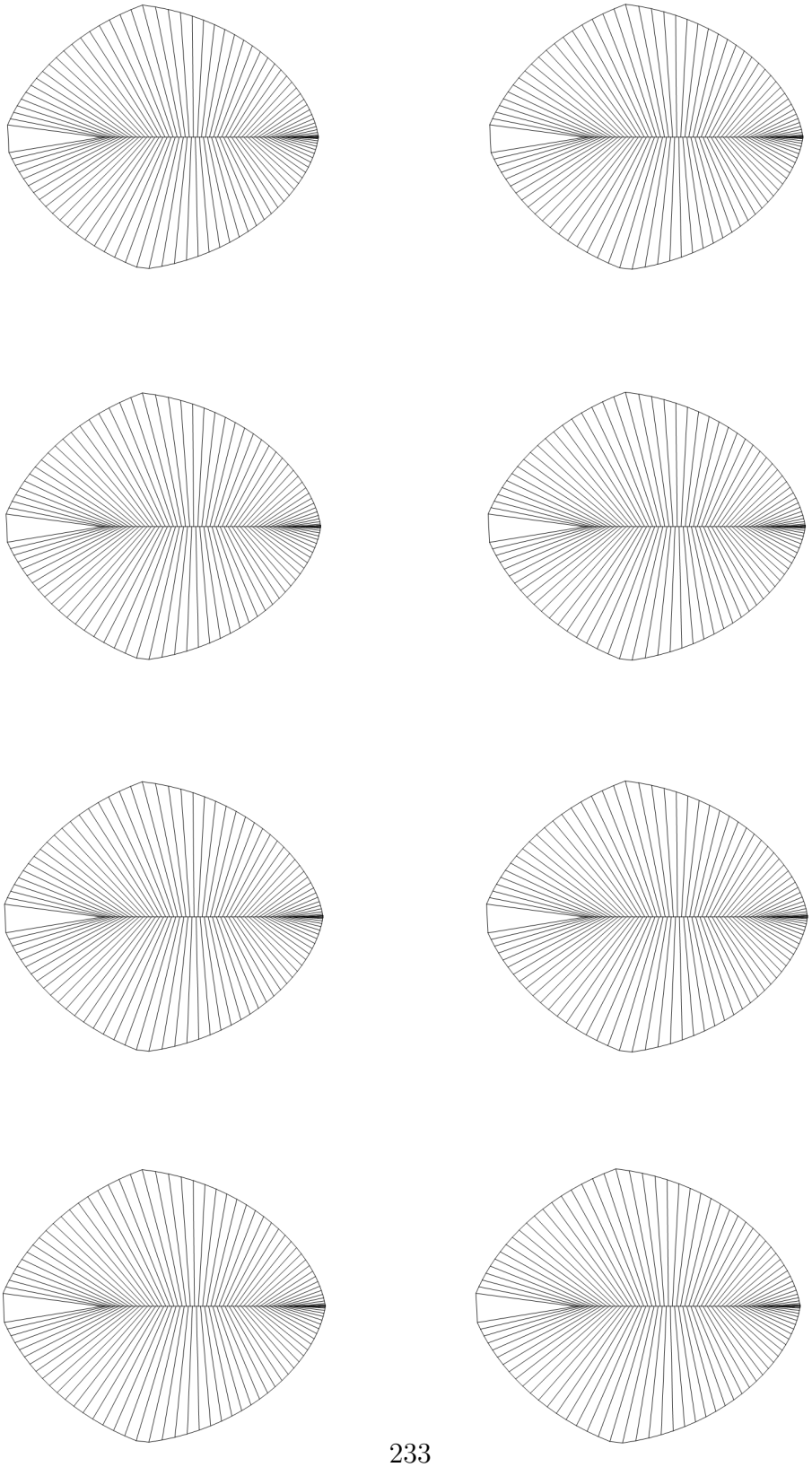

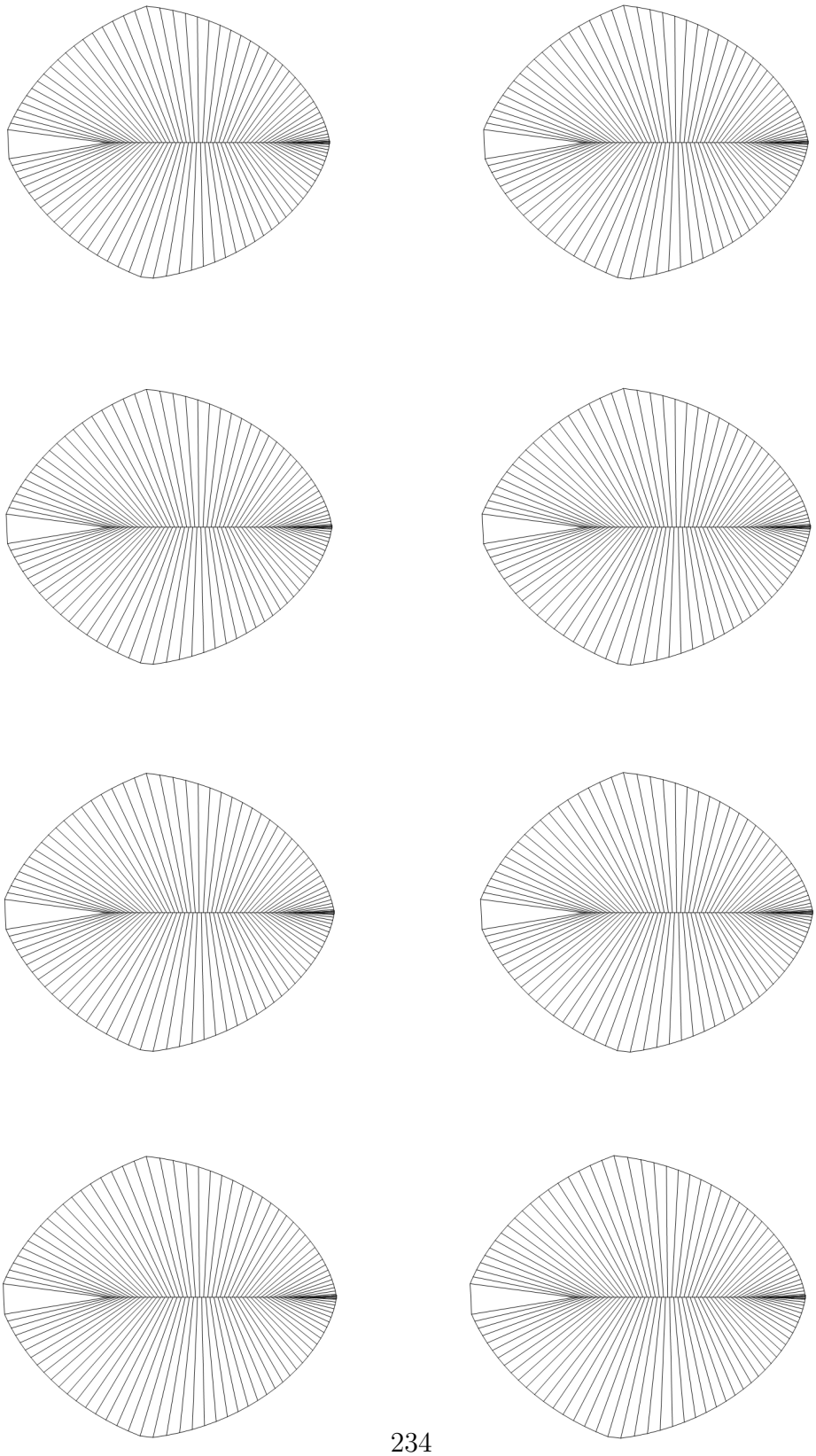

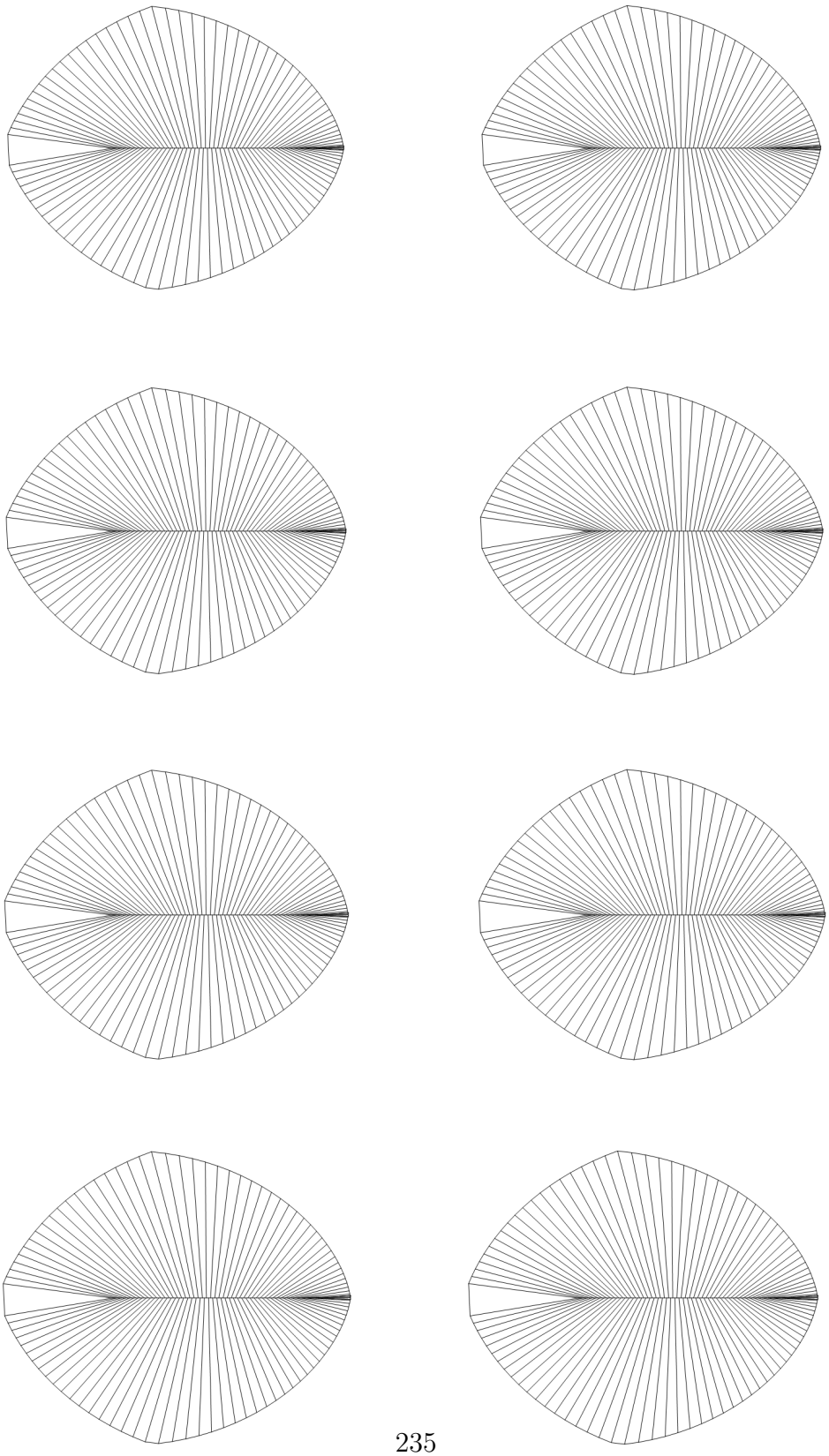

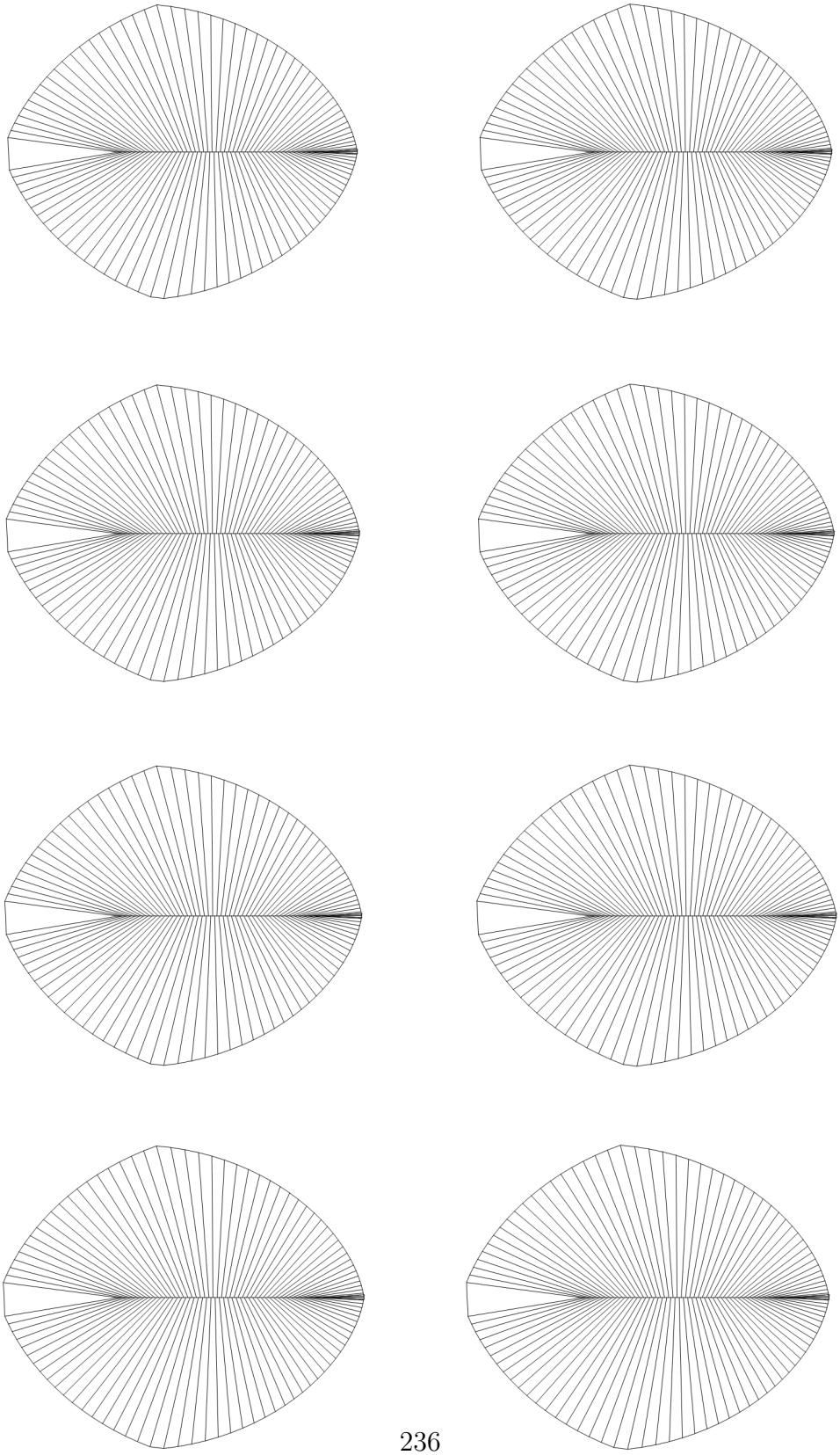

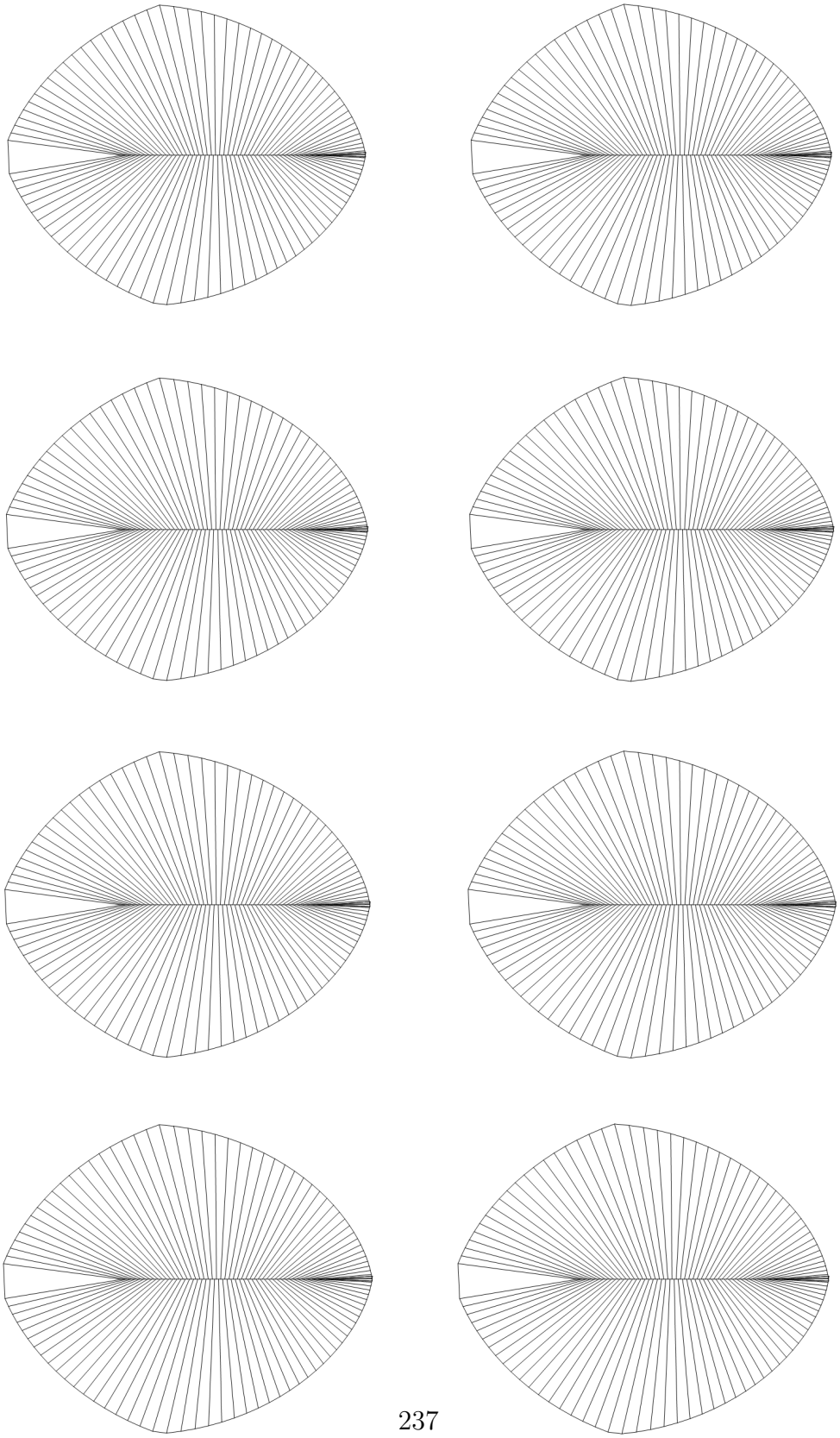

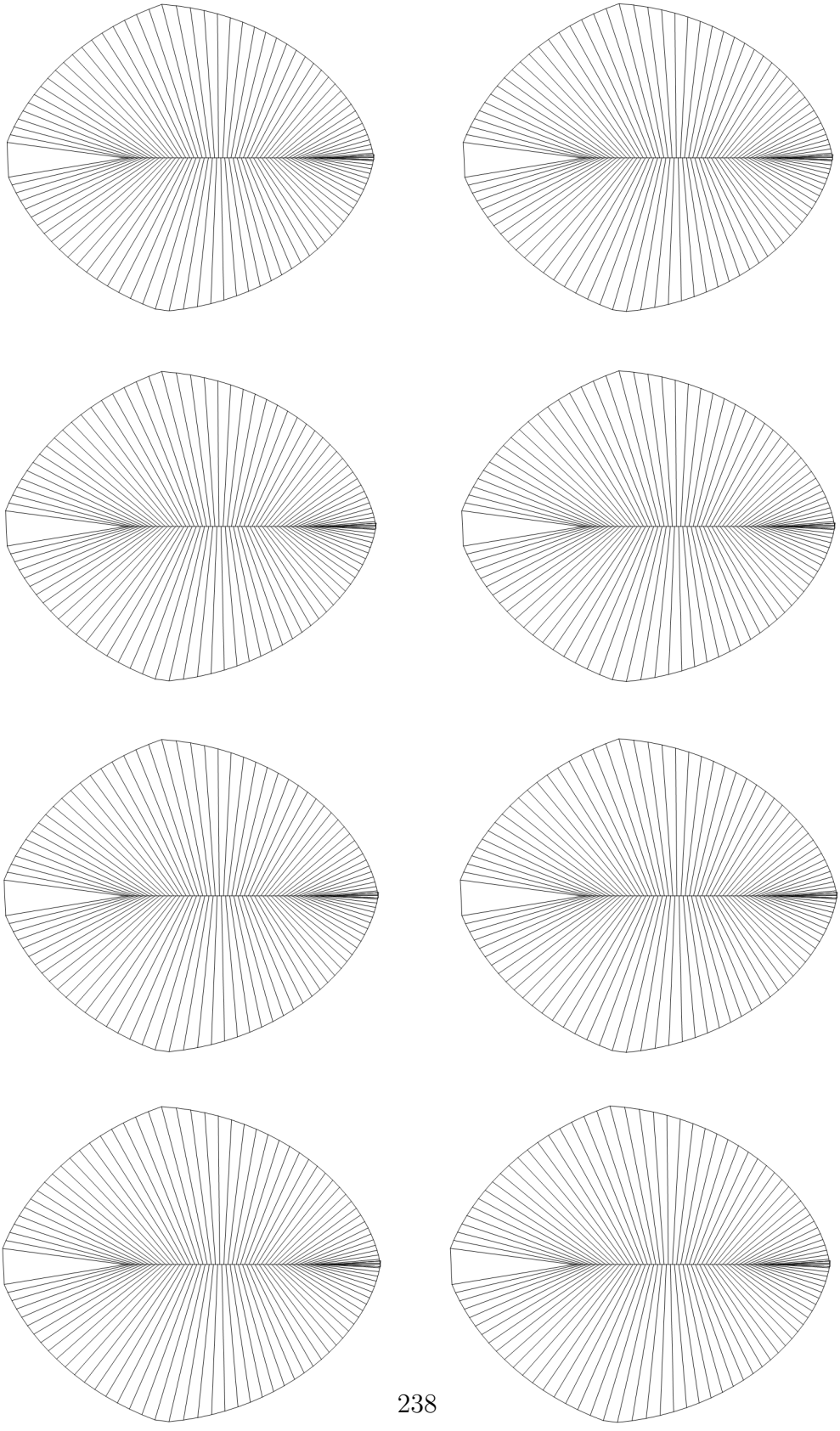

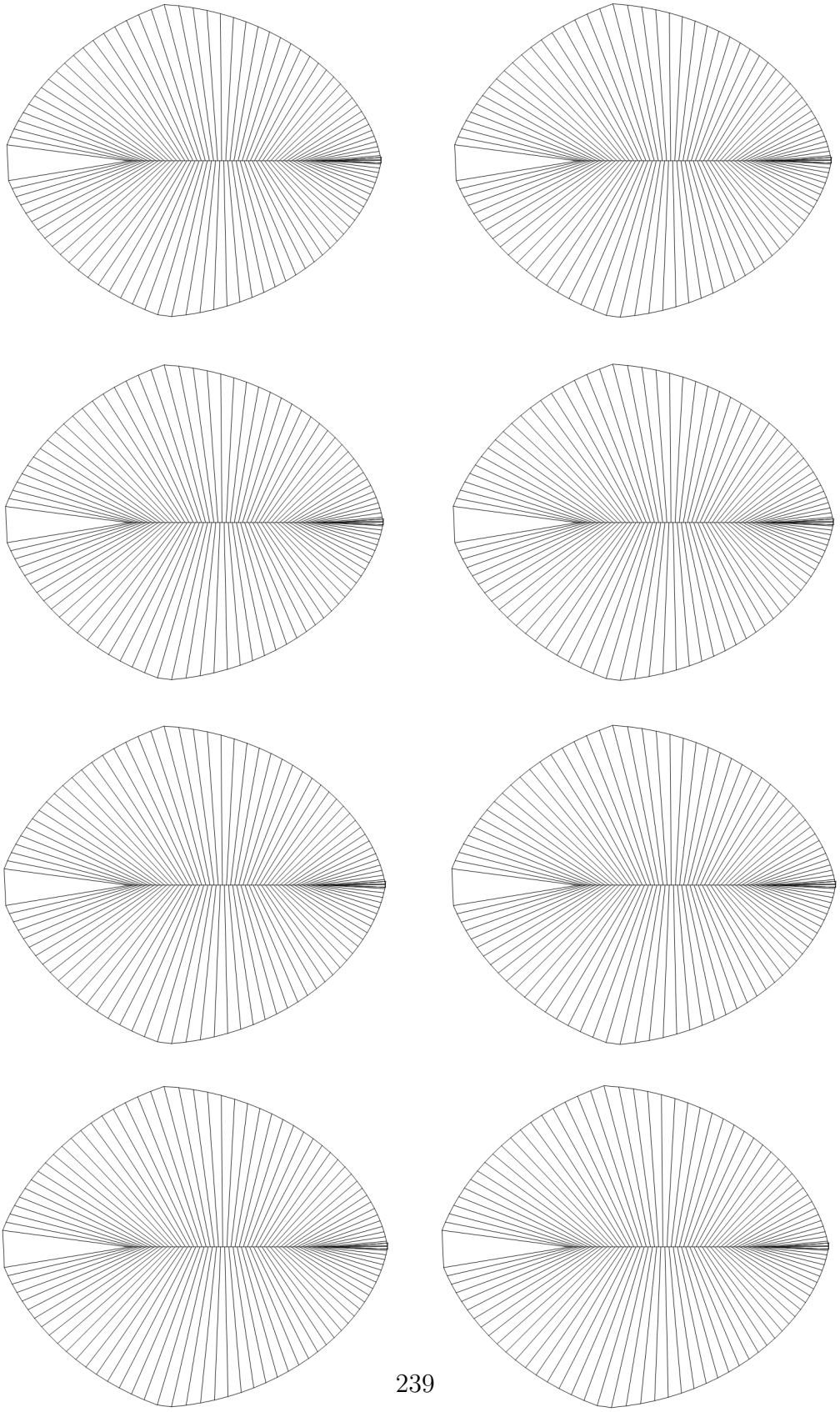

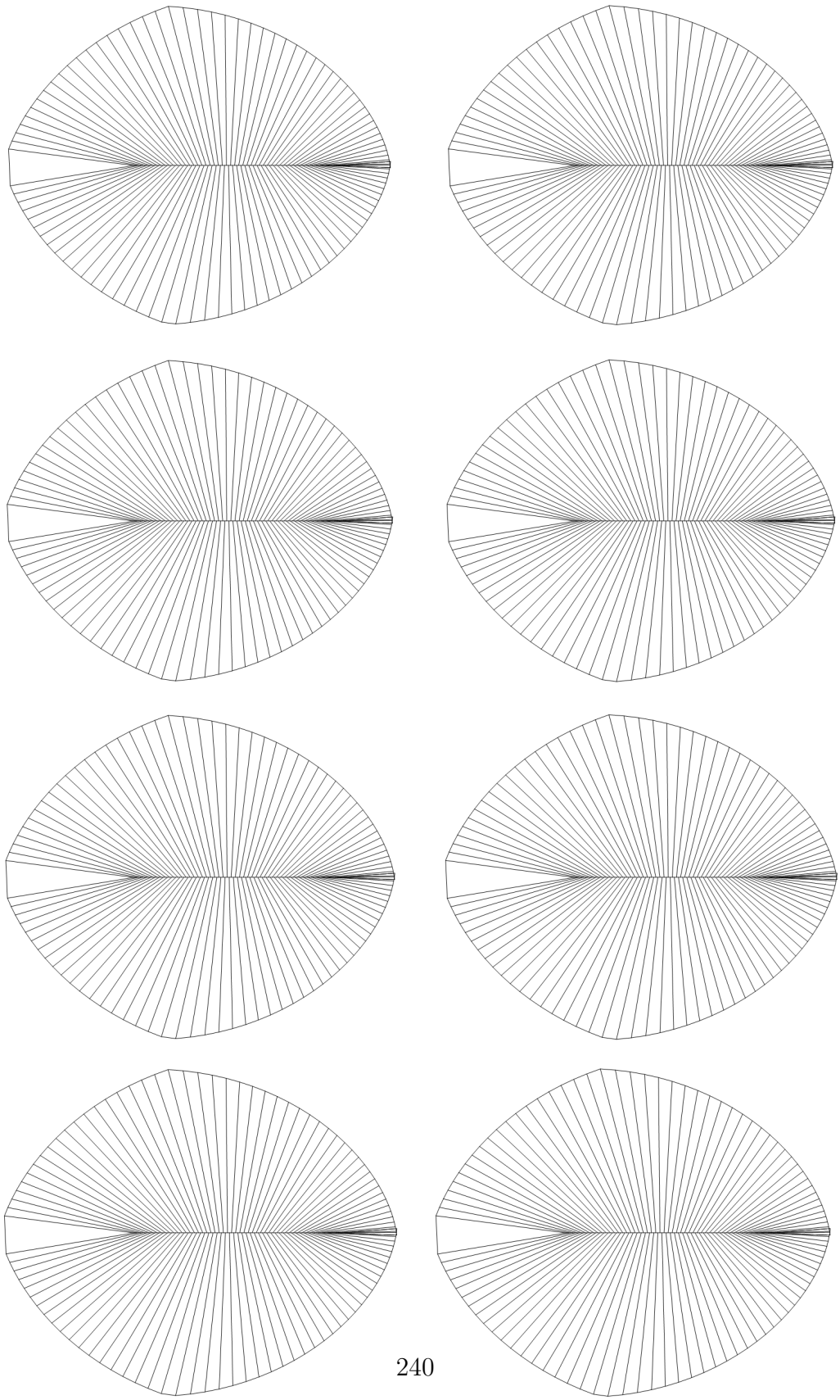

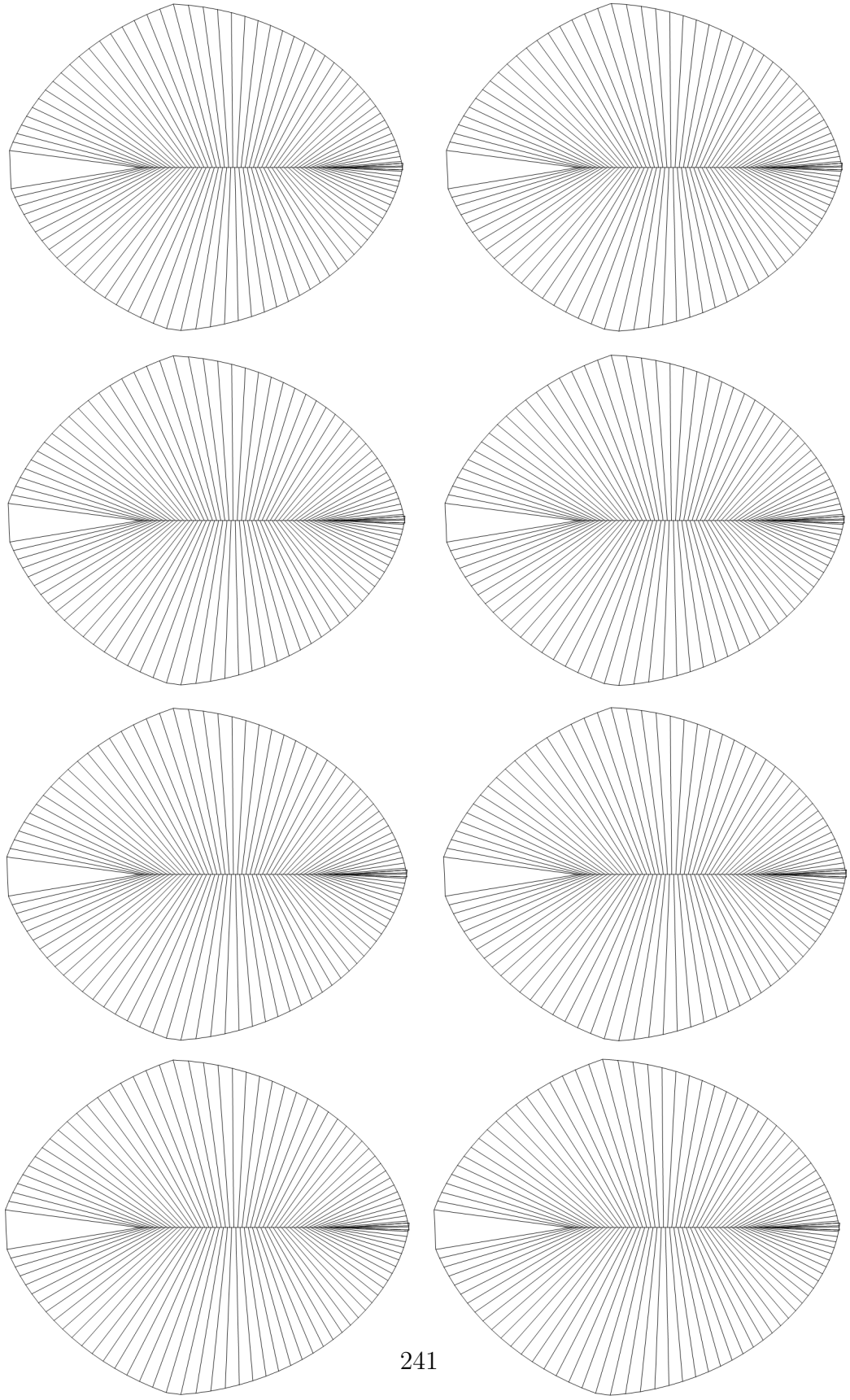

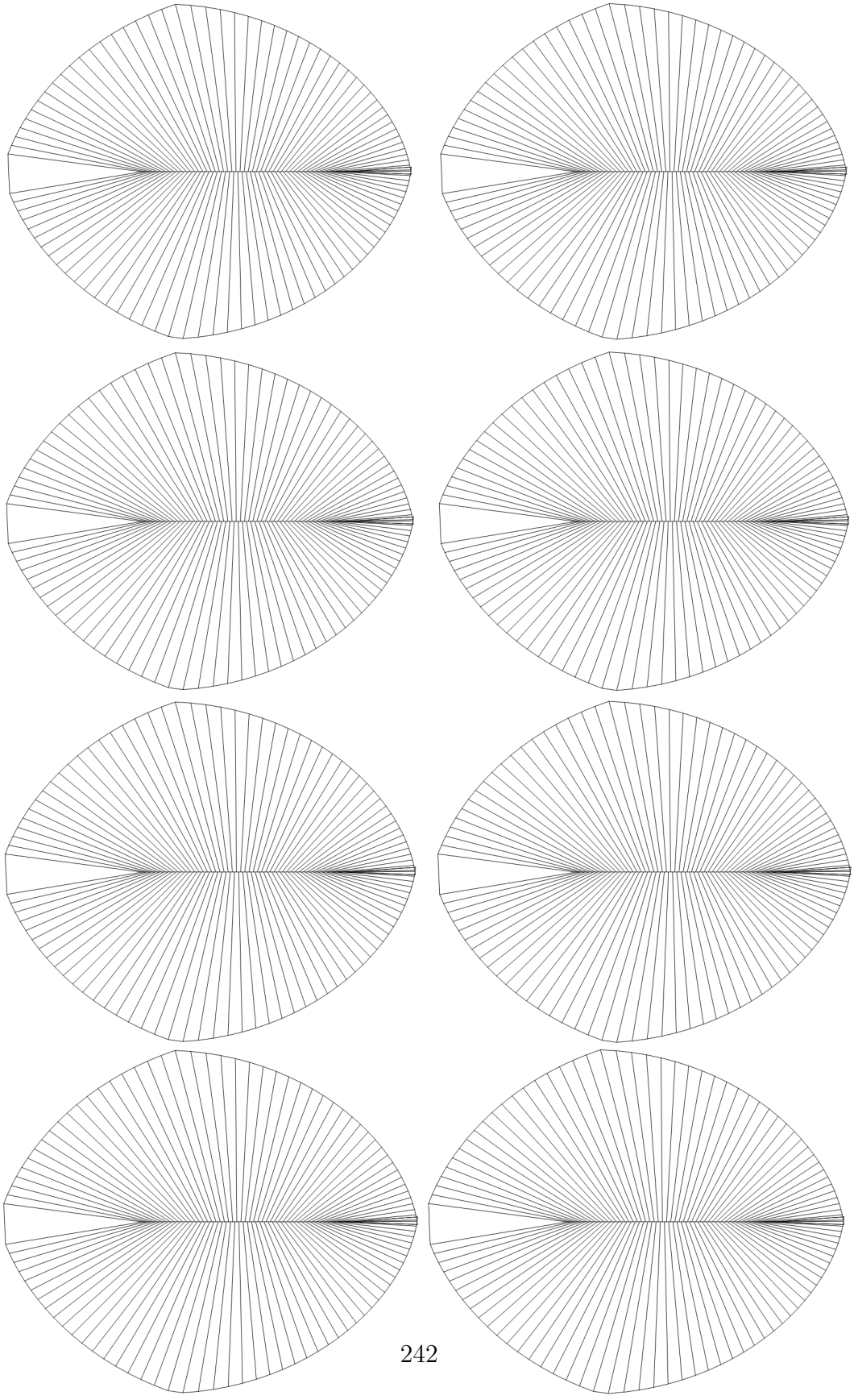

Appendix B

Growth model for *Charnia masoni*

The next pages show the growth model for the taxon *Charnia masoni* reconstructed in Chapter 4. The morphology is shown in 50 timesteps, where each timestep represents the insertion of one branch for as long as the branches are inserted. The insertion stops after 35 branches. The snapshot at the moment of the insertion stop is framed to indicate when this transition occurs.

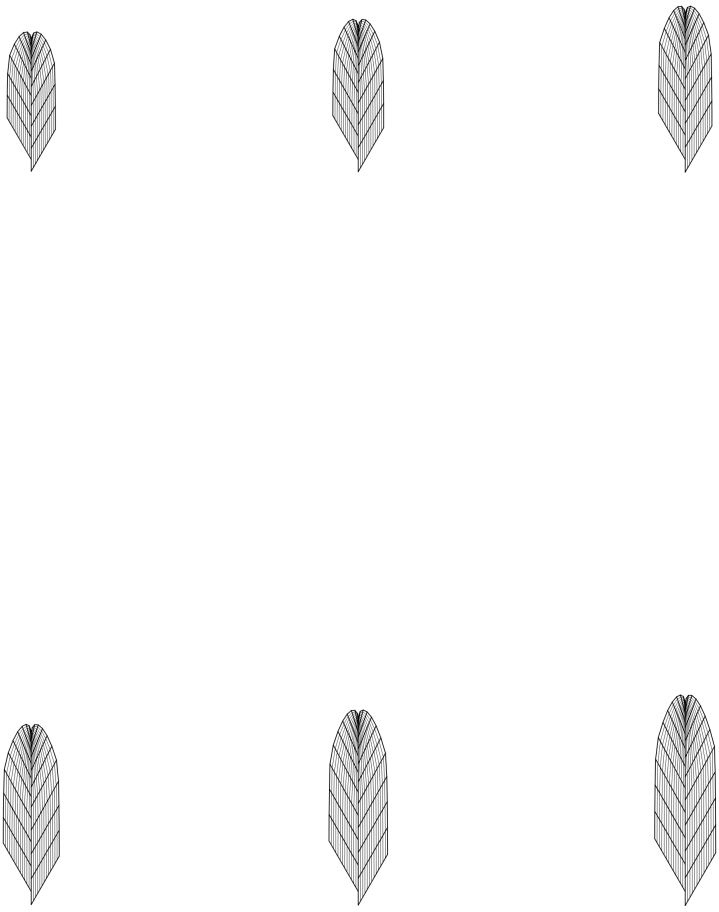

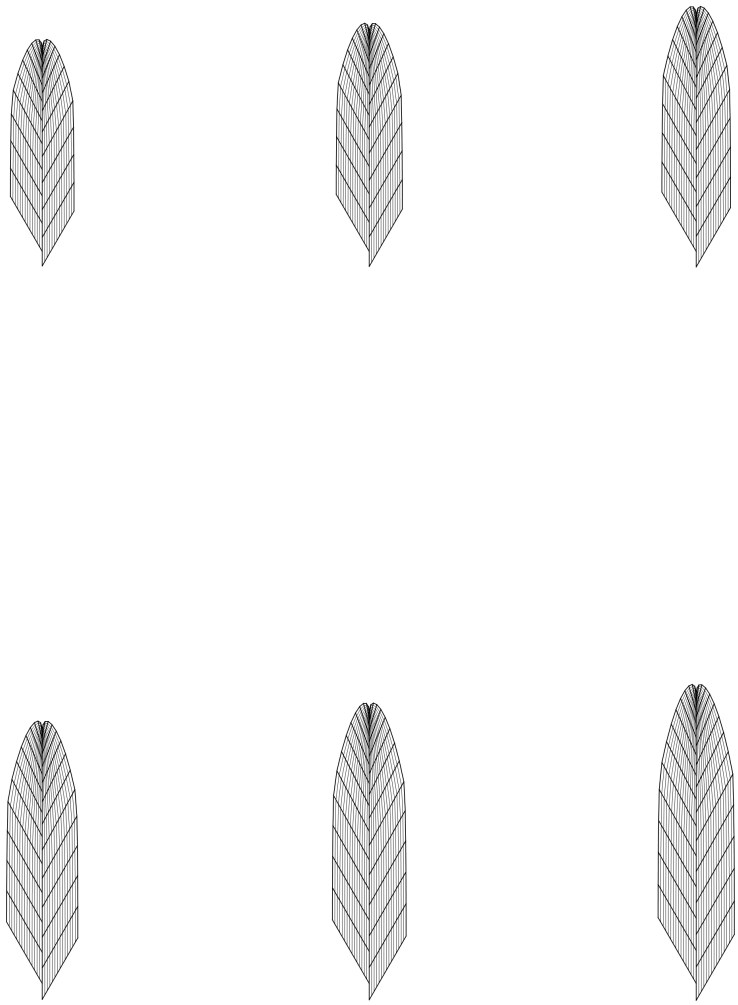

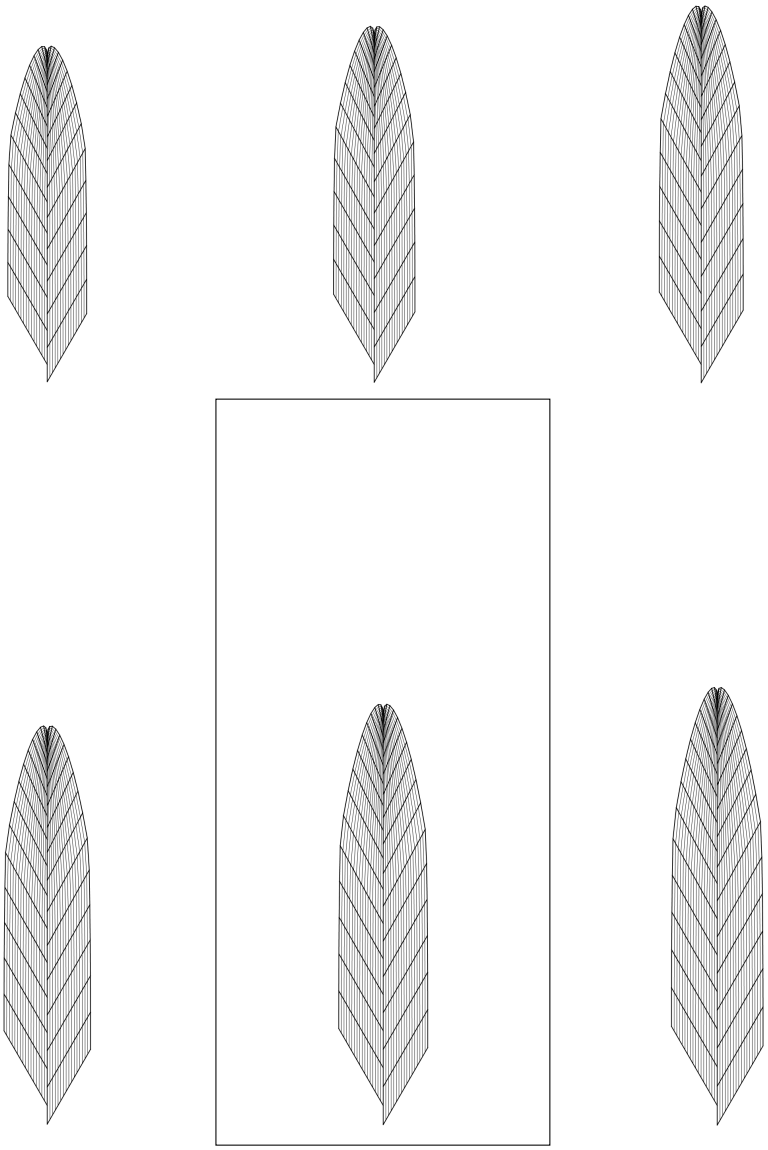

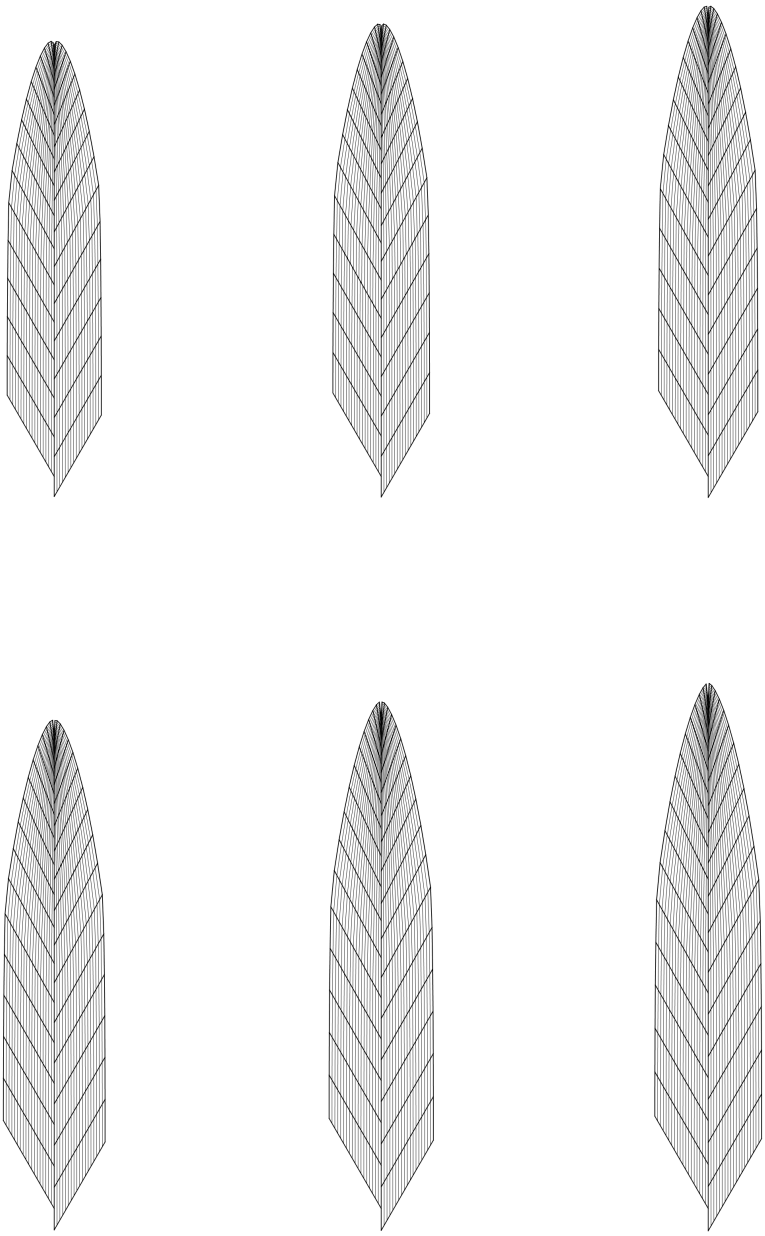

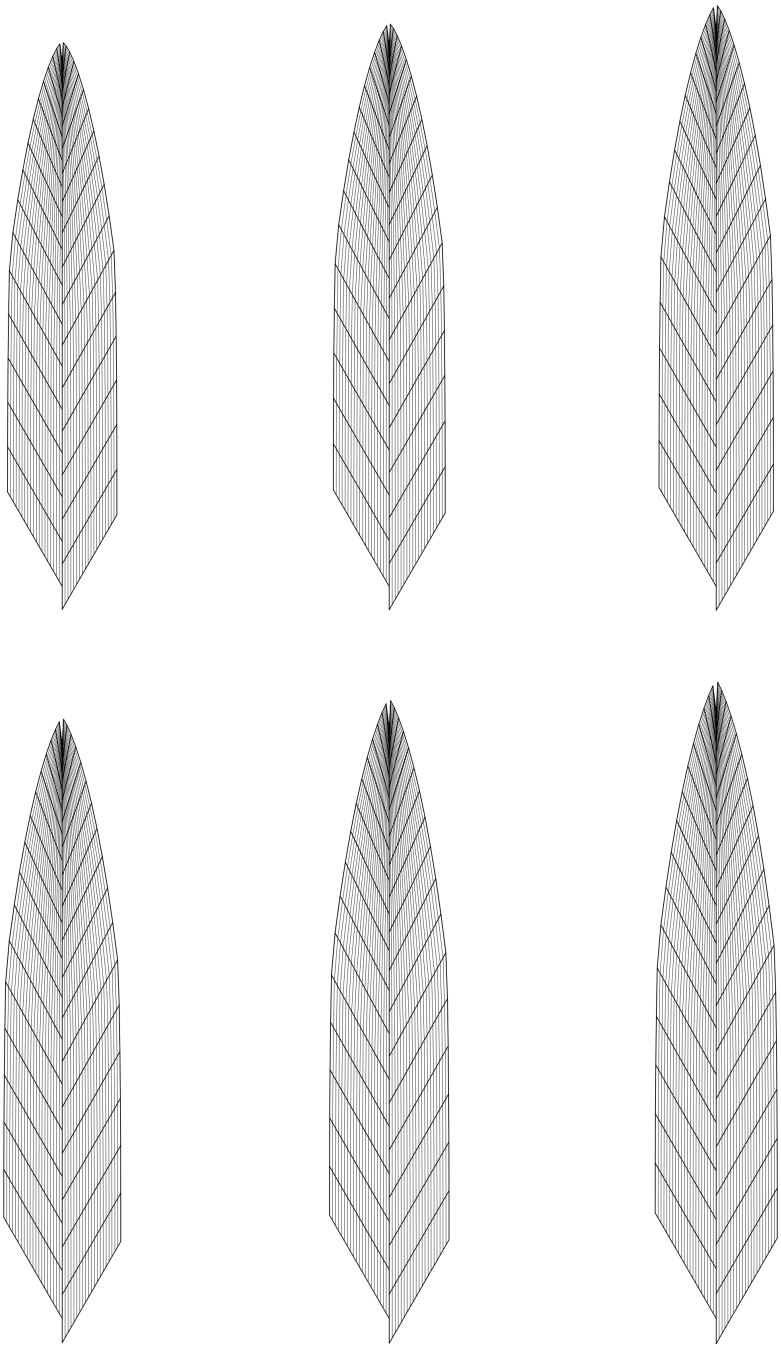

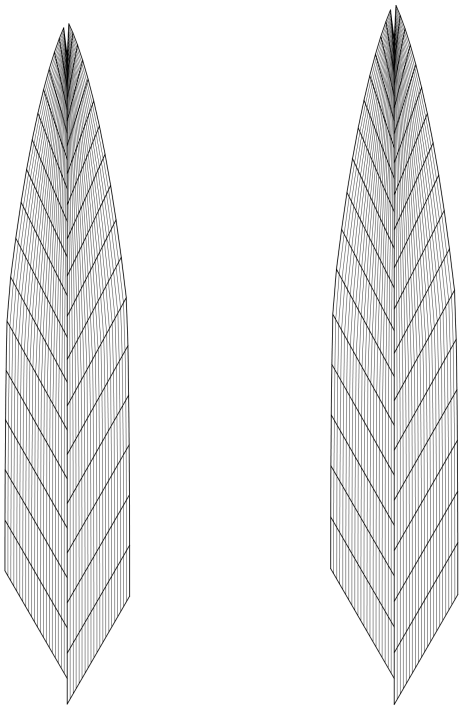

Appendix C

Paleodictyon

C.1 Interface hexagonal Faraday wave over time

The interface movement resulting from a hexagonal Faraday wave was calculated in Périnet et al. (2009). The model is a combination of a theoretical model and a numerical solution of the Navier-Stokes equation in three dimensions. The hexagonal pattern is formed by the interference of three two-dimensional spatial waves with wavenumbers k_c, $2k_c$ and $\sqrt{3}k_c$, which vary in amplitude over time. Here k_c is the wavenumber that corresponds to the primary wavelength with the relationship $k_c = 2\pi/\lambda$. The height of the interface is given by:

$$\begin{aligned}\zeta &= \langle\zeta\rangle + A_{k_c}(t)\sum_{j=1}^{6} e^{ik_c\mathbf{e}_j\cdot\mathbf{x}} \\ &\quad + A_{2k_c}(t)\sum_{j=1}^{6} e^{i2k_c\mathbf{e}_j\cdot\mathbf{x}} \\ &\quad + A_{\sqrt{3}k_c}(t)\sum_{j=1}^{6} e^{i\sqrt{3}k_c\mathbf{e'}_j\cdot\mathbf{x}} + \text{higher order terms.}\end{aligned} \tag{C.1}$$

Here $\langle\zeta\rangle$ is the expectation value of the interface height. The dot product $\cdot$ appears between $\mathbf{x} = (x, y)$ and the two-dimensional vectors $\mathbf{e}_j$ and $\mathbf{e'}_j$, which are given by:

$$\mathbf{e}_j = \begin{pmatrix} \cos(\pi j/3) \\ \sin(\pi j/3) \end{pmatrix} \tag{C.2}$$

and

$$\mathbf{e'}_j = \begin{pmatrix} \cos(\pi/6 + \pi j/3) \\ \sin(\pi/6 + \pi j/3) \end{pmatrix} \tag{C.3}$$

These vectors manifestly show the $\pi/3$ rotational symmetry of the hexagonal lattice. The time-dependent amplitudes $A_{k_c}(t)$, $A_{2k_c}(t)$ and $A_{\sqrt{3}k_c}(t)$ were calculated numerically and are shown in Fig. C.1. The numerical data of these amplitudes was given to me by Nicholas Périnet.

The next few pages show the height of the interface ζ given by equation C.1 in 48 timesteps. Here $\langle\zeta\rangle$ is set to zero and the higher order terms are neglected. In the first few snapshots the vertices of the pattern go downward. Then there is a transition in which the edges of the hexagons go downward and then upward entirely. Then the mid-egde points go upward for a while. Then the

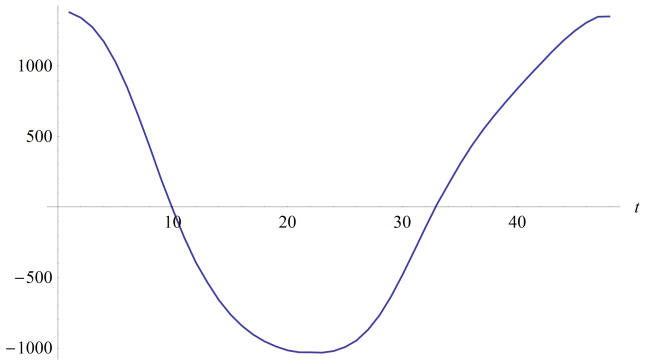

(a) $A_{k_c}(t)$

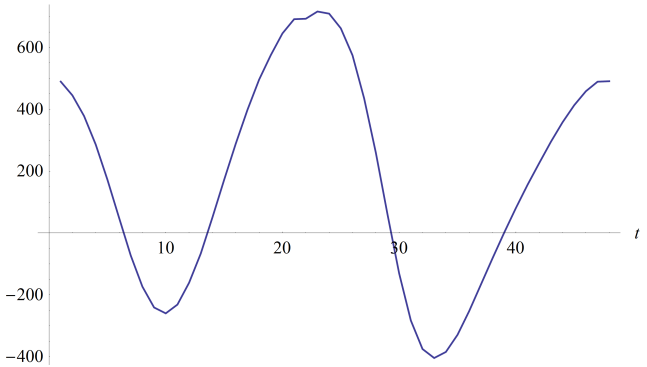

(b) $A_{2k_c}(t)$

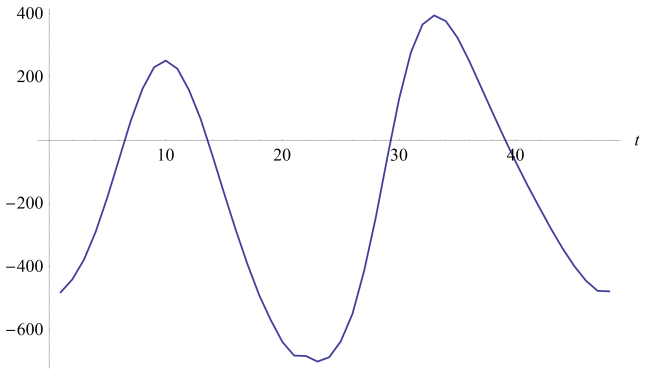

(c) $A_{\sqrt{3}k_c}(t)$

Figure C.1: Relative temporal amplitudes of the different wavenumbers. The data is shown in 48 timesteps, which is the period of the hexagonal Faraday mode and twice the period of the driving vibration.

transitioning phase happens in the reversed order. Then the vertices go down again and we are back at the start of the period.

Note that the transition phases are the only times that the vertices go upward slightly and the mid-edge points go downward. The fact that the mid-edge points go mostly upward and the vertices go mostly downward, results in the asymmetry observed in the pattern of in the upward maxima and downward maxima calculated in Chapter 5.

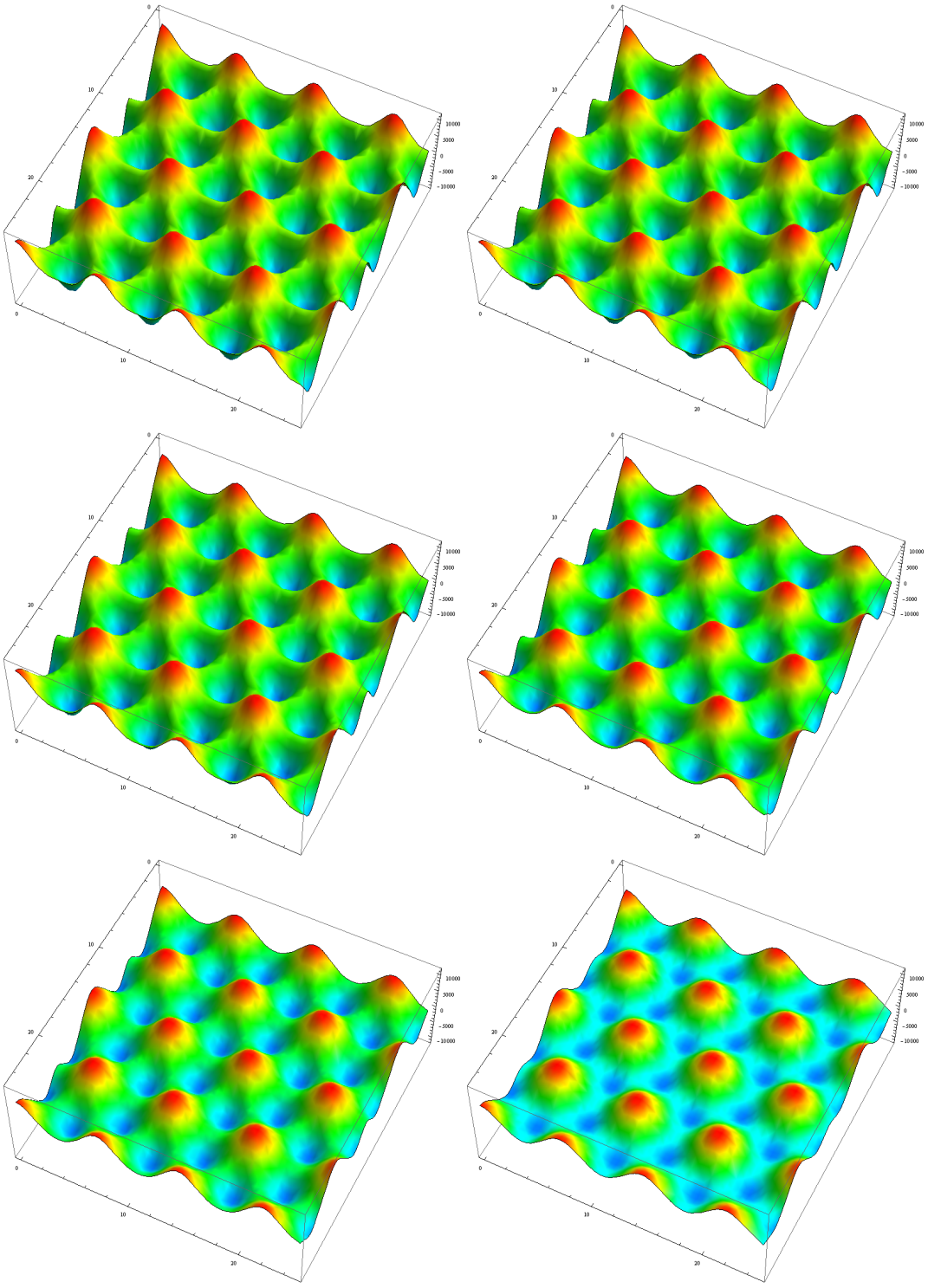

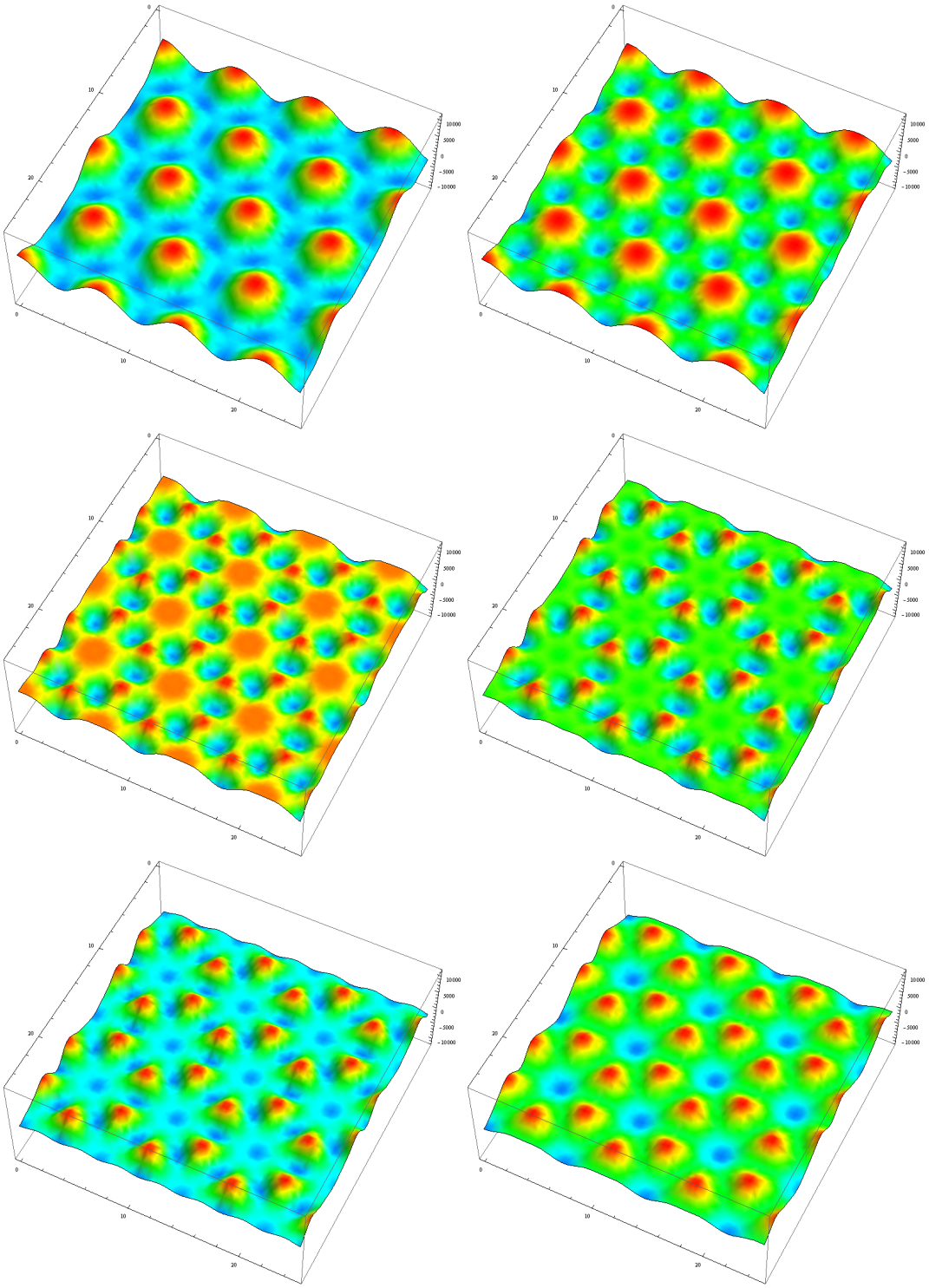

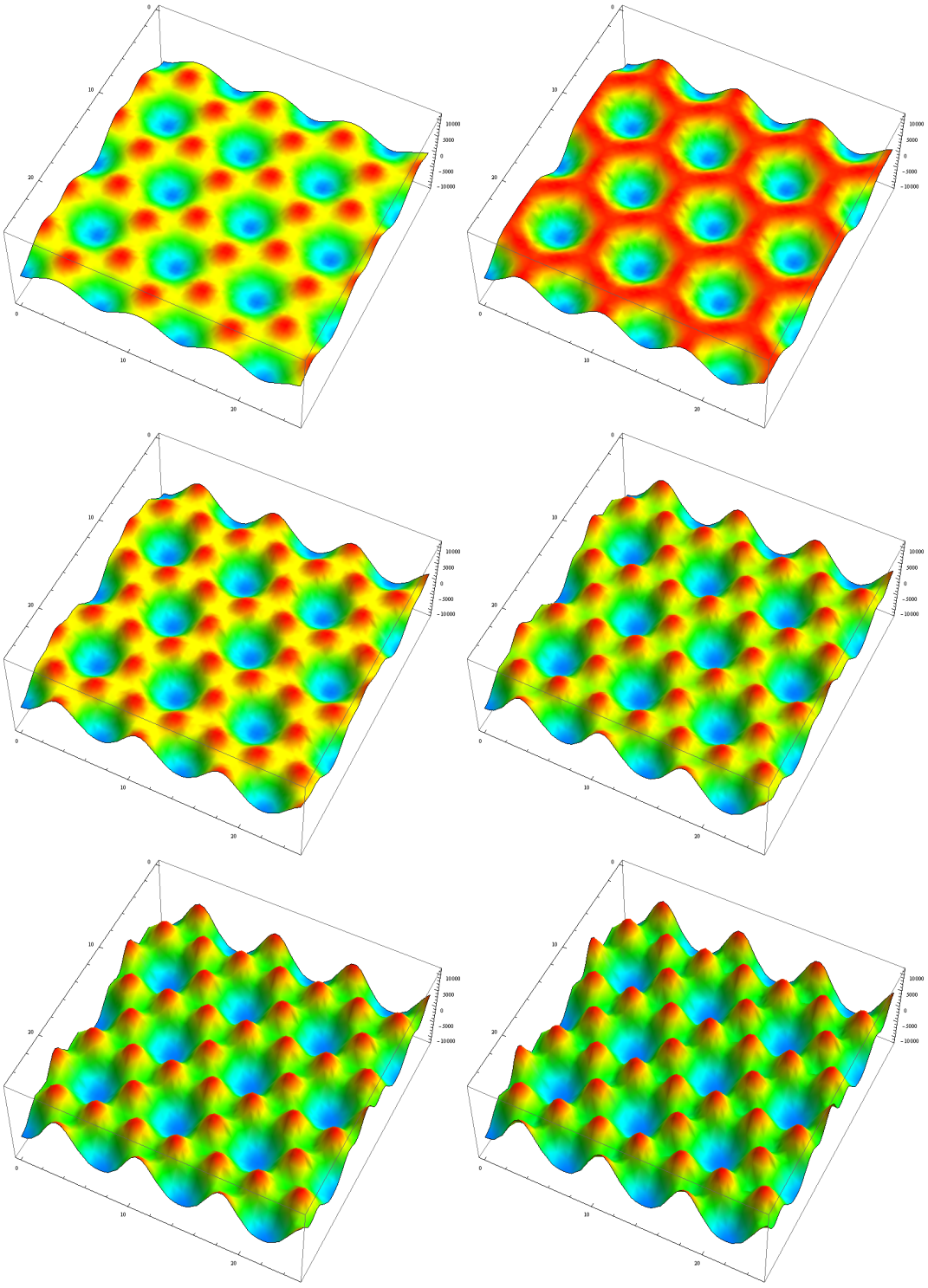

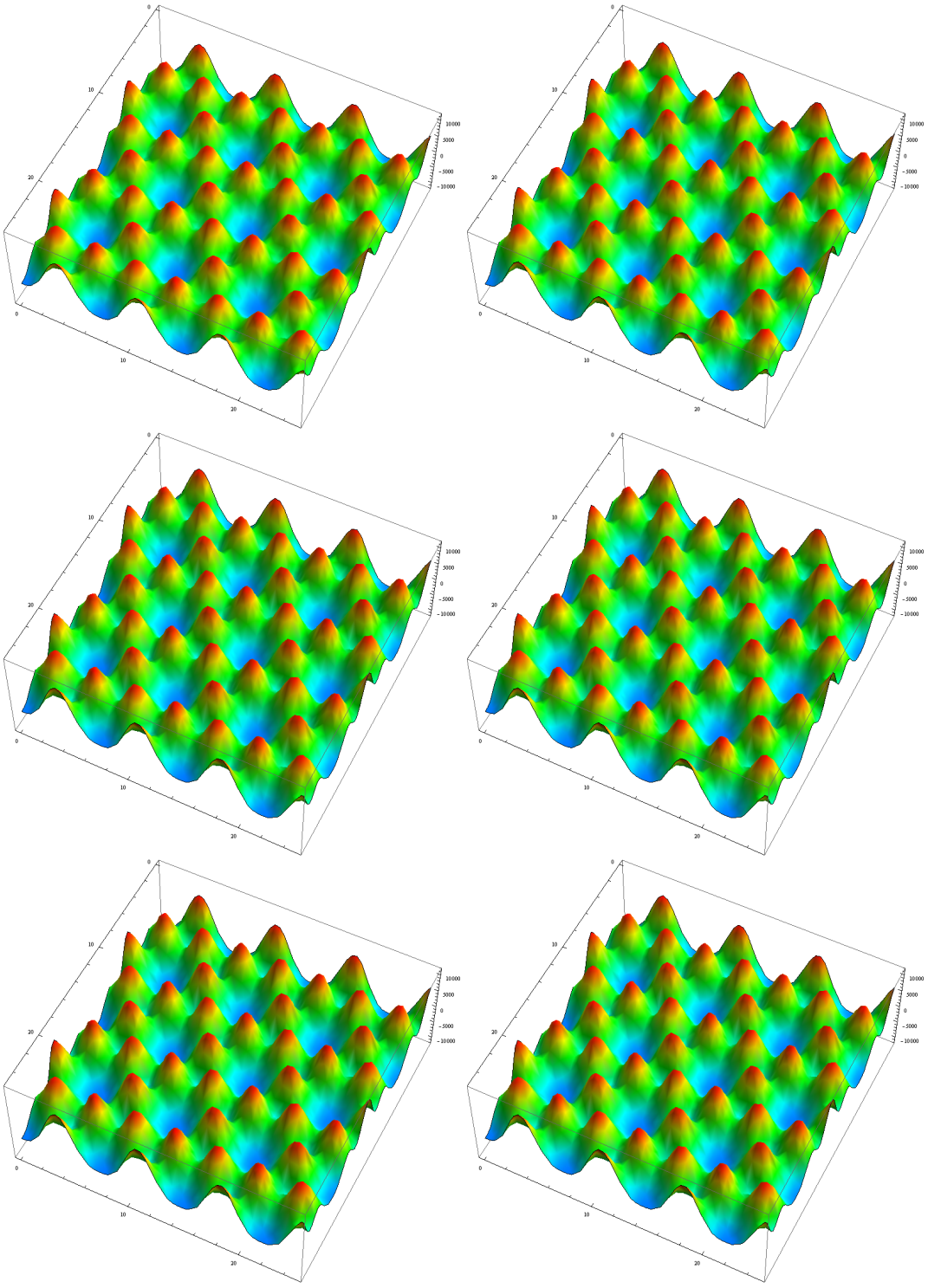

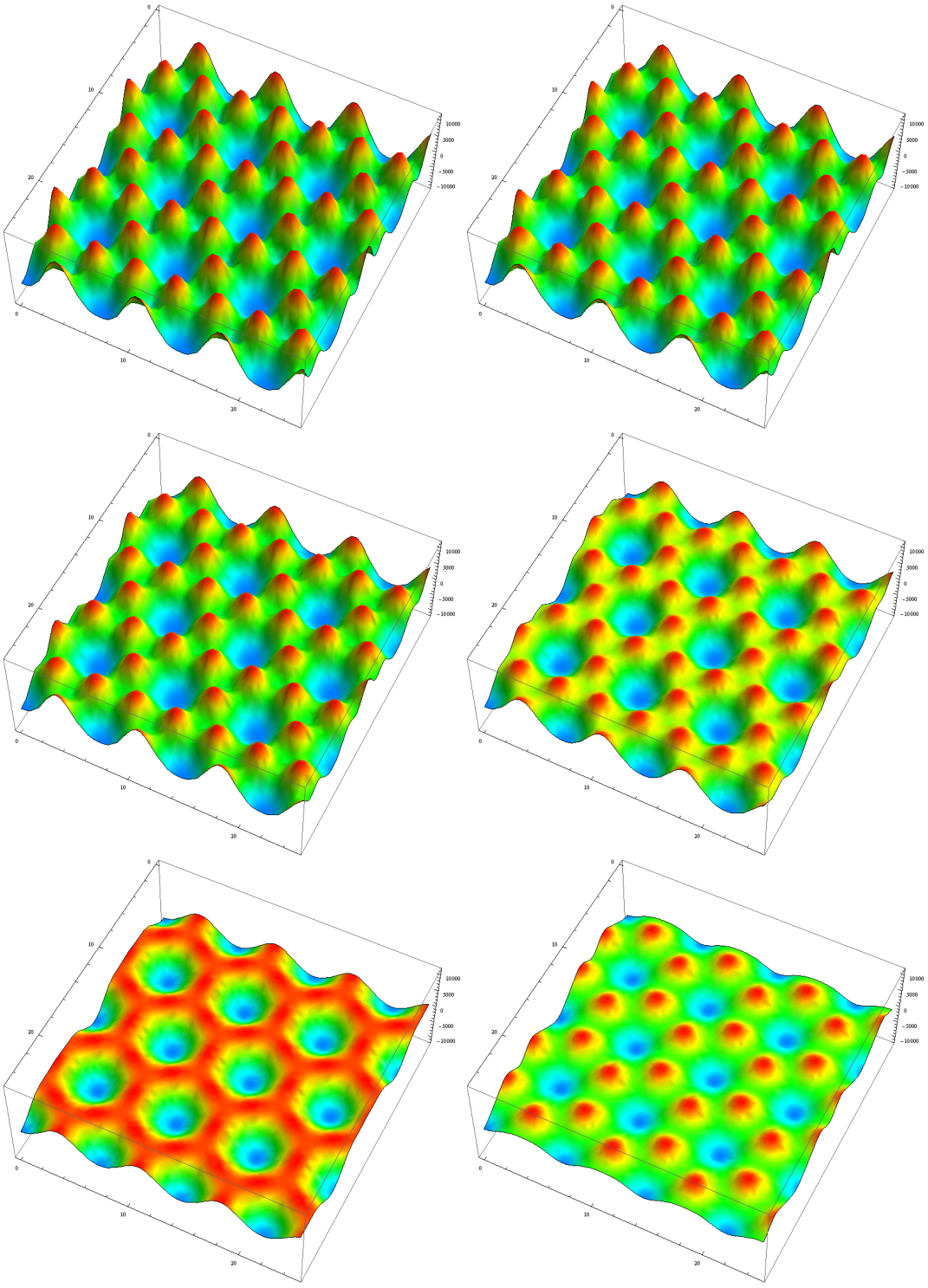

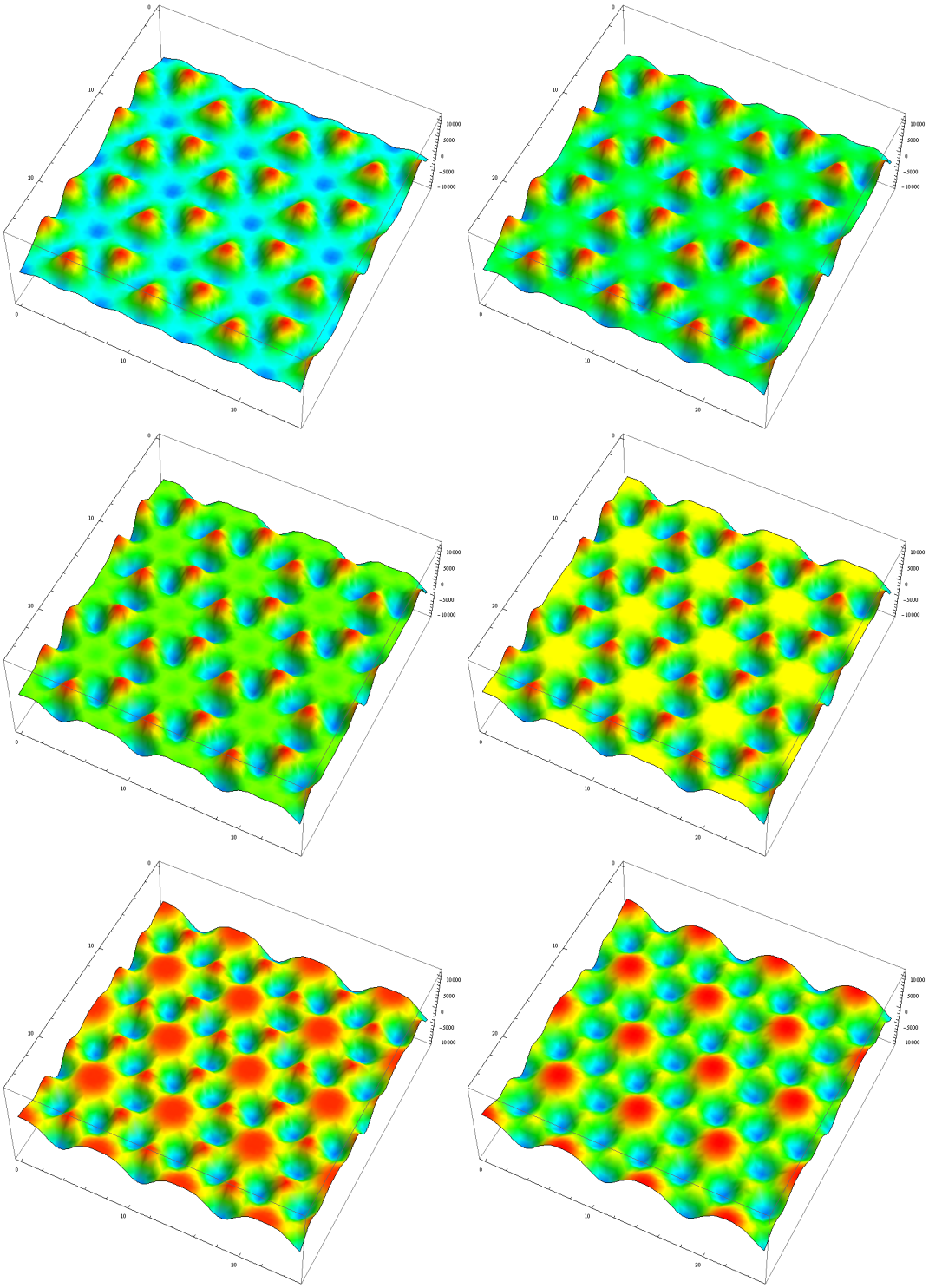

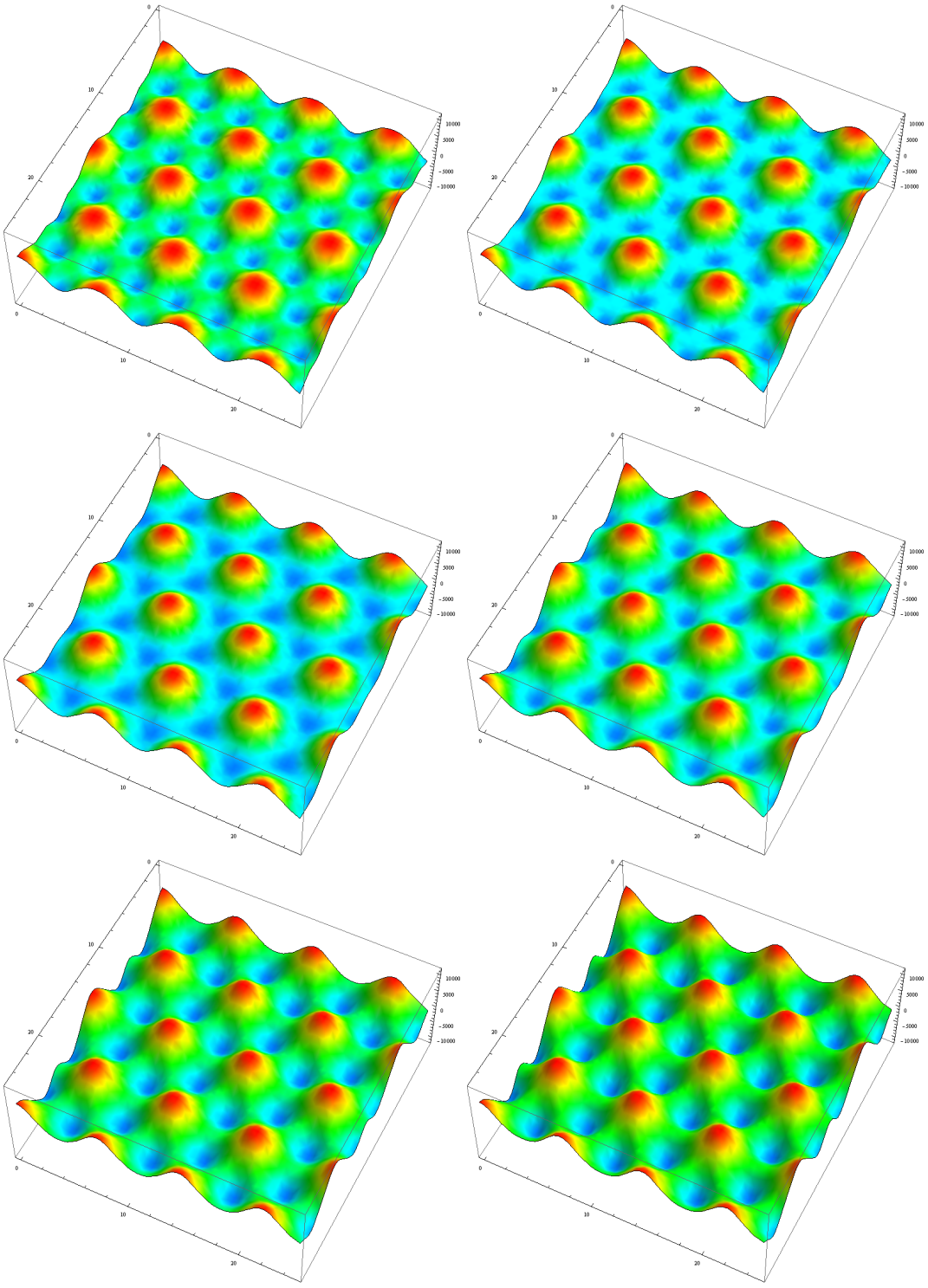

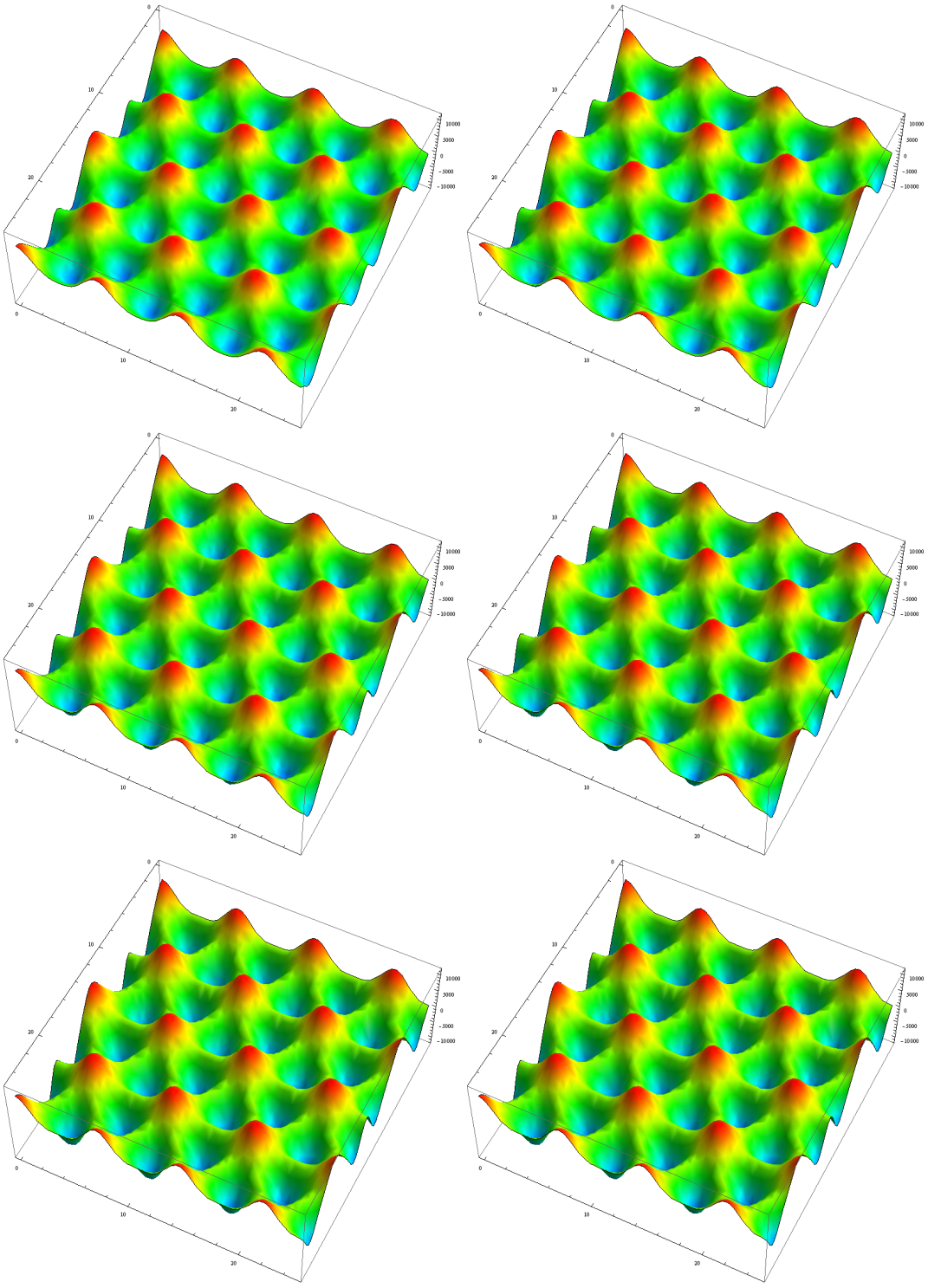

C.2 Velocity field of the hexagonal Faraday wave

C.2.1 View from top

The following pages show the velocity field of a three-dimensional simulation of the hexagonal Faraday wave as a function of time, in a top-down view. The data was provided by Nicholas Périnet.

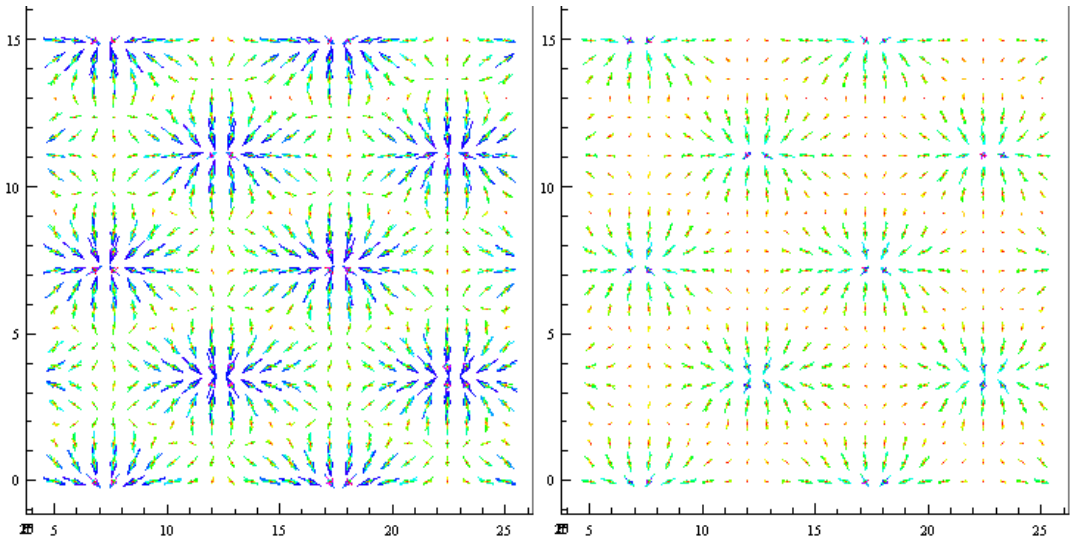
15
10
5
0
5
10
15
20
25
15
10
5
0
5
10
15
20
25

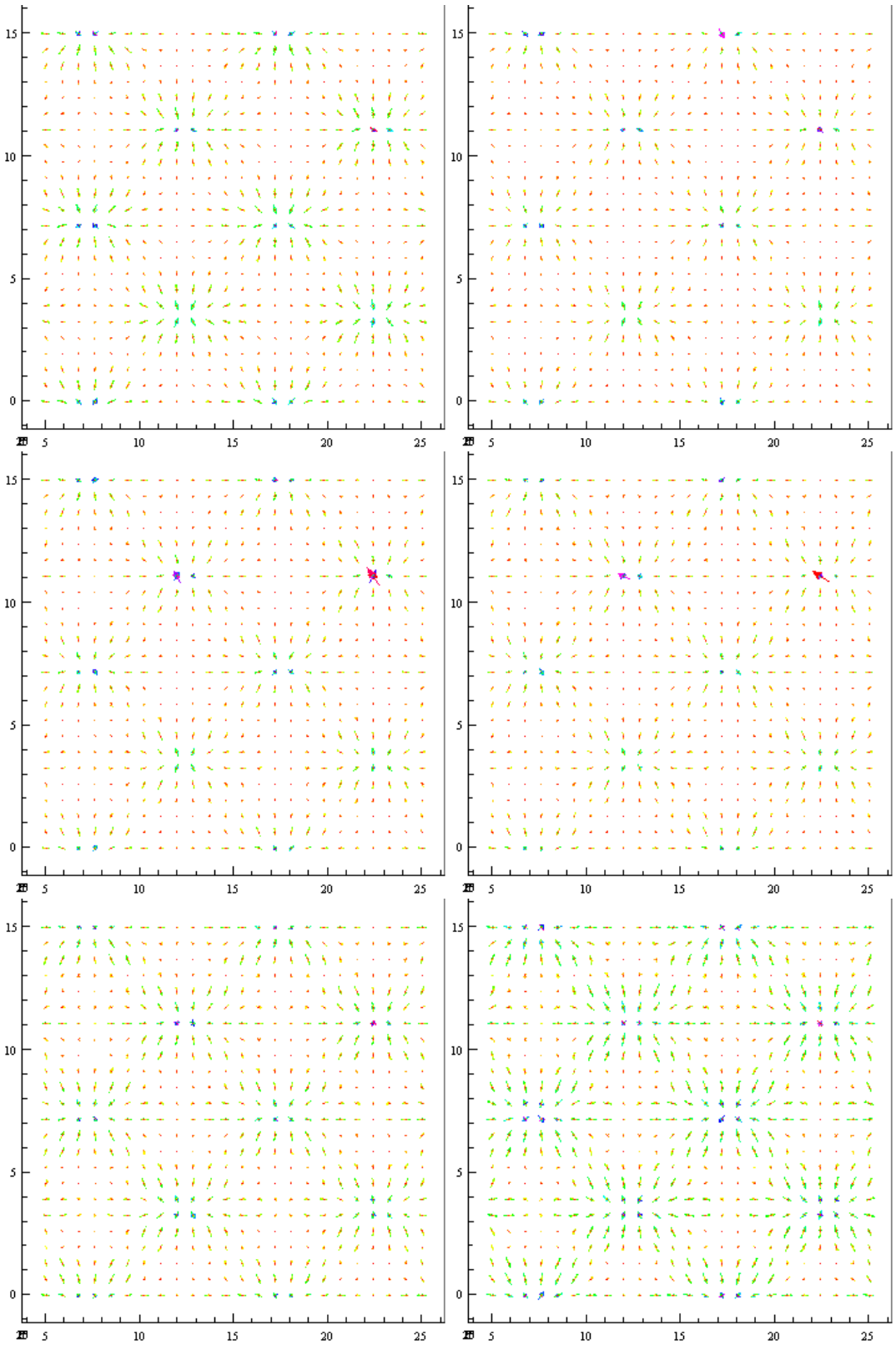
0
5
10
15
20
25

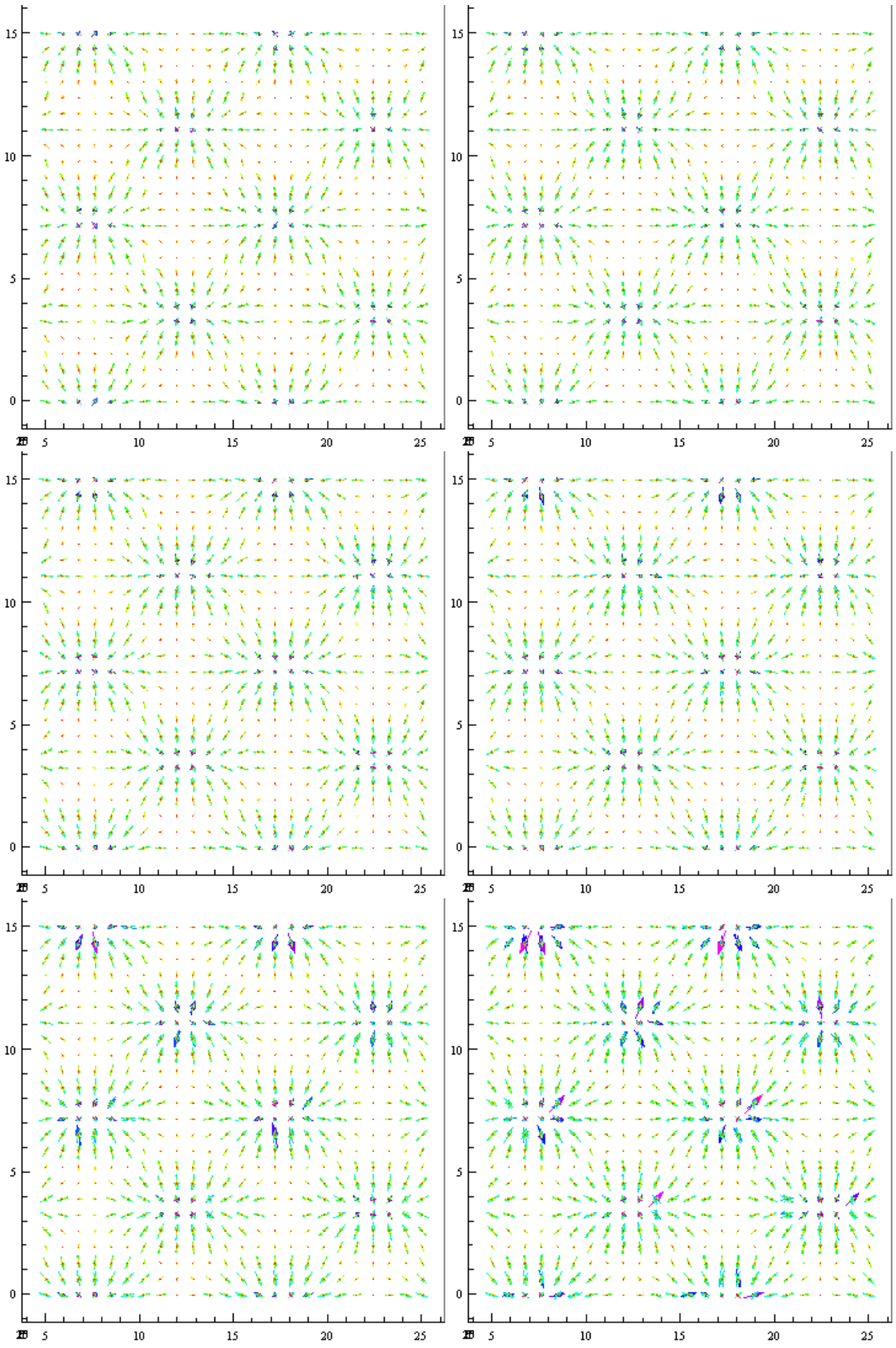
0
5
10
15
20
25

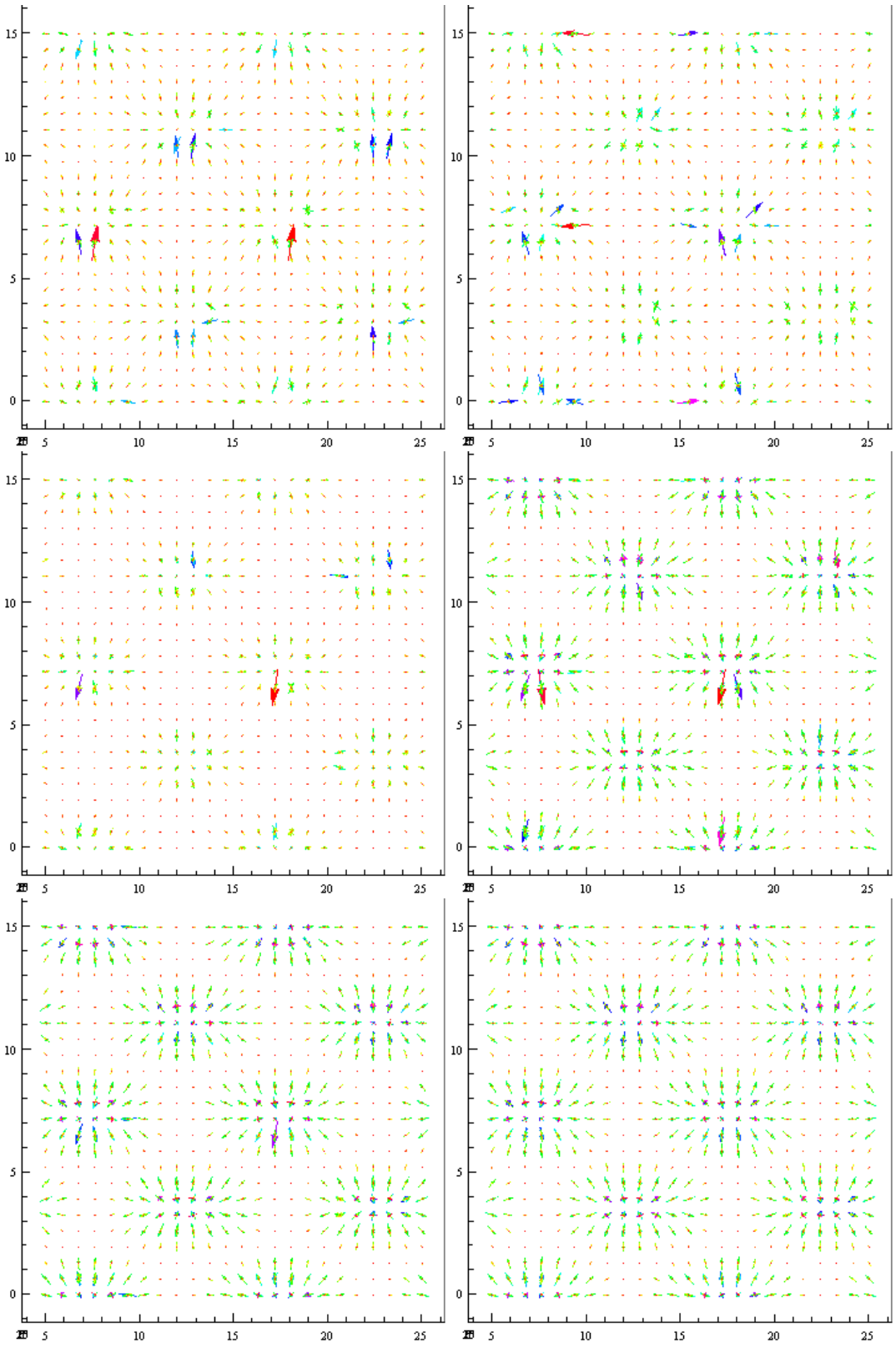
0
5
10
15
20
25

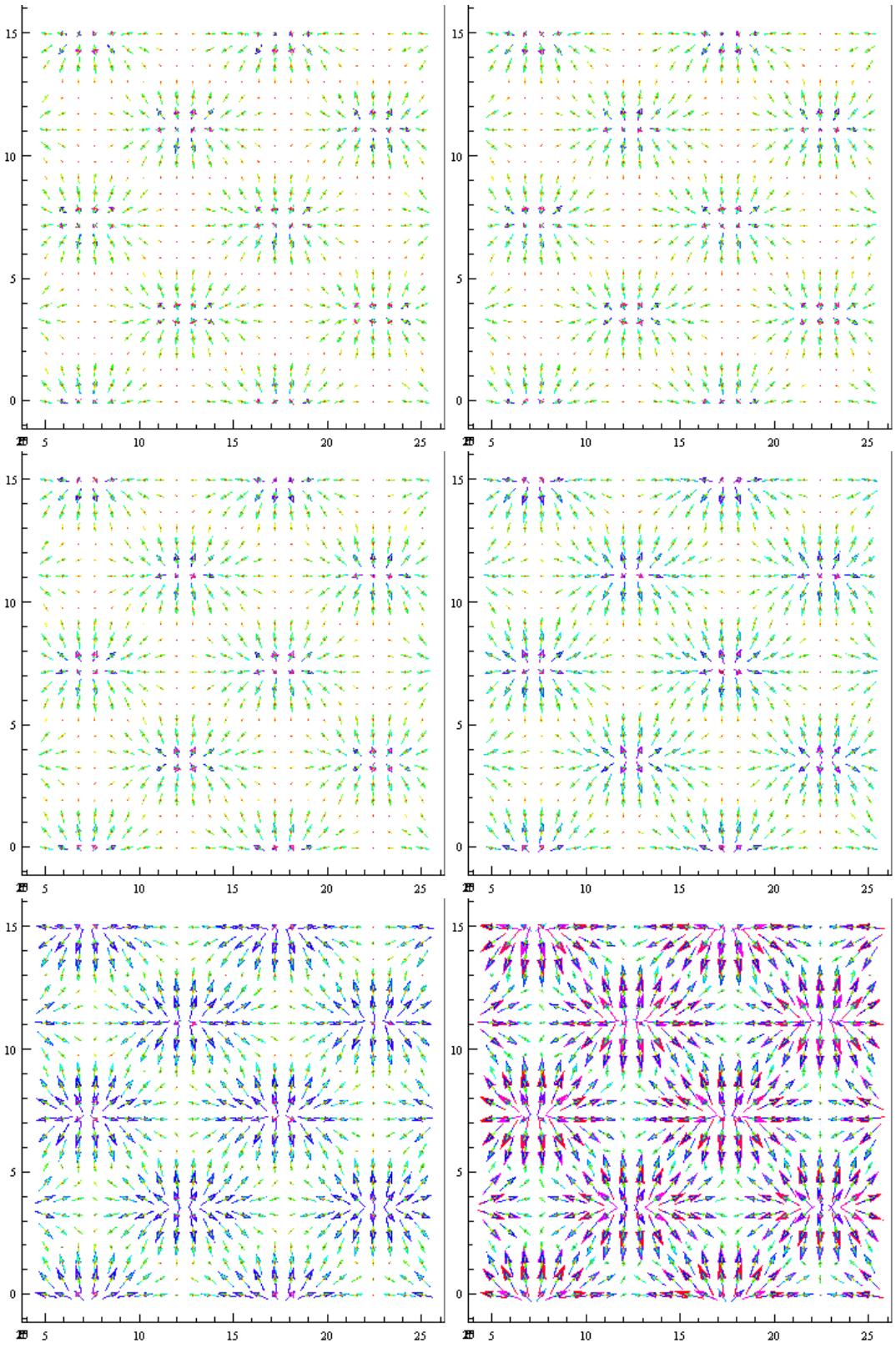
15
10
5
0
5
10
15
20
25

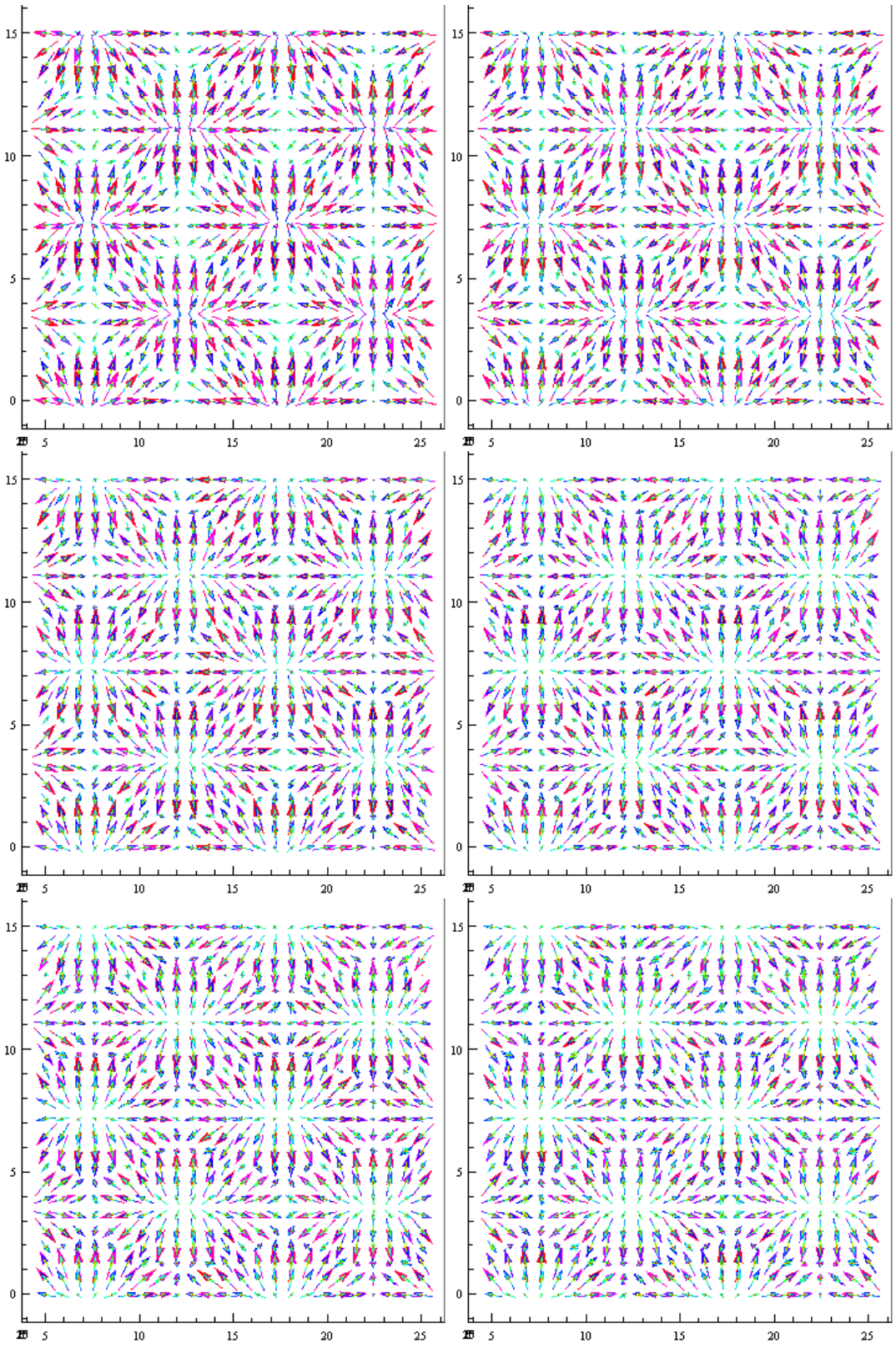
15
10
5
0
5
10
15
20
25

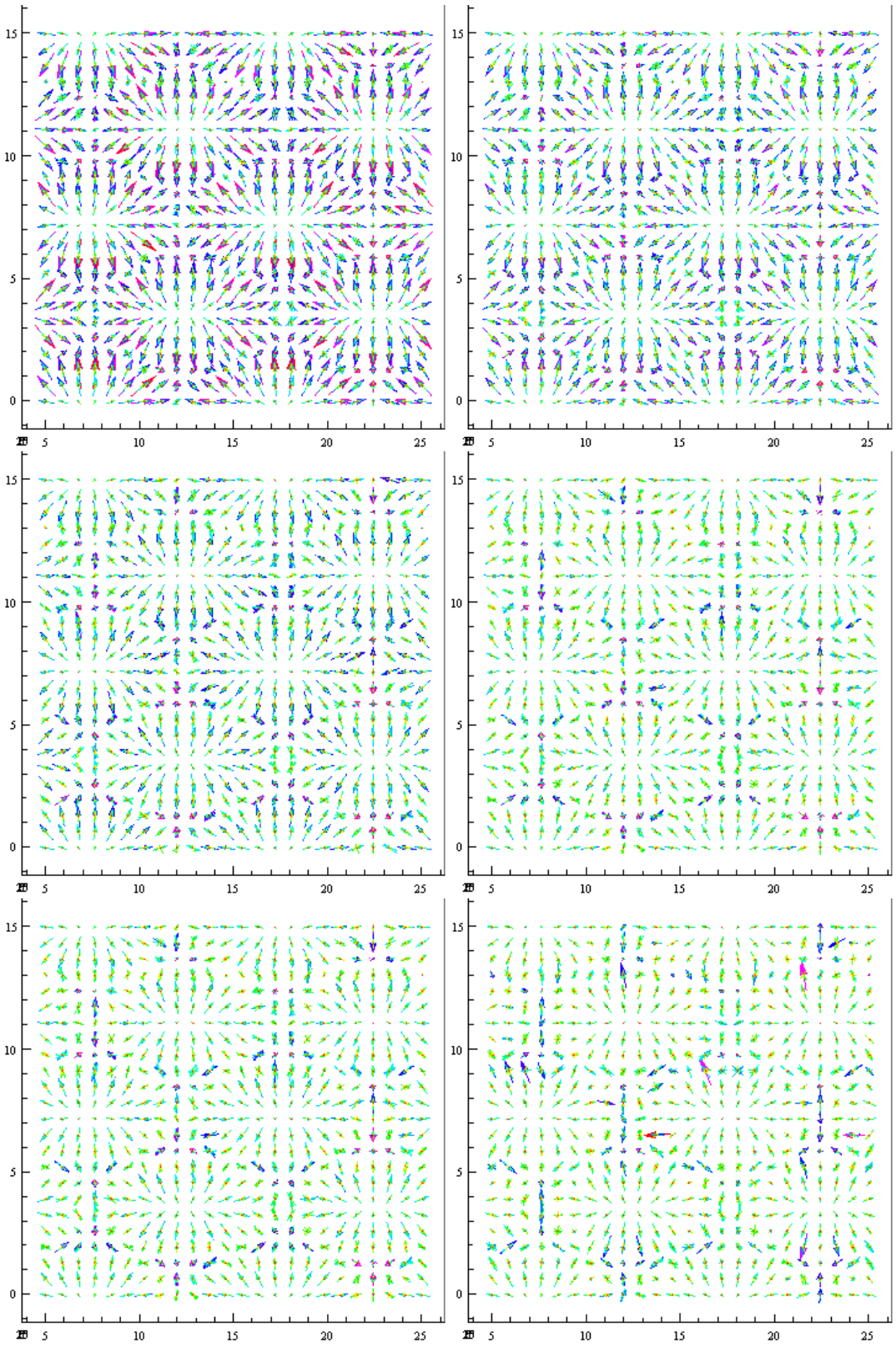
15
10
5
0
5
10
15
20
25

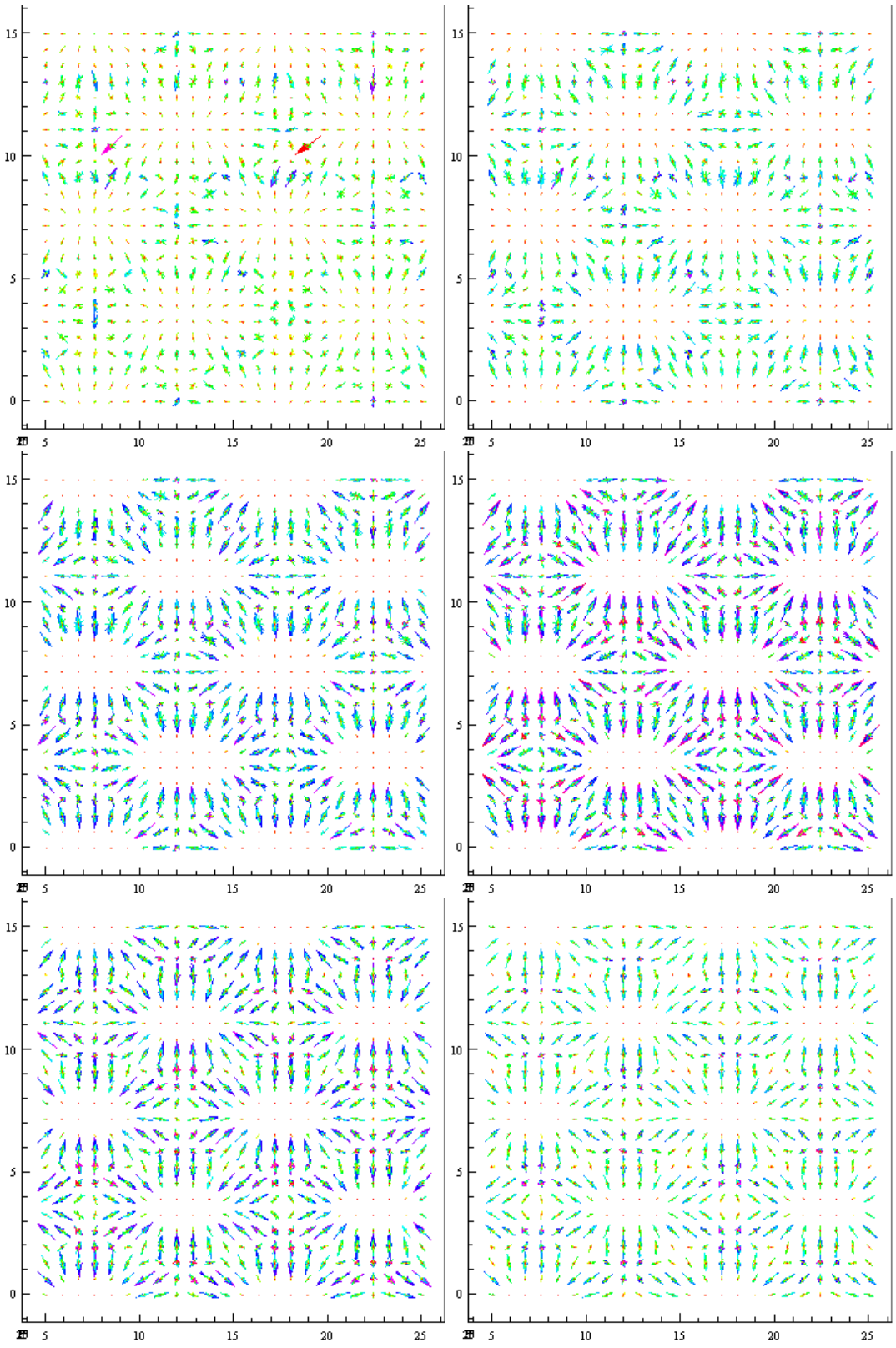
15
10
5
0
5
10
15
20
25

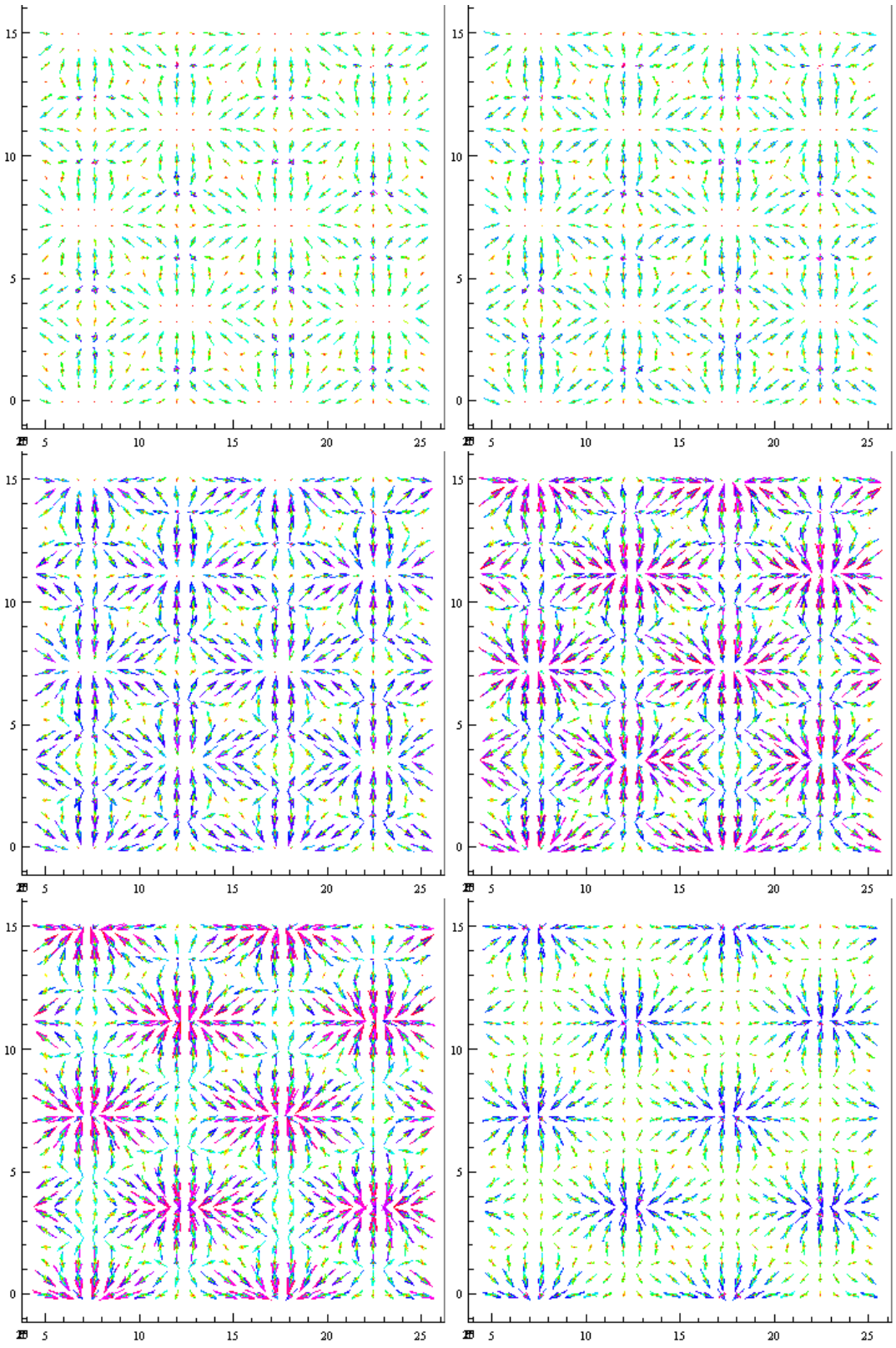
0
5
10
15
20
25

C.2.2 Three-dimensional view

The following pages show the velocity field of a three-dimensional simulation of the hexagonal Faraday wave as a function of time, in side view that shows the three-dimensional structure. The data was provided by Nicholas Périnet.

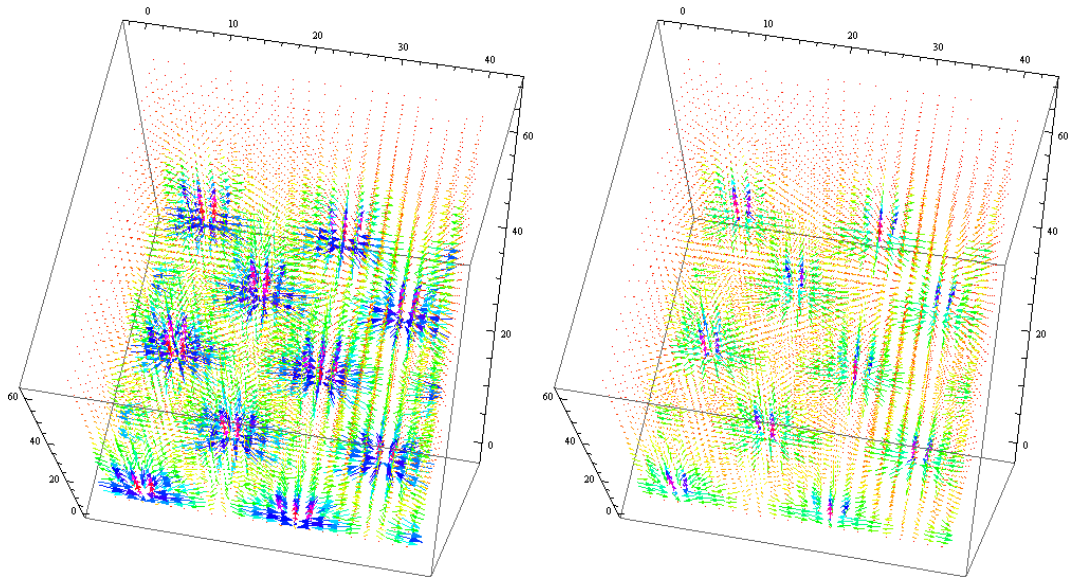
0
10
20
30
40
60
40
20
0
0
10
20
30
40
60
40
20
0

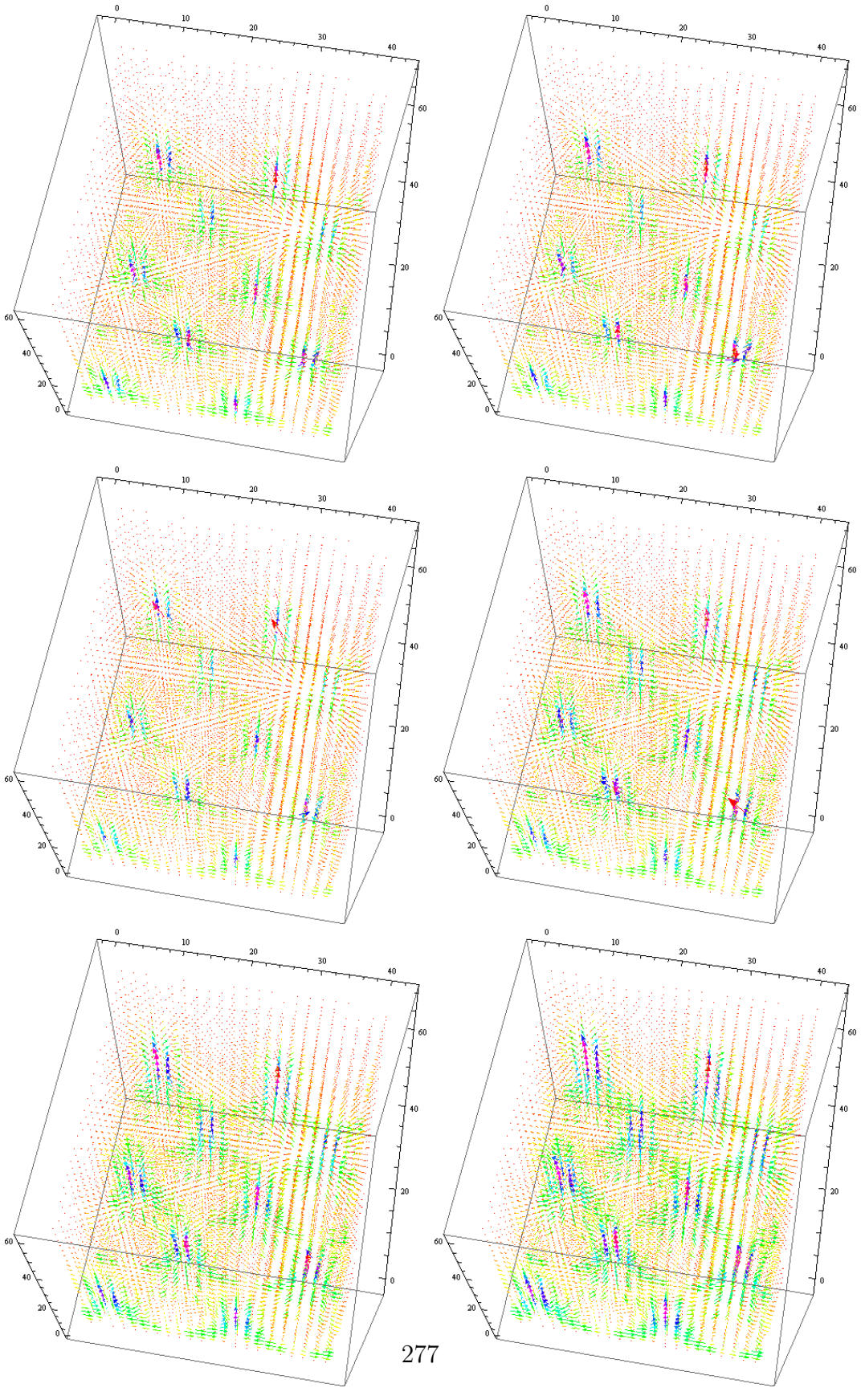

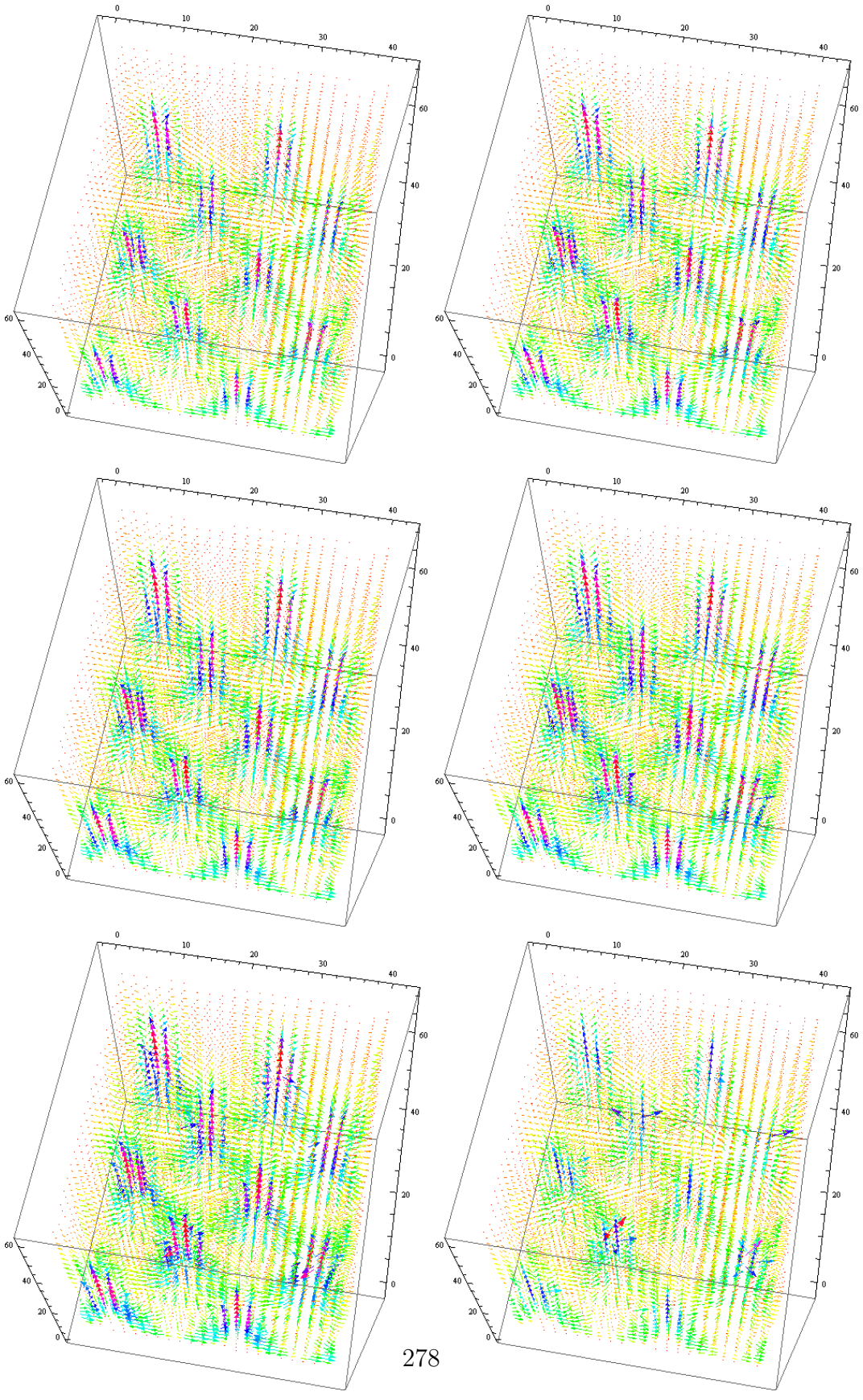
0
10
20
30
40
60
40
20
0

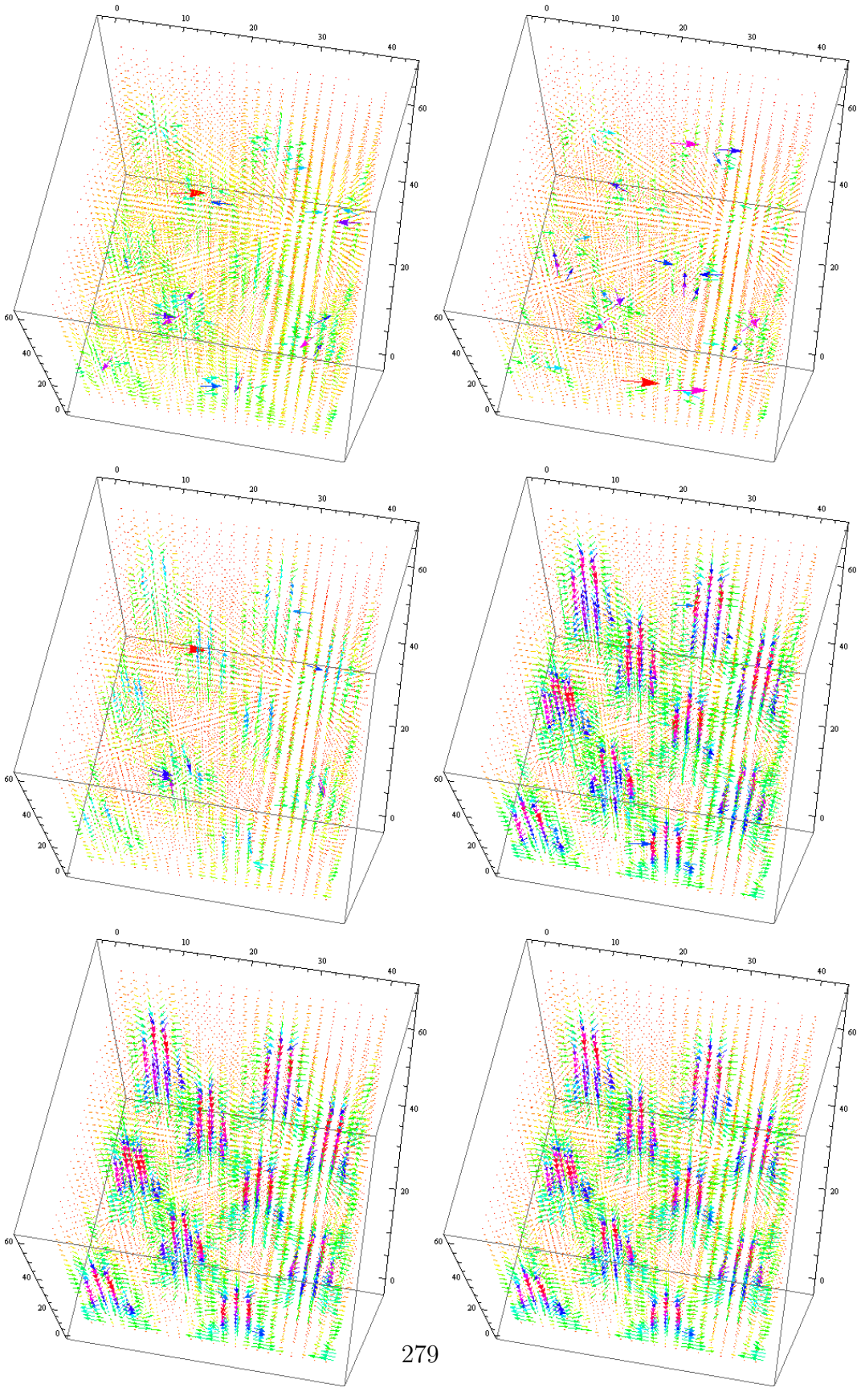

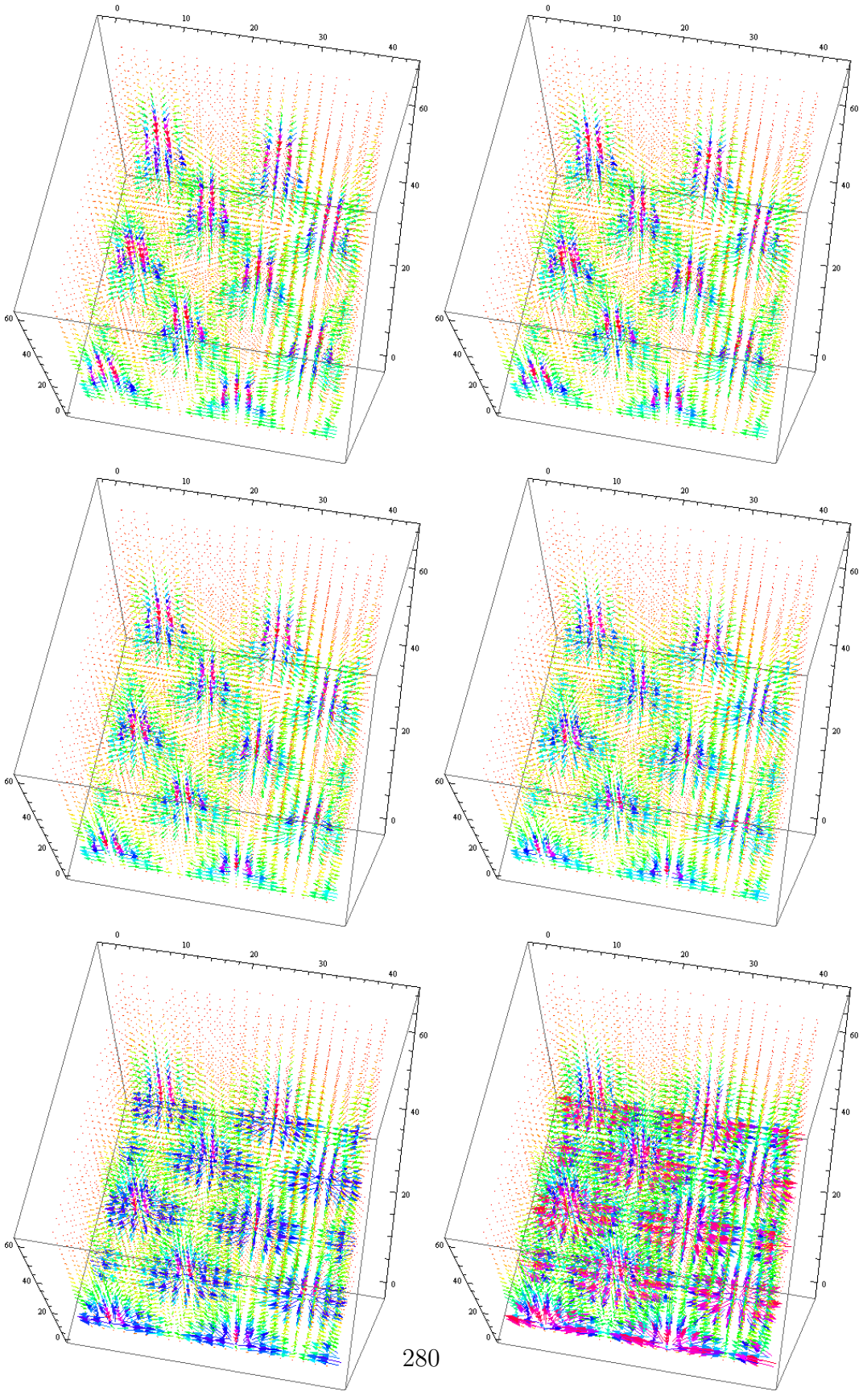

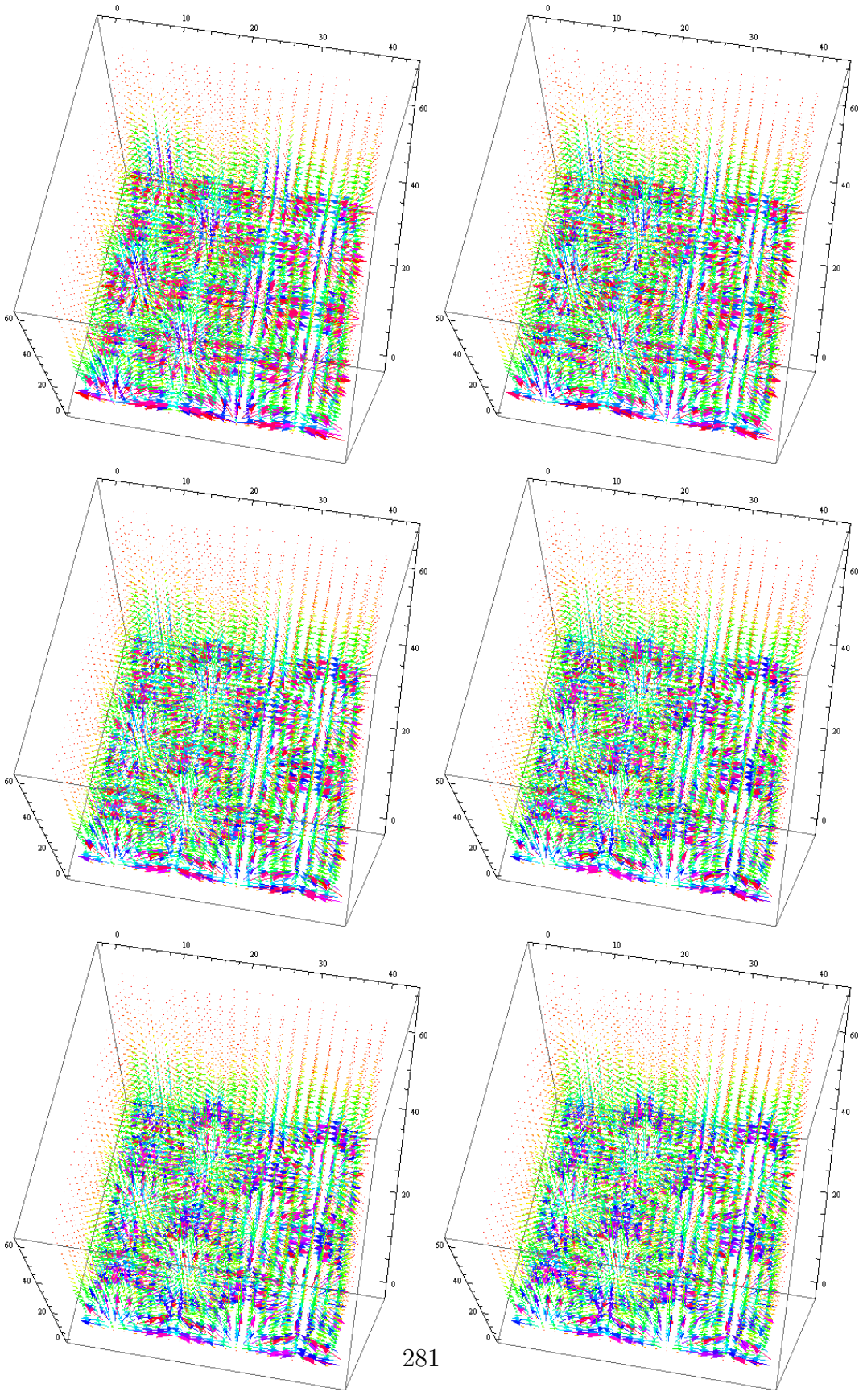

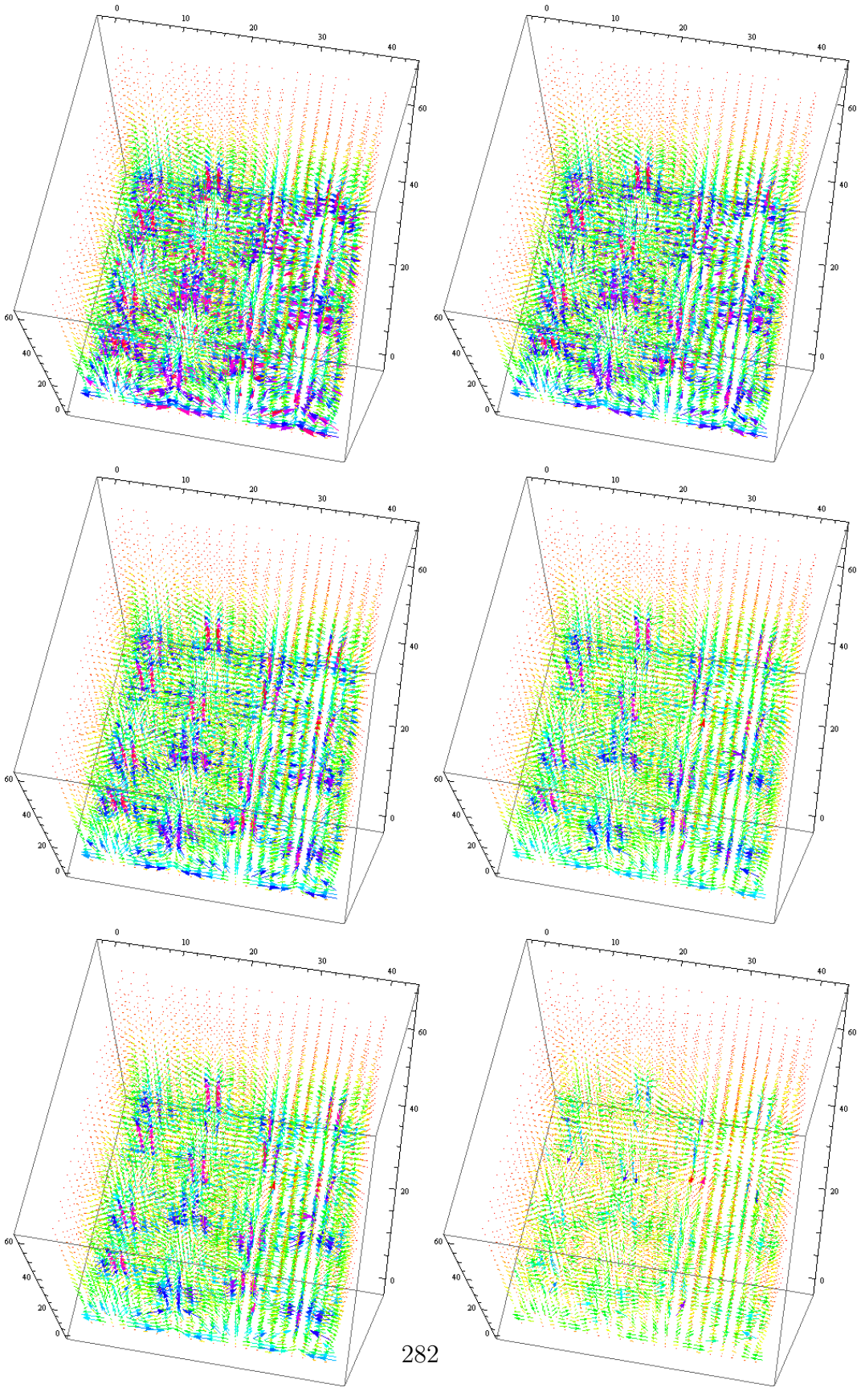

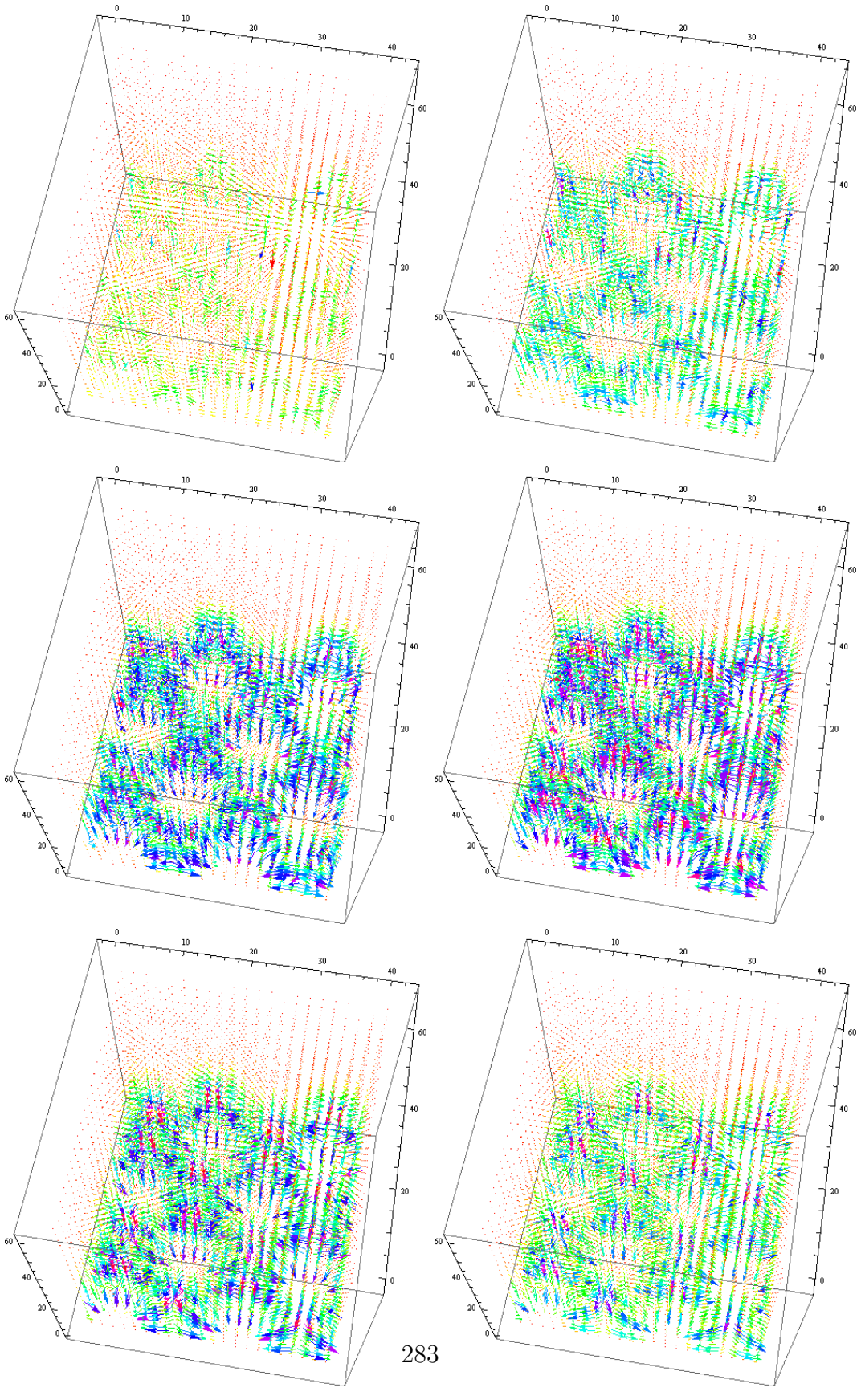

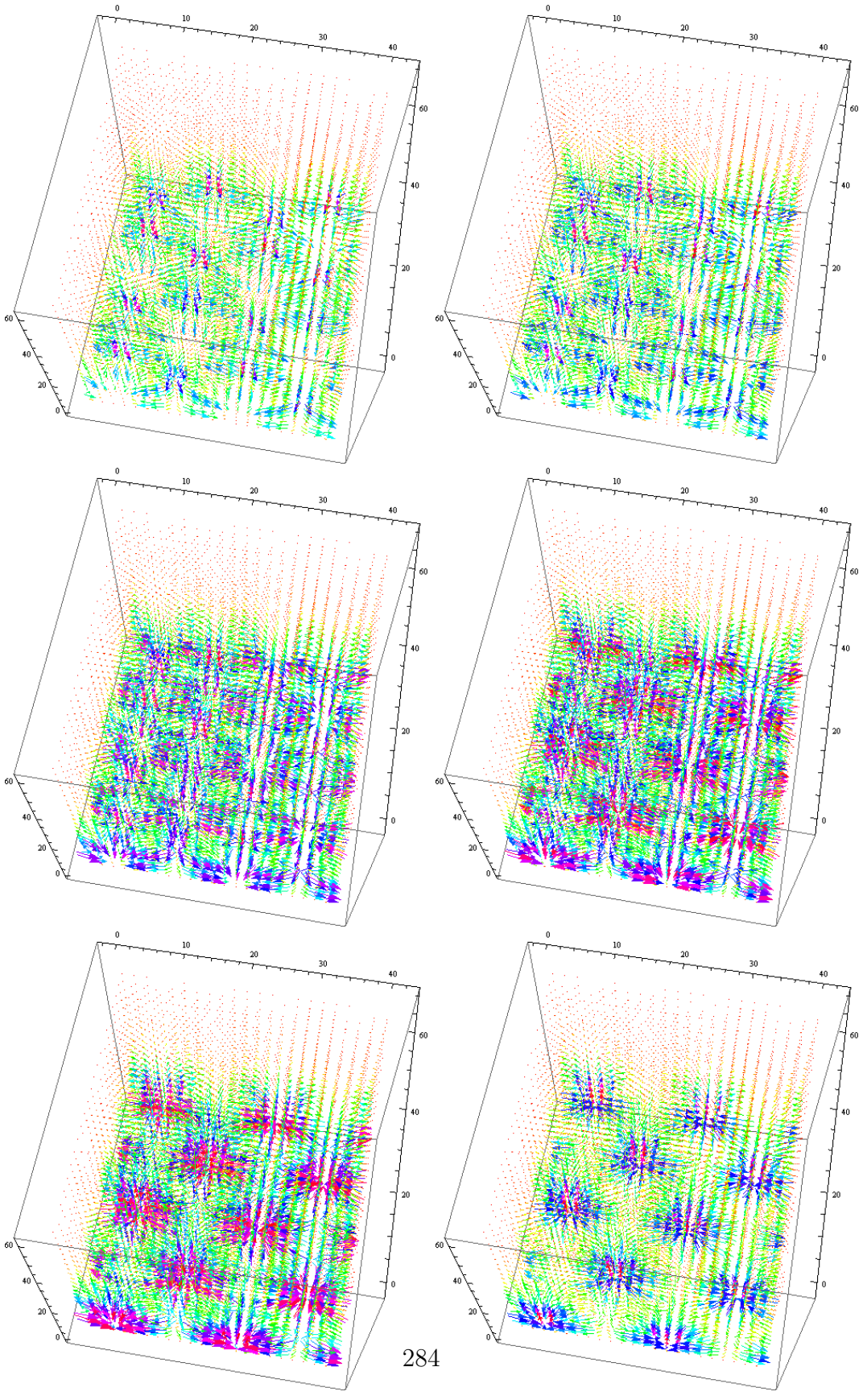

C.3 Size measurements of *Paleodictyon* from the literature

Here I give a list of the articles that were used to compile Fig. 5.18 with measurements of *Paleodictyon*.

Webby (1969)

Crimes and Harper (1970)

Corbo (1979)

Ekdale (1980)

Paczesna (1985)

Pickerill (1990)

Leszczynski (1991)

Hantzpergue and Branger (1992)

Stanley and Pickerill (1993)

Kozur et al. (1996)

Tchoumatchenco and Uchman (2001)

Wetzel (2000)

Buatois et al. (2001)

Mikuláš et al. (2004)

Uchman et al. (2005)

Fursich et al. (2007)

Monaco (2008)

López Cabrera et al. (2008)

Rona et al. (2009)

Lan and Chen (2010)

Nielsen et al. (2010)

Rodríguez-Tovar et al. (2010)

Metz (2012)

Jensen et al. (2013)

Bibliography

Antcliffe, J. B. (2013). Questioning the evidence of organic compounds called sponge biomarkers. *Palaeontology*, pages 1–9.

Antcliffe, J. B. and Brasier, M. D. (2007a). *Charnia* and sea pens are poles apart. *Journal of the Geological Society*, 164(1):49–51.

Antcliffe, J. B. and Brasier, M. D. (2007b). Towards a morphospace for the Ediacara biota. *Geological Society, London, Special Publications*, 286(1):377–386.

Antcliffe, J. B. and Brasier, M. D. (2008). *Charnia* At 50: Developmental Models for Ediacaran Fronds. *Palaeontology*, 51(1):11–26.

Antcliffe, J. B., Gooday, A. J., and Brasier, M. D. (2011). Testing the protozoan hypothesis for Ediacaran fossils: a developmental analysis of *Palaeopascichnus*. *Palaeontology*, 54(5):1157–1175.

Archer, A. W. and Maples, C. G. (1984). Trace-fossil distribution across a marine-to-nonmarine gradient in the Pennsylvanian of southwestern Indiana. *Journal of Paleontology*, 58(2):448–466.

Benton, M. and Harper, D. A. T. (2009). *Introduction to Paleobiology and the Fossil Record*. Wiley-Blackwell.

Boyd, D. W. (1975). False or misleading traces. In *The Study of Trace Fossils*, pages 65–83. Springer.

Brasier, M. and Antcliffe, J. (2004). Decoding the Ediacaran enigma. *Science*, 305(5687):1115–1117.

Brasier, M. D. and Antcliffe, J. B. (2008). *Dickinsonia* from Ediacara: A new look at morphology and body construction. *Palaeogeography, Palaeoclimatology, Palaeoecology*, 270(3-4):311–323.

Brasier, M. D., Antcliffe, J. B., and Liu, A. G. (2012). The architecture of Ediacaran Fronds. *Palaeontology*, 55(5):1105–1124.

Bright, M. (2014). The giant ciliate *Zoothamnium niveum* and its thiotrophic epibiont *Candidatus* Thiobios zoothamnicoli : a model system to study interspecies cooperation. *Frontiers in Microbiology*, 5(April):1–13.

Bromley, R. G. (1990). *Trace Fossils: Biology and Taphonomy, Special topics in paleontology, 3*. Unwin Hyman, London.

Buatois, L. a., Mángano, M. G., and Sylvester, Z. (2001). A diverse deepmarine Ichnofauna from the Eocene Tarcau sandstone of the Eastern Carpathians, Romania. *Ichnos*, 8(1):23–62.

Cabeza, C. and Rosen, M. (2007). Complexity in Faraday experiment with viscoelastic fluid. *International Journal of Bifurcation and Chaos*, 17(5):1599–1607.

Callow, R. H. and Brasier, M. D. (2009). Remarkable preservation of microbial mats in Neoproterozoic siliciclastic settings: Implications for Ediacaran taphonomic models. *Earth-Science Reviews*, 96(3):207–219.

Chen, Z., Zhou, C., Xiao, S., Wang, W., Guan, C., Hua, H., and Yuan, X. (2014). New Ediacara fossils preserved in marine limestone and their ecological implications. *Scientific reports*, 4(4180):1–10.

Chipman, A. D. (2010). Parallel evolution of segmentation by co-option of ancestral gene regulatory networks. *BioEssays*, 32(1):60–70.

Chipman, A. D. and Akam, M. (2008). The segmentation cascade in the centipede Strigamia maritima: Involvement of the Notch pathway and pair-rule gene homologues. *Developmental Biology*, 319(1):160–169.

Clapham, M. and Narbonne, G. (2002). Ediacaran epifaunal tiering. *Geology*, 30(7):627–630.

Clapham, M. E., Narbonne, G. M., and Gehling, J. G. (2003). Paleoecology of the oldest known animal communities : Ediacaran assemblages at Mistaken Point, Newfoundland. *Paleobiology*, 29(4):527–544.

Corbo, S. (1979). Vertical distribution of Trace Fossils in a Turbidite Sequence, Upper Devonian, New York State. *Palaeogeography, Palaeoclimatology, Palaeoecology*, 28:81–101.

Crimes, T. P. and Harper, J. C. (1970). *Trace Fossils*.

Crimes, T. P. and McCall, G. J. H. (1995). A diverse ichnofauna from Eocene-Miocene rocks of the Makran Range (S.E. Iran). *Ichnos*, 3(4):231–258.

Dequéant, M.-L. and Pourquié, O. (2008). Segmental patterning of the vertebrate embryonic axis. *Nature Reviews Genetics*, 9(5):370–382.

Dolnik, M. and Rovinsky, A. (1999). Standing Waves in a Two-Dimensional Reaction-Diffusion Model with the Short-Wave Instability. *The Journal of Physical Chemistry A*, 103(1):38–45.

Douady, S. and Fauve, S. (1988). Pattern Selection in Faraday Instability. *Europhysics Letters*, 6(3):221–226.

Dray, N., Tessmar-Raible, K., Le Gouar, M., Vibert, L., Christodoulou, F., Schipany, K., Guillou, A., Zantke, J., Snyman, H., Béhague, J., Vervoort, M., Arendt, D., and Balavoine, G. (2010). Hedgehog signaling regulates segment formation in the annelid *Platynereis*. *Science (New York, N.Y.)*, 329(5989):339–342.

Droser, M. L., Gehling, J. G., and Jensen, S. R. (2006). Assemblage palaeoecology of the Ediacara biota: The unabridged edition? *Palaeogeography, Palaeoclimatology, Palaeoecology*, 232(2-4):131–147.

Dzik, J. and Ivantsov, A. Y. (1999). An asymmetric segmented organism from the Vendian of Russia and the status of the Dipleurozoa. *Historical Biology*, 13(4):255–268.

Edwards, W. S. and Fauve, S. (1994). Patterns and quasi-patterns in the Faraday experiment. *Journal of Fluid Mechanics*, 278:123–148.

Ekdale, A. (1980). Graphoglyptid burrows in modern deep-sea sediment. *Science*, 207(4428):304–306.

Ekdale, A. A. (1985). Paleoecology of the marine endobenthos. *Palaeogeography, Palaeoclimatology, Palaeoecology*, 50:63–81.

Ekdale, A. A., Bromley, R. G., and Pemberton, S. G. (1984). *Ichnology: the use of trace fossils in sedimentology and stratigraphy*. Society of Economic Paleontologists and Mineralogists.

Engels, P., Atherton, C., and Hoefer, M. (2007). Observation of Faraday Waves in a Bose-Einstein Condensate. *Physical Review Letters*, 98(9):095301.

Erwin, D. H., Laflamme, M., Tweedt, S. M., Sperling, E. A., Pisani, D., and Peterson, K. J. (2011a). The Cambrian Conundrum: Early Divergence and Later Ecological Success in the Early History of Animals. *Science*, 334(November):1091–1098.

Erwin, D. H., Laflamme, M., Tweedt, S. M., Sperling, E. a., Pisani, D., and Peterson, K. J. (2011b). The Cambrian conundrum: early divergence and later ecological success in the early history of animals. Supporting material. *Science*, 334(6059):1091–7.

Evans, S. D., Droser, M. L., and Gehling, J. G. (2015). Dickinsonia liftoff: Evidence of current derived morphologies. *Palaeogeography, Palaeoclimatology, Palaeoecology*, 434:28–33.

Falkowski, P. G., Katz, M. E., Knoll, A. H., Quigg, A., Raven, J. A., Schofield, O., and Taylor, F. J. R. (2004). The Evolution of Modern Eukaryotic. *Science*, 305(July):354–361.

Faraday, M. (1831). On a peculiar class of acoustical figures; and on cer-

tain forms assumed by groups of particles upon vibrating elastic surfaces. *Philosophical Transactions of the Royal Society of London*, 121:299–340.

Fedonkin, M. (1998). Metameric features in the Vendian metazoans. *Italian Journal of Zoology*, 65(1):11–17.

Fedonkin, M. and Cope, J. (1985a). Precambrian Metazoans: The Problems of Preservation, Systematics and Evolution. *Philosophical Transactions of the Royal Society B: Biological Sciences*, 311:27–45.

Fedonkin, M. and Waggoner, B. (1997). The Late Precambrian fossil *Kimberella* is a mollusc-like bilaterian organism. *Nature*, 388(August):868–871.

Fedonkin, M. A. (1990). Systematic description of Vendian metazoa. *The Vendian System*, 1:71–120.

Fedonkin, M. A. and Cope, J. C. W. (1985b). Precambrian Metazoans: The Problems of Preservation, Systematics and Evolution [and Discussion]. *Philosophical Transactions of the Royal Society B*, 311(1148):27–45.

Fedonkin, M. A., Gehling, J. G., Grey, K., Narbonne, G. M., and Vickers-Rich, P. (2007a). *The rise of animals: evolution and diversification of the kingdom Animalia*. John Hopkins University Press.

Fedonkin, M. A., Simonetta, A., and Ivantsov, A. Y. (2007b). New data on *Kimberella*, the Vendian mollusc-like organism (White Sea region, Russia): palaeoecological and evolutionary implications. *Geological Society, London, Special Publications*, 286(1):157–179.

Folgueira, M., Bayley, P., Navratilova, P., Becker, T. S., Wilson, S. W., and

Clarke, J. D. W. (2012). Morphogenesis underlying the development of the everted teleost telencephalon. *Neural Development*, 7(1):32.

Foote, M. (1989). Perimeter-Based Fourier Analysis: A New Morphometric Method Applied to the Trilobite Cranidium. *Journal of Paleontology*, 63(6):880–885.

Foote, M. (1990). Nearest-Neighbor Analysis of Trilobite Morphospace. *Systematic Zoology*, 39(4):371–382.

Ford, T. D. (1958). Pre-Cambrian Fossils From Charnwood Forest. *Proceedings of the Yorkshire Geological Society*, 31(3):211–217.

Fortey, R. and Bell, A. (1987). Branching geometry and function of multiramous graptoloids. *Paleobiology*, 13(1):1–19.

Fursich, F. T., Taheri, J., and Wilmsen, M. (2007). New Occurrences of the Trace Fossil *Paleodictyon* in Shallow Marine Environments: Examples From the Triassic-Jurassic of Iran. *Palaios*, 22(4):408–416.

Galetzka, J., Melgar, D., Genrich, J. F., Geng, J., Owen, S., Lindsey, E. O., Xu, X., Bock, Y., Avouac, J.-P., Adhikari, L. B., Upreti, B. N., Pratt-Sitaula, B., Bhattarai, T. N., Sitaula, B. P., Moore, A., Hudnut, K. W., Szeliga, W., Normandeau, J., Fend, M., Flouzat, M., Bollinger, L., Shrestha, P., Koirala, B., Gautam, U., Bhatterai, M., Gupta, R., Kandel, T., Timsina, C., Sapkota, S. N., Rajaure, S., and Maharjan, N. (2015). Slip pulse and resonance of the Kathmandu basin during the 2015 Gorkha earthquake, Nepal. *Science*, 349(6252):1091–1095.

Garlick, G. D. and Miller, W. C. (1993). Simulations of burrowing strategies and construction of *Paleodictyon*. *Journal of Geological Education*, 41:159.

Gavrilets, S. and Gravner, J. (1997). Percolation on the fitness hypercube and the evolution of reproductive isolation. *Journal of theoretical biology*, 184(1):51–64.

Gehling, J. (1999). Microbial mats in terminal Proterozoic siliciclastics; Ediacaran death masks. *Palaios*, 14(1):40–57.

Gehling, J. G. and Droser, M. L. (2009). Textured organic surfaces associated with the Ediacara biota in South Australia. *Earth-Science Reviews*, 96:196–206.

Gehling, J. G. and Droser, M. L. (2013). How well do fossil assemblages of the Ediacara Biota tell time? *Geology*, 41(4):447–450.

Gehling, J. G., Droser, M. L., Jensen, S. R., and Runnegar, B. N. (2005). Ediacara organisms: relating form to function. *Evolving form and function: Fossils and Development; Proceedings of a Symposium Honouring Adolf Seilacher for His Contributions to Paleontology, in Celebration of His 80th Birthday*, pages 43–66.

Glaessner, M. (1961). Pre-Cambrian animals. *Scientific American*, 204:72–79.

Glaessner, M. (1962). Pre-Cambrian Fossils. *Biological Reviews*, 37:467–494.

Glaessner, M. and Wade, M. (1966). The late Precambrian fossils from Ediacara, South Australia. *Palaeontology*, 9:599–628.

Glaessner, M. F. (1959). Precambrian Coelenterata from Australia, Africa and England. *Nature*, 183:1472–1473.

Gold, D. A., Runnegar, B., Gehling, J. G., and Jacobs, D. K. (2015). Ancestral state reconstruction of ontogeny supports a bilaterian affinity for *Dickinsonia*. *Evolution & Development*, 17(6):315–324.

Gould, S. J. (1991). The Disparity of the Burgess Shale Arthropod Fauna and the Limits of Cladistic Analysis : Why We Must Strive to Quantify Morphospace. *Paleobiology*, 17(4):411–423.

Grazhdankin, D. (2004). Patterns of distribution in the Ediacaran biotas: facies versus biogeography and evolution. *Paleobiology*, 30(2):203–221.

Grazhdankin, D. (2014). Patterns of Evolution of the Ediacaran Soft-Bodied Biota. *Journal of Paleontology*, 88(2):269–283.

Grazhdankin, D. and Seilacher, A. (2002). Underground Vendobionta from Namibia. *Palaeontology*, 45(1):57–78.

Grazhdankin, D. and Seilacher, A. (2005). A re-examination of the Nama-type Vendian organism *Rangea* schneiderhoehni. *Geological Magazine*, 142:571–582.

Grotzinger, J. P., Watters, W. A., and Knoll, A. H. (2000). Calcified metazoans in thrombolite-stromatolite reefs of the terminal Proterozoic Nama Group, Namibia. *Paleobiology*, 26(3):334–359.

Gürich, G. (1929). Die bislang ältesten Spuren von Organismen in Südafrika. In *International Geological Congress. South Africa*, volume 2, pages 670–680.

Gürich, G. (1933). Die Kuibis-Fossilien der Nama-Formation von Südwestafrika. *Paläontologische Zeitschrift*, 15(2-3):137–154.

Hantzpergue, P. and Branger, P. (1992). L'ichnogenre *Paleodictyon* dans les depots neritiques de l'Oxfordien superieur nord-aquitan (France). *GeoBios*, 25(2):195–205.

Harazim, D., McIlroy, D., Edwards, N. P., Wogelius, R. A., Manning, P. L., Poduska, K. M., Layne, G. D., Sokaras, D., Alonso-Mori, R., and Bergmann, U. (2015). Bioturbating animals control the mobility of redox-sensitive trace elements in organic-rich mudstone. *Geology*, 43(11):1007–1010.

Höld, I. M., Schouten, S., Jellema, J., and Sinninghe-Damste, J. S. (1999). Origin of free and bound mid-chain methyl alkanes in oils, bitumens and kerogens of the marine, Infracambrian Huqf Formation (Oman). *Organic Geochemistry*, 30(11):1411–1428.

Honeycutt, C. E. and Plotnick, R. (2005). Mathematical analysis of *Paleodictyon*: a graph theory approach. *Lethaia*, 38(4):345–350.

Hoyal Cuthill, J. F. and Conway Morris, S. (2014). Fractal branching organizations of Ediacaran rangeomorph fronds reveal a lost Proterozoic body plan. *Proceedings of the National Academy of Sciences of the United States of America*, 111(36):13122–6.

Hughes, N. C. (2003). Trilobite body patterning and the evolution of arthropod tagmosis. *BioEssays*, 25(4):386–395.

Ivantsov, A. (2011). Feeding traces of proarticulatathe Vendian metazoa. *Paleontological Journal*, 45(3):237–248.

Ivantsov, A. Y. (2001). Traces of active moving of the large late Vendian Metazoa over the sediment surface. *Ecosystem Restructure and the Evolution of the Biosphere*, 4:119–120.

Ivantsov, A. Y. and Fedonkin, M. A. (2001). Locomotion trails of the Vendian invertebrates preserved with the producers body fossils, White Sea, Russia. In *North American Paleontologica/Convention, Berkeley. California, Program and Abstracts*, page 72.

Jenkins, R. (1995). The problems and potential of using animal fossils and trace fossils in terminal Proterozoic biostratigraphy. *Precambrian Research*, 73:51–69.

Jenkins, R. J. F. (1992). Functional and ecological aspects of Ediacaran assemblages. In *Origin and early evolution of the Metazoa*, pages 131–176. Springer.

Jensen, S., Buatois, L. A., and Mangano, M. G. (2013). Chapter 5 Testing for palaeogeographical patterns in the distribution of Cambrian trace fossils. *Geological Society, London, Memoirs*, 38(1):45–58.

Ke, Z., Hong-Li, W., Chun, Q., and Qi, O. (2006). Hexagonal Standing-Wave Patterns in Periodically Forced Reaction - Diffusion Systems. *Chinese physics letters*, 23(6):1414–1417.

Kloiber, U., Pflugfelder, B., Rinke, C., and Bright, M. (2009). Cell proliferation and growth in *Zoothamnium niveum* (Oligohymenophora, Peritrichida) Thiotrophic bacteria symbiosis. *Symbiosis*, 47:43–50.

Knoll, A., Walter, M., Narbonne, G., and Christie-Blick, N. (2006). The Ediacaran Period: a new addition to the geologic time scale. *Lethaia*, 39(1):13–30.

Knoll, A. H., Grotzinger, J. P., Kaufman, A. J., and Kolosov, P. (1995). Integrated approaches to terminal Proterozoic stratigraphy: an example from the Olenek Uplift, northeastern Siberia. *Precambrian Research*, 73:251–270.

Kozur, H. W., Krainer, K., and Mostler, H. (1996). Ichnology and Sedimentology of the Early Permian Deep-water Deposits from the Lercara-Roccapalumba Area (Western Sicily , Italy). *Facies*, 34:123–150.

Ksikiewicz, M. (1970). Observations on the ichnofauna of the Polish Carpathians. *Trace fossils*, pages 283–322.

Kudrolli, A., Abraham, M., and Gollub, J. (2001). Scarred patterns in surface waves. *Physical Review E*, 63(2):026208.

Kudrolli, A. and Gollub, J. P. (1996). Patterns and spatiotemporal chaos in parametrically forced surface waves: a systematic survey at large aspect ratio. *Physica D: Nonlinear Phenomena*, 97(1):133–154.

Kudrolli, A., Pier, B., and Gollub, J. (1998). Superlattice patterns in surface waves. *Physica D: Nonlinear Phenomena*, 123(1):99–111.

Kumar, K. (1996). Linear theory of Faraday instability in viscous liquids. *Proceedings: Mathematical, Physical and Engineering Sciences*, 452(1948):1113–1126.

Kummel, B. and Teichert, C. (1970). *Stratigraphy and paleontology of the Permian-Triassic boundary beds, Salt Range and trans-Indus ranges, West Pakistan*. University Press of Kansas.

Laflamme, M., a.F. Darroch, S., Tweedt, S. M., Peterson, K. J., and Erwin, D. H. (2013). The end of the Ediacara biota: Extinction, biotic replacement, or Cheshire Cat? *Gondwana Research*, 23(2):558–573.

Laflamme, M., Narbonne, G. M., and Anderson, M. M. (2004). Morphometric Analysis of the Ediacaran frond *Charniodiscus* from the Mistaken Point formation, Newfoundland. *Journal of Paleontology*, 78(5):827–837.

Laflamme, M., Xiao, S., and Kowalewski, M. (2009). Osmotrophy in modular Ediacara organisms. *Proceedings of the National Academy of Sciences*, 106(34):14438–14443.

Lan, Z. and Chen, Z. Q. (2010). *Paleodictyon* from a nearshore paleoenvironmental setting in the Guadalupian (Middle Permian) of the Carnarvon Basin, Western Australia. *Australian Journal of Earth Sciences*, 57(4):453–467.

Laurent, M. C. Z., Gros, O., Brulport, J.-P., Gaill, F., and Bris, N. L. (2009). Sunken wood habitat for thiotrophic symbiosis in mangrove swamps. *Marine environmental research*, 67(2):83–8.

Lehane, J. R. and Ekdale, A. A. (2013). Fractal Analysis of Graphoglyptid Trace Fossils. *Palaios*, 28(1):23–32.

Leszczynski, S. (1991). Oxygen-Related Controls on Predepositional Ichnofa-

cies in Turbidites, Guipuzcoan Flysch (Albian - Lower Eocene), Northern Spain. *Palaios*, 6(3):271–280.

Li, J. and Liu, Y. Y. (2008). Particle-wave duality and coherent instability control in dense gas–solid flows. *Chemical Engineering Science*, 63(3):732–750.

Lindenmayer, A. (1968a). Mathematical models for cellular interactions in development I. Filaments with one-sided inputs. *Journal of Theoretical Biology*, 18(3):280–299.

Lindenmayer, A. (1968b). Mathematical models for cellular interactions in development II. Simple and branching filaments with two-sided inputs. *Journal of Theoretical Biology*, 18(3):300–315.

Liu, A., Kenchington, C., and Mitchell, E. (2014). Remarkable insights into the paleoecology of the Avalonian Ediacaran macrobiota. *Gondwana Research*.

Liu, A. and Matthews, J. (2014). *Haootia quadriformis* n. gen., n. sp., interpreted as a muscular cnidarian impression from the Late Ediacaran period (approx. 560 Ma). *Proceedings of the Royal Society B*, 281(20141202).

Liu, A., McIlroy, D., Matthews, J., and Brasier, M. (2013). Exploring an Ediacaran 'nursery': growth, ecology and evolution in a rangeomorph palaeocommunity. *Geology Today*, 29(1):23–26.

Liu, A. G., Mcilroy, D., Antcliffe, J. B., and Brasier, M. D. (2011a). Effaced preservation in the Ediacara biota and its implications for the early macrofossil record. *Palaeontology*, 54(3):607–630.

Liu, A. G., McIlroy, D., Antcliffe, J. B., and Brasier, M. D. (2011b). Effaced preservation in the Ediacara biota and its implications for the early macrofossil record. *Palaeontology*, 54(3):607–630.

Livio, M. (2002). *The Golden Ratio: The Story of Phi, the World's Most Astonishing Number*. Broadway Books.

López Cabrera, M. I., Olivero, Eduardo B. Carmona, N. B., and Ponce, J. J. (2008). Cenozoic trace fossils of the Cruziana, Zoophycos and Nereites ichnofacies from the Fuegian Andes, Argentina. *Ameghiniana*, 45(2):377–392.

Love, G. D., Grosjean, E., Stalvies, C., Fike, D. A., Grotzinger, J. P., Bradley, A. S., Kelly, A. E., Bhatia, M., Meredith, W., Snape, C. E., Bowring, S. A., Condon, D. J., and Summons, R. E. (2009). Fossil steroids record the appearance of Demospongiae during the Cryogenian period. *Nature*, 457(7230):718–721.

Manton, S. M. and Harding, J. P. (1967). The polychaete *Spinther* and the origin of the Arthropoda. *Journal of Natural History*, 1(1):1–22.

Marshall, C. R. and Valentine, J. W. (2010). The importance of preadapted genomes in the origin of the animal bodyplans and the Cambrian explosion. *Evolution; international journal of organic evolution*, 64(5):1189–201.

Martin, M., Grazhdankin, D., Bowring, S., Evans, D., Fedonkin, M., and Kirschvink, J. (2000). Age of Neoproterozoic Bilatarian Body and Trace Fossils , White Sea , Russia: Implications for Metazoan Evolution. *Science*, 288(May):841–845.

McCaffrey, M. A., Michael Moldowan, J., Lipton, P. A., Summons, R. E., Peters, K. E., Jeganathan, A., and Watt, D. S. (1994). Paleoenvironmental implications of novel C30 steranes in Precambrian to Cenozoic Age petroleum and bitumen. *Geochimica et Cosmochimica Acta*, 58(1):529–532.

McCann, T. and Pickerill, R. K. (1988). Flysch Trace Fossils from the Cretaceous Kodiak Formation of Alaska. *Journal of Paleontology*, 62(3):pp. 330–348.

McGhee, G. (1999). *Theoretical Morphology: The Concepts and Its Applications*. Columbia University Press.

McGowan, a. J. and Dyke, G. J. (2007). A morphospace-based test for competitive exclusion among flying vertebrates: did birds, bats and pterosaurs get in each other's space? *Journal of evolutionary biology*, 20(3):1230–6.

McIlroy, D., Worden, R., and Needham, S. (2003). Faeces, clay minerals and reservoir potential. *Journal of the Geological Society*, 160(3):489–493.

Metz, R. (2012). The Trace Fossil *Paleodictyon* within The Cruziana Ichnofacies: First Record from The Devonian in Pennsylvania. *Ichnos*, 19(4):190–193.

Mikuláš, R., Lehotský, T., and Bábek, O. (2004). Trace fossils of the Moravice Formation from the southern Nízký Jeseník Mts.(Lower Carboniferous, Culm facies; Moravia, Czech Republic). *Bulletin of Geosciences*, 79(2):81–98.

Miller, W. (1991). Paleoecology of graphoglyptids. *Ichnos*, 1(4):305–312.

Miller, W. (2014). Mystery of the graphoglyptids. *Lethaia*, 47(1):1–3.

Minter, N. J., Buatois, L. A., Lucas, S. G., Braddy, S. J., and Smith, J. A. (2006). Spiral-shaped graphoglyptids from an Early Permian intertidal flat. *Geology*, 34(12):1057–1060.

Mitchell, E. G., Kenchington, C. G., Liu, A. G., Matthews, J. J., and Butterfield, N. J. (2015). Reconstructing the reproductive mode of an Ediacaran macro-organism. *Nature*.

Mitteroecker, P. and Huttegger, S. M. (2009). The Concept of Morphospaces in Evolutionary and Developmental Biology: Mathematics and Metaphors. *Biological Theory*, 4(1):54–67.

Monaco, P. (2008). Taphonomic Features of *Paleodictyon* and Other Graphoglyptid Trace Fossils in Oligo-Miocene Thin-Bedded Turbidites, Northern Apennines, Italy. *Palaios*, 23(10):667–682.

Moore, R. C. and Harrington, H. J. (1956). Conulata. *Treatise on Invertebrate Paleontology: Part F. Coelenterata. Geol. Soc. Am., Univ. Kansas*, pages F54—-F66.

Murchison, R. I., Savi, P., and Meneghini, G. (1850). *Memoria sulla struttura geologica delle Alpi degli Apennini e dei Carpazi: diretta specialmente a provare un passaggio dalle rocce secondarie alle terziarie e lo sviluppo dei depositi eocenici nell'Europa meridionale*. Stamperia granducale.

Nakayama, H., Matsuo, Y., Takeshi, O., and Nakahara, A. (2013). Position control of desiccation cracks by memory effect and Faraday waves. *The European physical journal. E, Soft matter*, 36(1):1.

Narbonne, G., Saylor, B., and Grotzinger, J. (1997). The youngest Ediacaran fossils from southern Africa. *Journal of Paleontology*, 71(6):953–967.

Narbonne, G. M. (2004). Modular construction of early Ediacaran complex life forms. *Science*, 305(5687):1141–4.

Narbonne, G. M., Laflamme, M., Trusler, P. W., Dalrymple, R. W., and Greentree, C. (2014a). Deep-Water Ediacaran Fossils from Northwestern Canada: Taphonomy, Ecology, and Evolution. *Journal of Paleontology*, 88(2):207–223.

Narbonne, G. M., Laflamme, M., Trusler, P. W., Dalrymple, R. W., and Greentree, C. (2014b). Deep-Water Ediacaran Fossils from Northwestern Canada: Taphonomy, Ecology, and Evolution. *Journal of Paleontology*, 88(2):207–223.

Narbonne, G. M., Xiao, S., and Shields, G. (2012). The Ediacaran Period. In *Geological Timescale*, chapter The Ediaca, pages 427–449.

Nielsen, J., Gormus, M., Uysal, K., and Kanbur, S. (2010). First records of trace fossils from the Lake District, southwestern Turkey. *Bulletin of Geosciences*, 85(4):691–708.

Niklas, K. J. (1994). Morphological Evolution Through Complex Domains of Fitness. *Proceedings of the National Academy of Sciences*, 91(15):6772–6779.

Olivero, E. and Lopez, C. (2010). Eocene graphoglyptids from shallow-marine, highenergy, organic-rich, and bioturbated turbidites, Fuegian Andes, Argentina. *Acta Geológica Polonica*, 60(1):77–91.

Paczesna, J. (1985). Ichnorodzaj *Paleodictyon* Meneghini Z dolnego kambru Zbilutki (Góry Świtokrzyskie). *Kwartalnik Geololiczny*, 29(3/4):589–596.

Parry, L., Vinther, J., and Edgecombe, G. D. (2015). Cambrian stem-group annelids and a metameric origin of the annelid head. *Biology Letters*, 11:1–5.

Peel, A. D., Chipman, A. D., and Akam, M. (2005). Arthropod segmentation: beyond the Drosophila paradigm. *Nature reviews. Genetics*, 6(12):905–916.

Penny, A., Wood, R., Curtis, A., Bowyer, F., Tostevin, R., and Hoffman, K.-H. (2014). Ediacaran metazoan reefs from the Nama Group, Namibia. *Science*, 344(6191):1504–1507.

Périnet, N., Juric, D., and Tuckerman, L. S. (2009). Numerical simulation of Faraday waves. *Journal of Fluid Mechanics*, 635:1–26.

Périnet, N., Juric, D., and Tuckerman, L. S. (2012). Exotic Behavior of Hexagons in Faraday Waves. *Revista Cubana de Física*, 29(1):6–8.

Peterson, K. J., Waggoner, B., and Hagadorn, J. W. (2003). A fungal analog for Newfoundland Ediacaran fossils? *Integrative and comparative biology*, 43(1):127–36.

Pi, H.-J., Park, S.-y., Lee, J., and Lee, K. J. (2000). Super-lattice, rhombus, square, and hexagonal standing waves in magnetically driven ferrofluid surface. *arXiv preprint*, cond-mat/0.

Pickerill, R. (1990). Nonmarine *Paleodictyon* from the Carboniferous Albert Formation of southern New Brunswick. *Atlantic Geology*.

Pueyo, J. I., Lanfear, R., and Couso, J. P. (2008). Ancestral Notch-mediated segmentation revealed in the cockroach Periplaneta americana. *Proceedings of the National Academy of Sciences of the United States of America*, 105(43):16614–16619.

Raup, D. (1966). Geometric analysis of shell coiling: general problems. *Journal of Paleontology*, 40(5):1178–1190.

Raup, D. and Michelson, A. (1965). Theoretical morphology of the coiled shell. *Science*, 147(3663):1294–1295.

Rivera, A. S. and Weisblat, D. A. (2009). And Lophotrochozoa Makes Three: Notch/Hes Signaling in Annelid Segmentation. *Development Genes and Evolution*, 219(1):37–43.

Rodríguez-Tovar, F. J., Uchman, A., Payros, A., Orue-Etxebarria, X., Apellaniz, E., and Molina, E. (2010). Sea-level dynamics and palaeoecological factors affecting trace fossil distribution in Eocene turbiditic deposits (Gorrondatxe section, N Spain). *Palaeogeography, Palaeoclimatology, Palaeoecology*, 285(1-2):50–65.

Rona, P. A. and Merrill, G. F. (1978). A benthic invertebrate from the Mid-Atlantic Ridge. *Bulletin of Marine Science*, 28(2):371–375.

Rona, P. a., Seilacher, A., de Vargas, C., Gooday, A. J., Bernhard, J. M., Bowser, S., Vetriani, C., Wirsen, C. O., Mullineaux, L., Sherrell, R., Frederick Grassle, J., Low, S., and Lutz, R. a. (2009). *Paleodictyon nodosum*: A living fossil on the deep-sea floor. *Deep Sea Research Part II: Topical Studies in Oceanography*, 56(19-20):1700–1712.

Rozhnov, S. V. (2010). From Vendian to Cambrian: the beginning of morphological disparity of modern metazoan phyla. *Russian Journal of Developmental Biology*, 41(6):357–368.

Runnegar, B. (1982). Oxygen requirements, biology and phylogenetic significance of the late Precambrian worm *Dickinsonia*, and the evolution of the burrowing habit. *Alcheringa*, 6(3):223–239.

Sebens, K. P. (1987). The Ecology of Indeterminate Growth in Animals. *Annual Review of Ecology and Systematics*, 18(1):371–407.

Seilacher, A. (1967). Bathymetry of trace fossils. *Marine Geology*, 5(5-6):413–428.

Seilacher, A. (1974). Flysch trace fossils: evolution of behavioural diversity in the deep-sea. *Neues Jahrbuch f{ü}r Geologie und Pal{ä}ontologie, Monatshefte*, 1974:233–245.

Seilacher, A. (1977). Evolution of trace fossil communities. *Developments in Palaeontology and Stratigraphy*, 5:359–376.

Seilacher, A. (1989). Vendozoa: organismic construction in the Proterozoic biosphere. *Lethaia*, 22:229–239.

Seilacher, A. (1992). Vendobionta and Psammocorallia: lost constructions of Precambrian evolution. *Journal of the Geological Society*, 149(4):607–613.

Seilacher, A. (2007a). The nature of vendobionts. *Geological Society, London, Special Publications*, 286(1):387–397.

Seilacher, A. (2007b). *Trace fossil analysis*. Springer.

Seilacher, A., Grazhdankin, D., and Legouta, A. (2003). Ediacaran biota: The dawn of animal life in the shadow of giant protists. *Paleontological Research*, 7(1):43–54.

Shen, B., Dong, L., Xiao, S., and Kowalewski, M. (2008). The Avalon explosion: evolution of Ediacara morphospace. *Science (New York, N.Y.)*, 319(5859):81–84.

Sperling, E. and Vinther, J. (2010). A placozoan affinity for *Dickinsonia* and the evolution of late Proterozoic metazoan feeding modes. *Evolution & development*, 209:201–209.

Sprigg, R. C. (1947). Early Cambrian (?) jellyfishes from the Flinders Ranges, South Australia. *Transactions of the Royal Society of South Australia*, 71:212–224.

Stanley, D. and Pickerill, R. (1993). Shallow marine *Paleodictyon* from the Upper Ordovician Georgian Bay Formation of southern Ontario. *Atlantic Geology*.

Stearns, S. C. (1992). *The evolution of life histories*. Oxford University Press.

Steeves, T. A. (1963). Morphogenetic studies of fern leaves. *Journal of the Linnean Society*, 58(373):401–415.

Stollewerk, A., Schoppmeier, M., and Damen, W. G. M. (2003). Involvement of Notch and Delta genes in spider segmentation. *Nature*, 423(6942):863–865.

Swinbanks, D. D. (1982). *Paleodictyon*: the traces of infaunal xenophyophores? *Science*, 218(4567):47–49.

Tarhan, L., Droser, M., and Gehling, J. (2010). Taphonomic controls on Ediacaran diversity: uncovering the holdfast origin of morphologically variable enigmatic structures. *Palaios*, 25(12):823–830.

Tchoumatchenco, P. and Uchman, A. (2001). The oldest deep-sea Ophiomorpha and Scolicia and associated trace fossils from the Upper Jurassic - Lower Cretaceous deep-water turbidite deposits of SW Bulgaria. *Palaeogeography, Palaeoclimatology, Palaeoecology*, 169:85–99.

Turner, S. and Vickers-Rich, P. (2007). Sprigg, Glaessner and Wade and the discovery and international recognition of the Ediacaran fauna. *Geological Society, London, Special Publications*, 286(1):443–445.

Tyszka, J. and Topa, P. (2005). A new approach to modeling of foraminiferal shells. *Paleobiology*, 31(3):522–537.

Uchman, A. (1995). Taxonomy and palaeoecology of flysch trace fossils. *Beringeria*.

Uchman, A. (2003). Trends in diversity, frequency and complexity of graphoglyptid trace fossils: evolutionary and palaeoenvironmental aspects. *Palaeogeography, Palaeoclimatology, Palaeoecology*, 192(1-4):123–142.

Uchman, A. (2004). Phanerozoic history of deep-sea trace fossils. *Geological Society, London, Special Publications*, 228(1):125–139.

Uchman, A., Abbassi, N., and Naeeji, M. (2005). Persichnus igen. nov. and Associated Ichnofossils From the Upper Cretaceous to Eocene Deep-Sea Deposits of the Sanandaj Area, West Iran. *Ichnos*, 12(2):141–149.

Valentine, J. (1992). *Dickinsonia* as a polypoid organism. *Paleobiology*, 18(4):378–382.

Vickers-Rich, P. and Ivantsov, A. (2013). Reconstructing *Rangea*: new discoveries from the Ediacaran of southern Namibia. *Journal of Paleontology*, 87(1):1–15.

Wade, M. (1972). *Dickinsonia*: Polychaete worms from the late Precambrian Ediacran fauna, South Australia. *Memoirs of the Queensland Museum*, (162):171–190.

Wagner, C., Müller, H. W., and Knorr, K. (1999). Faraday Waves on a Viscoelastic Liquid. *Physical Review Letters*, 83(2):308–311.

Webby, B. (1969). Trace fossils (Pascichnia) from the Silurian of New South Wales, Australia. *Paläontologische Zeitschrift*, 43(1/2):81–94.

Wetzel, A. (2000). Giant *Paleodictyon* in Eocene flysch. *Palaeogeography, Palaeoclimatology, Palaeoecology*, 160:171–178.

Wilby, P., Kenchington, C., and Wilby, R. (2015). Role of low intensity environmental disturbance in structuring the earliest (Ediacaran) macrobenthic tiered communities. *Palaeogeography, Palaeoclimatology, Palaeoecology*, 434:14–27.

Wilby, P. R., Carney, J. N., and Howe, M. P. a. (2011). A rich Ediacaran assemblage from eastern Avalonia: Evidence of early widespread diversity in the deep ocean. *Geology*, 39(7):655–658.

Wood, D. A., Dalrymple, R. W., Narbonne, G. M., Gehling, J. G., and Clapham, M. E. (2003). Paleoenvironmental analysis of the late Neoprotero-

zoic Mistaken Point and Trepassey formations, southeastern Newfoundland. *Canadian Journal of Earth Sciences*, 40(10):1375–1391.

Xiao, S. and Laflamme, M. (2009). On the eve of animal radiation: phylogeny, ecology and evolution of the Ediacara biota. *Trends in ecology & evolution*, 24(1):31–40.

Yun, M. H., Gates, P. B., and Brockes, J. P. (2014). Sustained ERK activation underlies reprogramming in regeneration-competent salamander cells and distinguishes them from their mammalian counterparts. *Stem Cell Reports*, 3(1):15–23.

Zhuravlev, A. Y., Wood, R. A., and Penny, A. M. (2015). Ediacaran skeletal metazoan interpreted as a lophophorate. *Proceedings of the Royal Society B*, 282:1–10.